The Application of a Charge Coupled Device to Astronomical Image Processing

by

Colin Lloyd Davies, B.Sc., A.R.C.S.

September 1980

A thesis submitted for the
degree of Doctor of Philosophy
at the University of London
and for the Diploma of
Imperial College

Astronomy Group,
Blacket Laboratory,
Imperial College,
London, SW7.

ABSTRACT

Optical images from large telescopes are seriously degraded by the point spread function introduced by the atmosphere, but image processing using speckle interferometry can recover diffraction limited information. The image processing is most efficiently carried out using digital techniques and various types of signal generator are assessed for this purpose. It is concluded that the charge coupled device (CCD) shows the greatest promise.

The construction of a camera using a Fairchild 202 CCD and its interface to a digital mini-computer are described. Laboratory assessment of the CCD performance suggested that it had several shortcomings as an analogue device, but that it would be very useful when used in a single bit quantization mode.

The CCD and computer were used in the laboratory reduction of speckle data. Speckle images were recorded on cine film using the Imperial College speckle interferometer and imaged onto the CCD so that two dimensional spatial autocorrelations could be computed for recovery of diffraction limited information.

Measurements of two binary star systems are presented. Investigation of the distorted shape of the autocorrelation function showed that this was caused by detector sampling effects. Subsequently, the expected form of the autocorrelation function was obtained for four stellar systems using data obtained from different telescope sites in different seeing conditions.

Tests of the CCD demonstrated that a prior stage of intensification would be necessary for unambiguous detection of single photoelectrons. The characteristics of such an intensifier and some experiments using available intensifiers are reported. These conclude that a new type of intensifier using a microchannel plate is necessary and a preliminary design is described.

Acknowledgements

I wish to record my sincere thanks to the following people.

First and foremost to my supervisor, Dr. Brian L. Morgan, who suggested the project and gave much needed advice, encouragement and criticism during the course of this work. Secondly to Mr. Peter Sharp for his instruction and vital assistance in the black art of electronics. Thanks are also owed to Mr. Robert W. Airey, Dr. Richard J. Scaddan and Dr. John G. Walker for many invaluable conversations, and to numerous members of the Imperial College Astronomy Group for providing apparatus, information and advice during this research.

I am grateful to the Science Research Council for the provision of a CASE studentship throughout the duration of the research.

Finally, I wish to thank Mr. W.C. Baker of Decca Radar Ltd., for permission to use Company facilities in the production of this thesis, and in particular for allowing the very patient Mrs J. Watson to type the manuscript.

List of Contents

List of Figures

List of Tables

CHAPTER ONE

INTRODUCTION

Optical images obtained using large telescopes are degraded in two ways. Firstly, there is photon noise which arises from the quantum nature of radiation and secondly there is a spatial point spread function introduced by the atmosphere. Image processing is necessary if the maximum amount of information is to be recovered from the raw data and modern digital techniques have greatly enhanced the ability of the astronomer in this respect. Ultimately the image processing will be performed in real-time leading to more efficient use of the telescope and effectively putting the astronomer back at the eyepiece.

The angular resolution limit of a telescope is often quoted (on the basis of Rayleigh's criterion) as:

$$\Theta = \frac{1.22\lambda}{D} \tag{1.1}$$

where Θ is in radians, λ is the wavelength of the light and D the diameter of the telescope aperture. However, although the theoretical limit of a large telescope such as the 98 inch Isaac Newton Telescope, may be about 0.05 arcseconds, in a conventional long exposure observation it is about one or two arcseconds at best. This is the angular diameter of the typical time averaged point spread determined by the atmospheric turbulence.

Since the 1920's, following the success of Michelson and his collaborators in using the interferometric properties of light to obtain high resolution optical data (reviewed by De Vorkin 1975), similar techniques were used successfully in radio astronomy and new optical techniques have measured angular stellar diameters as small as 0.001 arcseconds (reviewed by Hanbury Brown 1968, Labeyrie 1976 and 1978).

It had been noticed by astronomers that short exposure photographs (about 10ms) of the seeing disc exhibited a fine structure, and in 1970 Labeyrie correctly identified this as the so-called "speckle" pattern.

Speckle refers to the grainy structure observed when partially coherent light is reflected from, or transmitted through, a rough medium whose average phase fluctuations are greater than one wavelength of light. The speckle grains can be identified with the coherence domains of the Bose-Einstein statistics (Dainty 1974) and it has been shown by Lowenthal and Arsenault (1970), that in an imaging geometry, the characteristic size of these grains is determined by the diffraction limit. Labeyrie (1970) deduced that it should be possible to recover diffraction limited information about astronomical objects from the speckle pattern.

Recovery of this information is further hampered by the presence of photon noise due to the quantum nature of radiation. When the observation time is longer than the coherence time of the radiation the photon statistics are Poissonian; for a mean arrival rate of N photons per pixel, there is a noise of $\sqrt{N}$. The theory of how speckle interferometry is carried out under these circumstances is reviewed in Chapter Four.

In the case of photon counting photometry processing techniques to remove the atmospheric point spread function are not employed, but it is important to integrate the signal for as long as possible so that the signal-to-noise ratio (given by $S/N = \sqrt{N}$ when other noise sources are negligible) is maximised.

Digital image processing for this kind of observation has the important advantage over photography and electronography that the size of the integrating store can be arbitrarily increased, avoiding saturation effects. The manipulation of image arrays is considerably simplified by single bit quantization of the intensity at a point in the image. This implies that single photoelectrons must be detected for no distortion to occur (see Chapter Seven) although in some circumstances, a posteriori correction for single bit quantization of analogue signals can recover the original information (e.g. Chapter Four).

The initial experimental problem then is to record the position in space and time of each incident photon. Real detectors depart considerably from this ideal. The performance of practical detectors can be measured by their detective quantum efficiency (DQE) defined as (Rose 1946):

$$E_D = \frac{[S/N]^2_{\text{out}}}{[S/N]^2_{\text{in}}} , \qquad (1.2)$$

where S/N is the signal-to-noise ratio. An alternative formulation of this, due to Shaw (1963) is:

$$\varepsilon_D\ (u, v) = \frac{\varepsilon_D\ (o, o)\ \mathrm{MTF}^2\ (u, v)}{N(u, v)} \tag{1.3}$$

where ε_D (o, o) is the macroscopic DQE, MTF (u, v) is the modulation transfer function, N(u, v) is the noise power spectrum and u, v are spatial frequency co-ordinates.

If each detected photon is recorded with the same statistical weight, then:

$$\varepsilon_D\ (o, o) = \varepsilon_r \tag{1.4}$$

where ε_r is the responsive quantum efficiency, otherwise, from the work of Mandel (1959):

$$\varepsilon_D\ (o, o) = \frac{\varepsilon_r\ f}{1 + \dfrac{\overline{\Delta^2 g}}{\bar{g}^{\,2}}} \tag{1.5}$$

where f is the fraction of detected photons recorded, and $\bar{g}$ is the statistical weight of each detected photon.

Clearly then it is important that in general, most signal generating devices available at present require a prior stage of intensification in order that single photons will be detected unambiguously. The intensifier can either be coupled optically, or by direct electron bombardment, to a cascade intensifier or a microchannel plate intensifier.

One of the earliest systems that employed an intensifier and TV camera to record single photo-electron events from an image (in the laboratory) was constructed by Mende (1971) and this important paper discussed many of the problems that face constructors of image photon counting systems. One of the advantages of single photo-electron recording coded by a single bit is that digital signal storage can be extended indefinitely. The single bit digitising does, however, limit the photon rate that the system can handle. Mende also indicated the need for good phosphor to signal generator spectral matching, efficient optical coupling and photo-electron event centroid finding, but we will return to these topics in Chapter Seven. Soon after, Boksenberg and Burgess (1972) announced the University College Image Photon Counting System (IPCS) which comprised of a four-stage cascade intensifier optically connected to a TV camera and a digitising unit feeding a mini-computer equipped with a large memory. An important feature of this device is its centroid finding scheme that greatly improves resolution and linearity (Fort, Boksenberg and Coleman 1976). This system has since been updated and is now in routine use (e.g. Boksenberg 1972, Boksenberg et al 1976, Sargent et al 1978).

In recent years there have been a large number of image photon counting systems built, employing a wide variety of signal generator and intensifier combinations but lately there has been a move towards using all solid state signal generators that can avoid some of the problems encountered when using TV cameras (e.g. Beaver and McIlwain 1971 , Geary et al 1976, Currie 1976). The choice of an intensifier to extend the dynamic range of the CCD signal generator discussed in this thesis is presented later in Chapter Seven, but in the next section, the properties of various classes of signal generators are described.

a) Image Dissectors

In this device, photo-electrons produced by the photo-emissive cathode are accelerated and focussed along the tube as in an intensifier. A single channel photomultiplier is located in the "image" plane, and the electronic image is swept across it (and so dissected) by deflection coils.

The most successful system in routine use is the Lick Observatory scanner (Robinson and Wampler 1976, Miller et al 1976, Gaskell and Robinson 1978). As there is no storage in the dissector, a buffer memory has to be provided by long persistence phosphors in the preceding intensifier and this causes the pulse height distribution to be broad and unpeaked. Indeed, 1% of the initial image may persist for several minutes and as a result, the counting statistics are very poor. Considerations of phosphor decay time, dissector aperture and scan rate restrict its capacity to 4096 channels.

b) Television Cameras

Television cameras have been extensively used in the astronomical community both in an integrating analogue mode and in photon counting systems, because their technology is relatively well established, thus minimising system development. The most popular types of camera belong to the vidicon family; in particular the SIT tube with a structured mosaic of photodiodes as a target providing a limiting resolution of about 20 lp/mm, and the Plumbicon tube with an unstructured lead oxide target and a limiting resolution of about 25 lp/mm. Great care must be taken in arranging the scanning fields of the electron beam readout to avoid uncertain geometric registration and distortions (e.g. Mende 1971, Morton 1972).

The thermal distribution of electrons in the readout beam can cause non-linear readout at low light levels because only the high velocity electrons in the beam can land on the areas of the target that have had little exposure to light (Mende 1971, Colgate et al 1975). This can prevent the weaker scintillations in the pulse height distribution of the intensifier from being detected. The problem can be alleviated by provision of a uniform background illumination to improve the linearity of the TV camera (Mende 1971, Boksenberg and Burgess 1972). A gamma figure of 0.95 can be achieved using Plumbicon TV cameras but the gamma figure of other vidicons is somewhat lower (Stupp and Levitt 1971). The dynamic range of a TV camera is limited at the low signal end of the transfer characteristic by system noise (Colgate et al 1975, Westphal and Kristian 1976) and by saturation at the high signal end.

Television cameras suffer badly from lag, that is the retention of signal charge from field to field. This can be up to 30% in the third field of some vidicons, although the modern Plumbicon camera has reduced lag to around 6% (Stupp and Levitt 1971). The principal causes of lag are (a) the combined target capacitance and readout resistance, (b) the presence of trapping states in the target (particularly for silicon vidicons) or (c) at low light levels, the inability of the electron beam to fully recharge the target due to the thermal distribution of velocities in the electron beam.
In the silicon vidicon, the photodiode capacitance is particularly high (Gilbert et al 1976); Lowrance et al (1976) report that this causes detected events to be counted twice on average in their

photon counting system, with a consequent degradation of statistics. For accurate image measurement, an elaborate target preparation sequence is required. McCord et al (1975) have found that to operate an integrating television camera in such a way that successive frames of the same object are reproducible to within 1% requires a target preparation sequence of seven steps before each exposure.

c) Integrated Diode Arrays (IDA)

The problems encountered with electron beam scanned devices stimulated work on solid state signal generators based on the photodiode. The photodiode is simply a reverse biased silicon diode that forms a small capacitor which is then exposed to light. Incident photons are absorbed in, or near, the depletion layer creating hole-electron pairs that discharge the capacitor, and because this is a photoconduction process where the electrons do not have to leave the material, the relative quantum efficiency of this process (RQE), is much higher than for photo-emissive cathodes. There is also, of course, a thermal leakage current that will tend to discharge the photodiodes. At the end of the exposure, the charge required to replenish the diode is a measure of the incident light flux. Incident photons of wavelength greater than about 1.1 - 1.2μm, will generally fail to raise an electron from the valence to the conduction band, so that the response of the photodiode will fall dramatically after about 1μm, while photons from the blue end of the spectrum will tend to create carriers in the surface layers that will recombine before penetrating to the depletion layer of the photodiode thus causing a fall in response at the opposite end of the spectrum (Fry 1975, Geary 1976). The size of the band gap increases as the temperature of the device falls, so that the wavelength response of the photodiode shifts towards the blue end of the spectrum with decreasing temperature (Geary 1976, Livingston 1976). The greater penetration of photons from the red end of the spectrum increases the probability of carriers diffusing sideways into adjacent photodiodes before creating charge and this leads to a progressive loss of resolution as the energy of the incident photons decreases (Geary 1976, Vicars-Harris 1975).

Early solid state devices (e.g. Horton et al 1964) did not integrate the image between scans and must therefore be considered as belonging to the image dissector class of signal generators, but techniques for integrating soon followed and also a method of multiplexing the photo-diode outputs on-chip (for a review see Fry 1975).

Arrays based on serially multiplexed photodiode arrays known as integrated diode arrays (IDA) are popular in the astronomical community because of their good photometric performance (e.g. Livingston 1975, Dravins 1975, Livingston 1976, Geary 1976, Vogt et al 1978) but the one dimensional arrays are most popular, either for direct observation or with a prior stage of intensification. The hard-wired nature of the readout from these devices avoids the problems associated with electron beam readout in conventional TV cameras; in particular there is no measurable image lag associated with these devices. (A possible measurement of lag at 1.5% by Livingston et al (1975) has been shown by Geary (1976) to be probably caused by insufficient bandwidth in the preamplifier). The linearity of photodiode arrays has been measured to about 0.2% (Geary 1976, Dravins 1975) and although some possible causes of non-linearity have been suggested by Geary, none have been observed in practice.

The main sources of noise in integrated diode arrays are as follows:

a) Reset Noise

Each photodiode has an effective capacity C_D and when this is recharged, there remains an uncertainty in the diode charge given by:

$$N_e \simeq \frac{1}{e} \sqrt{kTC_D} \qquad (1.6)$$

where N_e is the number of electrons uncertainty, e the electronic charge, k is Boltzmann's constant, and T the temperature (Barbe 1975).

b) Amplifier Noise

Whether the output amplifier is on the chip or external to the array there is a noise associated with it that is proportional to the effective video line capacitance (Geary 1976).

c) Dark Current Noise

As mentioned earlier, this is noise created by thermal generation of hole-electron pairs in the photosite. Theoretically this should follow the generation of equilibrium charge density for intrinsic silicon, i.e.

$$I_D(T) \propto n_i^2 (T) = \text{const.} \times T^3 e^{-Eg/kT} \qquad (1.7)$$

where Eg is the band gap energy. For photodiodes, Geary (1976) has found significant departures from this law below $0^{o}C$, and derived the empirical relationship:

$$I_D(T) = I_D(To)\ 2^{(T - To)/\alpha} \qquad (1.8)$$

where To and α are experimental constants. Loh and Wilkinson (1975) have found that equation 1.7 is obeyed by CCD's down to -50°C. This disagrees with the results of Dyck and Jack (1974) who observed departures from equation 1.7 for CCD's below about -20°C.

d) System Noise

In the Reticon type of photodiode array a particular problem is stochastic noise coupled onto the video lines.

The first two types of noise can be considerably reduced by using output techniques such as correlated double sampling or distributed floating gates (Barbe 1975). Dark current noise is dramatically lowered by cooling the photodiode array as is shown by the figures assembled by Livingston (1975) from the work of others in Table 1.1.

It appears to be the case that integrated diode arrays will be limited by the system noise to an uncertainty of the order of hundreds of electrons per readout (e.g. Livingston 1975 and Livingston et al 1976).

The saturation level of photodiode arrays is of the order of 10^7 electrons giving a dynamic range of about 10^5 (Geary 1976).

TABLE 1.1: The variation in dark current with temperature for an IDA

Temperature (^{o}C)	Dark Current (Electron/Sec per Element)
20	1×10^7
0	1×10^6
- 76 (Dry ice)	6×10^2
-183 (LO_2)	2×10^{-2}

The inter-diode variation in response for a typical IDA is very good. Livingston et al (1976) have observed that a Reticon array type RL512B-24 has an inter-diode uniformity of about 0.5% and an end to end variation of about 2% (see also Dravins 1975).

The large number of circuit elements required to fabricate these devices makes it difficult to construct two dimensional arrays and also increases system noise and power dissipation. At the time of writing, a 100 x 100 element Reticon array is available, but it is difficult to see the size of IDA's increasing beyond this because the required packing density becomes too great.

d) Charge Coupled Devices

An alternative technology known as the charge coupled device (CCD) was conceived by Boyle and Smith (1970).

In this device potential wells are formed in a doped silicon substrate under metal electrodes held at a constant potential. Charge created by incident photons collects in the potential wells during the integration period. By clocking the electrodes in sequence, the stored charge packets can be moved along the array and out of the device.

Early CCD's were surface channel devices where the minimum of the potential well was near the substrate/SiO_2 interface and the interaction of signal charge with interface states gave rise to transfer-inefficiency (Barbe 1975). These limitations were overcome by placing a layer of opposite polarity silicon between the substrate and the $Si\ O_2$ layer, thus shifting the minimum of

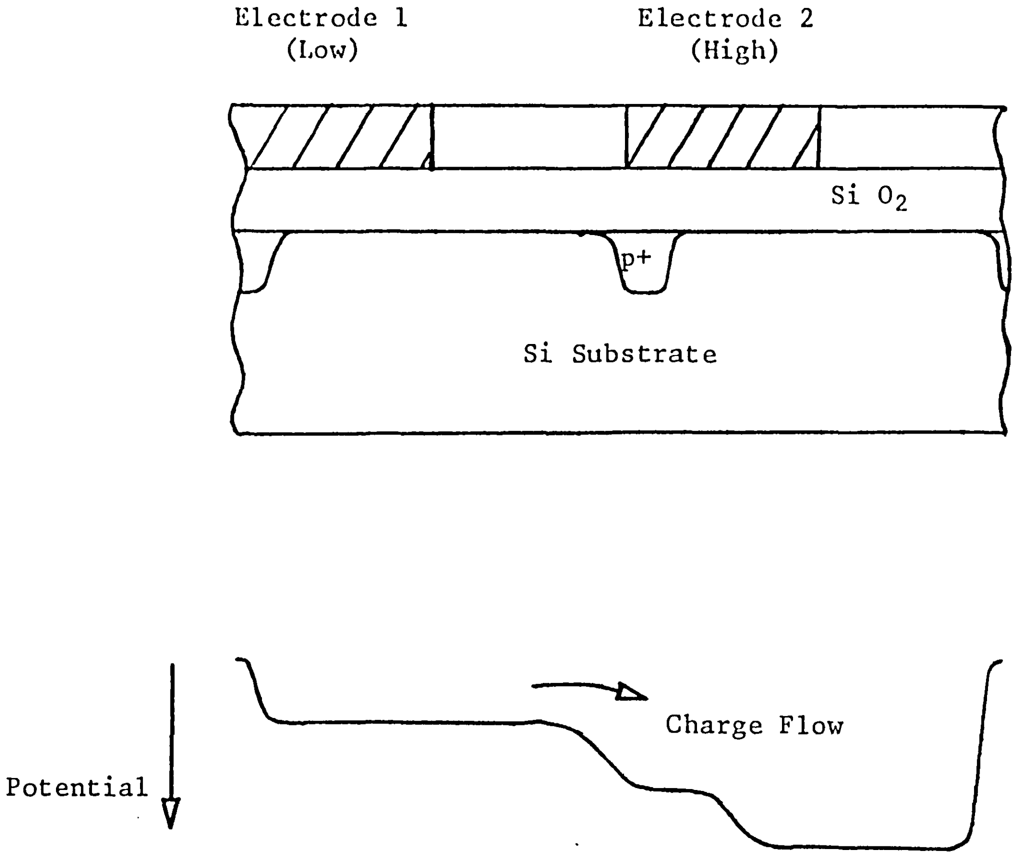

FIG. 1.1: Charge Transfer in CCD

the potential well away from the surface and into the bulk (Barbe 1975). The necessary assymetry required for unambiguous direction of charge transport is provided by ion implanted barriers (Figure 1.1).

Imaging arrays are organised in one of two ways (Figure 1.2). The first is the frame transfer scheme in which each line of video is clocked into a covered storage area and then read out line by line. This has the advantage of no dead area between photosites which reduces aliassing and improves stellar photometric accuracy, but because the charge transfer takes place along the uncovered photosites while the image is still incident, there is a danger of image smearing. The second is the interline transfer scheme where the contents of each photosite are moved sideways into a covered shift register before being read out line by line. Image smear is avoided in this scheme, but the penalty is that about half the array is dead area.

The mechanism of interaction between photons and CCD photosites is the same as for photodiodes, described in the last section on IDA's. However, the CCD enjoys the following advantages over the IDA:

i) The video line capacitance is about one hundred times smaller.

ii) They are not limited by clocking noise, and when cooled, noise figures of 50 - 60 electrons per readout have been obtained (at -40^{o}C and readout rate of 1.8×10^{4} pixels/sec; Chodil et al 1978). Since the CCD has a saturation level of about 10^{6} electrons per photosite, the dynamic

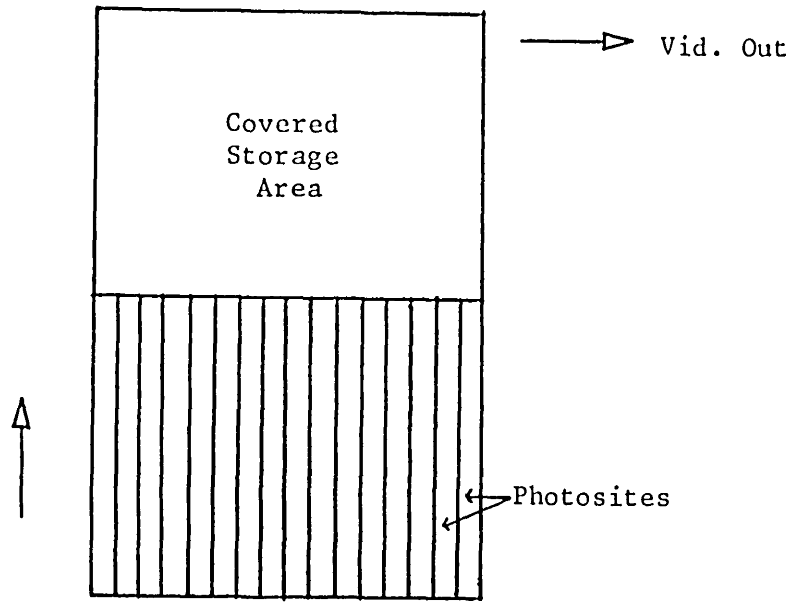

(a)

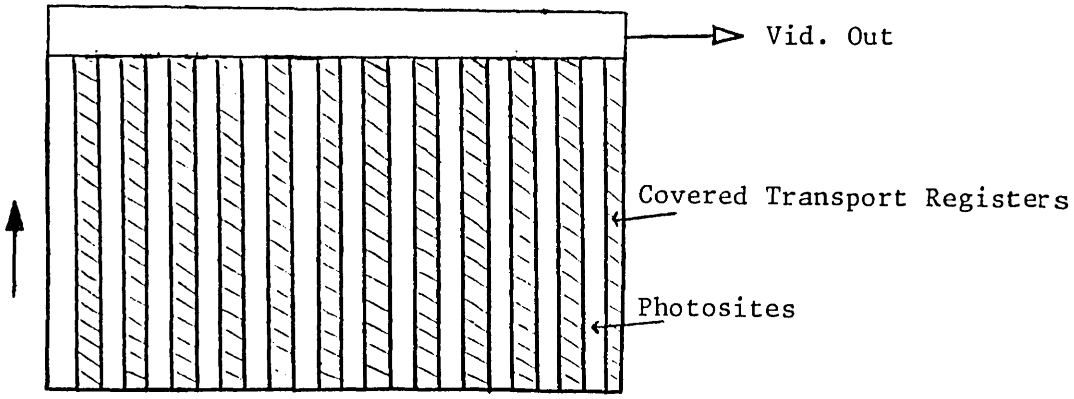

(b)

FIG. 1.2: (a) Frame Transfer Scheme
(b) Line Transfer Scheme

range can be of the order of 10^5.

iii) Their simple architecture leads to more resolution elements per unit area.

One of the most important disadvantages is their greater non-uniformity of photosites, and indeed, some photosites have such an anomalously high dark current that they appear as white spots in the video picture. In the Fairchild 202 (100 x 100) class B device (CCD's are classified according to the number of white spots in the picture), there are 9 defective photosites on average (Fairchild 1976). The number is falling as manufacturing processes improve and the newer Fairchild CCD 211 (244 x 190) claims 22 defective photosites in the class B version.

e) Charge Injection Device (CID)

Each photosite in a CID consists of a dual MOS capacitor, i.e. the depletion region is under two closely spaced metal electrodes. For a 2-D array, one capacitor is connected to a row of like elements and the other to a column. Every time that the voltage on one of the electrodes is altered, some (or all) of the charge can be transferred from under one electrode to the other and a displacement current flows that is a measure of the photo-generated charge (Barbe 1975). Thus the signal in each photosite can be sampled non-destructively. For destructive readout, the appropriate row and column is addressed simultaneously and the charge contained in that particular photosite is released into the substrate causing a current to flow. Photosites can, of course, be addressed sequentially or in random order.

CID's should have similar electro-optic properties to CCD's with perhaps slightly more readout noise caused by the higher video line capacitance (Livingston 1976). A General Electric Company CID based system has been under development at Kitt Peak National Observatory for some time, and some of its properties were detailed in Aikens et al (1976). The spectral sensitivity covered the same range as a CCD, but with the peak response coming, somewhat surprisingly, around 0.6μm and some fringing effects were observed with monochromatic light (c.f. Chapter Two). The linearity was ± 0.25% and a dynamic range of 6×10^3 was measured. Non destructive readout was obtained for 9000 frames at 77°K with a loss of not more than 10^{-3} carriers per pixel per readout and this feature can be used to improve the signal-to-noise ratio by averaging over many non-destructive reads.

A CID camera system is under development by Wattson et al (1976) for a programme of astronomical observation.

Choice of Detector

Despite the low number of pixels in comparison with conventional television cameras, solid state area imaging devices are very attractive in all other aspects of performance. A further advantage to add to those listed earlier is that the CCD is small, robust and does not require scanning coils, heater current or high voltages. Thus the solid state imager seemed well suited to the image processing described in this thesis.

At the time that the decision on the choice of signal generator was made, relatively little was known about the electro-optic performance of the CID and none were available as discrete devices in the United Kingdom, so the choice fell between a CCD or IDA.

The IDA has a better inter-diode uniformity than the CCD (0.5% as opposed to 5%) but the devices have similar performance in all other aspects. The reason for this is not clear and the difference between these devices may well become very small once CCD manufacturing techniques are as well established as photodiode manufacturing techniques. It also appears likely that the size of IDA arrays will not increase much in the future whereas CCD arrays are already available in a 244 x 190 format. Recently the Jet Propulsion Laboratory in America has placed an order with Texas Instruments Ltd., for a 400 x 400 element CCD and prototype arrays are now becoming available for testing (Fahlman et al 1979). Initially a Fairchild 201 CCD with 100 x 100 elements was purchased for use in the work described in this thesis. This was an ion implanted barrier, two phase CCD with interline transfer organization. Later this device was replaced by the Fairchild 202 that has the same physical structure but improved electro-optic performance.

The driving circuitry required to operate the Fairchild CCD 202 is described in Chapter Two, along with the electro-optic tests considered necessary to determine its suitability for the image processing work described in this thesis. The digitising of the CCD video signal and its interface to the mini-computer via a buffer store is described in Chapter Three.

The primary use of the CCD and computer is in the laboratory reduction of speckle interferometry, and the theory of this processing is reviewed in Chapter Four. Chapter Five is a description of the experimental arrangement, preliminary tests and calibration of the speckle reduction apparatus, while some results from astronomical data and their interpretation are discussed in Chapter Six.

Some preliminary experiments in using the CCD as a signal generator behind an image intensifier are set out in Chapter Seven and the requirements for a more efficient intensifier are detailed with some preliminary design ideas. Finally the conclusions and an outline of the possible course of future work are discussed in Chapter Eight.

CHAPTER 2

THE FAIRCHILD 202 CCD

2.1 Functional Description

The Fairchild CCD has been designed to be compatible with broadcast television standards and this imposes two constraints upon the architecture (Fairchild 1974a and 1976).

i) There is an aspect ratio of 4:3. This is achieved by making the separation of the photosites in the x direction 40μm and 30μm in the y direction (Figure 2.1).

ii) The scanning is interlaced i.e. odd numbered lines are read out before even numbered lines.

The particular layout shown in Figure 2.1 is a compromise between resolution and the picture smearing that is present in designs that do not use a separate masked vertical transport register. (Barbe 1975, Chpt. 1).

Incident photons pass through a transparent polycrystalline silicon gate structure and are absorbed in the substrate creating hole-electron pairs. The resulting signal charge (minority carriers) is collected in the photosites during the integration period when the photogate voltage (ØP) is HIGH. At the end of this time, ØP is lowered and alternate lines of charge packets are transferred sideways in the covered vertical transport register. The charge packets are clocked to the horizontal transport register via a vertical transfer stage by a minimum of 51 cycles of the clocks $ØV_1$ and $ØV_2$. After the removal of the first field, a second field cycle is initiated to receive information from even numbered photosites.

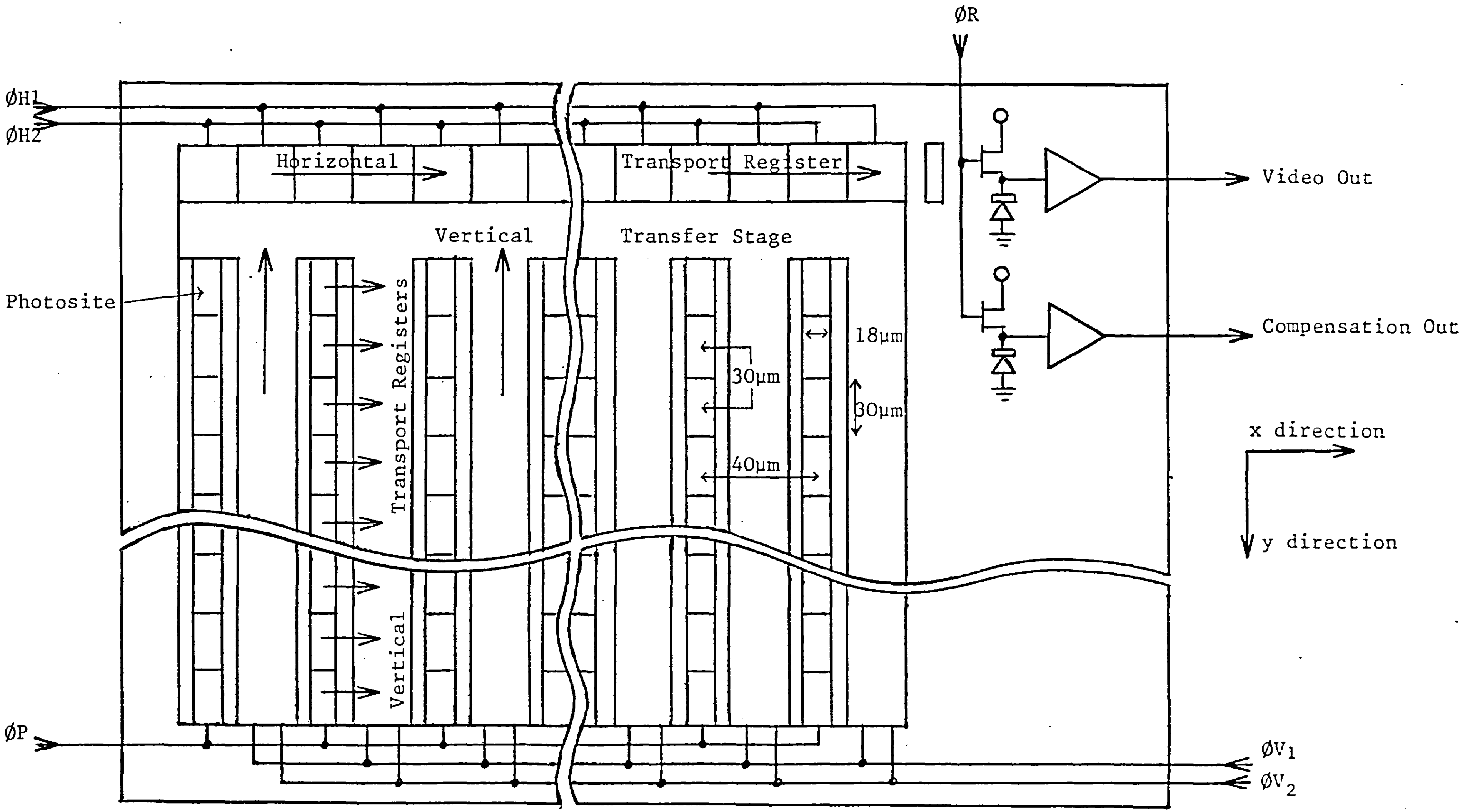

FIG. 2.1: LAYOUT OF FAIRCHILD CCD 202 IMAGING DEVICE

Data is moved through the horizontal output register to the on-chip output amplifier by a minimum of 102 cycles of the clocks $\emptyset H_1$ and $\emptyset H_2$.

The charge packets enter a pre-charged diode whose potential changes linearly in response to the quantity of signal charge delivered. This potential is applied to the gate of the first stage of a two stage n-channel MOS amplifier producing a signal output at VIDEO-OUT. A reset transistor, driven by clock ØR, recharges the diode before each signal charge packet.

Present in the output waveform are reset pulses from ØR. These can be cancelled using the COMP-OUT signal by differential amplification.

The timing waveforms are shown in Figure 2.2. The swing of each clocking waveform necessary for efficient charge transfer is individual to each CCD (Fairchild 1974a) and these values are supplied by the manufacturer. The values suggested for this particular device were found to be suitable for good CCD performance; alteration of each waveform swing had the following effects.

ØP Except for extreme values, this did not appear to affect the output waveform greatly.

ØR Again this has little effect except at extreme values when the signal level was diminished.

ØV, ØH These can alter the uniformity, shading and bordering of the CCD video picture, but interact in a complex manner that is difficult to quantify.

Similar tests for several different Fairchild 211 CCD's have been carried out by Chodil et al (1978). They also concluded that adjusting the drive voltages affected the CCD performance in a

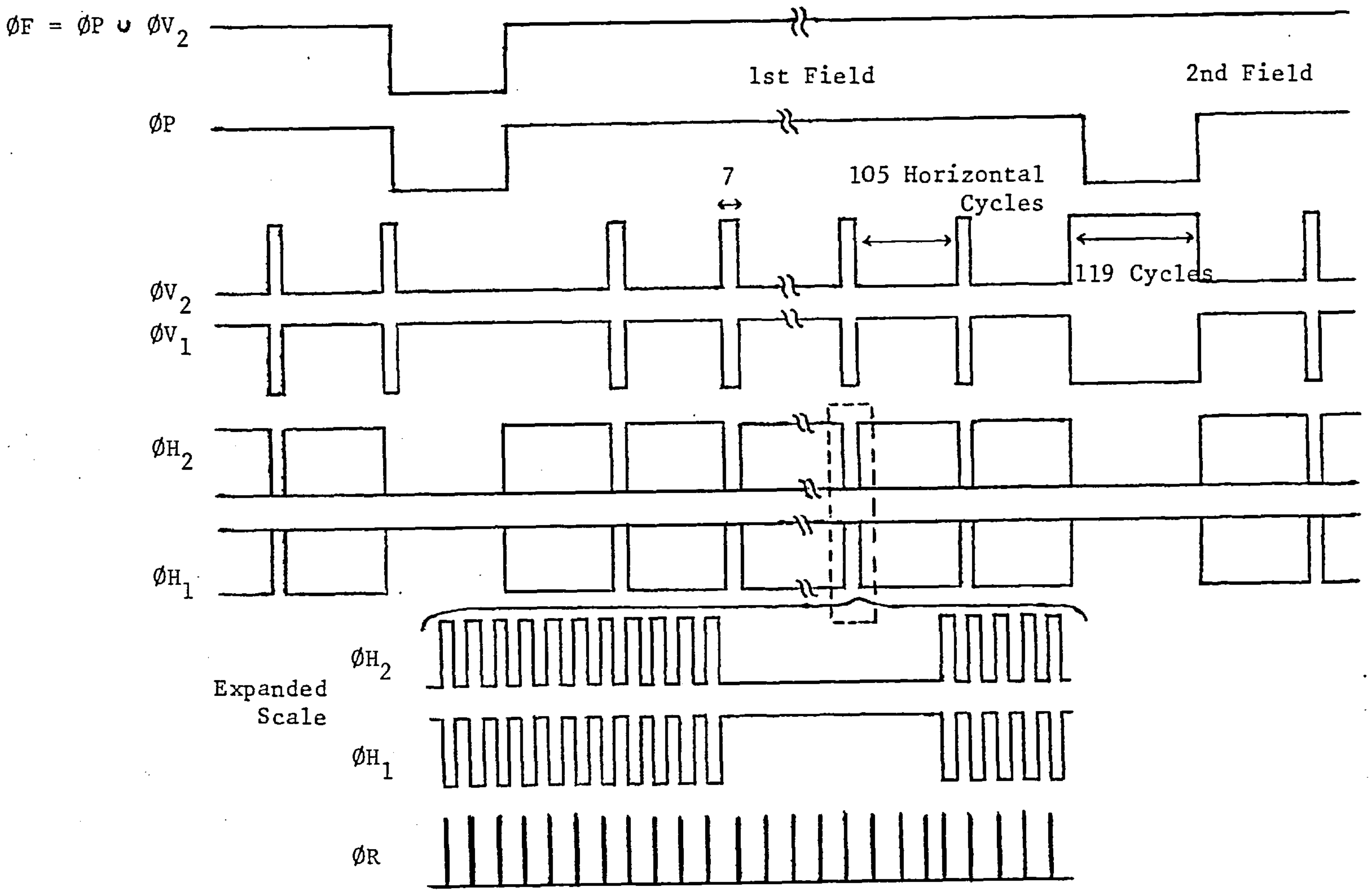

FIG. 2.2: TIMING DIAGRAM OF DRIVE SIGNALS

CLOCK PERIOD 1·2 μs; ØH Period 2·4 μs

complex and individual manner.

2.2 CCD Driving Circuitry

2.2.1 Digital

The digital circuits that provide the necessary clocking waveforms for the CCD were based on that suggested by Fairchild (1974b) with minor modifications due to the unavailability of some TTL logic devices at the time. These are shown in Appendix 1. When the original CCD 201 was replaced by the CCD 202 (Fairchild 1976), no modification to the logic circuits was required.

Figure 2.3 shows a block diagram of the complete driving circuit.

The TTL digital waveforms are generated by the logic circuits in the block marked "waveform logic". These waveforms are shifted to the levels necessary for CCD operation by the level shifters that can be manually adjusted. A horizontal and vertical ramp generator, (Appendix A) controlled by the waveform generator, are used to display the digitized video picture.

The CCD 202 has a maximum and minimum clocking rate of 6.0 MHz and 100 KHz, respectively. It is necessary to clock the array as fast as possible for best temporal resolution. Unfortunately an upper limit was placed on the clocking rate by the timing requirements of the interface memory devices (see Chapter 3). The clocking frequency chosen was about 1 MHz.

2.2.2 Analogue

Unavailability of the original transistors required the original Fairchild (1974b) driving circuit to be modified to the design shown in Figure 2.4(a).

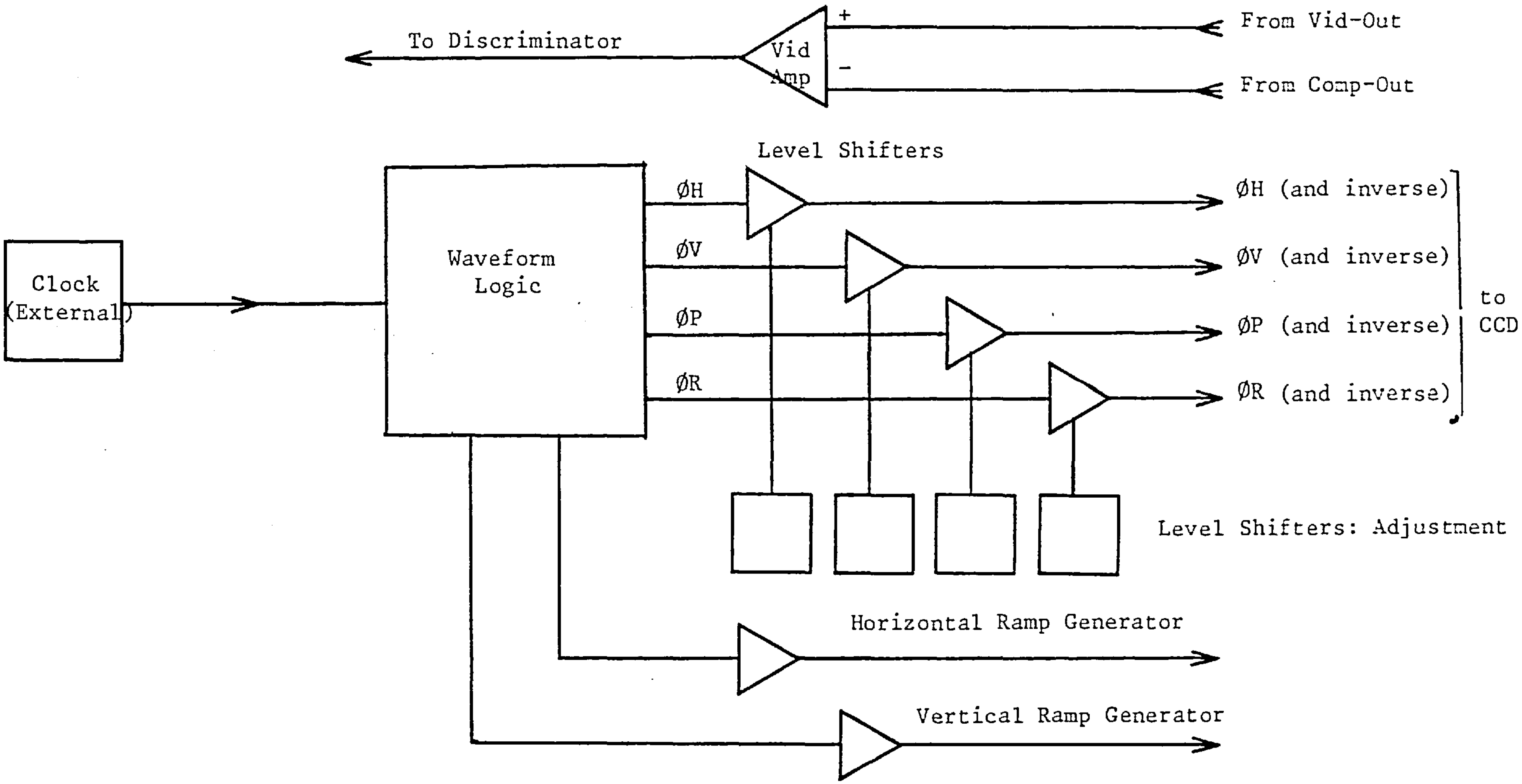

FIG. 2.3: BLOCK DIAGRAM OF CCD DRIVING CIRCUITS

The transistors used were the complimentary pair of high speed switching transistors TIS 49 and TIS 50 manufactured by Texas Instruments. The sum of the turn on time, storage time and turn-off time of these transistors is about 50ns (Texas 1970); this is longer than the minimum rise time of 15ns required for efficient charge transfer (Fairchild 1976).

The rise times obtained using the component values shown in Figure 2.4(a) were better than 100ns on all waveforms (ØP, ØR, ØH, ØV) and this was sufficient to provide good imaging.

Clocking levels were adjusted using the control circuit shown in Figure 2.4(b). The transistor simply acts as a voltage follower controlled by VR1 or VR2.

2.2.3 Video Amplifier

Some further amplification of the video signal was required for the digitising process.

The timing requirements of the interface memory devices demanded that the "boxcar" form of the video output have a rise time better than 100ns, but the amplifier circuit configuration supplied by Fairchild (1974b) was deliberately designed to smooth the video output so that it will appear as a continuous analogue television signal. Thus in order to preserve the discrete nature of the video signal, the video amplifier must have a minimum bandwidth given by $f = 0.35/t$, i.e. 3 MHz. The μA733 integrated video amplifier with a (large signal) bandwidth of 20 MHz (Texas 1971b) appeared to be suitable for these purposes.

The circuit diagram employed is shown in Figure 2.5 and this gave a gain of about five.

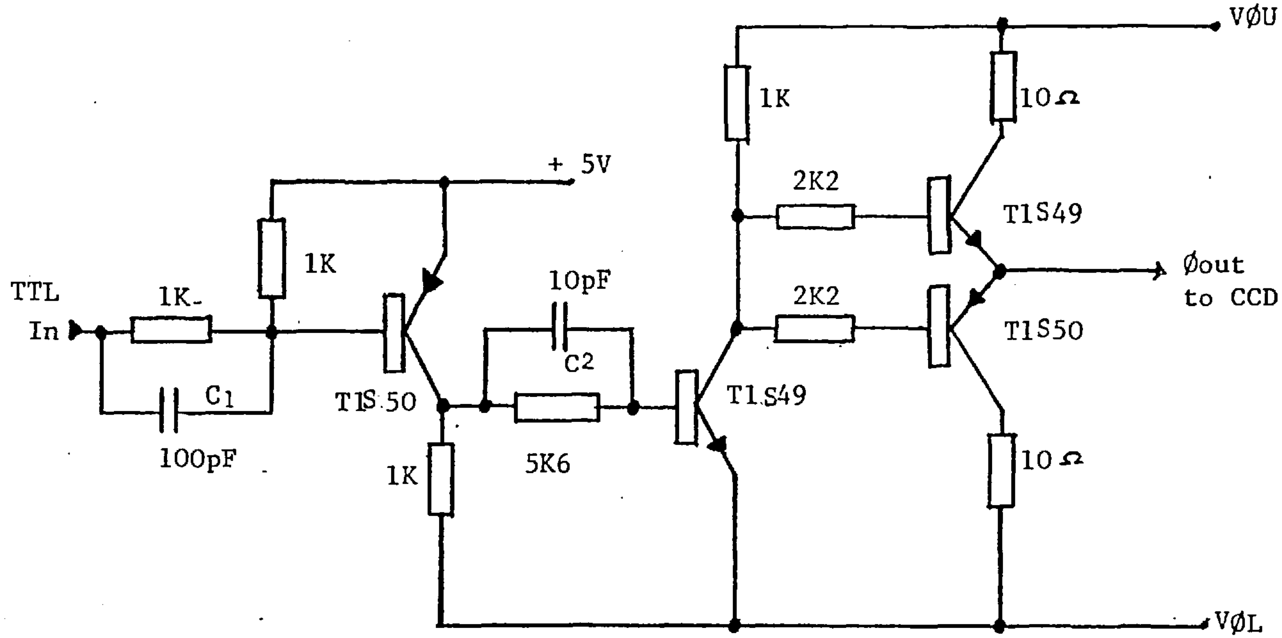

FIG. 2.4(a): LEVEL CONVERTER/DRIVER

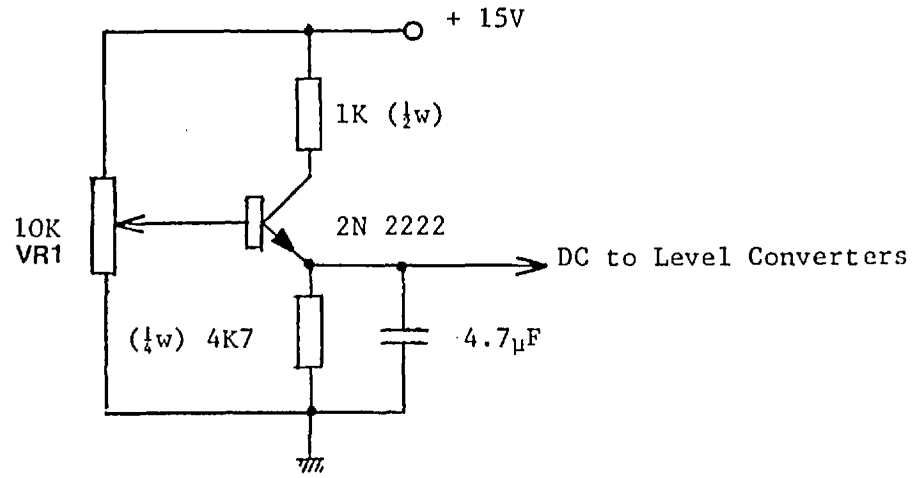

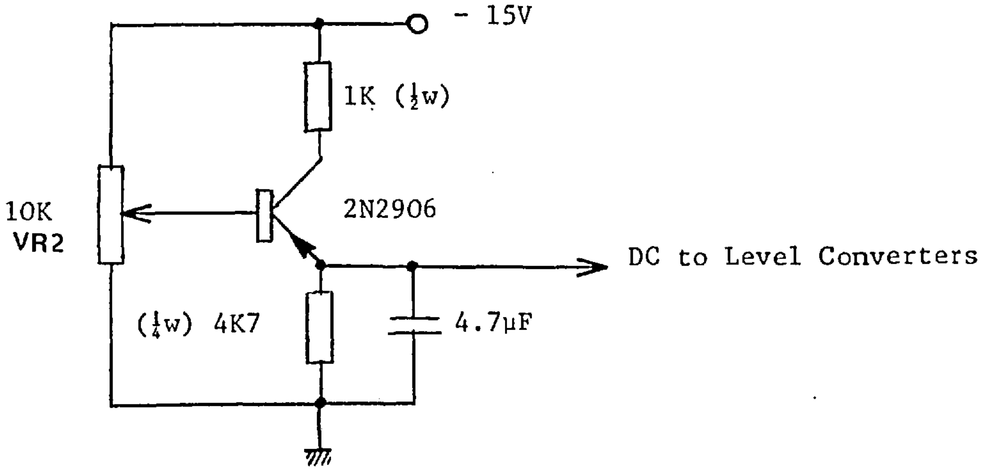

FIG. 2.4(b): DC SUPPLIES TO LEVEL CONVERTERS

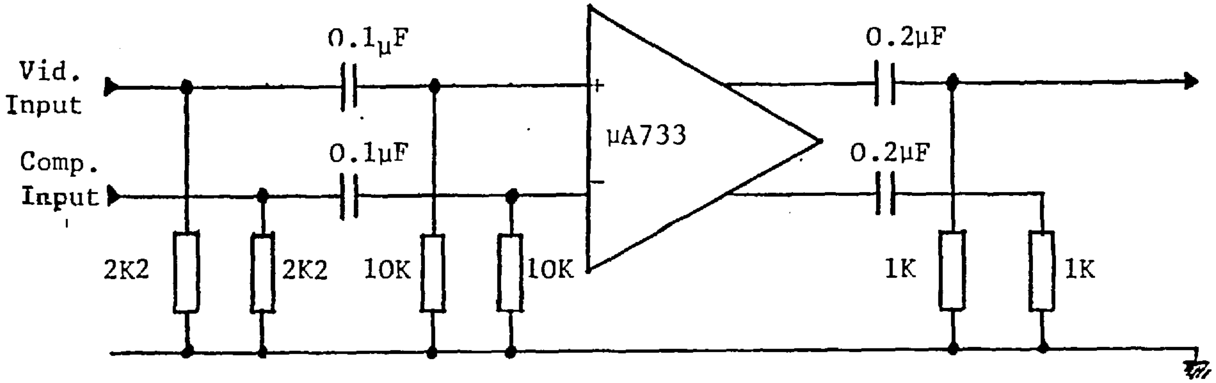

FIG. 2.5: VIDEO AMPLIFIER

2.3 Performance Tests

In this section white light was used for testing the uniformity and the MTF to determine the performance of the CCD when illuminated by the film projector (Chapter 5) used for speckle interferometry data reduction. The crosstalk and lag tests were conducted using a red light emitting diode as a point source of light in order to simulate photo-electron events on a red phosphor in a proposed image intensifier (Chapter 7). Tests to discover the extent of changes in CCD imaging properties with changes in incident light wavelength are currently being conducted.

A guide to these changes can be obtained from the work of other researchers. For example Vicars-Harris (1975) has found that the crosstalk between an excited and adjacent photosite changes from 5% at 0.5/0.6µm, 12% between 0.7 and 0.8µm and 21% between 0.8 to 1.1µm. Both Vicars-Harris and Livingston et al (1976) report a loss of MTF as the wavelength of the incident light increases, although they disagree on the amount. As a worst case, Livingston reports that the MTF at 8 diodes separation falls from about 1.0 at 0.6µm to about 0.75 at 1.0µm; the fall is faster at higher spatial frequencies. Finally, Loh and Wilkinson (1975) and Marcus et al (1979) report that inter-diode non uniformity gets worse towards the red end of the spectrum although no figures are given.

2.3.1 Uniformity and Noise

The tests described in this section were performed using a spatially uniform, thermally generated white light source that was measured by a photomultiplier to be within ± 0.5% of the mean level over an area of several square centimetres.

A typical line of video from near the centre of the array is shown in Figure 2.6 a, b and c, with three different levels of illumination: (c) with no illumination, (b) with illumination at an arbitrary level and (a) at saturation. The first three and last three photosites in a line have an anomalously high response to the photon flux.

This signal which is not present in the dark, very rapidly rises to saturation level upon the introduction of a relatively small signal, but does not "bloom" as the signal is increased further until the rest of the array is saturated. This creates a border around the video picture that can be removed by a computer programme (P - E; see Appendix B).

There are two components to the noise. The first is a "fixed pattern noise" that takes the form of a variation in zero level from photosite to photosite; in particular there are fixed "white spots" (photosites that have an anomalously high dark current) and these are scattered randomly around the array with a rather higher density towards the edges. A mapping of their position can be stored in the computer and it was found that they do not vary on a time scale of at least several weeks. It has been reported by several authors that the fixed pattern noise exists on a column basis when the array is cooled to sub-zero temperatures. This was not observed in the experiments reported here as the high thermal dark current at room temperature probably forms a "fat-zero".

It is also possible for fringes to be observed across CCD arrays due to Fabry-Perot interference in the Polycrystalline layer (Livingston et al (1976), Livingston (1976), Geary (1976)). This

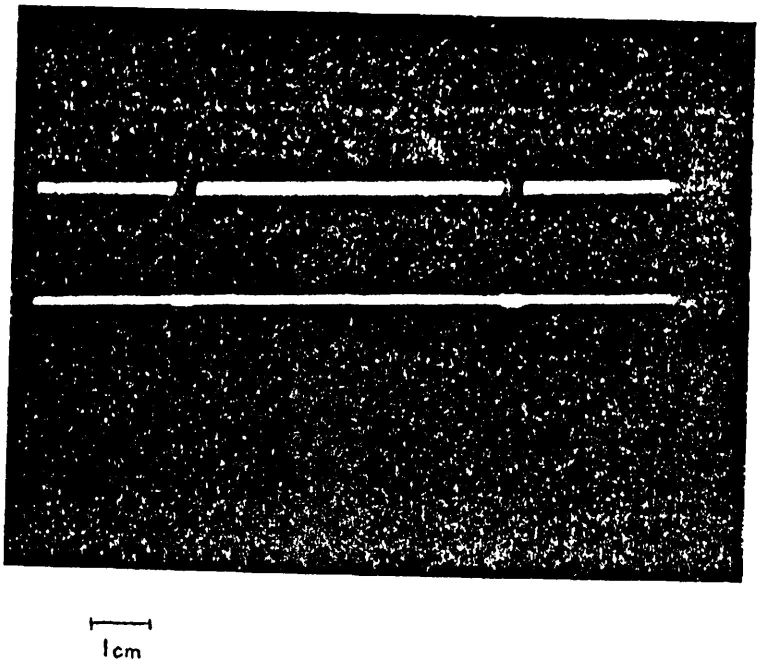

Fig. 2.6(a): A Single Line of Video at Saturation Level
Vertical Scale 2V/cm
Horizontal Scale 50μs/cm

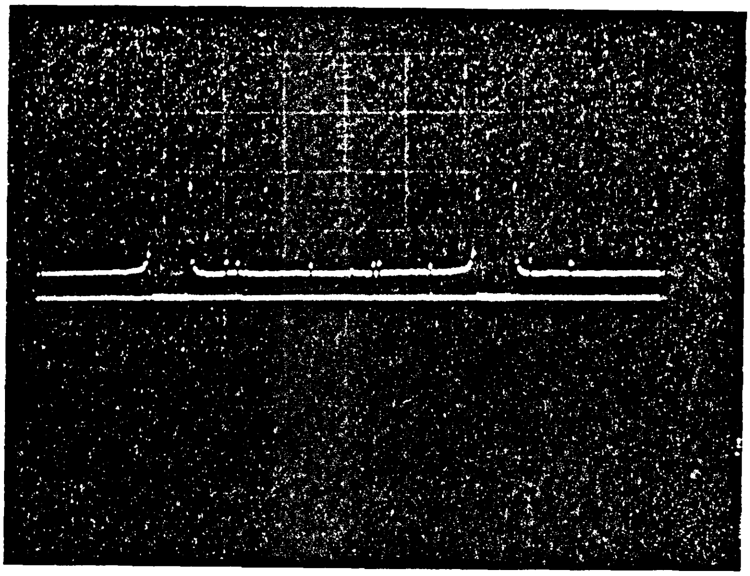

Fig. 2.6(b): A Single Line of Video at Arbitrary Level of Illumination
Scales as for Fig. 2.6(a)

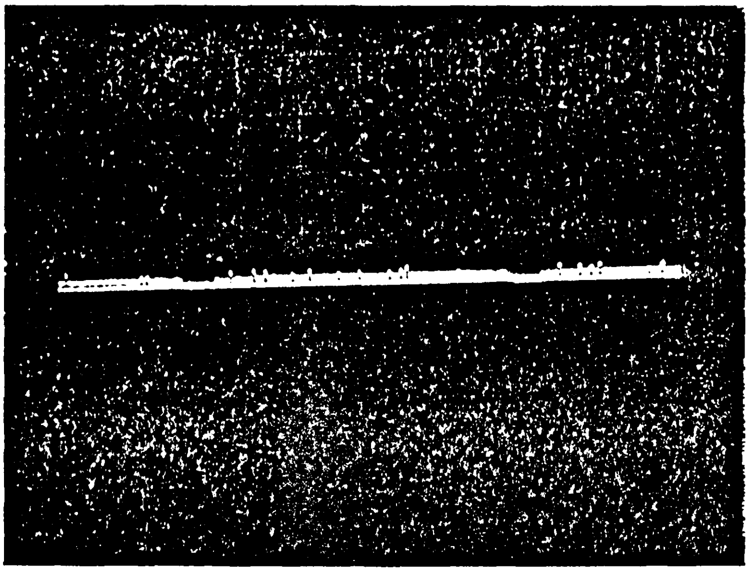

Fig. 2.6(c): A Single Line of Video with no Illumination.
Scales as for Fig. 2.6(a)

was not observed with the CCD 202 in question and was tested for in the spectral response (see 2.3(iv)).

The temporal noise is caused by thermal carriers and electronic noise (e.g. amplifier noise, diode reset noise, trapping noise etc.). Loh and Wilkinson (1975) have reported that the noise power spectrum follows an $(f)^{-1}$ dependance to 100 KHz and more recently Chodil et al (1978) have found that it follows $(f)^{-1}$ to 40 KHz due mainly to amplifier noise. The thermal noise follows the classical silicon response down to -128°C (Chodil et al 1978, Geary 1976).

Non-uniformity in the array response was measured in two ways; as a variation in mean response from one end of a line to the other, and as a variation in response from photosite to photosite.

a) Shading

Shading is the change in mean diode response from one end of the video frame to the other in the x and y directions. In the x direction this was measured as ± 2% of saturation level and in the y direction the value was ± 1%. These values conform to the tolerance limits set by Fairchild (1976). The mean light level was about half of saturation. There is no shading in the absence of illumination or at saturation. This compares very favourably with the result for integrated diode arrays of about 2% (Dravins 1975, Livingston et al 1976).

b) Uniformity of Response

Assuming that the response of a photosite to the photon flux is linear, (see 2.3(ii)), we can write for the output of the i^{th} photosite:

$$V_i\ (\lambda) = M_i\ (\lambda)\ E(\lambda) + C_i \qquad (2.1)$$

where $E(\lambda)$ is the photon flux, $M_i\ (\lambda)$ the RQE, C_i the dark signal background and $V_i\ (\lambda)$ the output of the photosite. The uniformity of response depends on the uniformity of $M_i\ (\lambda)$ and C_i (Loh & Wilkinson 1975).

The tests were carried out using the one-bit digitised output to the mini-computer described in Chapter 3, and consisted of setting a discriminator level and counting the number of photosites whose output is greater than this level.

At each discriminator setting, twenty readings were taken for an approximate mean and standard deviation to be calculated. The mean value was taken as a measure of the fixed pattern noise.

No Illumination

In Figure 2.7 the mean number of events is plotted against threshold voltage for zero light level.

Fairchild (1976) have defined a blemish (or "white spot") as a photosite that has a dark current response that is 10% of the the saturation level. In the absence of illumination, the number of photosites above this level is about 100 and is much higher than the average of 10 claimed by Fairchild (1976) although the ambient temperature was the same in both cases ($T = 25^{o}C$). It can also be seen from this graph that about 250 photosites were outside the 5% uniformity level also set by Fairchild.

Uniform Signal Background (Half Saturation Level)

Figure 2.8 shows the variation of the mean count versus threshold voltage with and without the bordering photosites. The number of photosites above the 10% limit is now 200 while those above the 5%

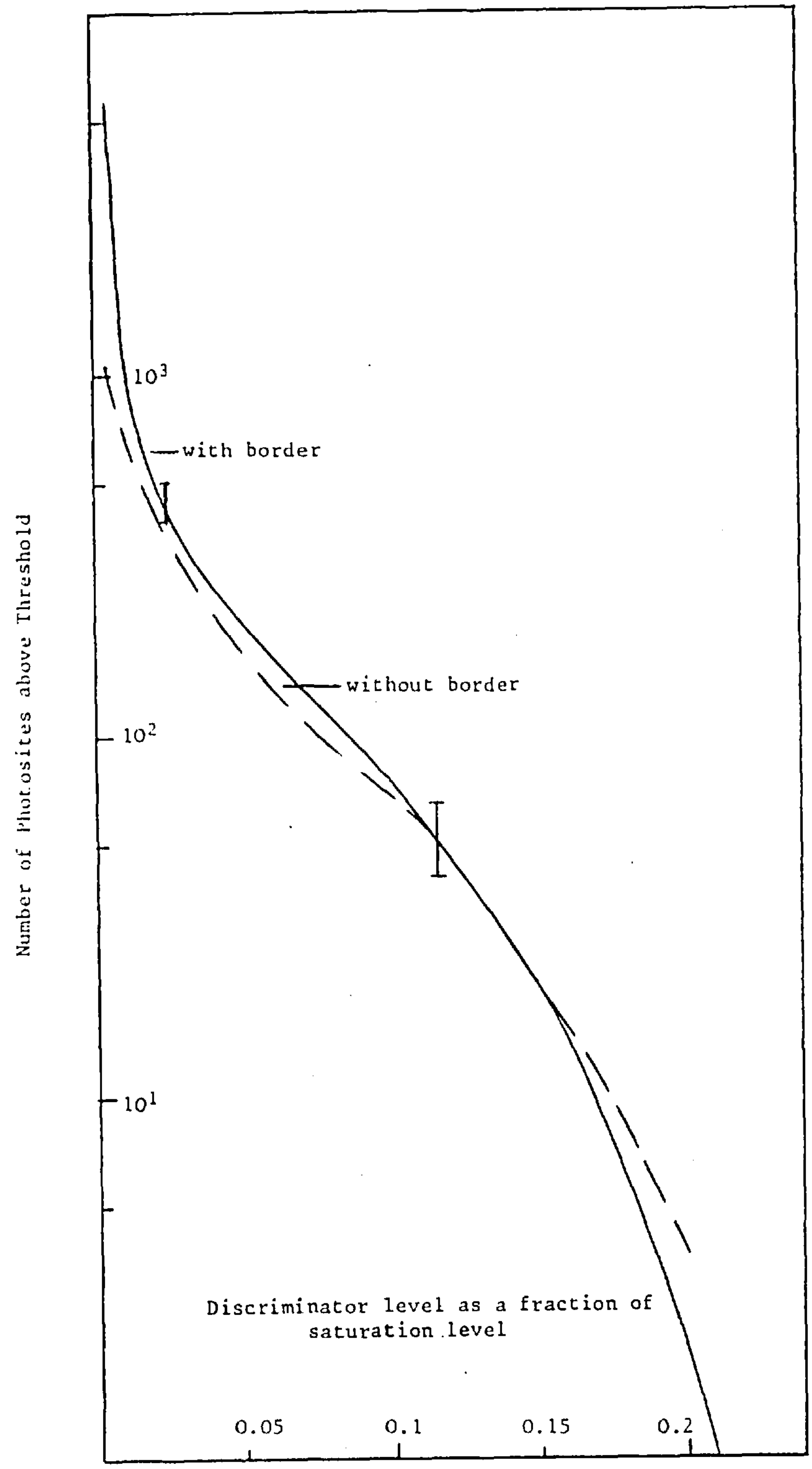

Fig. 2.7: Mean Number of Photosites above Threshold at 25°C (with no illumination)

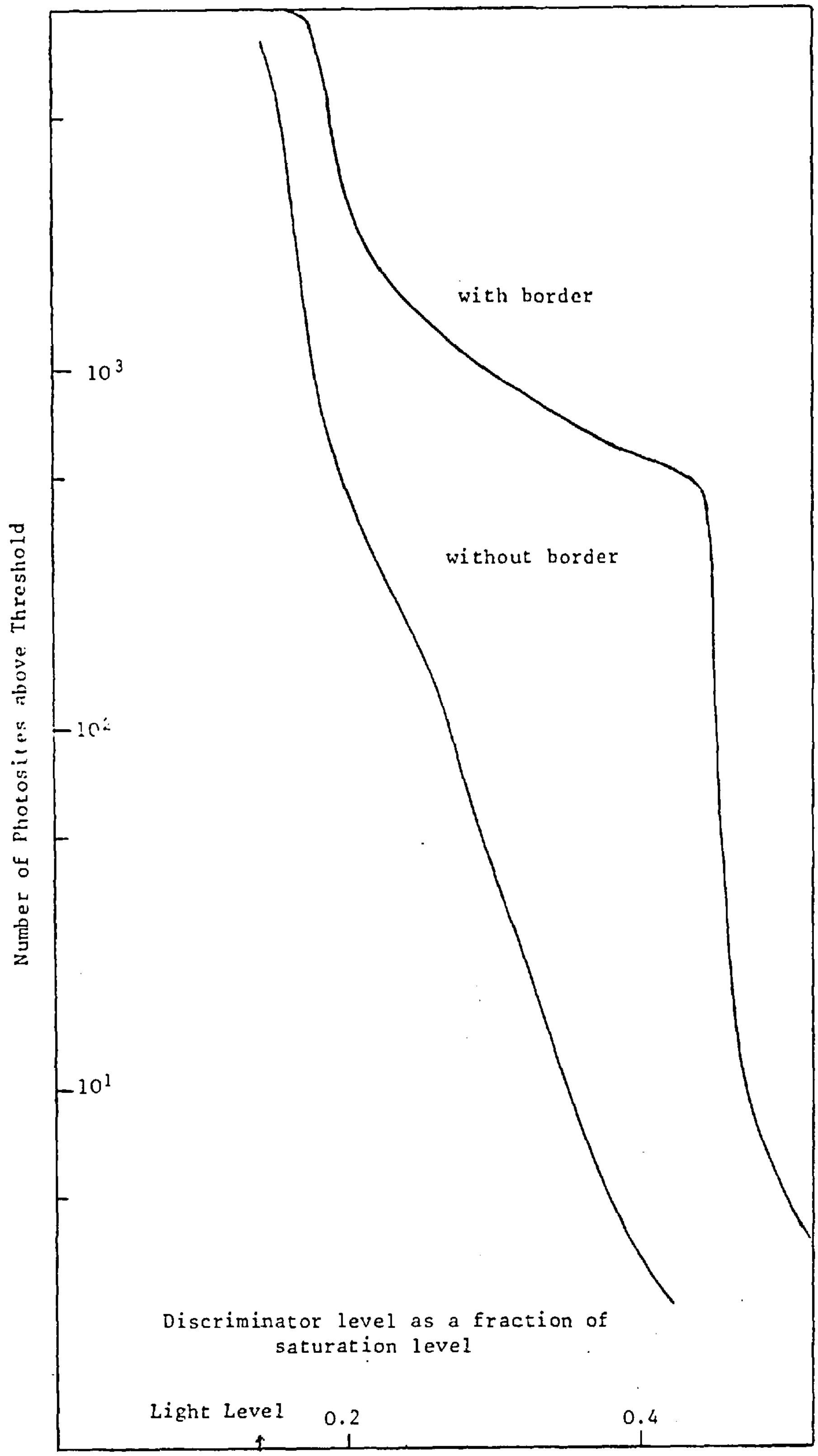

Fig. 2.8: Mean number of photosites above threshold at 25°C and arbitrary level of illumination

limit number 1000.

This was unexpected and suggested that the fixed pattern noise may be signal dependant, that is, the quantity $M_i(\lambda)$ in equation 2.1 varies from photosite to photosite. It has since been suggested by Chodil et al (1978) that this dependence is non-linear.

c) Increase in the Number of B~~ol~~lemishes with Temperature

The number of blemishes above the threshold level increases dramatically as the temperature rises, and this is illustrated in Figure 2.9. In this experiment, conducted in a dark room, the threshold level was set at 20% of the saturation level and the CCD temperature allowed to rise from room temperature to the CCD working temperature. The temperature indicated was the air temperature within the CCD camera. Some 350 photosites are above the threshold level at the normal working temperature of about 35°C, but this could be reduced to a very small number (< 10) with only a moderate amount of cooling (< 15°C).

Figures 2.10a and b are digitized video pictures of the blemishes when there is no illumination on the CCD. Figure 2.10(a) is a mapping of the hot spots with the discriminator level at 20% of saturation and Figure 2.10(b) is the same picture with a discriminator level of 50% of saturation. The temperature in both cases was about 25°C.

2.3.2 Linearity

The linearity of the CCD was tested using an apparatus for the routine measurement of the relative quantum efficiency of photocathodes devised by Wilcock (1966). In this arrangement, the flux from a standard 2854°K tungsten lamp at a known distance passes through

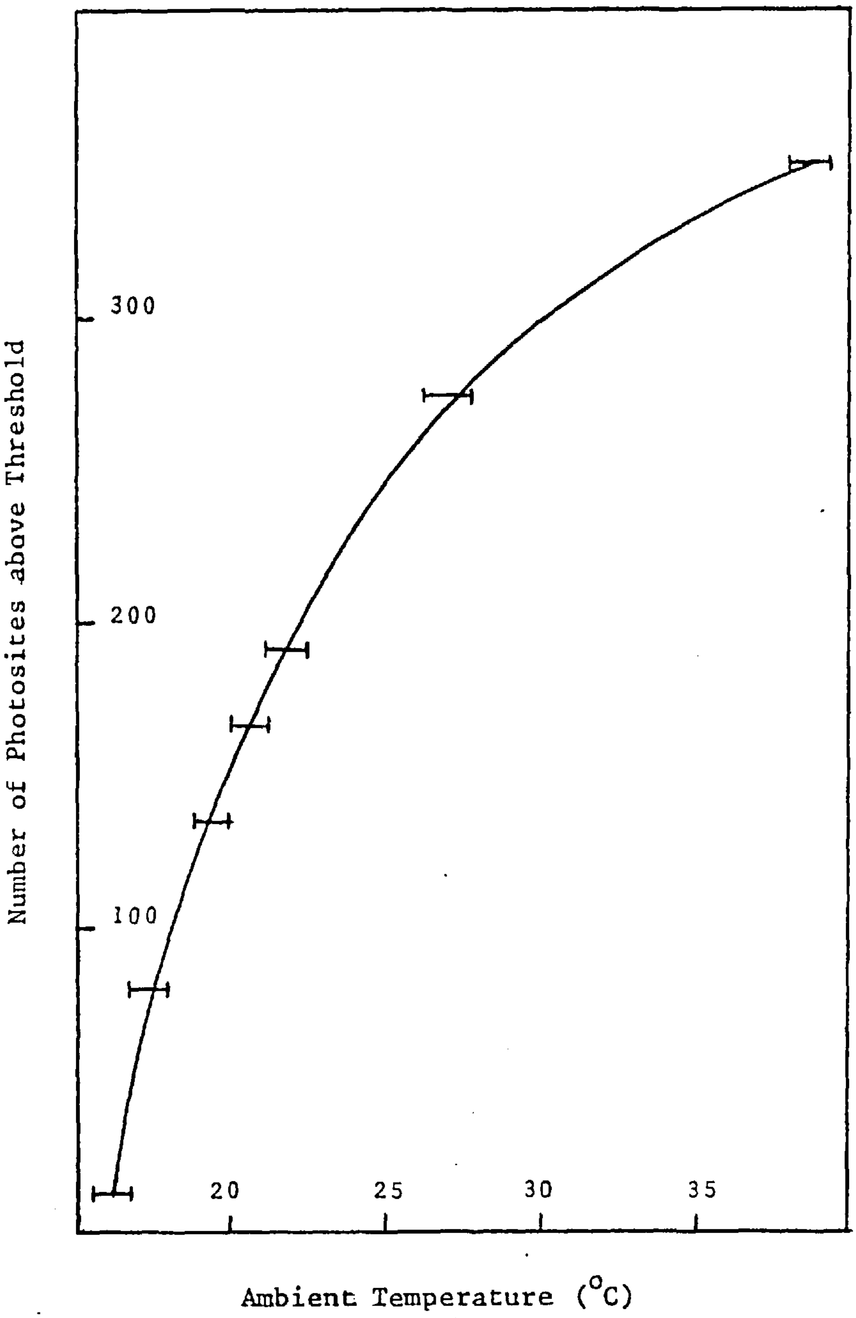

Fig. 2.9: Variation in the number of photosites above a fixed threshold (20% of saturation) with temperature (border removed).

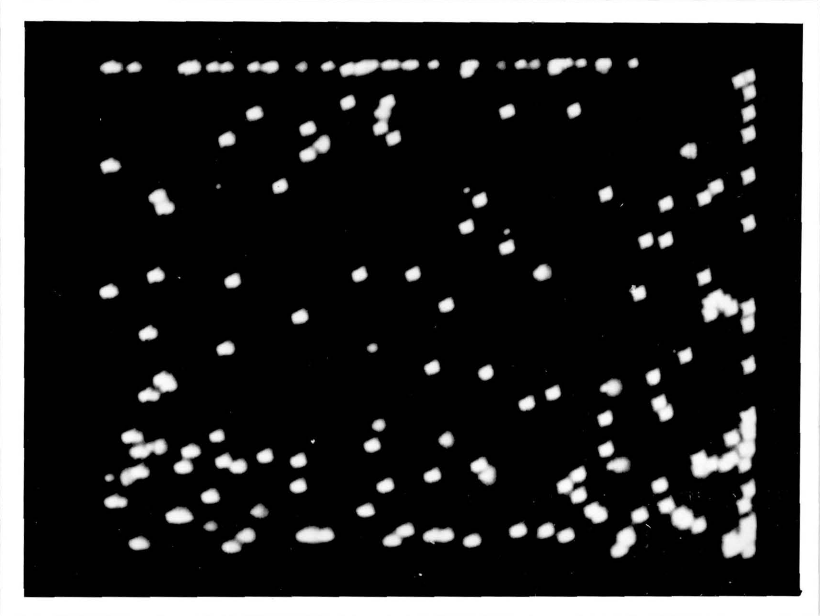

Fig. 2.10(a): A digitised video picture of the CCD output at 25°C (dark field) and the discriminator set at 20% of saturation level.

Fig. 2.10(b): The same picture as 2.10(a) with the discriminator set at 50% of saturation level.

an aperture and filter before falling on the CCD.

Let J be the radiant intensity of the standard lamp in the direction of the aperture, $E(\lambda)$ its relative power distribution as a function of wavelength λ, Ω the solid angle subtended by the aperture at the lamp filament, $I(\lambda)$ the spectral transmittance of the filter and $\sigma(\lambda)$ the responsive quantum efficiency of the cathode. The number of photons in the wavelength range $\lambda \to \lambda + d\lambda$ which reach the CCD in unit time is $p(\lambda)\, d\lambda$, where

$$p(\lambda) = \frac{J\Omega\, \lambda\, E(\lambda)\, \tau(\lambda)}{hc\int_0^\infty E(\lambda)\, d\lambda} \qquad (2.2)$$

Hence the total number of photons (n) reaching the CCD in unit time is given by:

$$n = \int_0^\infty p(\lambda)\, d\lambda$$

i.e

$$n = \frac{J\Omega}{hc} \frac{\int_0^\infty \lambda\, E(\lambda)\, \tau(\lambda)\, d\lambda}{\int_0^\infty E(\lambda)\, d\lambda} \qquad (2.3)$$

The luminous intensity (I) of the tungsten lamp is defined by

$$I = K_m J \frac{\int_0^\infty E(\lambda)\, \bar{y}(\lambda)\, d\lambda}{\int_0^\infty E(\lambda)\, d\lambda} \qquad (2.4)$$

where $\bar{y}(\lambda)$ is the CIE standard luminosity function and K_m is the luminous efficiency of radiant flux at the wavelength for which $\bar{y}(\lambda)$ has its maximum value of unity; the accepted value for K_m is 680 lm/W.

Defining $F = I\Omega$

and $$k = hc\, K_m \frac{\int_0^\infty E(\lambda)\, \bar{y}(\lambda)\, d\lambda}{e\int_0^\infty E(\lambda)\, \tau(\lambda)\, d\lambda} \qquad (2.5)$$

then

$$n = \frac{F}{ke} \tag{2.6}$$

Values of k for various glass filters have been calculated by Wilcock, who also showed that the error in assuming that all the photons passing through the filter have the same wavelength is less than 10%. Wratten neutral density filters were used to reduce the number of photons reaching the CCD.

With an aperture of 0.5cm diameter, a luminous flux of 5478×10^{-6} lumens and an integration time of 28ms, the following results for the number of photons required for saturation were obtained.

Mean Wavelength	No. of Photons
0.545μm	3.33×10^6 (± 15%)
0.644μm	2.86×10^6 (± 15%)
0.795μm*	1.12×10^6 (± 20%)

(* - This result has a higher error because of the uncertain performance of Wratten neutral density filters beyond 0.700μm (Kodak 1967)).

A plot of a single photosite output (abcissae) versus photon flux of wavelength 0.644μm (ordinates) is shown in Figure 2.11. When a mean noise level of 0.025 arbitrary units is subtracted, the photosite exhibits good linearity with $\gamma = 0.96$ (± .05); a similar result for 0.545μm photons is $\gamma = 1.05$ (± .05).

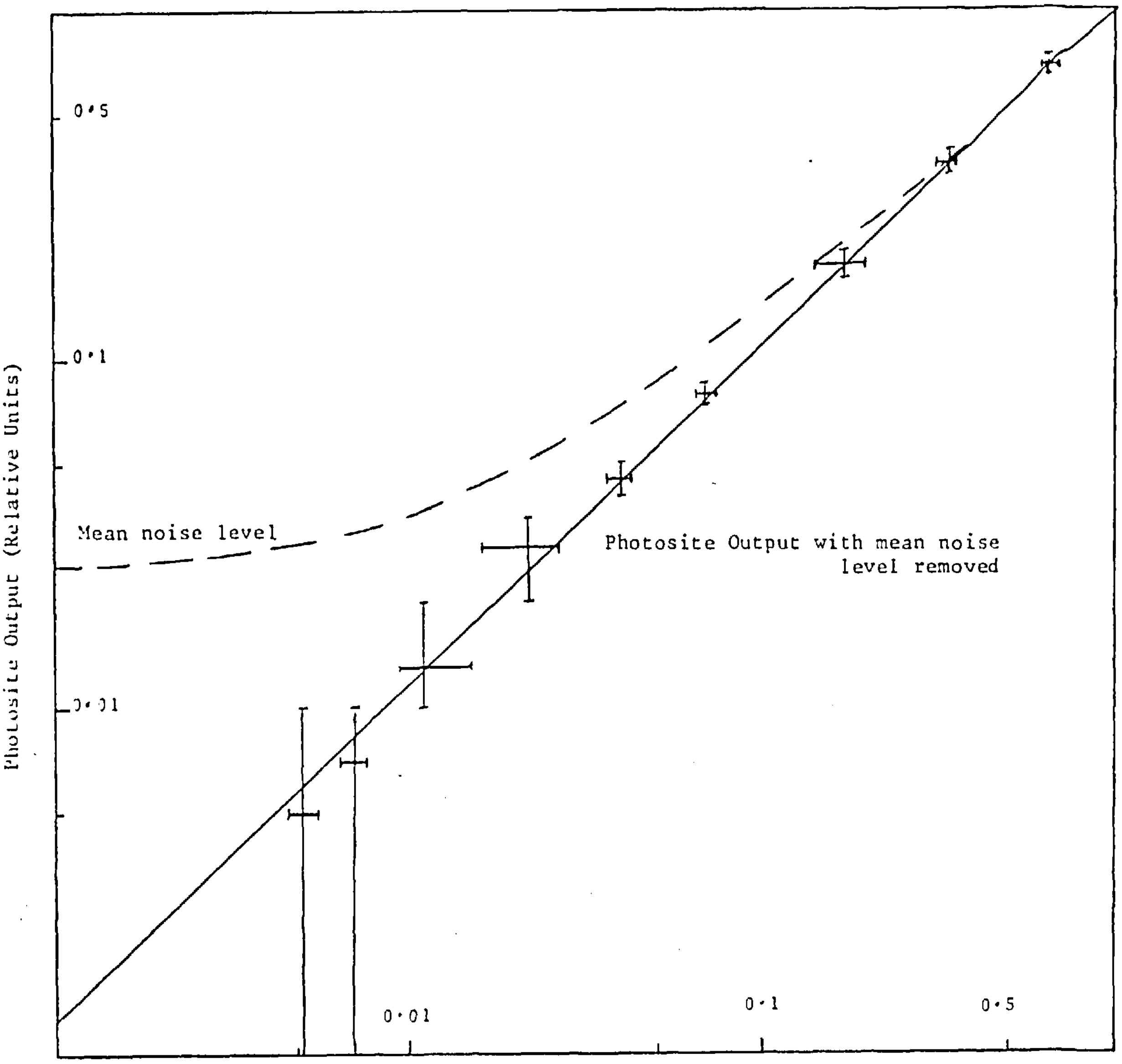

Fig. 2.11: Variation of Photosite Output with Photon Flux (Arbitrary Units)

For a mean noise level of 0.025 arbitrary units, and a saturation level of approximately 3×10^6 carriers, the mean noise is $\frac{3}{4} \times 10^5$ carriers and the rms noise is 2.74×10^2 carriers.

Thus defining the dynamic range as

$$D = \frac{S}{n_{\mathrm{rms}}}$$

where S is the number of carriers required to saturate a photosite, we find that the dynamic range is better than 10^3.

Applying the same analysis to the data of Loh and Wilkinson (1975) shows that D in excess of 10^4 is obtainable at liquid nitrogen temperatures.

Extreme linearity is, of course, to be expected from silicon devices (Vicars-Harris (1975), Dyck and Jack (1974), Dravins (1975), Livingston et al (1976)).

2.3.3 Crosstalk, MTF and Transfer Efficiency

a) Transfer Efficiency

The transfer efficiency of the CCD shift register is a measure of the amount of charge left behind as a signal charge packet is transferred from one cell to the next. If significant, it causes dispersion of the spatial frequencies and loss of modulation transfer function (Berglund 1971, Joyce and Bertram 1971, Solomon 1974).

Much work has been done on improving this figure, resulting in an efficiency of better than 99.995% per transfer at 1 MHz (Vicars-Harris 1975). For the 100th photosite of the 100th row of the CCD 202, the total transfer efficiency is given by

$$T = 1 - nE \qquad (2.7)$$

where n is the total number of transfers and E is the inefficiency at each transfer providing that $nE \ll 1$ (Barbe 1975). Thus after 200 transfer there is an efficiency of 99% which has a negligible effect on the modulation transfer function.

b) Modulation Transfer Function

In the absence of any transfer inefficiency, the modulation transfer function can be calculated up to the sampling limit by the Fourier transform of the basic integration cell (Barbe 1975), and for the CCD 202 this is

$$\mathrm{MTF}(w) = \frac{\sin\left(\frac{\omega\pi a}{\omega_m p}\right)}{\left(\frac{\omega\pi a}{\omega_m p}\right)} \qquad (2.8)$$

where ω_m is the maximum spatial frequency given by $\omega_m = \frac{2}{p}$, p is the periodicity and a is the cell length. For the CCD 202, the cell lengths in the vertical and horizontal directions are 30μm and 18μm respectively while the periodicity in the vertical and horizontal directions are 30μm and 40μm respectively. The MTF measurements made by Fairchild (1974, 1976) correspond to equation 2.8.

Figure 2.12 (a, b, c) shows the Baum test pattern projected onto the CCD by a Baum projector (Baum 1962) in the vertical direction (a), the horizontal direction (b), and at an arbitrary angle (c). The video picture has been digitised with single bit accuracy before display and the discriminator level set for maximum resolution. From these pictures it can be seen that a limiting resolution of about 12 lp/mm can be expected in the vertical and horizontal directions.

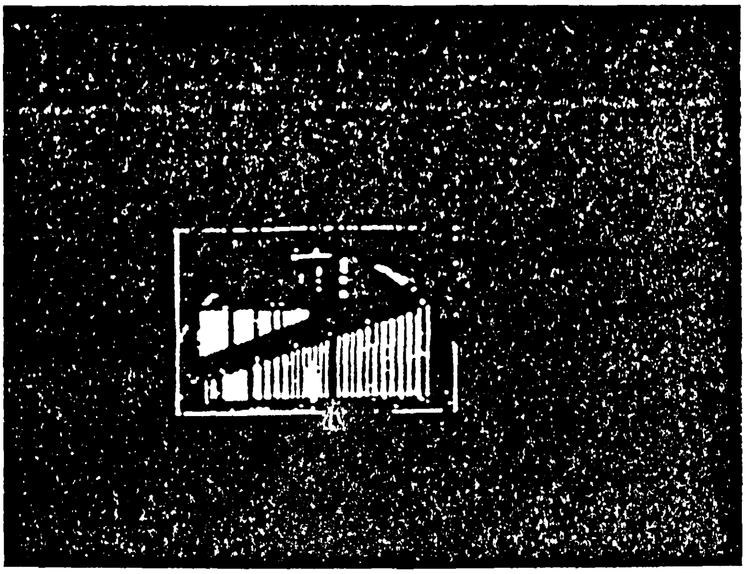

Fig. 2.12(a): The Baum Pattern projected onto the CCD and Digitised by a Single Bit. The Resolution Wedge in the Horizontal Direction shows a Limiting Resolution of about 12 lp/mm (arrowed).

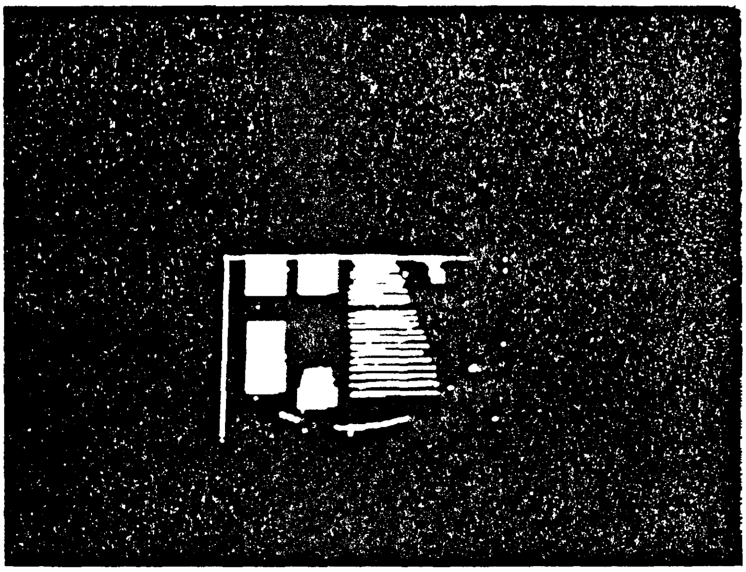

Fig. 2.12(b): The Baum Pattern rotated through 90°. The Limiting Resolution is still about 12 lp/mm.

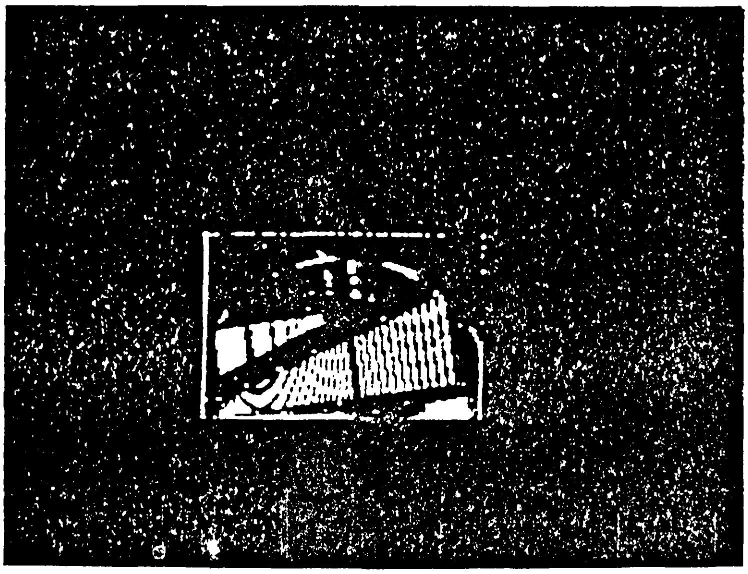

Fig. 2.12(c): The Baum Pattern Projected in an Arbitrary Direction.

c) Crosstalk

The crosstalk between adjacent photosites was measured by projecting a reduced image of a red (λ ~ 0.6μm) light emitting diode onto a single photosite near the end of the array. With a diameter of 20μm the spot of light produced no measurable crosstalk in the horizontal direction while the vertical column crosstalk is about 7% of the saturation voltage (the original photosite is at about 50% of saturation). (Figure 2.13).

When the spot diameter was increased to 33μm diameter the horizontal crosstalk is about 8% of saturation level and the spot overlaps 2 photosites in the vertical direction. These values are similar to those found by Vicars-Harris (1975).

Since the charge created by the LED is clocked through a maximum number of registers, we can see from Figure 2.13 that there is no measurable transfer ineffiency because the leading and trailing photosites on either side of the main photosite have the same height.

Lag

The CCD was tested for lag, i.e. the retention of signal charge from frame to frame, by flashing a light emitting diode (LED) onto the CCD every other frame period. This was achieved by using the ØF signal from the control logic (that marks the start of a frame period (Chapter 3)) through a divide-by-two counter.

The resulting output from the CCD is shown in Figure 2.14. Since the image of the LED covered several photosites, the LED signal charge appears in both half fields during the frame period. Thus in Figure 2.14, each frame period contains two signal spikes.

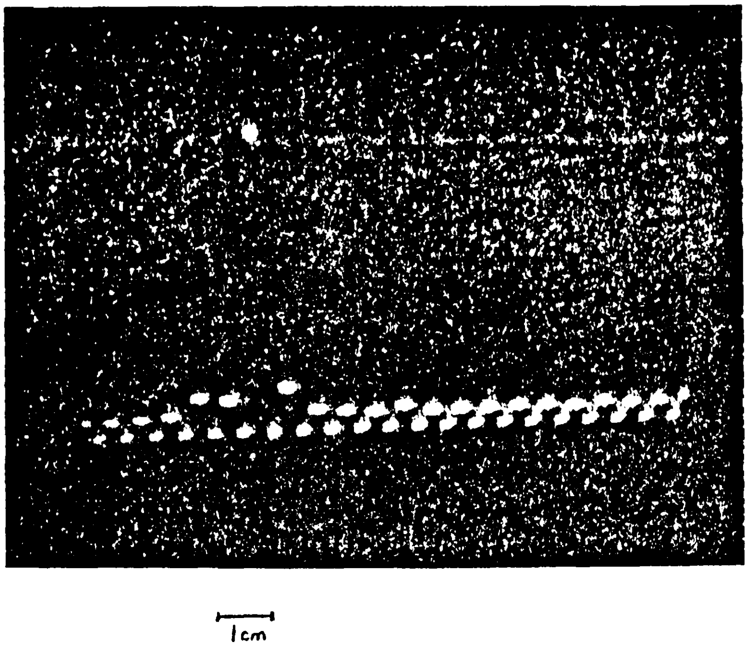

Fig. 2.13(a): Crosstalk between adjacent Photosites, the Excited Photosite on the extreme left is a "Hot Spot". Vertical scale $\frac{1}{2}$V/cm, Horizontal scale 5 μs/cm.

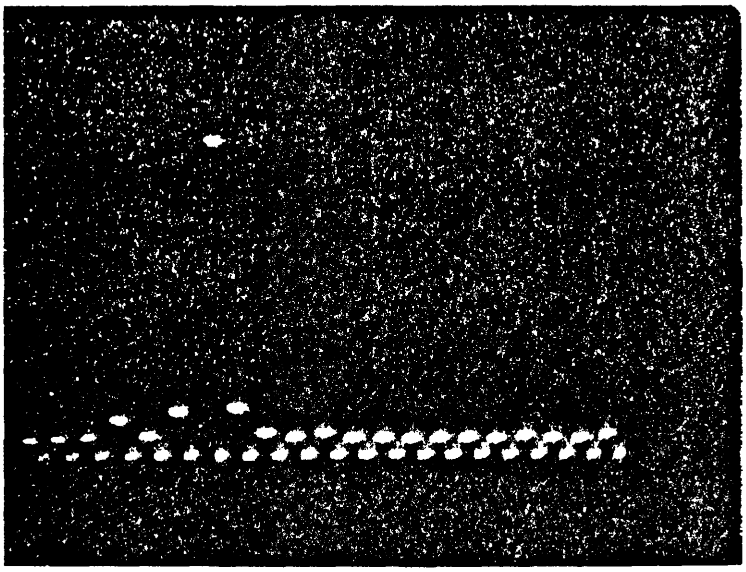

Fig. 2.13(b): As for Fig. 2.13(a) but with the Spot shifted by One Photosite.

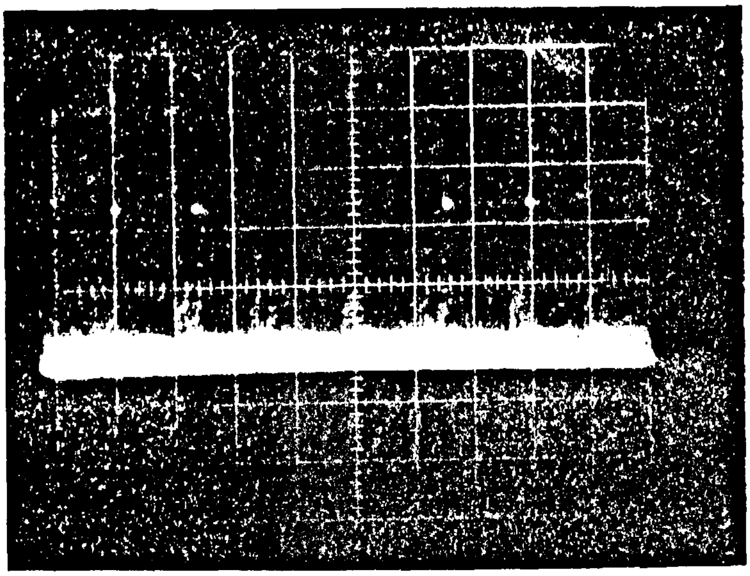

Fig. 2.14: Test for Lag between Frames
Vertical scale 1V/cm
Horizontal scale 10ms/cm

Three frame periods are shown in this photograph but it can be seen that the middle frame period does not exhibit any signal charge above the noise level, i.e. any charge retention is less than the thermal and electronic noise charge. It is to be expected from the "hard-wired" nature of the CCD that there should be no lag, but it is interesting to note that Livingston et al (1976) have reported lag in a Reticon IDA array of about 1.5% probably due to insufficient pre-amplifier bandwidth (Geary 1976).

2.3.4 Spectral Response

The spectral response of the CCD was measured using a Hilger and Watts F 1497 Prism monochromator; the Wilcock box (Section 2.3.2) was rejected because of the limited number of filters available, and their relatively large bandwidth (~ 70nm). The monochromator was first calibrated using a standard mercury source. To allow the maximum light to fall on the CCD, the entrance slit was widened to increase the flux, but this reduced the resolution which was estimated as 8 - 10nm (e.g. Born and Wolf 1975).

The resulting spectral response, corrected for the spectral curve of the source (Eberhardt 1968), is shown in Figure 2.15. The response of the CCD is averaged over several photosites. As expected, the CCD exhibits a silicon device type response peaking in the red to near infra-red region at 0.97μm.

The loss of response beyond 1.1μm is due to the incident photons not having enough energy to raise an electron from the valance to the conduction band. For photons of higher energy (towards 0.3μm) the reduction in response is caused by increasing absorption of high energy photons in the surface layers of silicon away from the depletion layer (Fry 1975).

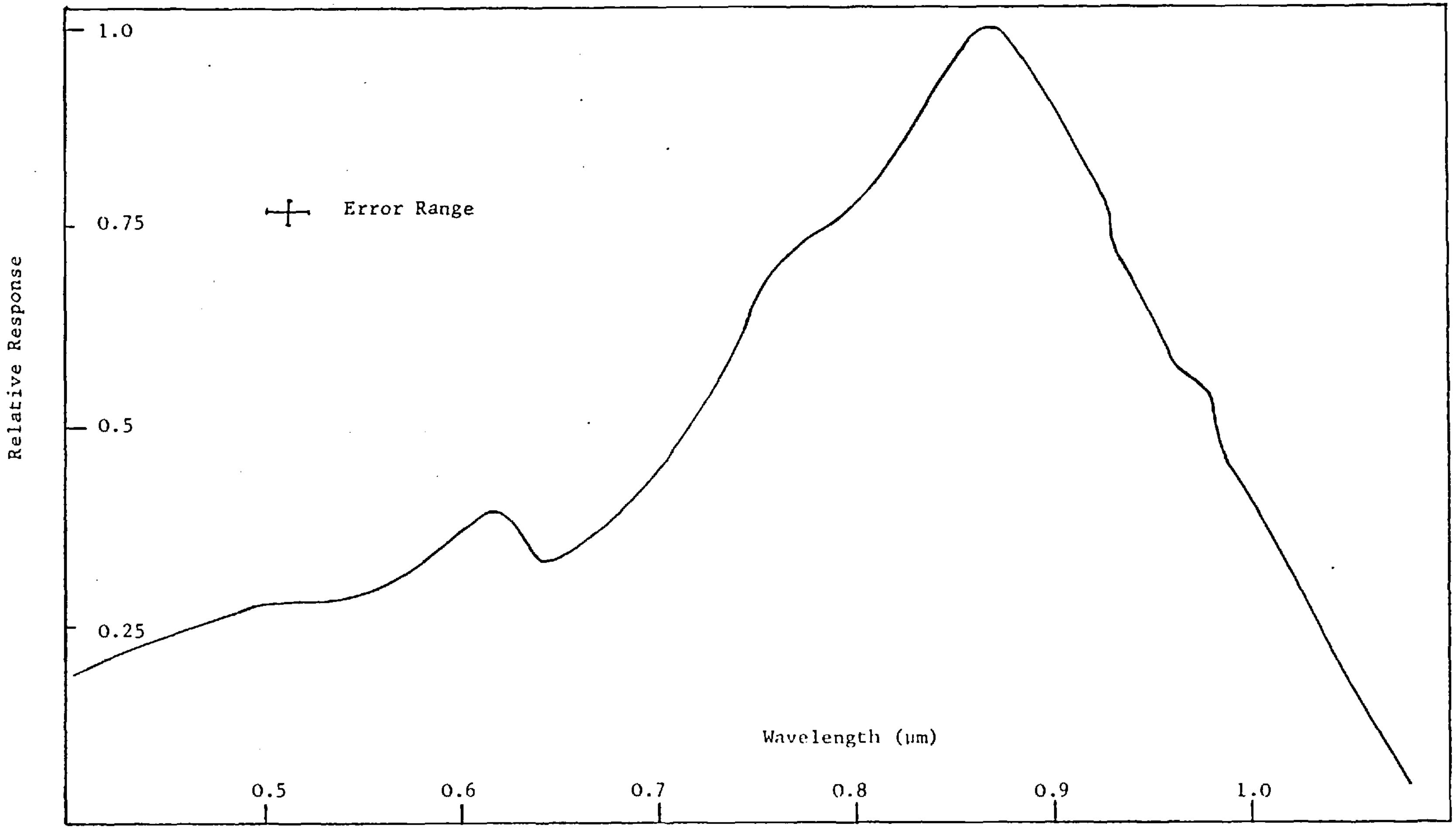

Fig. 2.15: The Spectral Response of the CCD

Fabry-Perot type interference effects in the SiO_2 layer have been the cause of some concern (Geary 1976, Livingston 1976, 1975), since these can cause light and dark bands across the array. Childs (1978) reports that this effect causes dips of about 40 - 50 nm in the measured spectral response of an unspecified CCD. This effect is suggested in one or two regions of Figure 2.15 but is clearly not a problem with this particular device and at this low wavelength resolution.

2.3.5 Blooming

Figure 2.16 shows the effect of progressively saturating the CCD. The image of a square spot has been focussed onto the CCD by a Baum projector in which the light level can be continuously varied. In Figure 2.16(a) the spot is just below the saturation level of the CCD; this is shown as a single bit digitised video picture and also as a single video line profile through the centre of the spot image. As the CCD reaches saturation level, the line profile flattens at the top (Figure 2.16(b)). Soon after saturation occurs, blooming begins in the vertical direction (Figure 2.16(c)). Photosites are not physically separated in the vertical direction, and in the horizontal direction, the blooming spills into the vertical transport register which is normally filled by the same photosite. When the light level of Figure 2.16 (d) has been reached, blooming has spread completely across the array in the vertical direction, and is now spreading in the horizontal direction. The apparent blooming of the border on the left is due to stray light on the CCD.

Blooming causes no permanent damage to the CCD and the excess charge is quickly removed in subsequent readouts.

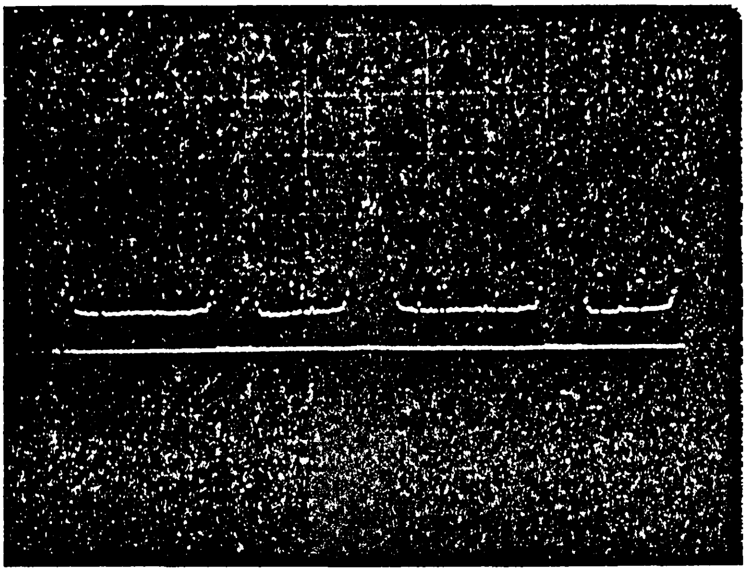

Fig. 2.16: Blooming Test.

(a) Light level below saturation. This is a single line of video through the image.

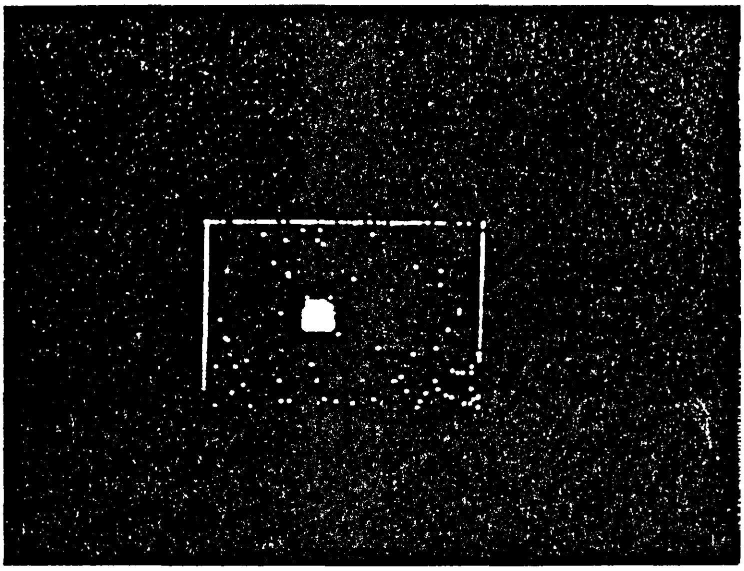

Fig. 2.16(a): The Digitised Video Image

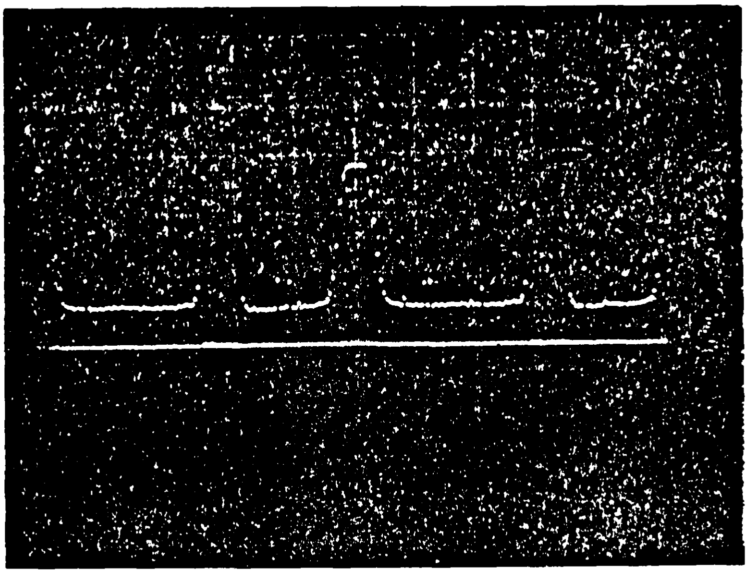

Fig. 2.16(b): Light level increased to just saturation level. The profile of the image is beginning to flatten.

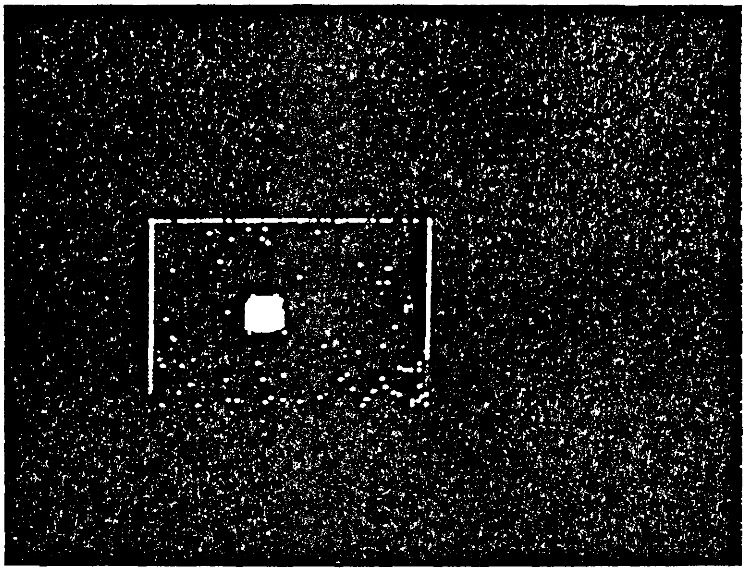

Fig. 2.16(b): The digitized image just below saturation level with no evidence of blooming.

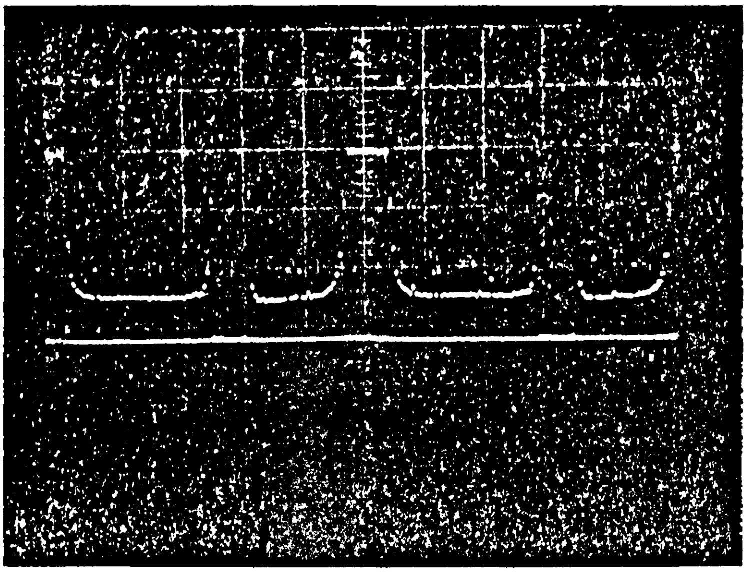

Fig. 2.16(c): The light level is past saturation with the profile well flattened.

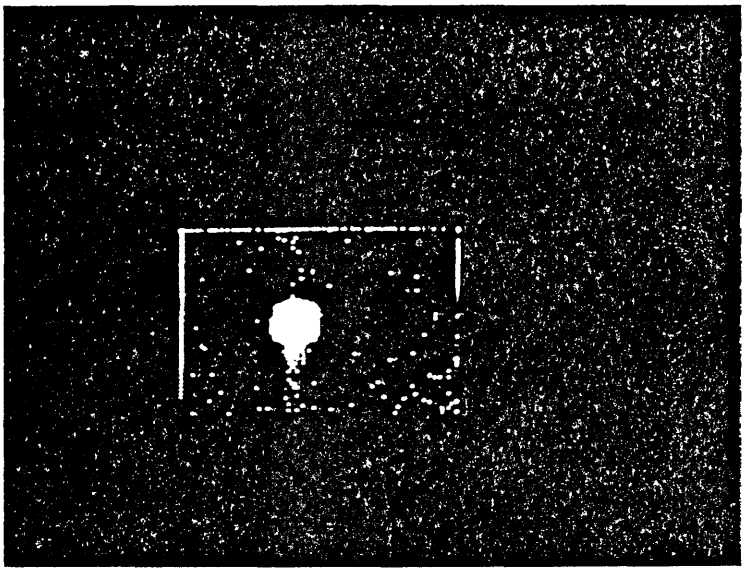

Fig. 2.16(c): Blooming begins in the vertical direction.

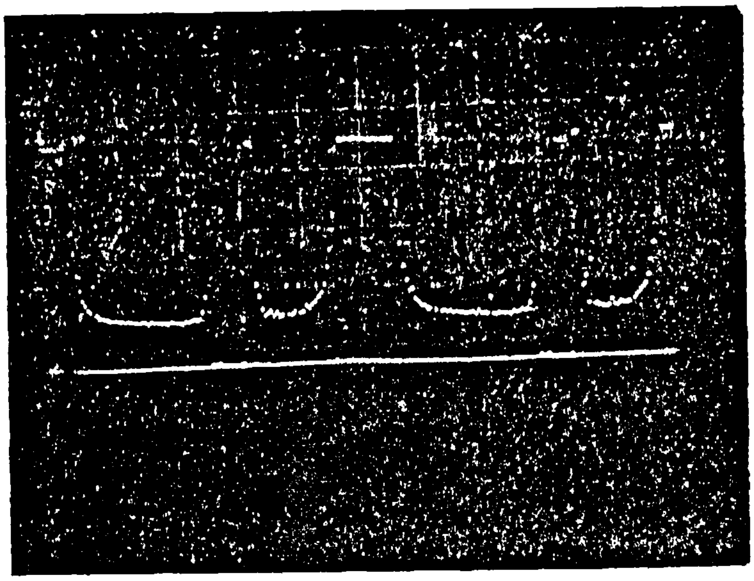

Fig. 2.16(d): Light level increased and blooming begins in the horizontal direction.

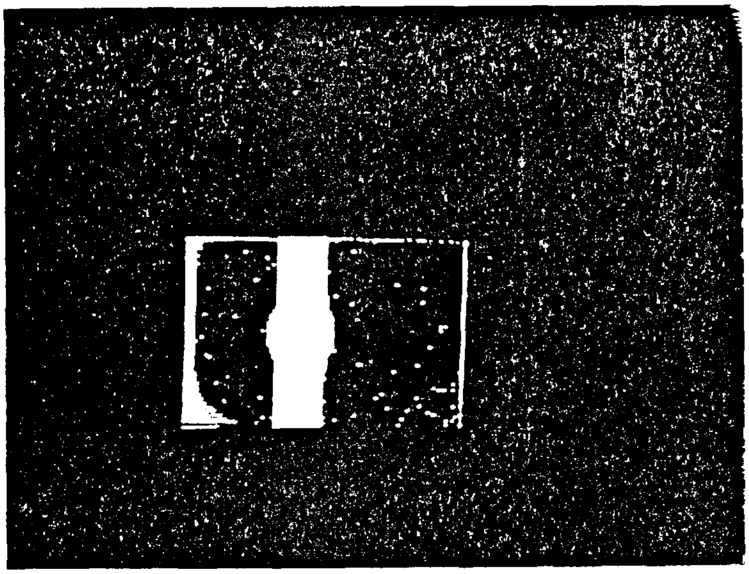

Fig. 2.16(d): The CCD is completely bloomed in the vertical direction and there is also some horizontal spreading. The border on the left is due to light leakage around the image.

2.4 Non-Uniformity Removal

The results of these tests indicated that while there were many deficiencies in the imaging qualities of the CCD, its performance is adequate for the purposes described in this thesis involving single bit quantization. The most serious source of noise is the presence of "hot spots" above the threshold level which appear as spurious "photo-electron events" or "speckles"; accordingly a computer programme (ACNE) was written to remove these events. A dark field of the CCD containing only spurious events is stored on a magnetic disc file in the Interdata mini-computer and is subtracted out of subsequent data fields.

To avoid the operating time overheads involved in software noise removal, a hardwired noise removal circuit is proposed. This is based on a charge coupled analogue shift register (Fairchild CCD 321A (1978)), which is a broadcast quality video delay line of 910 bits. Eleven such devices would be connected in series to form a circulating analogue memory. In this particular type of CCD, the fixed pattern noise is a function of the length of time for which the clock is stopped, as well as temperature. If the signal is kept circulating at approximately 1 MHz, the clock stop period of ϕH (i.e. the time between video lines) would amount to about $2\,ms$ and from the Fairchild data, we note that at $25^{o}C$ this would result in a fixed pattern noise 0.02% of the saturation level. This is very small compared to the fixed pattern noise of the imaging CCD. Thus the memory will be able to remember the fixed pattern noise of the imaging CCD without significantly adding to it.

A schematic diagram of the proposed device is shown in Figure 2.17.

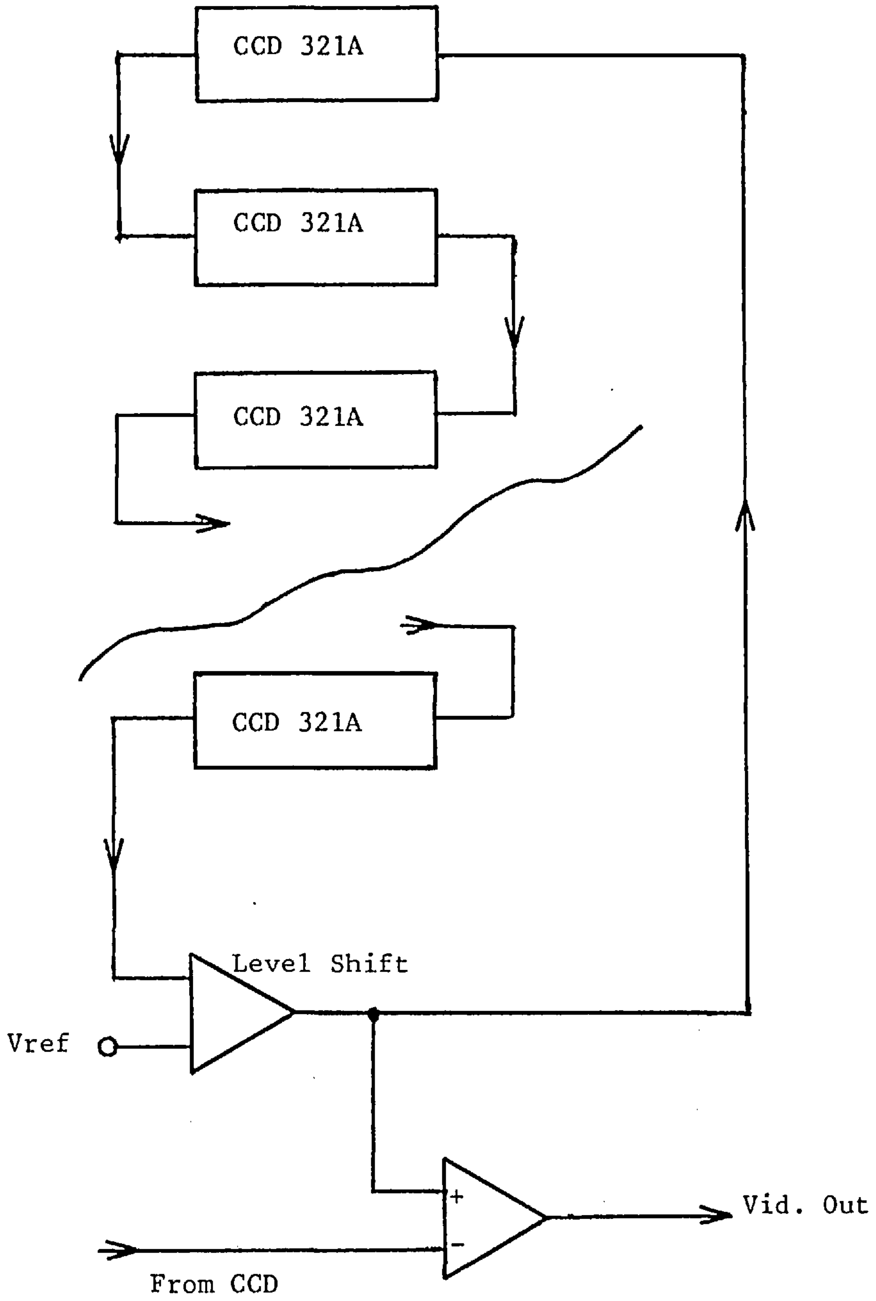

FIG. 2.17: POSSIBLE HOT SPOT REMOVAL

A dark field from the CCD is fed into the memory and subtracted from fields of data emerging from the CCD. Thermal leakage causes an increasing offset for the stored signal of about 4mV/ms at 25°C (Fairchild 1978). In one cycle, the stored dark field would receive an offset of about 120mV. This could be removed by a level shifting circuit before refreshing the circulating memory.

2.5 The Macroscopic DQE of the CCD 202

The term detective quantum efficiency (DQE) was introduced by Rose (1946) for the purpose of comparing detectors such as film, TV cameras and the human eye. This useful parameter has since been applied to many different systems (for a review see Shaw (1975)). As explained in Chapter One, one definition of DQE is

$$\mathrm{DQE} = \frac{(S/N)^2\mathrm{out}}{(S/N)^2\mathrm{in}} \qquad (2.9)$$

Assuming that the detection of photo-electrons is a Poisson process, it can be shown that for a mean arrival rate of $\bar{n}$ photons/sec, there is a root-mean-square fluctuation about the mean of $\bar{n}^{\frac{1}{2}}$ photons, which constitutes photon noise. Thus the input signal-to-noise ratio is

$$\left(\frac{S}{N}\right)\mathrm{in} = \sqrt{\bar{n}} \qquad (2.10)$$

Mandel (1959) has studied interactions in which a single photon or photo-electron primary gives rise to secondaries via a stochastic statistical process, and using the relationships arrived at in his paper, we may write:

$$\overline{m} = \varepsilon(\lambda)\,\overline{n} \tag{2.11}$$

$$\begin{aligned}\overline{\Delta^2 m} &= \varepsilon^2(\lambda)\,\overline{\Delta^2 n} + \overline{n}\,\overline{\Delta^2\varepsilon(\lambda)} \\ &= \overline{n}\,\varepsilon(\lambda)\end{aligned} \tag{2.12}$$

where $\overline{m}$ is the mean output rate, and $\varepsilon(\lambda)$ is the wavelength dependent relative quantum efficiency (RQE).

Generation of thermal carriers in a CCD is also a Poisson process (Barbe 1975), so that the rms thermal noise is $\sqrt{\overline{I}}$, where $\overline{I}$ is the mean rate of thermal carrier generation. The generation of thermal carriers is statistically independent of the signal noise, so that the total rms noise is (from 2.12);

$$N = (\overline{n}\,\varepsilon(\lambda) + \overline{I})^{\frac{1}{2}} \tag{2.13}$$

Equation 2.13 is the root mean square noise associated with a single photosite; in order to calculate the macroscopic DQE, we must take into account the inter-photosite variation $\overline{\Delta^2 D}$. Again assuming statistical independence, equation 2.13 becomes:

$$N = (\overline{n}\,\varepsilon(\lambda) + \overline{I} + \overline{\Delta^2 D})^{\frac{1}{2}} \tag{2.14}$$

Therefore the output signal-to-noise ratio is (from 2.11 and 2.14):

$$\frac{S}{N}_{\text{out}} = \frac{\overline{n}\,\varepsilon(\lambda)}{(\overline{n}\,\varepsilon(\lambda) + \overline{I} + \overline{\Delta^2 D}\,)^{\frac{1}{2}}} \tag{2.15}$$

Using 2.9 and 2.15 we obtain:

$$\varepsilon_D\,(o,\,o) = \frac{\overline{n}^2\,\varepsilon^2(\lambda)}{\overline{n}\,(\overline{n}\,\varepsilon(\lambda) + \overline{I} + \overline{\Delta^2 D}\,)} \tag{2.16}$$

and rearranging:

$$\varepsilon_D\,(o,\,o) = \frac{\varepsilon(\lambda)}{1 + \dfrac{\overline{I} + \overline{\Delta^2 D}}{\overline{n}\,\varepsilon(\lambda)}} \tag{2.17}$$

Thus we see that the DQE is signal dependent and at high light levels, ε_D (o, o) $\simeq \varepsilon(\lambda)$, i.e. the DQE is approximately equal to the RQE.

From Section 2.3.2, we know that the mean noise at 25°C is approximately 7.5 x 10^4 carriers per photosite per frame period. Assuming that the "hot-spots" are removed by signal processing, the inter-diode variation is about 5% of the saturation level (for no signal input) i.e. about 8 x 10^4 carriers per frame period. The statistics describing the inter-diode variation are unknown but we shall assume that the figure describing the inter-diode variation above is a reasonable estimate of the rms fluctuation.

Thus the total mean square noise becomes 15.5 x 10^4 carriers.

At a wavelength of 800nm (the peak response of the CCD) an RQE of 80% is possible (Vogt et al 1978).

Hence, from Equation 2

$$\varepsilon_D\,(o, o) \simeq \frac{0.8}{1 + \frac{2.10^5}{\bar{n}}} \qquad (2.18)$$

The values of ε_D (o, o) for various signal levels are shown in Table 2.1(a). Table 2.1(b) shows the same calculation for an RQE of 40%.

TABLE 2.1: The Variation in the DQE With Signal Level

(a) RQE = 80%

Signal % of Saturation	No. of Carriers	DQE (%)
100	1.6×10^6	71
50	0.8×10^6	64
10	1.6×10^5	36
1	1.6×10^4	6
0.1	1.6×10^3	.6

(b) RQE = 40%

Signal % of Saturation	No. of Carriers	DQE (%)
100	1.6×10^6	32
50	0.8×10^6	27
10	1.6×10^5	11
1	1.6×10^4	1.5
0.1	1.6×10^3	0.1

CHAPTER 3

THE INTERFACE

The minicomputer available for use in these experiments was an Interdata 70, 16 bit-halfword, general purpose machine. Sixty four kilobytes of core space are available and there is also a disc store that acts as virtual memory. In addition, the peripheral devices include two visual display units (VDU), a teletype, paper tape input and output, a line printer and card reader.

FORTH computer language has been adapted for use with the Interdata. FORTH is a high level language that makes extremely efficient use of core and time and is thus well suited for image processing work where a large number of data points in core have to be manipulated in the shortest possible time (Moore 1974).

To ease the problem of interfacing in a multi-user arrangement, a standardized instrumentation system for computer automated measurement and control (CAMAC) was designed and has subsequently become internationally accepted as a standard interface system. CAMAC is based on a modular arrangement of a crate and plug-in modules; connections to external analogue or digital devices are controlled by specified standards (EUR 5100 e and EUR 4100 e). The use of CAMAC in astronomy is discussed by Stephens and Van Breda (1972).

In the particular system used in these experiments, communication with the minicomputer was accomplished via a "systems" CAMAC crate located next to the minicomputer. A roving "remote crate" consisting of a CAMAC crate with appropriate modules and a VDU could be used alongside the experimental apparatus while the minicomputer was located some seven floors away in a controlled environment (see Fig. 3.1). The standardising requirements on CAMAC result in a rather inefficient transfer of data, and this is particularly true for the arrangement under discussion because of an operating

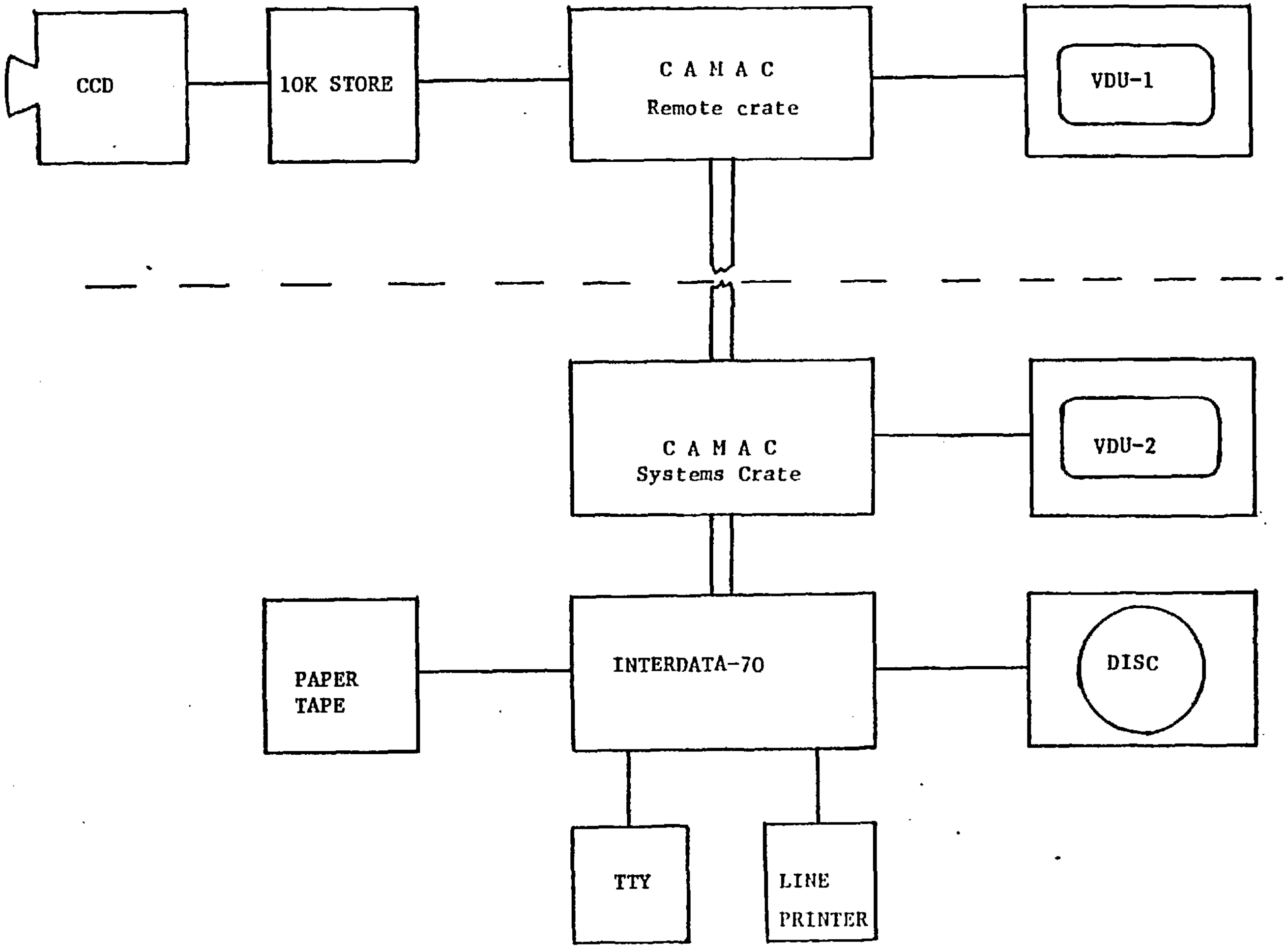

Fig. 3.1: The Computing Configuration

system that was not originally intended for use with CAMAC. Indeed it will be seen later in the chapter that about two seconds are required to read in one thousand 14 bit data points through the CAMAC crate. This data "bottleneck" is a familiar problem in image processing.

A good deal of literature has been generated on this subject, but there does not seem to be a universally accepted solution; each problem must be solved on its own merits (e.g. Toner et al 1978, Brignell and Young 1979, Millett 1976, Hale and Saraga 1974, Farrow 1974). Many data transfer schemes are based on the removal of redundant information since "pictures are not just arbitrary matrices, they do not occur equally often" (Rosenfeld 1969).

A great simplification was possible by digitising with single bit quantisation since the processing schemes discussed later (Chapters 4, 6, 7) allow the recovery of information in this circumstance. The data output from the CCD is 10^4 single bits in one frame period (30 ms), i.e. about 3.3×10^5 bits/sec. The CAMAC crate was found to be capable of passing approximately 7×10^3 bits/sec.

Some workers have used the storage target of the signal generator as a buffer store, and this results in an upper limit of several hundred "events" per frame if the transfer or processing is to take place in a frame period (e.g. Boksenberg and Burgess 1972, Blazit et al 1975 and 1977). With the extremely slow transfer rate of CAMAC, this strategy would result in an upper limit of about 15 events per picture; the number of fixed pattern noise events is considerably higher than this (Chapter 2, section 2.3.1).

The best approach appeared to be in using an intermediate buffer store, into which a frame of data could be deposited by the CCD and then read out into the computer via CAMAC in its own time. There would be an upper limit of 10^4 on the number of events per frame, but the CCD camera, while operating "on-line", would no longer be working in "real-time" as the frames of data generated during the computer read-out would be lost.

3.1 The Camac module and buffer scheme

The CAMAC module used was a Nuclear Enterprises type 9017 driver. The module contains a 24 bit parallel access register which functions as a one word store. An interrupt signal level at the front panel input establishes a look-at-me (LAM) status within the module which is continually tested in the programme. Receipt of the INTERRUPT signal causes the data (loaded in at the front panel multi-way socket) to be loaded into the register and gated onto the dataway; the LAM bistable is then cleared. This particular module has been modified so that the action of clearing the LAM bistable causes an output pulse to be sent to the external unit via a front panel socket marked CLEAR. Another mode of operation of this module, not used in this experiment, causes data to be loaded from the dataway to the external unit via the module register. The CAMAC system operates with inverse logic; a five volt level (HIGH) represents a logical zero while zero volts (LOW) represents a logical one.

A block diagram of the overall buffer interface is shown in fig. 3.2. D_1 is a "D" type bistable ($\frac{1}{2}$ x SN7474). For every 100 data bits in a line, there are 105 cycles of ϕ H, and for every 100 lines there are 102 blocks of ϕ H (Chapter 2). Thus the address of every data "event" is given by :

$$A = 105y + x \qquad (3.1)$$

where $0 < x \leqslant 105$

and $0 < A \leqslant 10{,}710.$

It was decided that in order to simplify construction, the extra cycles of ϕ H would be treated as though they were associated with true data events. This, and the interlacing of the picture, would be rearranged using software since the time required to perform this algorithm would be much shorter than the time required for data transfer.

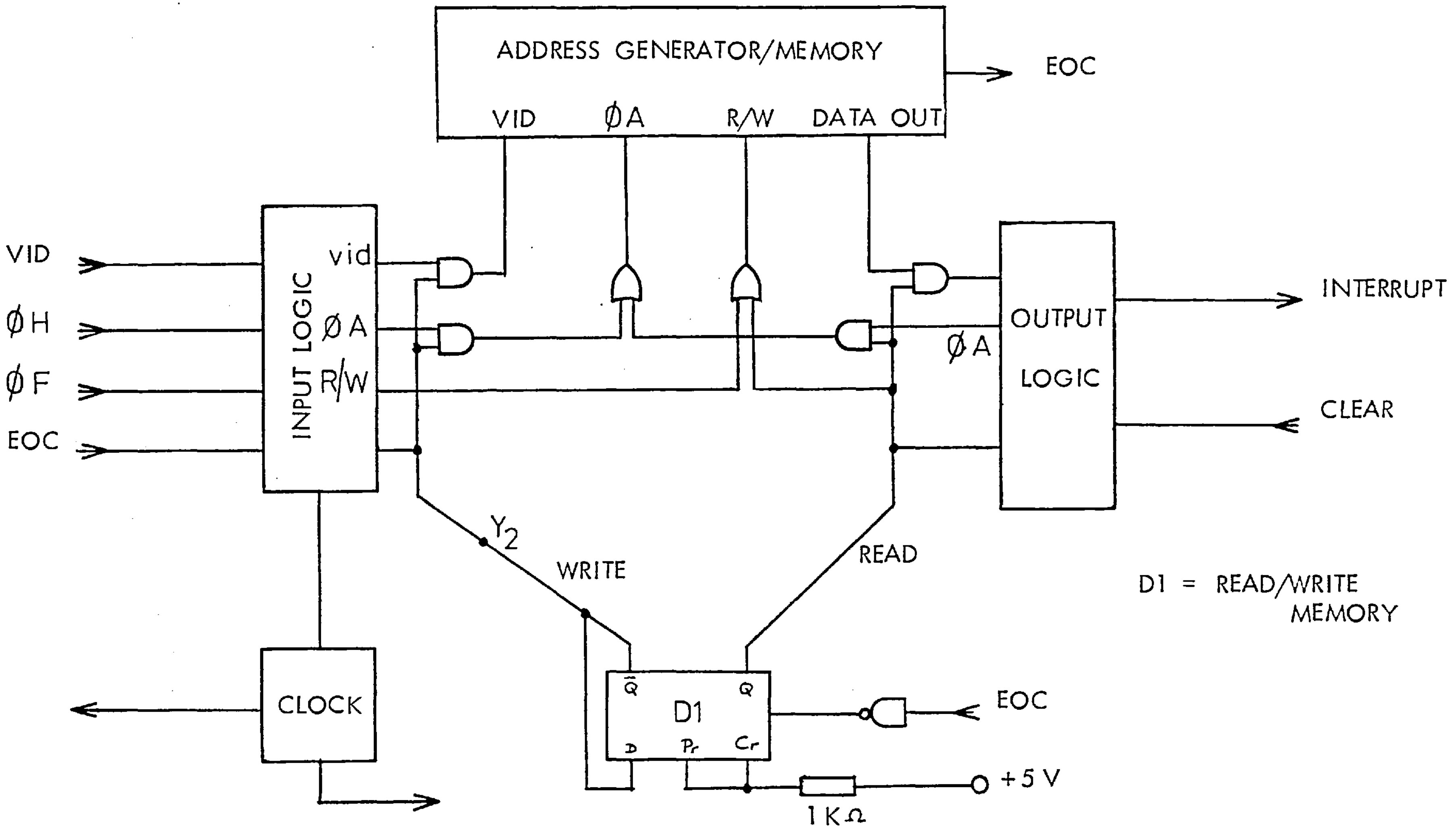

FIG. 3.2 BLOCK DIAGRAM OF THE BUFFER INTERFACE

a) Write-to-memory cycle

For this cycle, the read/write memory places the input logic in control of the buffer store. The input logic waits for the start of a frame of video, flagged by ϕ F, opens the input gates to allow the digitised data into the memory, and generates the necessary waveforms for enabling the write mode of memory operation. Each memory location is addressed by the address generator which keeps account of the current address. When the ultimate address of a frame of video is detected, an end-of-count (EOC) signal flips the read/write memory to start the read-from-memory cycle.

b) Read-from-memory cycle

The input gates to the buffer memory are now closed and the output logic takes over control. The output logic addresses each location of the memory in turn, and if the content is a "one", an INTERRUPT signal is communicated to the CAMAC module. Further examination of the memory is suspended while the CAMAC module reads the 14 bit address of this event and then sends a CLEAR signal to the output logic which restarts the search. This "handshake" process continues until the ultimate address of a frame of data is detected and the EOC signal switches the read/write memory back to the write-to-memory cycle.

3.2 Circuit Details

3.2.1 The Clock

Precise knowledge of the clock period is unnecessary in the buffer interface because all operations are timed relative to the clock, thus allowing a simplified design. Two monostables (SN74121; Texas 1971a) were employed in a simple feedback configuration (Fig. 3.3) to give an easily controlled mark-to-space ratio and a TTL output. The particular values shown generate a 50% duty cycle of period 1.2 μs.

Output to the (remote) CCD is done via a simple emitter follower buffer fed

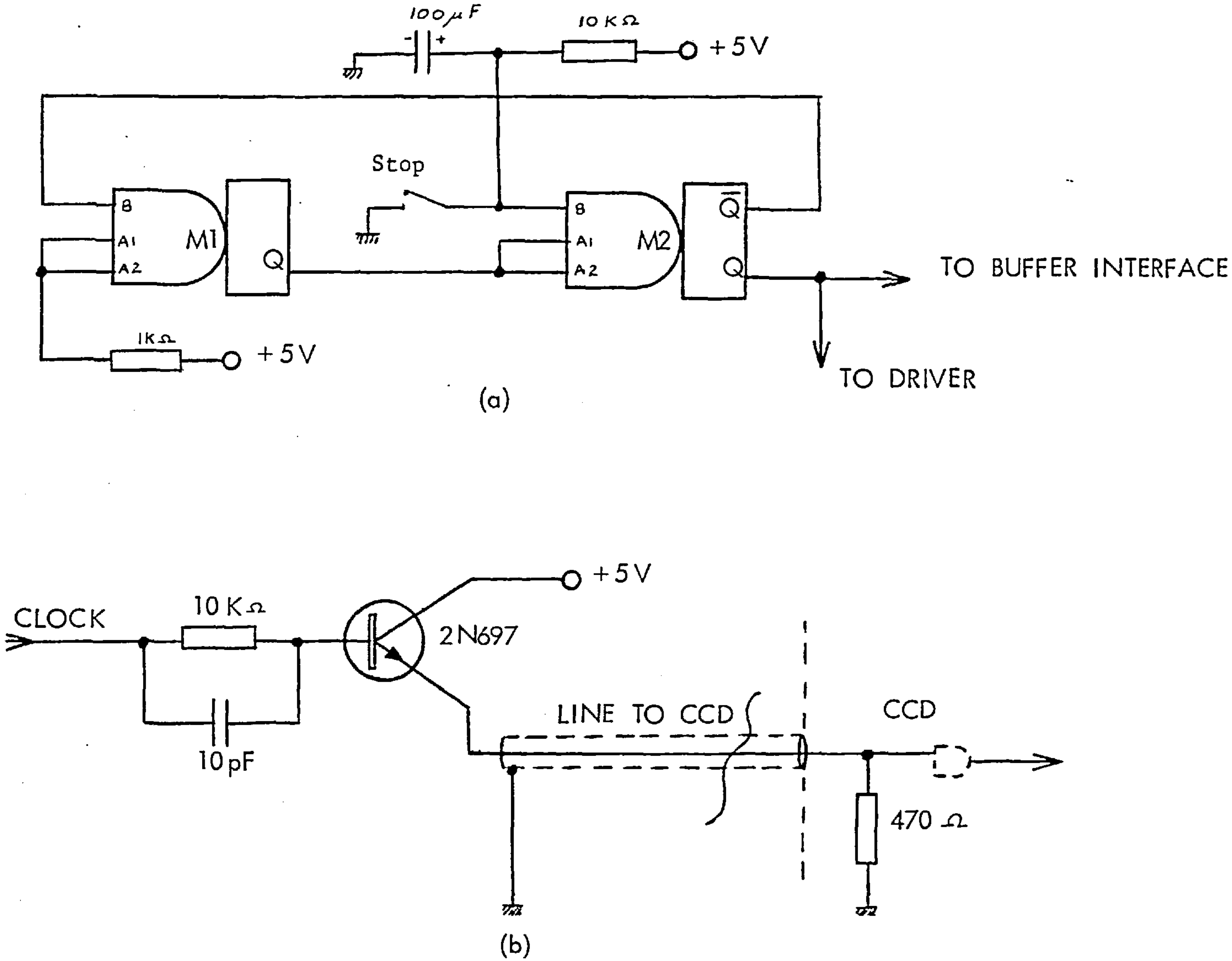

FIG. 3.3 : (a) CLOCK (b) LINE DRIVER TO CCD

into a co-axial cable. When switched on, the clock begins to function after about a second while C_1 charges via R_1, giving the rest of the logic time to settle. The STOP switch enables the operator to stop operation if, for example, the data transfer becomes stuck in an infinite loop.

3.2.2 The Discriminator

The timing requirements of the memory devices used demanded overlaps of the order of 100 ns. Early attempts at digitising, using an LM 311 operational amplifier, were only partially successful because this device had an input overdrive response time between 200 ns and 400 ns, resulting in a digitised pulse whose position in time varied with discriminator level (Fig. 3.4). Thus, some data pulses failed to register in the memory.

Eventually an SN 72710 comparator (Texas 1971b) with a rise time of 40 ns and a TTL compatible output was chosen and used in the configuration of Fig. 3.4. Any D.C. component of the video signal is blocked by the 1 μF capacitor and the small signal silicon diode D ensures that the negative going half of the video signal is clamped to - 0.7 volts.

3.2.3 Address Generator/Memory

Addresses corresponding to each data pulse are generated using four SN74161 asynchronous up-down counters (Fig. 3.5). Fourteen bits are required to specify the position of a data point within the 102 x 105 matrix. The SN7430 NAND gate (Texas 1971 a) "recognises" the ultimate address of a frame of data and its output level is the end-of-count (EOC) signal, which also clears and resets the counters. The fourteen logic inverters are necessary to change the address into reverse logic for CAMAC and also to protect the logic from the large amount of clocking noise present in the CAMAC system.

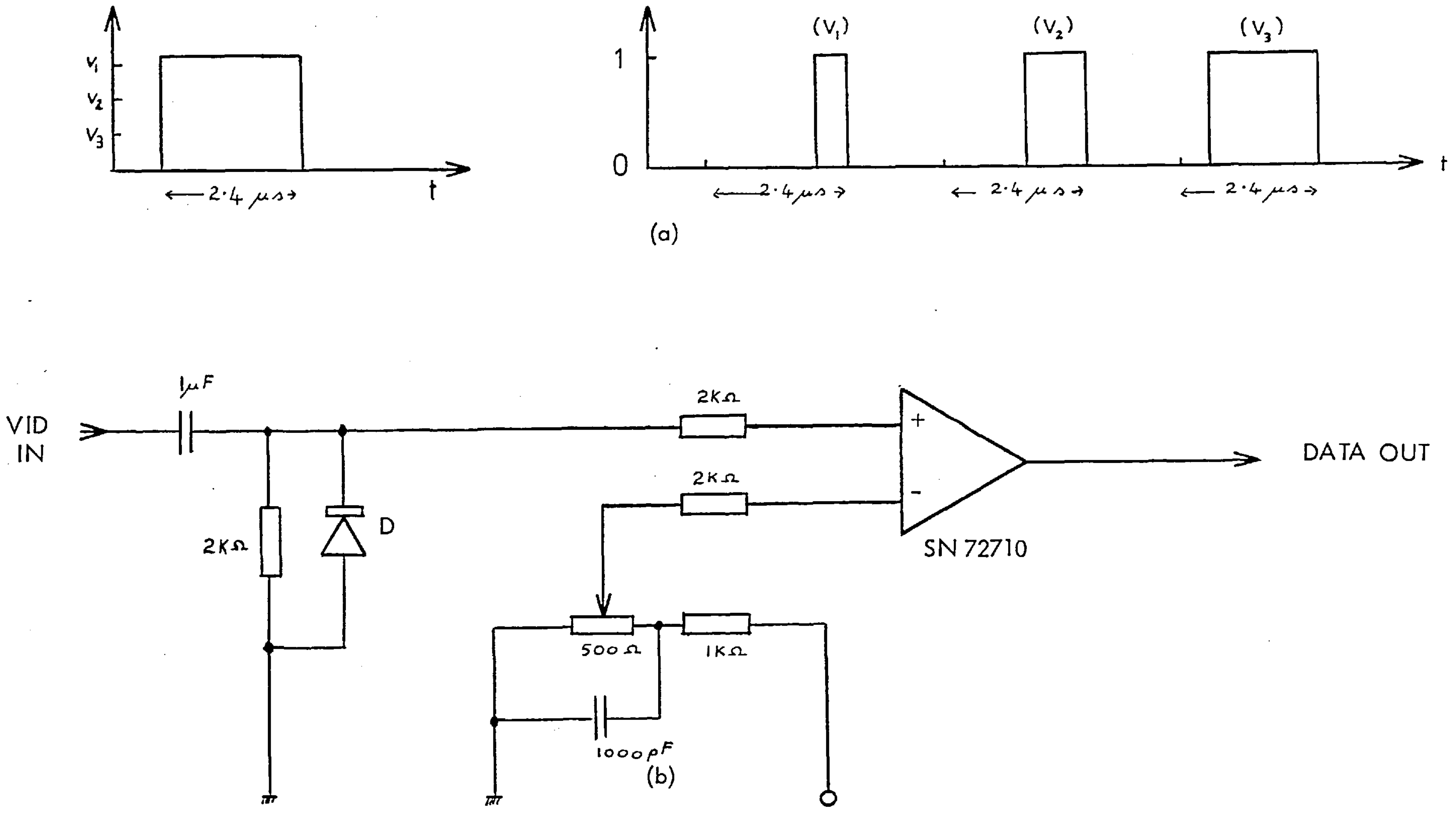

FIG. 3.4 (a) VARIATION OF PULSE WIDTH WITH DISCRIMINATOR LEVEL
(b) DISCRIMINATOR

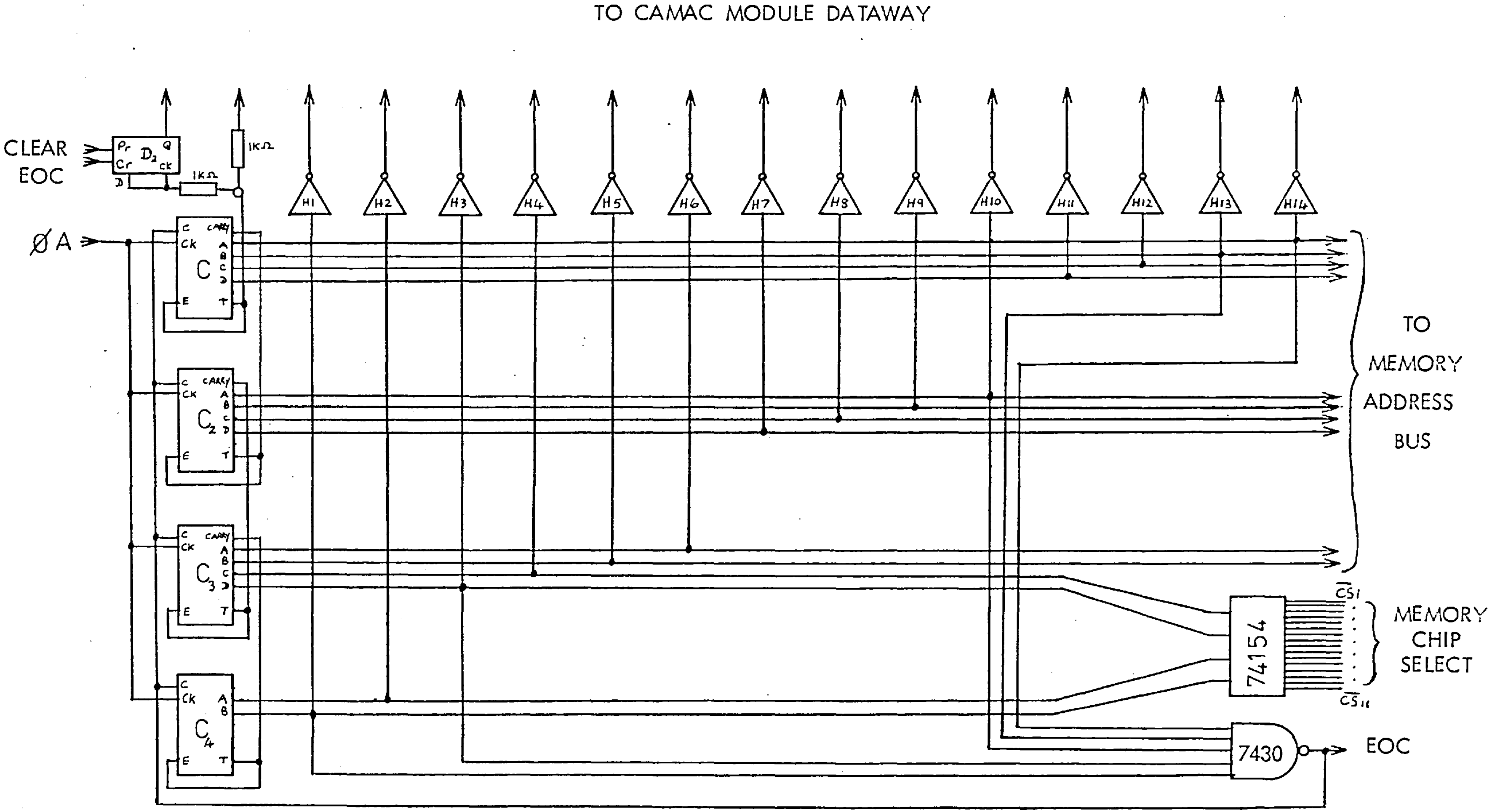

FIG. 3.5 THE ADDRESS GENERATOR

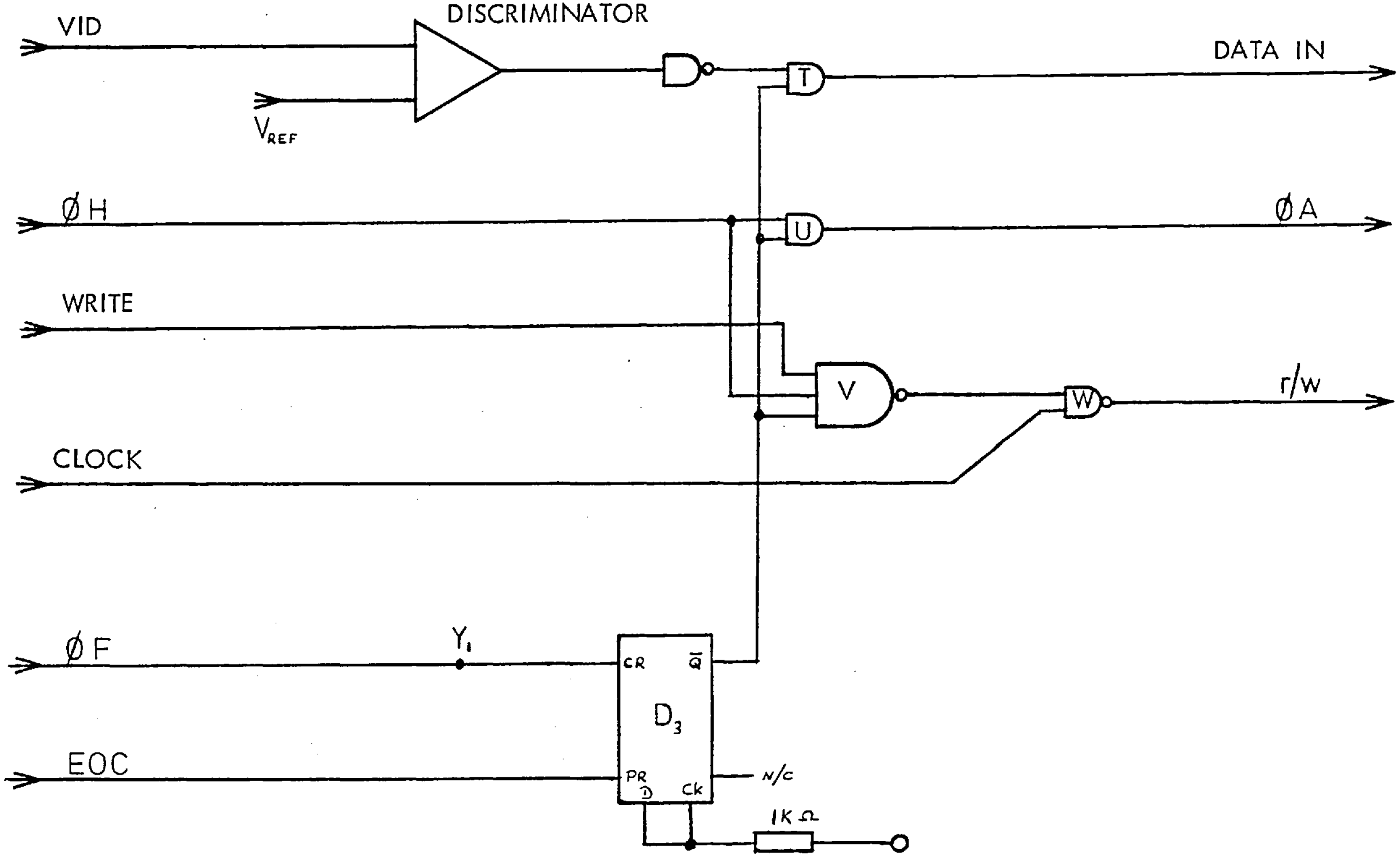

FIG. 3.7 THE INPUT LOGIC

The fastest memory devices available at the time were TMS4033 NL, 1024 by 1 bit static random access memories (RAMS) with a minimum access time of 450 ns (Texas 1974); this determined the maximum clock rate (Chapter 2). The circuit configuration is shown in Fig. 3.6.

Ten bits are required to specify a location within each device which is enabled by the chip select ($\overline{cs}$) input. The ten least significant bits of the event address are used to internally address each device while the remaining four bits are decoded into 16 lines by SN74154 (Texas 1971 a) that selects each device in turn.

3.2.4 Input logic

During the phase of operation, when data is to be written into the buffer memory, it is important that clocking of the address generator begins only at the start of a new frame of video or synchronisation is lost. An EOC signal from the previous read-to-CAMAC cycle will have set flip-flop D_3 (Fig. 3.7) into a state where $\overline{Q}$ is LOW, thus closing gates T, U, V and preventing clocking of the address generator at some arbitrary point during a video frame. As explained in Chapter 2, a start-of-frame signal is synthesised from ϕ P and ϕ V_2 and when communicated to S it causes $\overline{Q}$ to go HIGH; writing of data into the memory then commences.

A waveform known as R/W is necessary to ensure faithful recording of data in the memory (Texas 1974). During the output to CAMAC cycle this remains LOW, but for the write-into-memory cycle a 25% duty cycle signal is required and generated by gates V, W.

3.2.5 Output Logic

The output cycle is initialized when the EOC signal changes the read/write memory to the output cycle, and the address generator is clocked by the main clock, via a divide-by-two counter (Fig. 3.8). Each address accesses locations in the memory

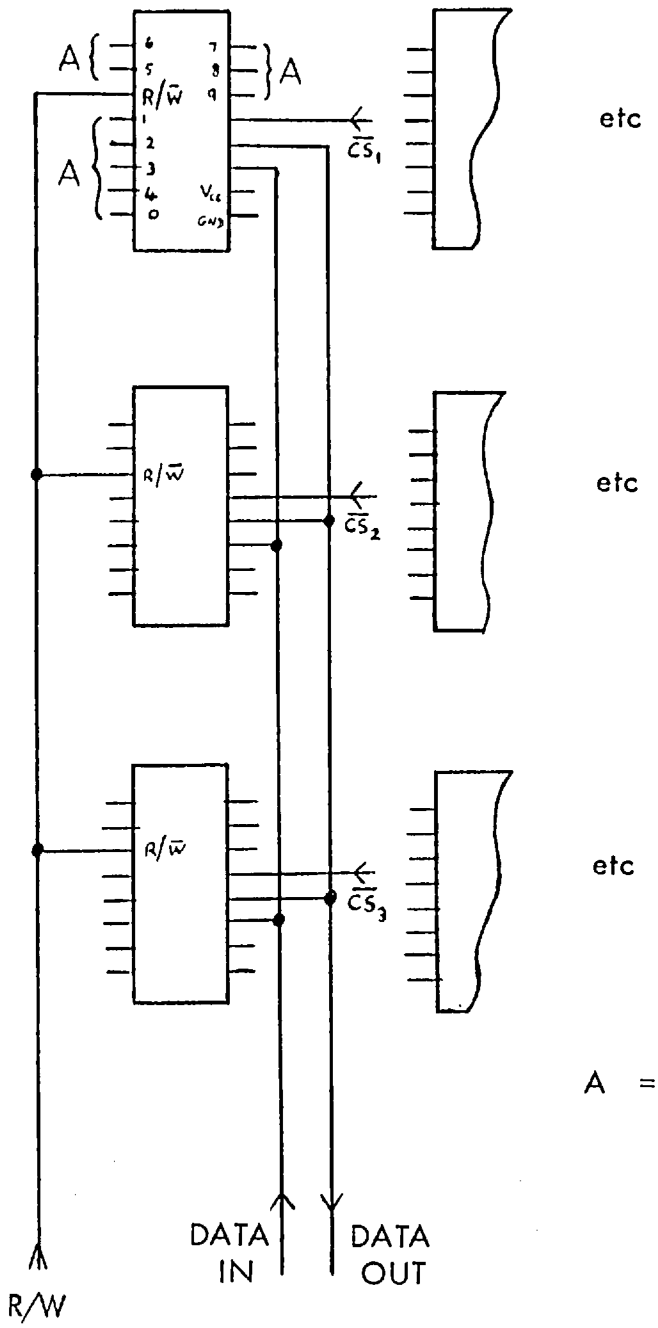

A = ADDRESS BUS TO MEMORY DEVICE

FIG. 3.6 THE MEMORY DEVICE CIRCUIT

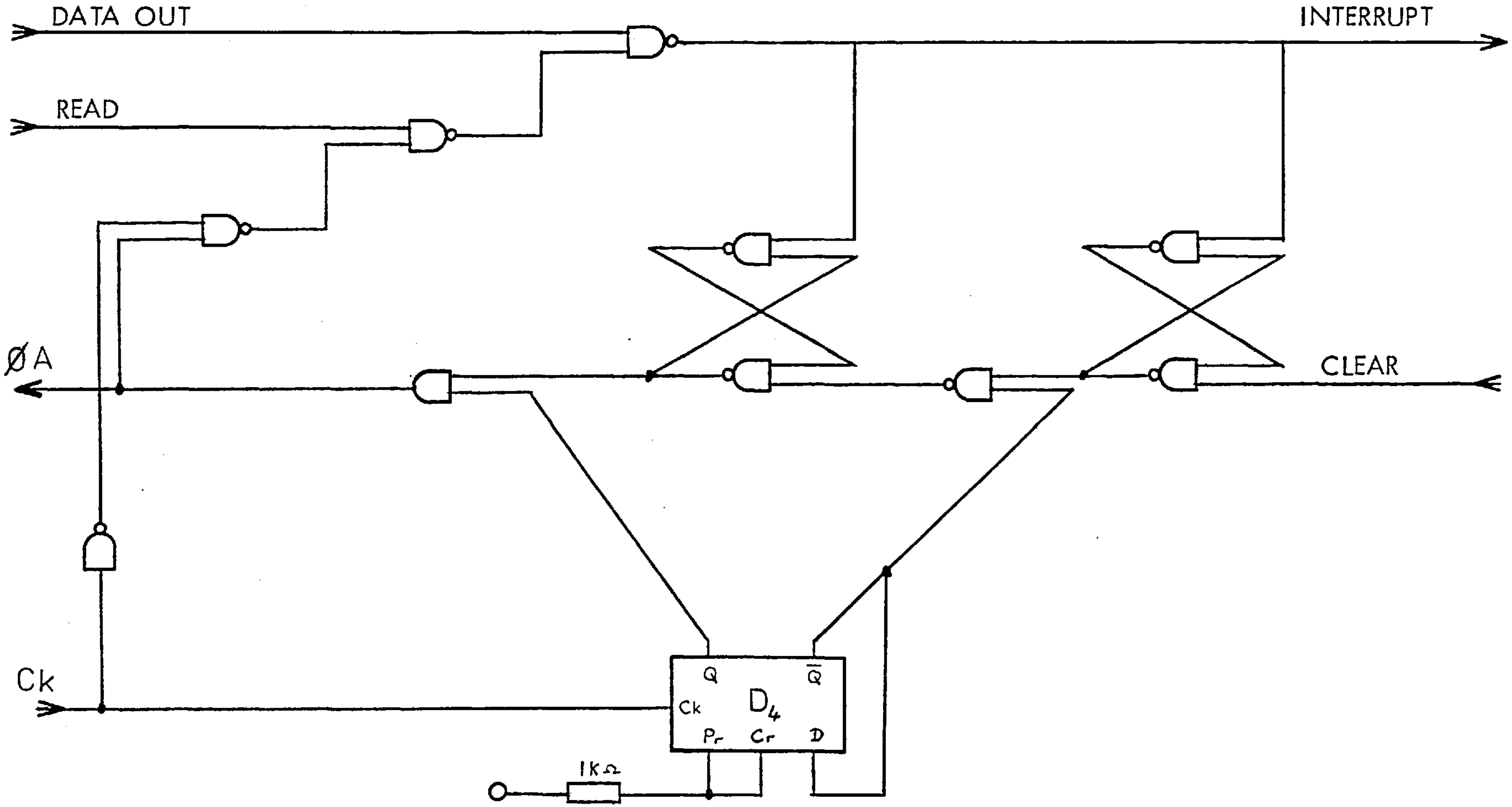

FIG. 3.8 THE OUTPUT LOGIC

until a ONE is found, and this sends a LOW interrupt signal to the CAMAC module while shutting off the clock from the address generator. The clock signal was NANDed to the output from the memory at G so that stopping the clock creates a "cut-throat" action ensuring that the interrupt signal is a pulse rather than a change of level.

The CAMAC module reads the address present on the address bus and returns the CLEAR signal to the output logic.

The complicated locking arrangement formed by flip-flops 1 and 2 are necessary because :

a) the width of the CLEAR signal can be longer than the clock period so that two or more addresses could be accessed before the CLEAR signal has ceased and their contents lost;

b) the clock train to the address generator must be started at the beginning of a clock cycle, otherwise the first pulse of the train would be long enough to clock the address generator but too short to activate the memory location.

It was found useful to use the EOC signal to set a bistable (D2 in Fig. 3.5) whose output is connected to the 16th line of the address bus. A LOW level on this line causes the address to be interpreted by the computer as negative, signifying the end of a frame of data. The CLEAR signal from reading this address resets the bistable.

3.3 Software

An information flow diagram of the programmes associated with the interface is shown in Fig. 3.9.

Two programmes exist for performing the CAMAC operations necessary to bring the data from the buffer memory onto the stack. The first, CLEAR-CCD, reads through a single frame of data in the buffer store, does not record the event addresses, but

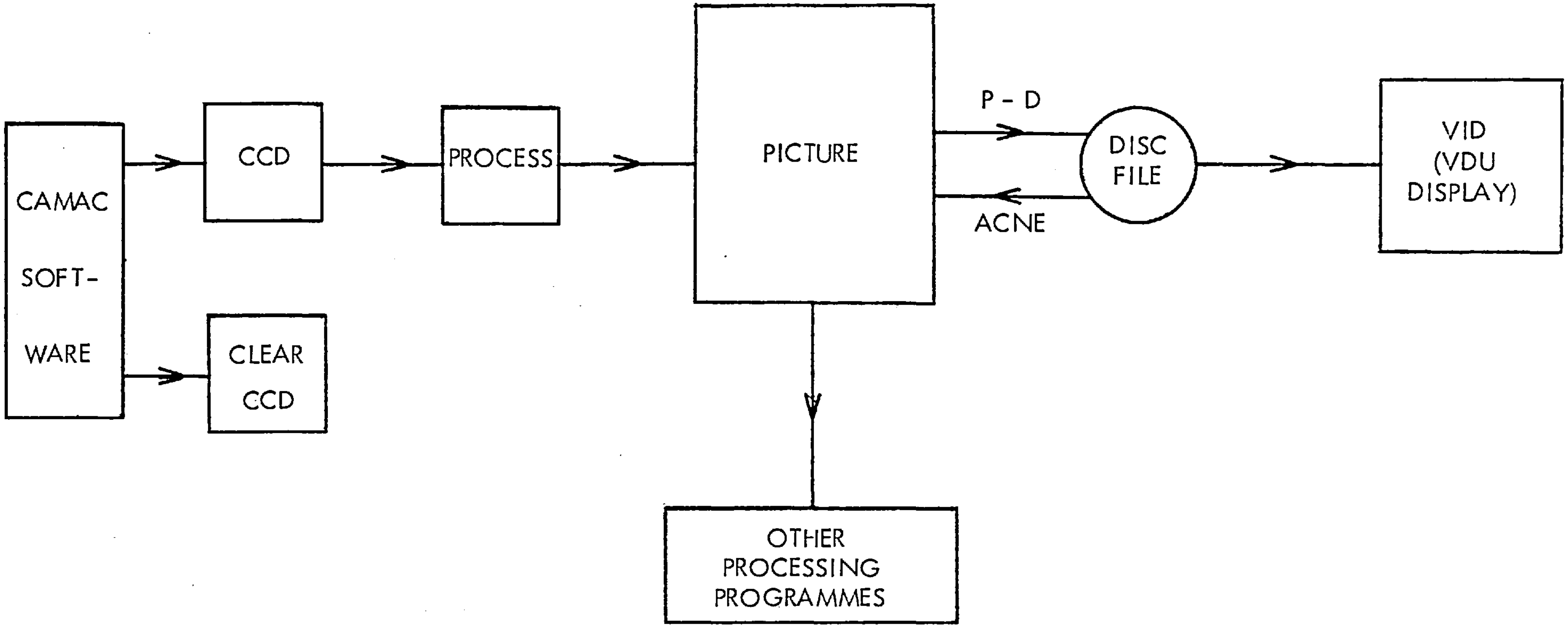

FIG. 3.9 INFORMATION FLOW THROUGH PROGRAMMES

displays the total number of events stored; this is useful for clearing the buffer memory for new data. The second, CCD, places the addresses into the holding array PICTURE after processing by the programme PROCESS (described later).

The array PICTURE is where further processing programmes (Chapters 4 - 7) obtain the raw data. For permanent storage the data can be transferred by programme P- E to a magnetic disc file. This is useful for storing a mapping of the "white spots" present in a dark field and these can be subtracted out of subsequent data fields in PICTURE using the programme ACNE. A further possibility is the display of data present on disc onto the VDU screen by VID which displays a 100 (x) x 100 (y) picture in two parts of 50 (x) x 100 (y) each, because the screen is limited to 64 characters width.

PROCESS

There are two parts to this programme :

i) Trimming of invalid data points

Each train of 100 video pulses per line is associated with 105 clocking pulses. Similarly the 100 lines are associated with 102 blocks of 105 pulses. The first line of each field of data contain no valid data, and when interlaced, these constitute the last two lines of the picture. The relationship between the true and recorded addresses of photosites along each line is based on the assumption that no data will be found associated with the five invalid addresses on a line. This is true if the CCD picture has not bloomed. Thus the relationship is

$$\begin{array}{r} \mathrm{R\,A} \\ 2 \\ 107 \\ 212 \\ 317 \\ 422 \\ 527 \end{array} \left(\begin{array}{r} \mathrm{T\,A} \\ 0 \\ 100 \\ 200 \\ 300 \\ 400 \\ 500 \end{array} \right) \begin{array}{c} \\ \ldots\ldots\ldots\ldots \\ \ldots\ldots\ldots\ldots \\ \ldots\ldots\ldots\ldots \\ \ldots\ldots\ldots\ldots \\ \ldots\ldots\ldots\ldots \\ \ldots\ldots\ldots\ldots \end{array} \begin{array}{r} \mathrm{R\,A} \\ 101 \\ 206 \\ 311 \\ 416 \\ 521 \\ 626 \end{array} \qquad \left(\begin{array}{r} \mathrm{T\,A} \\ 99 \\ 199 \\ 299 \\ 399 \\ 499 \\ 599 \end{array} \right)$$

etc.

where RA = recorded address, and TA = true address.

This leads to the simple algorithm for correction :

$$TA = RA - (5n_r + 2) \qquad (3.2)$$

where n_r is the recorded line number.

ii) Interlacing

The relationship between the true line number and recorded line number is :

n_r	n_t	
0	1	
1	3	
2	5	
⋮	⋮	1st data field
49	99	
50	101	
51	2	
52	4	
53	6	2nd data field
⋮	⋮	
98	96	
99	98	
100	100	
101	102	

where n_r = recorded line number and n_t = true line number.

The algorithm for re-interlacing the video picture is :

$$n_t = \begin{cases} 2n_r + 1 & \text{for } n_r < 51 \\ 2n_r - 100 & \text{for } n_r \geqslant 51 \end{cases} \qquad (3.3)$$

Both algorithms (eqns. 3.2 and 3.3) are combined to form the single programme PROCESS. A listing of all the programmes in this section can be found in Appendix B.

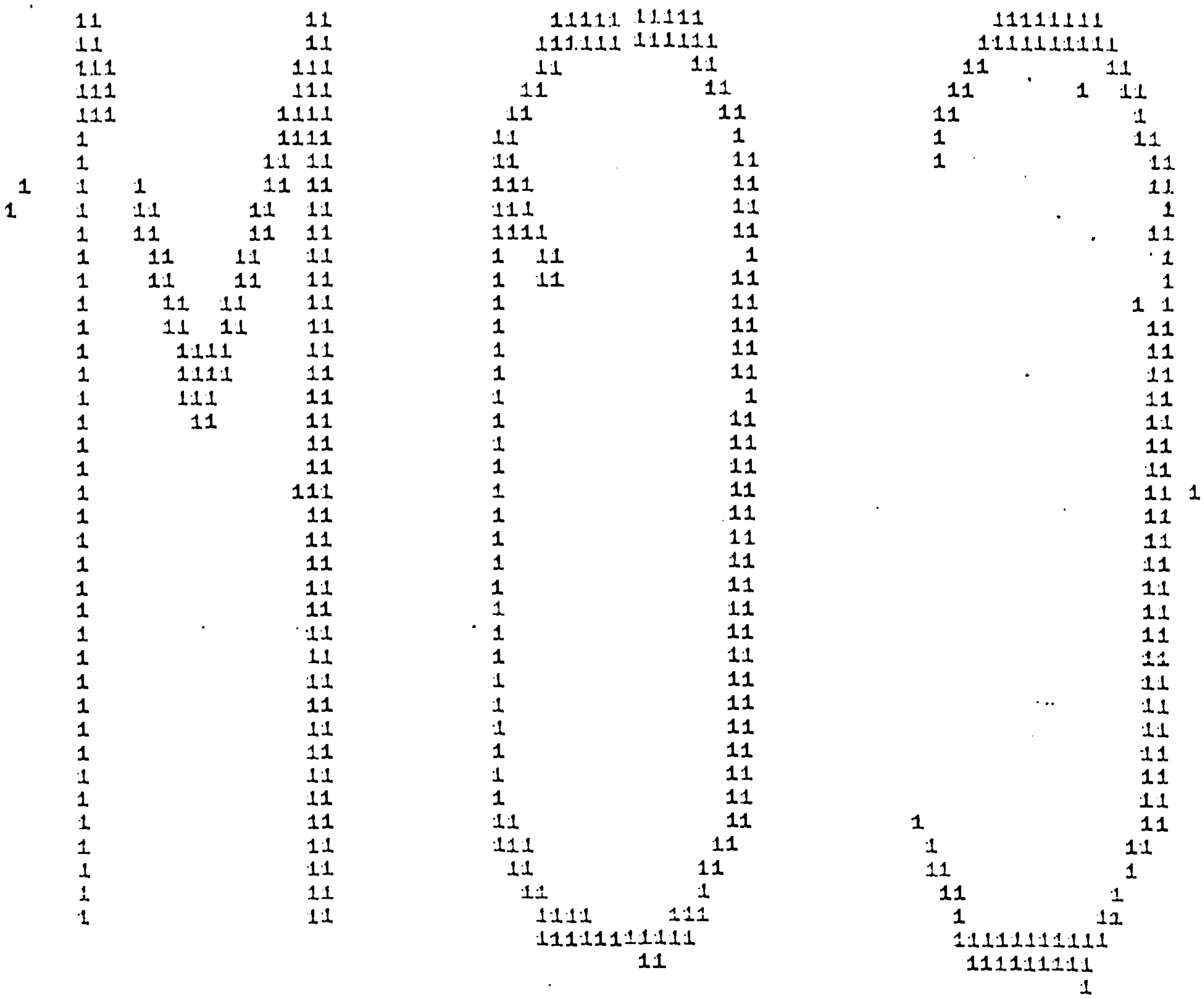

Fig. 3.10 (a): Computer Printout of Image (Reversed)

(b): Digitised Video Image

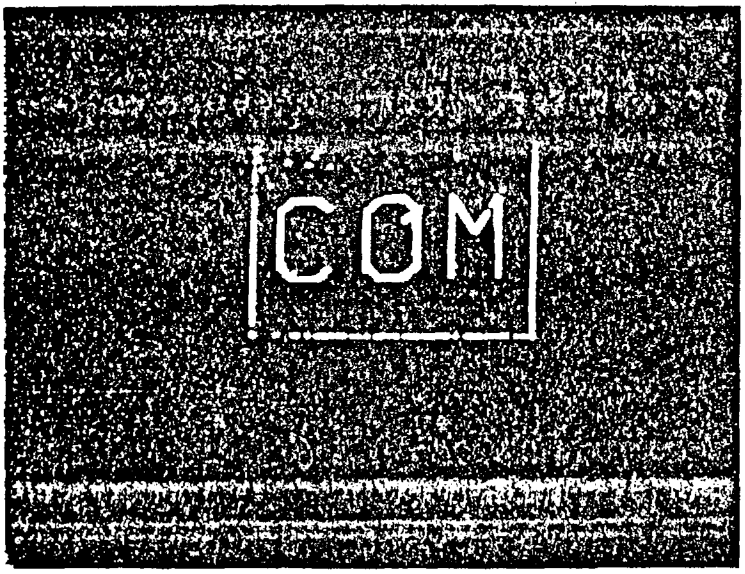

3.4 System Performance

Figure 3.10 (a) shows a simple single bit digitised image before being stored in the buffer. Figure 3.10 (b) is the stored computer image print out (reversed due to the printer format). From the uniformity tests of Chapter 2 it was found that when the discriminator level was well below the signal level, there was an average variation of 2 events per frame, and this is attributed to "dropped bits" in the logic. It was also found to be possible to keep a mapping of the "white spots" on disc for several weeks and successfully remove them from subsequent frames of data.

The time taken for the transfer of about 10^3 addresses to the array PICTURE, about 2 s, was disappointing, but could be improved by altering the operating system of the minicomputer. Although this was a considerable disadvantage for photon counting, the time taken for the autocorrelation of this number of data points in speckle interferometry, about 45 seconds, is very much greater than the data transfer time.

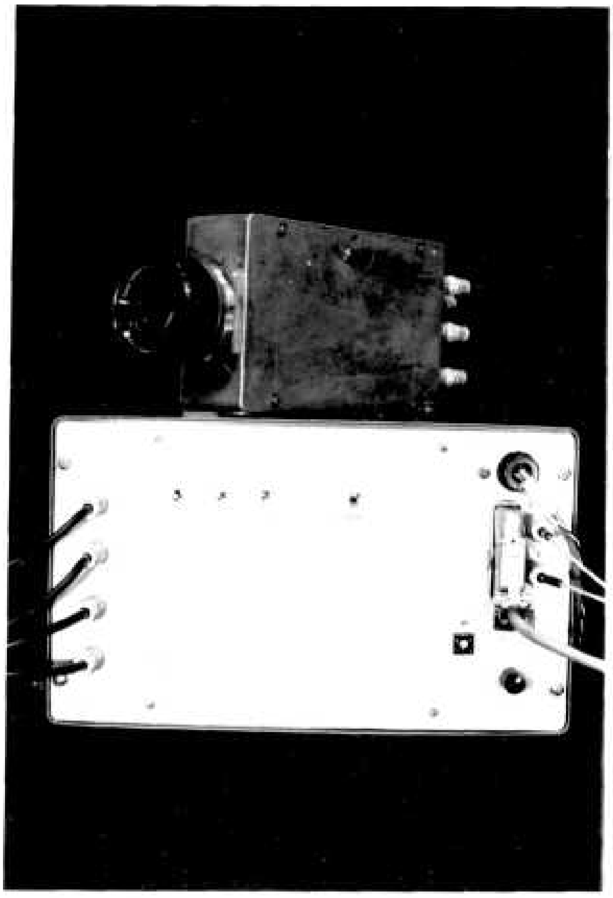

Fig. 3.11: Photograph of the CCD and Interface

CHAPTER 4

A REVIEW OF THE THEORY OF SPECKLE INTERFEROMETRY

It was explained in Chapter 1 that the introduction of atmospheric turbulence into the optical path between the object and observer causes the formation of speckle patterns in the image plane, and that it was deduced by Labeyrie (1970) that diffraction limited information could be obtained by studying the second order statistics of the speckle image.

4.1 Conditions necessary for recording good speckle images

The turbulence of the atmosphere has been extensively studied in recent years (for a review see Labeyrie, 1976), and it is apparent that a variety of mechanisms occur in the atmosphere to account for the disturbances in the optical path. This makes theoretical modelling very difficult. If it is assumed that the number of scattering cells is very large, then the properties of a speckle pattern are readily deduced in a statistical approach (reviewed by Goodman 1975). Dainty (1976) has pointed out that the atmosphere has a relatively small number of scattering cells within the telescope aperture and this causes the speckle image to be concentrated in a region near to the optical axis. The following conditions are necessary for recording speckle images :

1. The average number of speckles in the telescope aperture must be reasonably large so that the speckle image (and hence the spectrum of intensity fluctuations) is relatively unaffected by telescope aberrations and defocussing (Dainty, 1974).

2. The temporal frequency spectrum of atmospheric turbulence is largely governed by wind speeds and altitude levels. Roddier and Roddier (1975), in their study of turbulence degradation and exposure time, concluded that the power spectrum in the speckle technique is negligibly affected by exposure times of up to 20 m. sec. More recently, however, a series of experiments by Scaddan and Walker (1978) has suggested that an exposure time of 8 ms. is more appropriate. In practice, the exposure

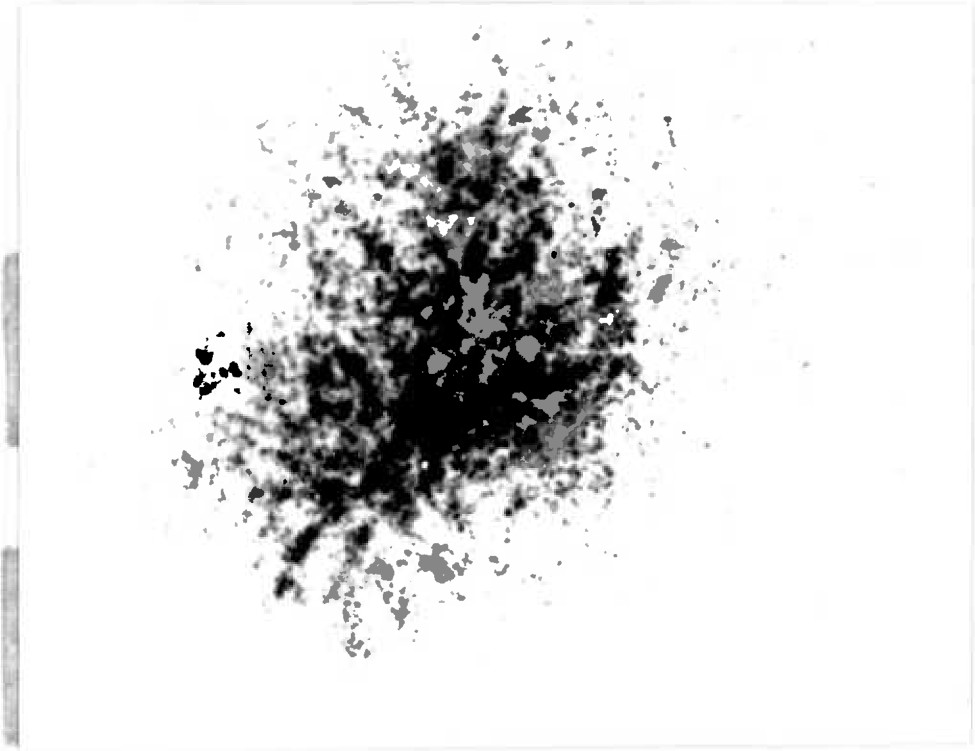

Fig. 4.1: A typical single frame speckle image taken at the Isaac Newton Telescope with a 10ms exposure time and a filter bandwidth of 30nm (centred on 520nm).

is never longer than 10 m.sec.

3. The scale of a speckle pattern is wavelength dependent. In a fairly wide-band optical system, the resulting speckle pattern can be regarded as the superposition of many speckle patterns from small frequency intervals and therefore the overall intensity distribution is smoothed, losing the high spatial frequency data. The bandwidth ($\delta\lambda$) of the filter necessary to avoid this has been discussed by Dainty (1973) and Korff (1973) and is given by :

$$\frac{\bar{\lambda}}{\delta\lambda} \gtrsim \frac{D}{d_0} \qquad (4.1)$$

where $\bar{\lambda}$ is the mean wavelength, D the seeing diameter and d_o is the diameter of the Airy disc.

4. The dispersion introduced by the atmosphere for stars not at the zenith must be corrected (Dainty, 1975).

Figure 4.1 shows a typical speckle image of the binary star system η Oph (ADS 10374) taken using the 98 inch Isaac Newton telescope.

4.2 The Interferometer

The Imperial College Speckle Interferometer was built in 1975 to begin a programme of binary star measurements (Beddoes et al, 1976). Its function is to record a large number of short exposure images of a star on cine film at the Cassegrain focus of a large telescope (Fig. 4.2).

Mounted at the Cassegrain focus, the image from the telescope enters the instrument via a hole in the base plate and is reflected from a mirror which transmits about 4% of the light to a wide-field eyepiece fitted with an illuminated crosswire. The image comes to a focus on a rotating shutter that determines the exposure time. Various shutters are available to give exposure times in the range 0.002 - 0.01 s. The 5 cm focal length microscope objective is used to provide a collimated beam of

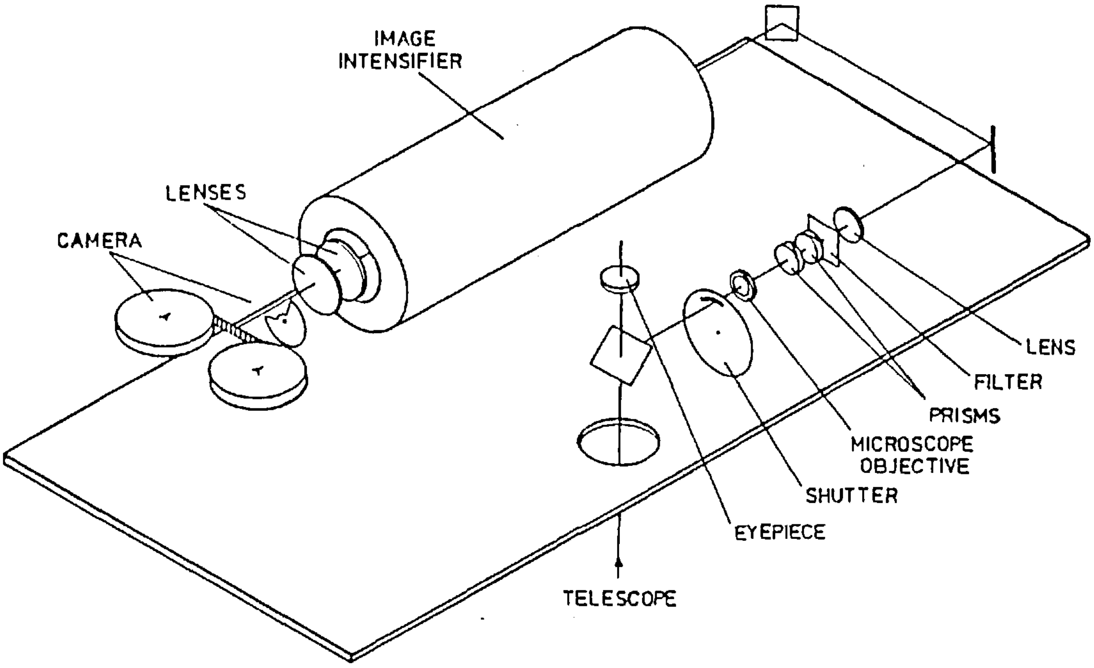

Fig. 4.2: A schematic diagram of the Imperial College Speckle Interferometer.

light from the star image. The nondeviating but dispersing prisms are set to produce an equal and opposite dispersion to that imparted by the atmosphere. Precomputed tables list the prism settings as a function of the object's declination and hour angle. The interference filter has a medium bandwidth; typically, a bandwidth of 30 nm centred at 520 nm is used in practice. An achromatic doublet (focal length 60 cms.) reimages the star onto the photocathode of an image intensifier via two mirrors that are included to fold the size of the apparatus. Not shown are an eyepiece and movable mirror for viewing the image falling on the photocathode, and a sliding shutter to protect the image intensifier when exposures are not being made.

The short exposure time and limited bandwidth imply that some form of intensification will be required to record a good image. A four stage, magnetically focussed, E.M.I. (type 9912) intensifier is used which has a maximum (blue) light gain greater than 10^6, and a resolution of 40 line pairs per mm. The magnetic field is supplied by a water-cooled solenoid. The final phosphor screen is imaged by a pair of f/1.2 Nikon 35 mm camera lenses in front-to-front configuration onto the focal plane of a 16 mm Vinten cine-camera. Using Kodak Tri-X Reversal type 7278 film and standard processing, the overall light gain of the system is just sufficient to record individual photoelectrons from the primary photocathode of the image intensifier. The cine camera and rotating shutter are driven syncronously by stepping motors, using a framing rate of about 8 frames per second.

The LED display of a calculator may be photographed via a movable mirror between the two f/1.2 lenses to record identification numbers at the start of each film.

The overall magnification of the optics and image intensifier is 11.5 at 36 KV to narrow the field of view.

4.3 Recovery of high spatial frequency data

Using short exposure electronographs of binary stars (whose components were unresolved), Rösch et al (1962) showed that at high light levels (i.e. the speckles are not significantly degraded by photon shot noise), the speckle patterns of each component of the binary are the same within an angular extent of about 3 arcseconds. This defines the isoplanatic patch (or angle); light from two objects, separated by greater than this amount, will not travel through the same turbulent column of air.

Labeyrie (1970) showed that for each instantaneous image the quasi-monochromatic imaging equation applies :

$$I(x, y) = O(x, y) \quad * \quad t(x, y) \qquad (4.2)$$

where :

$I(x, y)$ is the instantaneous image intensity,

$O(x, y)$ is the object intensity,

$t(x, y)$ is the instantaneous point spread function of the atmosphere/telescope system,

and $*$ denotes convolution.

The result of passing coherent light through such short exposures of a binary system is a set of cosine fringes (Debrus et al 1969, Labeyrie 1970) where the spacing of the fringes is scaled by the binary separation, the orientation of the fringes is determined by that of the binary system, and the depth of modulation depends on the magnitude difference of the two stars (Gezari et al, 1972). Diffraction limited information can be recovered without having to remove the transfer function of a single point source if care is taken (Beddoes et al, 1976; Morgan et al, 1978). An improvement is made by observing an unresolved star near to the binary system, computing its transfer function and dividing this out of the binary star power spectrum.

This method is known as the spatial power spectrum method. An alternative, but equivalent, method is to obtain the ensemble space autocorrelation of each short exposure (Dainty, 1974). The power spectrum and autocorrelation function are a Fourier transform pair related by the Weiner-Khintchine Theorem (e.g. Born and Wolf, 1975).

It will be shown in the next two sections that these methods of analysis yield the modulus of the Fourier transform of the object intensity (or its auto-correlation function), and the spatial phase information is lost. This is of no importance in the case of centro-symmetric objects, since their Fourier transform is a real function. Speckle interferometry therefore is well suited to the measurement of stellar diameters and the separation (and position angles) of binary star systems. These quantities are of great importance in the determination of stellar mass, the most important parameter of a star (Swihart 1968).

There have been several promising methods of recovering the intensity distribution for asymmetric objects proposed (Gough and Bates 1974, Knox and Thompson 1974, Lynds et al 1976). At present these require extensive data processing and are not yet producing routine results. Accordingly, we shall confine ourselves in the following discussion to centro - symmetric objects.

4.3.1 The Power Spectrum Method

a) Theory

In the spatial frequency domain the average squared modulus of the Fourier transform is found (i.e. the Weiner or power spectrum).

$$W(u,v) = \left\langle \left| i(u,v) \right| \right\rangle \qquad (4.3)$$

where i (u, v) is the Fourier transform of the image intensity distribution, $|\ \ |$ denotes the absolute value, $\langle\rangle$ denotes ensemble averaging, and u, v are spatial frequency co-ordinates. Using equation 4.3 and the convolution theorem, we obtain

$$W(uv) = \left| \sigma(u,v) \right|^2 . \left\langle \left| T(uv) \right|^2 \right\rangle \qquad (4.4)$$

where σ (u, v) and T (u, v) are the Fourier transforms of the object intensity distribution and atmospheric point spread function respectively.

For any isoplanatic, incoherent imaging system, the transfer function $T(u,v)$ is given by the space autocorrelation of the pupil function $H(h,j)$, i.e.

$$T(u,v) = \iint H(h,j).H(h+h',j+j')\, dh\, dj \qquad (4.5)$$

The variables h', j' represent distances in the pupil and are related to the spatial frequency variables by

$$h' = \lambda f u \quad , \quad j' = \lambda f v$$

where λ is the wavelength and f is the focal length. In this case the pupil function may be written as the product of the complex amplitude $A(h,j)$ due to light from a point source that is propagated through the atmosphere and the pupil function $H_o(h,j)$ of the telescope,

$$H(h,j) = A(h,j) . H_0(h,j) \qquad (4.6)$$

With this substitution, the average (long exposure) transfer function for conventional astronomical imaging may be written

$$\langle T(u,v)\rangle = T_0(u,v).C_A(\lambda fu , \lambda fv) \qquad (4.7)$$

where $T_o(u,v)$ is the transfer function of the telescope and is equal to the space autocorrelation of $H_o(h,j)$ and $C_A(\lambda fu \ ,\lambda fv\ )$ is the coherence function or transfer function of the atmosphere and is equal to the time average (ensemble average) autocorrelation of $A(h,j)$. Thus the seeing usually limits the resolution attainable with a large telescope.

The speckle interferometry transfer function is equal to the average squared modulus of $T(u,v)$.

$$\left\langle \left| T(u,v) \right|^2 \right\rangle = \iiiint_{-\infty}^{+\infty} H_0^*(h_1 j_1) . H_0(h_2 j_2)$$

$$\times \quad H_0(h_1 + h , j_1 + j).H_0^*(h_2 + h , j_2 + j)$$

$$\times \langle A^*(h_1 j_1) A(h_2 j_2) A(h_1 + h , j_1 + j)$$

$$\times \quad A^*(h_2 + h \quad j_2 + j) \; . \; dh_1 dj_1 dh_2 dj_2 \tag{4.8}$$

In order to find the fourth-order moment in this equation we must specify the probability distribution of $A(h, j)$. Although no one model for the complex amplitude of a wave propagated through the atmosphere is completely satisfactory, the most realistic for typical seeing is the log normal model; the log amplitude and phase are each assumed to have Gaussian or normal distributions. Using this model, Korff (1973) has computed $\left\langle \left| T(u,v) \right|^2 \right\rangle$ for various sizes of telescope and seeing and thus has shown that the speckle transfer function has a component that extends to the diffraction limit of the telescope. Dainty (1974) uses a simpler model that assumes that the real and imaginary parts of the field have a zero-mean Gaussian distribution; this simplifies the mathematics and is fairly realistic for poor seeing.

Both models result in a transfer function that can be written in the form :

$$\left\langle \left| T(u,v) \right|^2 \right\rangle \approx \left| \left\langle T(u,v) \right\rangle \right|^2 + k\, T_D(u,v) \tag{4.9}$$

where $\left| \left\langle T(u,v) \right\rangle \right|^2$ is the normal long exposure transfer function, $T_D(u,v)$ is the diffraction limited transfer function, and k is a constant given by :

$$k \approx \frac{1}{N} \tag{4.10}$$

and N is the total number of correlation cells in the telescope aperture.

Thus, Dainty and Korff have shown that the transfer function extends to the telescope diffraction limit.

The ability of this technique to provide useful measurements of stellar systems was confirmed experimentally by Gezari et al (1972).

b) Data Analysis

The data analysis follows the technique of Labeyrie (1970) and Gezari et al (1972) and is shown schematically in Fig. 4.3.

Coherent light from the He-Ne laser (λ = 633 nm) is passed through a pinhole and a microscope objective as a spatial filter to obtain uniform coherent illumination for the cine film. Each frame is then projected by a lens onto a piece of film where the squared modulus of the Fourier transform of the image is recorded. By running as many as 10^3 frames through the projector and co-adding their transforms on the same piece of film, good signal to noise ratios can be obtained, even in the case of images where photon shot noise predominates, eg Fig. 4.4.

c) Sources of Error

1. Light scattered from the emulsion surface limits the number of frames that can be co-added by adding to the fog level.

A liquid gate is being constructed to reduce the scattered light, and this should permit the co-addition of up to 10^4 frames (Beddoes et al 1976).

2. To obtain binary star magnitude differences (given by the contrast of the fringes (Gezari et al 1972) (sec 4.3), or to obtain the size of extended objects, it is necessary to calibrate the response curve of the film.

3. The zero-order (or undiffracted) laser beam is very bright compared to the rest of the transform, and, unless masked, it can cause halation effects.

4. Edge effects can occur unless apodization is employed in the cine film plane.

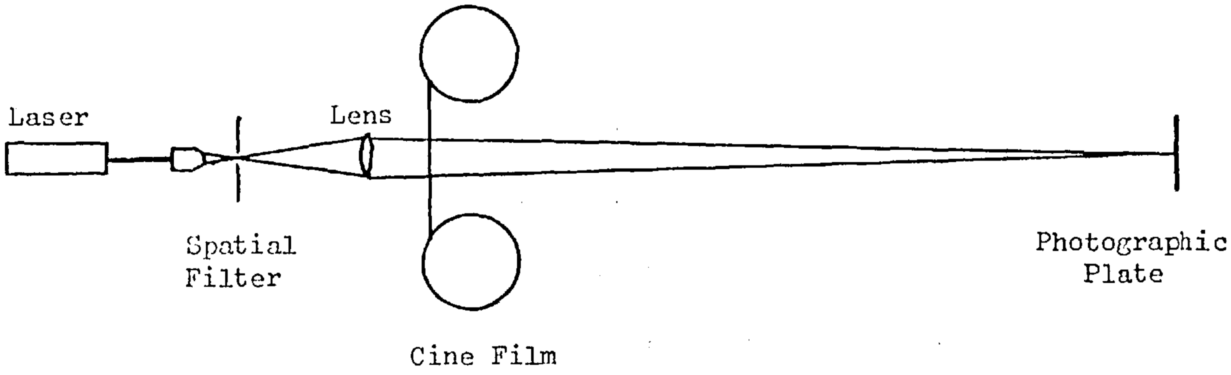

Fig. 4.3: A schematic diagram of the analogue data reduction apparatus (power spectrum method).

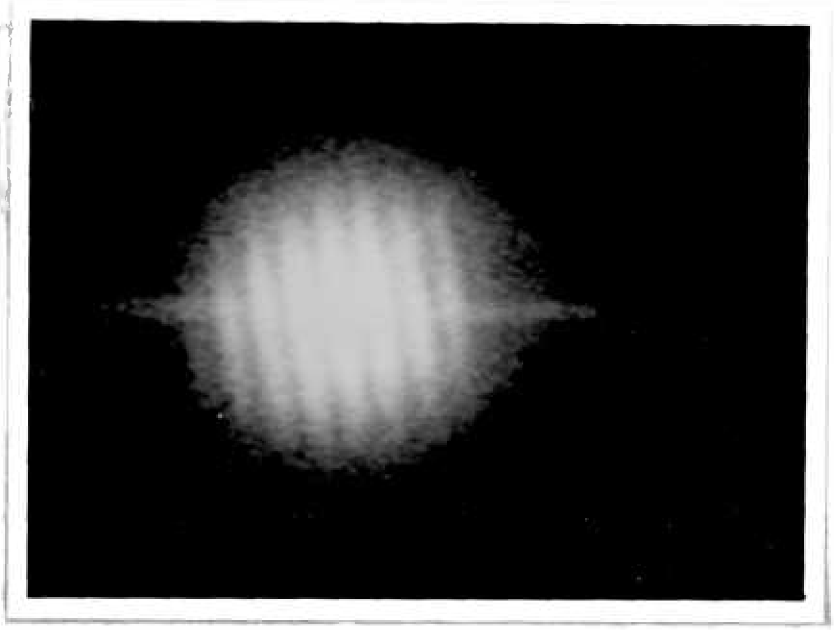

Fig. 4.4: The Power Spectrum of the binary star system ADS 10374 with the fringe structure clearly visible. The separation and position angle of this system are 0.290 arcsec and 276.9° respectively (Morgan et al 1978). About 250 frames of data were co-added to obtain this result.

d) Results using this method

The power spectrum method, effected by a coherent optics system, is now producing routine results (e.g. Gezari et al 1972, McAlister 1977).

Some initial results using the Imperial College Speckle Interferometer were published by Beddoes et al (1976) and the results of a further 35 observations on 30 objects were presented by Morgan et al (1978). In most cases binary star separations could be quoted with a formal error of a few milliarcseconds. This error was assigned by making a large number of measurements on a composite transform. Due to the symmetry of the image power spectrum there is an ambiguity of 180 degrees in the measured position angle, but the formal error was typically 2 degrees. The ambiguity can be resolved either by locating corresponding pairs of speckles in the original data or by comparison with previously deduced elements. It has been found difficult to obtain the magnitude difference in the binary components from the contrast of the fringes (Beddoes 1979) despite calibration using artificially generated binary pairs (Morgan et al 1978). This is probably due to the large number of other factors that can also influence fringe contrast (Dainty 1978). We will return to this problem in sec. 4b.

e) Alternative Data Reduction Techniques

i) Digital Reduction

In this process, the density of each frame of the cine film is scanned by a P.D.S. microdensitometer (Beddoes et al 1976). The scanning aperture used was 55 μm^2 and up to 1024 density levels were recorded in an array of 128 x 128 pixels with a step size of 50 μm (equivalent to 0.025 arcsec). A two dimensional fast Fourier transform is computed for each frame using a digital computer. The squared moduli of many such transforms are co-added to improve the signal-to-noise ratio, as before.

The digital approach allows more sophisticated image processing; by observing an unresolvable star near to the binary system it is possible to complete the transfer function of the speckle process and divide this out of the binary star power spectrum (see sec. 4.3). Averaging the transfer function over many frames is essential to minimize the noise introduced by this process. The results obtained by this method are impressive, but the time taken scanning and digitizing each frame is very long and precludes using this method for routine data reduction.

ii) On-line Digital Fourier Transform

It may be possible to perform fast Fourier transforms in real time using a television type detector and a "hard-wired" circuit for the transform computation (Gibbs 1977).

iii) On-line Optical Fourier Transform

This is a technique proposed by Nisenson and Stachnik (1975), based on a rapidly recyclable, electro-optic image storage device known as a PROM (Pockels Readout Optical Memory). Different types are available (Kazan 1974), but essentially an optical image can be stored on a crystal surface when charge is present. Readout is achieved by passing a laser beam through the crystal and obtaining the Fourier transform as in the photographic scheme (section 4.3.1). The image is then erased by first neutralizing the surface charge, and then uniformly recharging the crystal for the next image.

By directly coupling the PROM to the output of a high gain image intensifier (via fibre optics), speckle images can be stored on the crystal within a 20 ms. exposure. It is claimed that the PROM can work at 30 frames/sec, has a dynamic range in the image plane of 10,000 : 1 and a signal-to-noise ratio of 10^6 : 1 in the Fourier plane.

It is reported by Lipson and Nisenson (1974) that a PROM normally requires about 50 ergs/cm^2 for typical exposure (at 442 nm) but with baseline subtraction as little as 0.5 ergs/cm^2 can be used.

This device is intended to be combined with shearing interferometry for reconstruction of true images based on the Knox and Thompson (1974) algorithm, but it is not yet in routine operation.

4.3.2 The Autocorrelation method of Speckle reduction

a) The high frequency information contained in the speckle pattern of an image can be recovered by computing the ensemble average spatial autocorrelation instead of the power spectrum, i.e.

$$C(x,y) = \langle I(x,y) \otimes I(x,y) \rangle \qquad (4.11)$$

Substituting equation 4.2, we obtain

$$C(x,y) = \left\{ O(x,y) \otimes O(x,y) \right\} * \left\{ \langle t(x,y) \otimes t(x,y) \rangle \right\} \qquad (4.12)$$

where $\otimes$ denotes autocorrelation.

Working in one dimension for convenience, a binary star can be represented as

$$O(x) = \delta(x) + f\delta(x-a) \qquad (4.13)$$

where a is the binary separation, and f is the luminostiy of the companion expressed as a fraction of the primary.

Defining

$$\langle t(x) \otimes t(x) \rangle = \mathfrak{J}(x) \qquad (4.14)$$

we can substitute (4.14) and (4.13) into (4.12) :

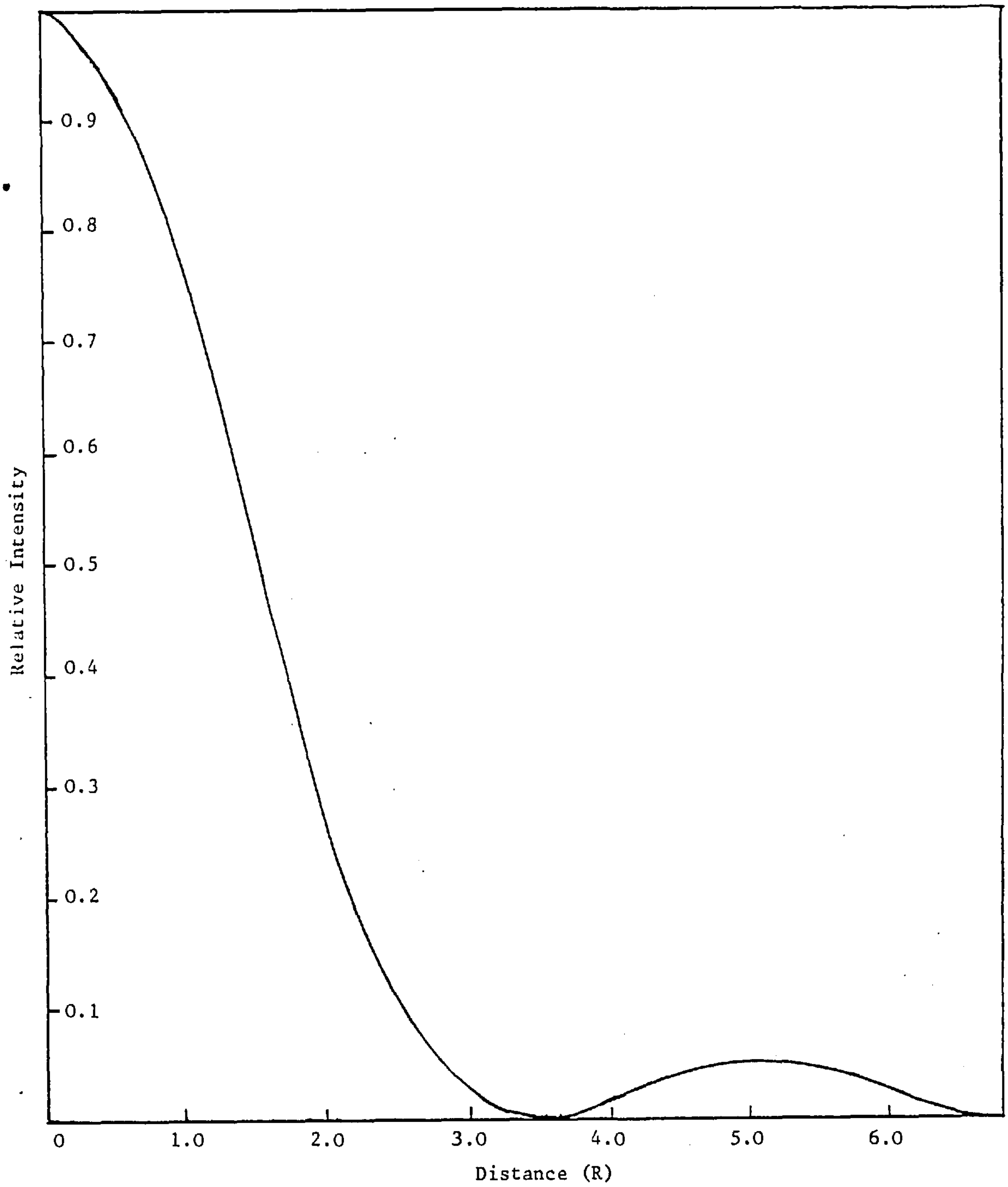

Fig. 4.5: The Airy Function for a Circular Aperture Telescope with a Central Obscuration. The Ratio of Obscuration Radius to Aperture Radius (t) is 0.3.

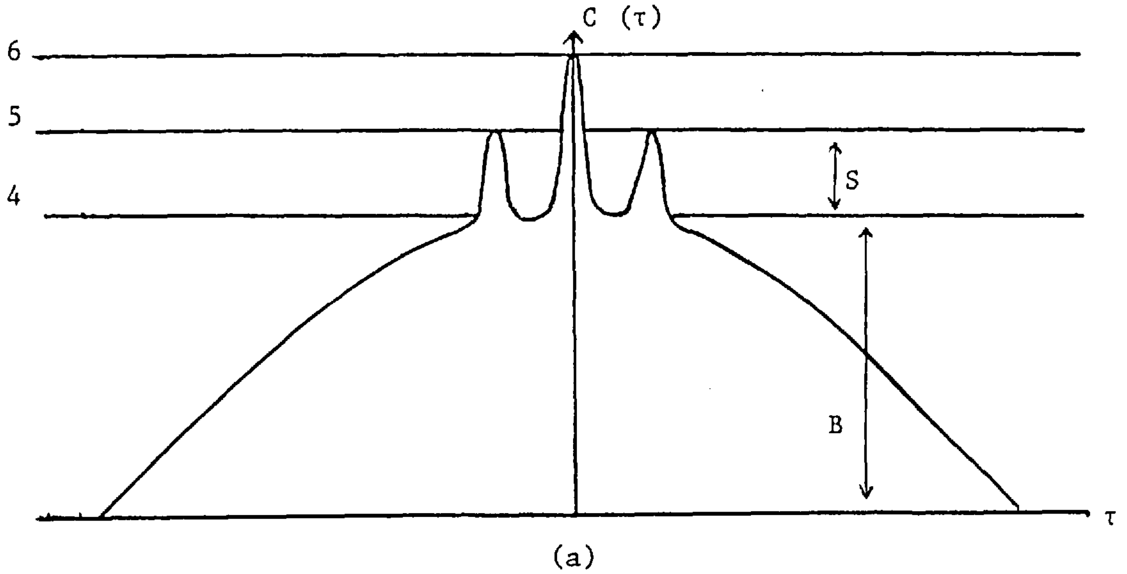

Fig. 4.6: A Sketch of the Autocorrelation Function for
(a) Small Separation (S/B = 0.25), and
(b) Large Separation (S/B = 1.0)

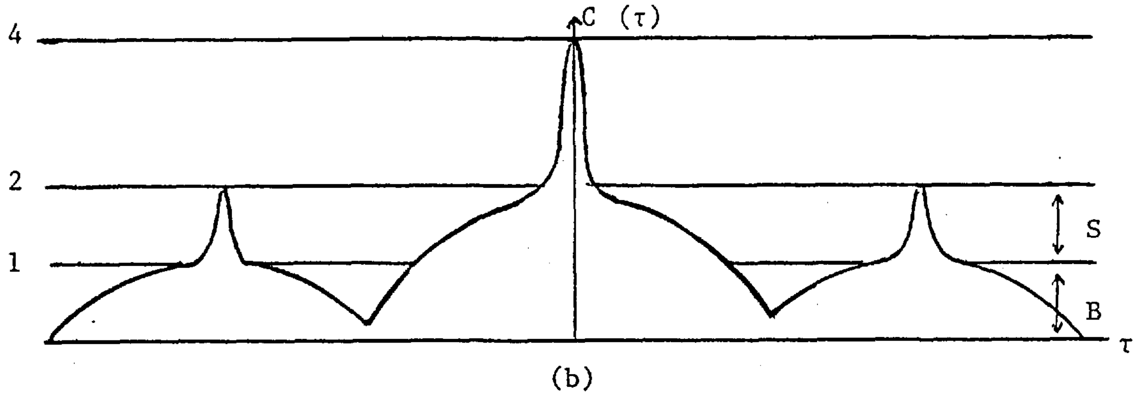

$$C(x) = f.\mathcal{J}(x+a) + (1+f^2).\mathcal{J}(x) + f.\mathcal{J}(x-a) \qquad (4.15)$$

In the case of a speckle pattern of infinite extent this function takes the form of the Airy function of the imaging system standing on an uncorrelated background (Lowenthal and Arsenault 1970, Goodman 1975). Thus, for a circular aperture modified by a central obscuration, the autocorrelation of the speckle pattern of a point source is :

$$\mathcal{J}(x) = \langle I\rangle^2 \left[1 + \left| \frac{2\left[\frac{J_1(x)}{x} - t^2\frac{J_1(tx)}{tx} \right]}{(1-t^2)^2} \right|^2 \right] \qquad (4.16)$$

where $t = \frac{d}{D}$ is the ratio of the primary mirror diameter (D) to the secondary mirror diameter (d). This function is plotted in figure 4.5.

As pointed out in section 4.1, the speckle image is confined to the optical axis with an overall envelope of approximately Gaussian form. Thus, the background of the autocorrelation function may be regarded as a Gaussian function of diameter 2 arcsec at the 1/e points (this is the "seeing" disc). The expected form of the autocorrelation function is sketched in figure 4.6 for the cases of large and small separation.

From equation 4.15 it can be seen that the relative heights of the central and secondary peaks contains information about the magnitude difference (Δ m) of the binary components since f and Δ m are related by :

$$f = (2{\cdot}5)^{-\Delta m} \qquad (4.17)$$

However, because of the overlap of the uncorrelated background of the primary and secondary peaks, the ratio of the secondary peak height to the total uncorrelated local background will depend on the magnitude difference of the binary pair and their separation. Defining the signal as the height of the secondary peak above the background (S in figure 4.6), then the ratio of the signal to background can be calculated (Dainty 1978). For large separations (i.e. wider than the Gaussian background),

$$\frac{S}{B} = 1 \cdot 0 \quad (\Delta m = 0)$$

(where B is the local background),

and for small separations,

$$\frac{S}{B} = 0 \cdot 25 \quad (\Delta m = 0)$$

When Δ m assumes an arbitrary value, the signal-to-background ratio at small separation can be calculated in the manner employed by Dainty (1978). The autocorrelation function $C(\tau)$ of the speckle image intensity $I(x)$ is defined as,

$$C(\tau) = \left\langle \int_{-\infty}^{+\infty} I(x)\, I(x+\tau)\, dx \right\rangle \qquad (4.18)$$

where $\langle \rangle$ denotes an ensemble average. The image intensity is defined by equation 4.2, 4.13 and 4.14, i.e.

$$I(x) = t(x) + f t(x-a) \qquad (4.19)$$

where $t(x)$ is the speckle pattern produced by a single unresolved star, and f is defined by equation 4.17. The ensemble average intensity in the image of an unresolved star is simply the "seeing disc" and is denoted by $\langle i(x) \rangle$. Assuming a negative exponential distribution of intensity, then :

$$\langle i^2(x)\rangle = 2\,\langle i(x)\rangle^2 \tag{4.20}$$

It is also convenient to normalize $\langle i(x)\rangle$, such that:

$$\int_{-\infty}^{+\infty} \langle i(x)\rangle^2\,dx = 1\cdot 0 \tag{4.21}$$

Substituting 4.19 into 4.18 and rearranging gives

$$C(\tau) = \int_{-\infty}^{+\infty} \Big\{ \langle t(x)\,t(x+\tau)\rangle + f\langle t(x-a)\,t(x+\tau)\rangle + f\langle t(x)\,t(x+\tau-a)\rangle + f^2\langle t(x-a)\,t(x+\tau-a)\rangle \Big\}\,dx \tag{4.22}$$

We now consider three particular values of the autocorrelation function at the points (i) $\tau = 0$, (ii) $\tau = a$, and (iii) $\tau \neq a$, but in the region of a : these values are the central value, signal + background, and background respectively. We shall consider a close binary but the separation will always be assumed to be greater than a speckle width, so that

$$\langle t(x)\,.\,t(x\pm a)\rangle \doteq \langle t(x)\rangle . \langle t(x\pm a)\rangle$$

i) $\tau = 0$

$$C(\tau) = \int_{-\infty}^{+\infty} \Big\{ 2\langle t(x)\rangle^2 + 2f\langle t(x-a)\,t(x)\rangle + 2f^2\langle t(x-a)\rangle^2 \Big\}\,dx$$

For a close binary (small a),

$$\langle i(x-a)\rangle \approx \langle i(x)\rangle$$

and therefore,

$$C(0) = 2(f^2 + f + 1)$$

ii) $\tau = a$

$$C(\tau) = \int_{-\infty}^{+\infty} \Big\{ \langle t(x)\rangle\langle t(x+a)\rangle + f\langle t(x-a)\rangle\langle t(x+a)\rangle + 2f\langle t(x)\rangle^2 + f^2\langle t(x-a)\rangle\langle t(x)\rangle \Big\} dx$$

Using similar arguments to those used in (i),

$$C(a) = f^2 + 3f + 1$$

iii) $\tau \neq a$, but in the region of a, such that

$$\langle i(x+a)\rangle \approx \langle i(x+\tau)\rangle$$

and

$$\langle i(x)\, i(x+\tau-a)\rangle = \langle i(x)\rangle^2$$

Applying these conditions to equation 4.22 results in

$$C(\tau \approx a) = f^2 + 2f + 1$$

The signal-to-background ratio S/B is given by :

$$\frac{S}{B} = \frac{C(a) - C(\tau \approx a)}{C(\tau \approx a)}$$

i.e.

$$\frac{S}{B} = \frac{f}{f^2 + 2f + 1} \qquad (4.23)$$

These relations have been tested in a computer simulation by Dainty (1978), but the following points must be borne in mind when trying to estimate Δ m.

a) The value of S/B is related to the binary separation, although the variation could be calibrated using simulated binary stars (Morgan et al 1978).

b) Due to the finite exposure time and bandwidth, and anomalous atmospheric effects, the assumption of strictly negative exponential statistics may not, in general, be valid.

c) Dainty (1978) has shown that an additive, uncorrelated, random noise can affect the S/B ratio, though this may only be true in the faintest cases (e.g. Labeyrie 1978).

d) Unless the pixel area is smaller than the speckle (or photo-electron event) size, the statistics will depart from negative exponential in nature. Also the peak of the secondary may well lie between the sampling intervals in the autocorrelation plane. Interpolation will be required to find the true signal level.

e) Non isoplanatic effects can be considerable in practice (Karo and Schneiderman (1979)).

4.4 The Effect of Photon Shot Noise

The results presented above also apply in the photon counting regime. Defining the normalized autocorrelation function $C'(\tau)$ as :

$$C'(\tau) = \frac{\left\langle \int_{-\infty}^{+\infty} I(x)\, I(x+\tau)\, dx \right\rangle}{\left\langle \int_{-\infty}^{+\infty} I(x)\, dx \right\rangle^2} \qquad (4.24)$$

and using the general relationship due to Jakeman (1973) :

$$\frac{\langle I_1(x)\ I_2(x)\rangle}{\langle I_1(x)\rangle\langle I_2(x)\rangle} = \frac{\langle N_1(x)\ N_2(x)\rangle}{\langle N_1(x)\rangle\langle N_2(x)\rangle} \qquad (4.25)$$

for $1 \neq 2$, it can be shown (Barnett and Parry (1977), Dainty (1978)) that 4·24 becomes :

$$C'(\tau) = \frac{\left\langle \int_{-\infty}^{+\infty} N(x)\ N(x+\tau)\ dx \right\rangle}{\left\langle \int_{-\infty}^{+\infty} N(x)\ dx \right\rangle^2} \qquad (4.26)$$

for $\tau \neq 0$.

Thus Dainty (1978) shows that the value of the signal-to-background ratio for the secondary peak remains unchanged, but the value of the central peak ($C(\tau = 0)$) increases.

c) The signal-to-noise ratio at low light levels

In this section we will follow the argument of Dainty (1978) and impose the conditions that (a) the binary has small separation, (b) there is no additive noise term such as dark current or sky background, and (c) each pixel is equal to the minimum speckle size.

At low light levels, the probability (p) of finding a photon in a speckle is given by

$$p \approx \frac{\langle n_{ph} \rangle}{\langle n_s \rangle} \tag{4.27}$$

The average value of the local background is given by the probability that two uncorrelated sample points both contain a photon, multiplied by the total number of statistically independent vector separations in the experiments, i.e.

$$\begin{aligned} C(\tau \approx a) = B &= p^2 \frac{\langle n_s \rangle n_{pic}}{2} \\ &= \frac{\langle n_{ph} \rangle^2}{\langle n_s \rangle} \frac{n_{pic}}{2} \end{aligned} \tag{4.28}$$

The number of statistically independent speckle pairs per picture is equal to half the number of speckles. This is the binary star case of Barnett and Parry (1977), who considered the statistics of an object of arbitrary shape, but smaller than the isoplanatic angle.

From 4.13 and 4.23 we know that

$$S = \frac{f}{1+2f+f^2} \cdot \frac{\langle n_{ph} \rangle^2}{\langle n_s \rangle} \frac{n_{pic}}{2} \tag{4.29}$$

The noise is the square root of the background, so that the signal-to-noise ratio is given by

$$R = \frac{S}{N} = n_{ph} \sqrt{\frac{n_p}{2\langle n_s \rangle}} \; \frac{f}{1+2f+f^2} \qquad (4.30)$$

Equation 4.30 differs considerably in result from that of Roddier (1975). For the case of equal magnitude components (f = 1), we can compare the two formulae,

$$R = \langle n_{ph} \rangle \sqrt{\frac{n_p}{2\langle n_s \rangle}} \qquad \text{(Dainty 1978)}$$

$$R = \frac{\frac{\langle n_{ph} \rangle}{\langle n_s \rangle} T_0(f) \, . \, n_p^{1/2}}{1 + \frac{\langle n_{ph} \rangle T_0(f)}{\langle n_s \rangle}} \qquad \text{(Roddier 1975)}$$

where $T_o(f)$ is the transfer function of the telescope.

It is interesting to compare the limiting magnitude suggested by these equations, using the values $\langle n_s \rangle = 10^3$, $n_p = 10^4$, $T_o(f) = \frac{1}{2}$, and the required signal-to-noise ratio, R, = 10. The average number of photons per picture $\langle n_{ph} \rangle$ is then 200 (Roddier) or 9 (Dainty). For a 4 metre telescope, a zero magnitude star provides 10^8 photons/s/A, and taking a detector primary quantum efficiency of 10%, a bandwidth of 250 A and an exposure time of 10^{-2}s, we arrive at a limiting magnitude of 16 (Dainty) and 12 (Roddier). This discrepancy is discussed by Aime and Roddier (1977) and Dainty (1978), who conclude that Roddier's estimate is low because of an unrealistic definition of signal, that does not take into account the magnitude difference of the binary system. It is important to note that the "signal" in an autocorrelation plot is a sensitive function of magnitude difference. Fig. 4.7 shows a plot of signal-to-background plotted against magnitude difference. It is

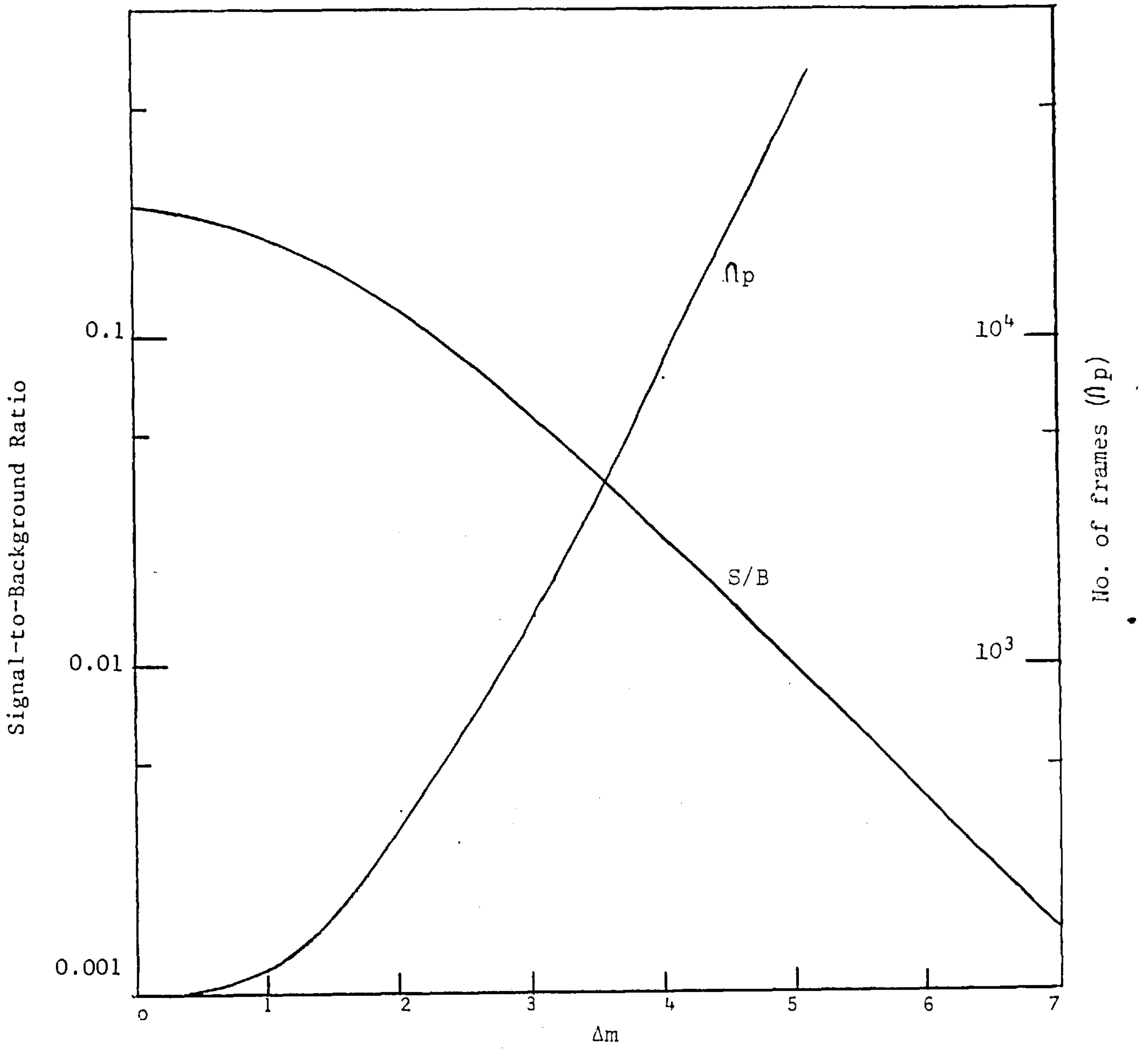

Fig. 4.7: The Variation in Signal-to-Background Ratio (S/B) with Magnitude Difference, of the Secondary Peak in the Autocorrelation of Speckle Data from a Binary Star.

clear that for the relatively modest magnitude differences frequently encountered in practice, the value of S/B falls rapidly. (This graph was obtained using equations 4.17 and 4.23). From equation 4.30,

$$R = \langle n_{ph} \rangle \sqrt{\frac{n_p}{2\langle n_s \rangle}} \cdot \frac{f}{1+2f+f^2}$$

we can see that to maintain a signal-to-noise ratio for a given $\langle n_{ph} \rangle$ and $\langle n_s \rangle$ then

$$n_p = \frac{2R^2}{\langle n_{ph} \rangle^2} \langle n_s \rangle \left\{ \frac{f^2+2f+1}{f} \right\}$$

Choosing R = 10 $\langle n_{ph} \rangle$ = 200, $\langle n_s \rangle$ = 10^3. This reduces to

$$n_p = 5 \left\{ \frac{f^2+2f+1}{f} \right\}^2 \qquad (4.31)$$

This function is also plotted in fig. 4.7.

4.5 Autocorrelation with single bit quantization

With fainter binary objects, photon shot noise dominates the speckle image and in the limiting case the speckle picture will consist of individual photo-electron scintillations arising from single photons incident at the photocathode. Obviously in this case information about the size and shape of the scintillation is irrelevant; it is sufficient to know that a photon has been detected. For this reason it is not necessary to digitize the analogue video output of the CCD with more than one bit. This digitising strategy is also applicable to high light level speckles. If the speckle image of a binary star is regarded as two overlapping identical speckle patterns displaced with respect to each other by the binary separation, then it could be expected that a measurement of all possible separations in the image must give an indication of the binary separation. Thus only the position of the speckles in the image needs to be recorded, but some information is lost in this scheme.

The simplified algorithm

In the case of discrete functions, we shall take as our definition of autocorrelation :

$$C(x_1,x_2) = \sum_{y_1} \sum_{y_2} y_1 \ y_2 \ P(y_1,y_2 \ ; x_1,x_2) \tag{4.32}$$

(e.g. Goldman 1953)

Assuming stationary statistics,

$$C(\Delta x) = \sum_{y_1} \sum_{y_2} y_1 \ y_2 P(y_1,y_2 \ ; x, x+\Delta x) \tag{4.33}$$

With one bit quantization, the value of y is restricted to 1 or 0, so that equation 4.32 reduces still further to :

$$C(\Delta x) = P(\ y(x) = 1 \ ; y(x+\Delta x) = 1\ ) \tag{4.33}$$

and assuming a large number of trials,

$$C(\Delta x) = n(\ y(x) = 1 \ ; \ y(x+\Delta x) = 1\ ) \tag{4.34}$$

that is, the value of the autocorrelation function at Δ x is given by the number of times that two events separated by distance Δ x occurs. (See also Blazit et al (1975) and Koechlin (1978)). Computing the autocorrelation function in these circumstances can be regarded as constructing a histogram of the vector separations of the events in a single frame of video, and averaging over many such frames. The number of subtractions performed per video frame is $\frac{n\,(n-1)}{2}$, where n is the number of photon or speckle events in that frame.

One bit quantization as a method of data compression

Kaiser and Angell (1956) have shown that quantization noise does not play a great part in limiting averaged functions, but it was pointed out by Blazit et al (1977) that clipping of high light level images will introduce distortions of the autocorrelation function owing to (a) poor linearity of the analogue video signal, and (b) the non-linearity of the clipping process. The CCD has superior linearity compared to commercial T.V. cameras of the type used by Blazit, and we can regard effect (a) as negligible (see Chapter 2). The problem of effect (b) is well defined, but applying an "a posteriori" correction is in general a difficult problem.

For the case of Gaussian statistics an elegant solution to the effect of clipping was found by Van Vleck (reprinted : Van Vleck and Middleton 1966) and this has been extensively used by radio astronomers in digital autocorrelators (e.g. Weinreb 1963, Davies et al 1969). Unfortunately this correction is not applicable to the negative exponential statistics of speckle patterns.

The problem of clipping applied to speckle images has been studied by Bates (1977) who has proposed a rigorous "a posteriori" correction for a generalized object. For a single unresolved star, the correction is,

$$C(\tau) = \left\{ \cosh\left[\frac{2\rho^{1/2}\Gamma}{(1-\rho)}\right] + \rho^{1/2}\sinh\left[\frac{2\rho^{1/2}\Gamma}{(1-\rho)}\right] \right\} \times \exp\left[-\frac{2\rho\Gamma}{(1-\rho)}\right] \tag{4.35}$$

where

$$\rho(\tau) = C'(\tau) - 1$$

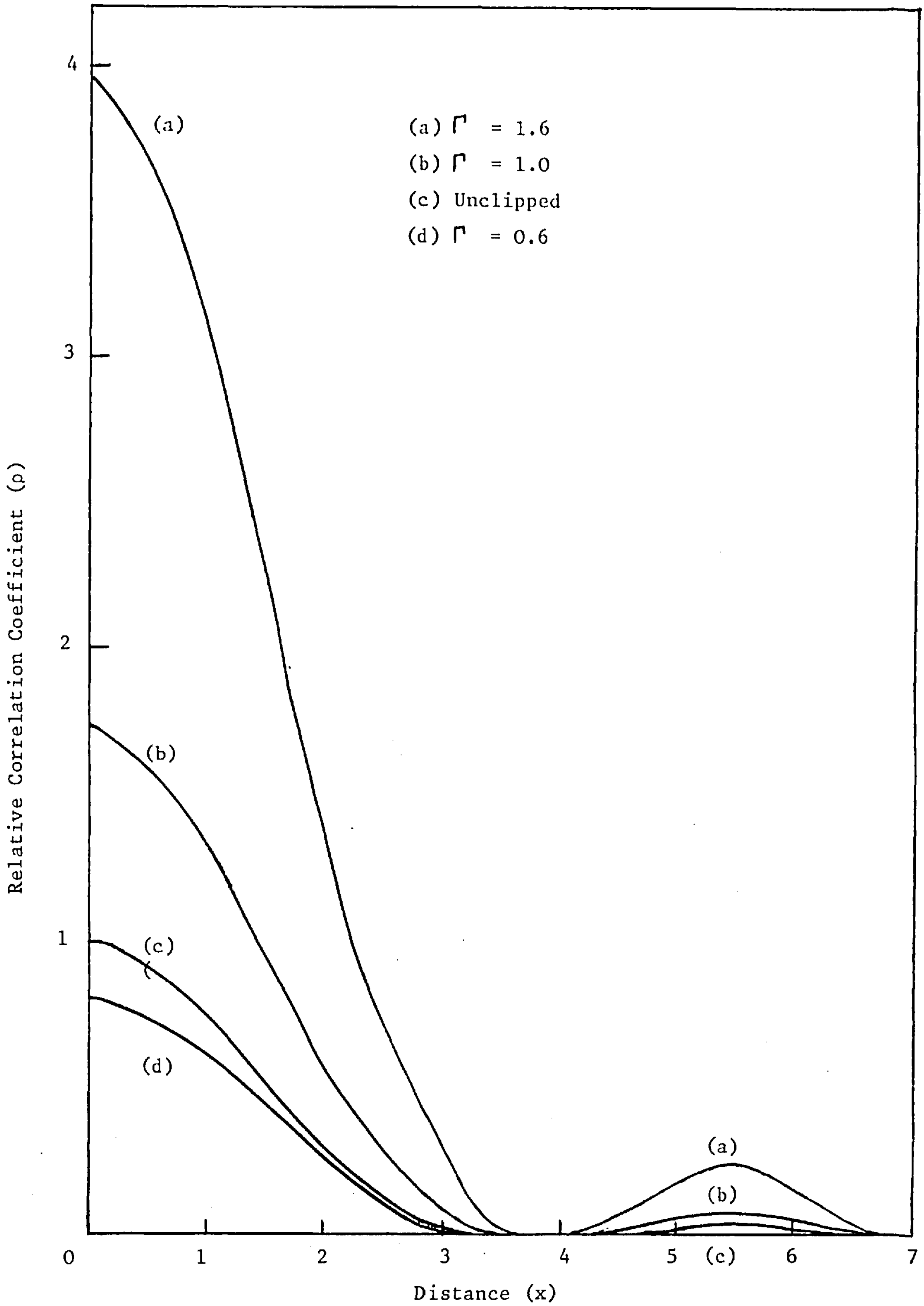

Fig. 4.8: The Effect of Clipping on the Airy Disc of Fig. 4.5 for Various Values of

$$\Gamma = \frac{I_D}{\langle I \rangle}$$

$C'(\tau)$ is the unclipped normalized autocorrelation function, $C(\tau)$ is the normalized clipped autocorrelation function, and $\Gamma = \frac{I_D}{\langle I \rangle}$, where I_D is the threshold intensity level and $\langle I \rangle$ is the mean intensity.

Fig. 4.8 has been constructed from values tabulated by Bates, and shows the effect that clipping at various levels has on the autocorrelation function (in this case a typical Airy function of diffraction limit 0.05 arcsecs). It is important to note that the position of the first minimum is unchanged by clipping. The relative height of the Airy function changes considerably with discriminator level.

It is clear from the work of Dainty, described in section 4.3.2, that the signal-to-background ratio is an important quantity, and equation 4.35 will allow the correction of this ratio for clipped autocorrelation functions.

The derivation of equation 4.35 departs from reality in two ways. Firstly, it is assumed that the statistics of the speckle pattern are negative exponential, and secondly it is assumed that the speckle pattern has an infinite spatial extent. In Chapter 6, section 6.4, it will be shown that these assumptions can affect the shape of the expected autocorrelation function with a consequent loss of high spatial frequency information.

CHAPTER 5

THE REDUCTION OF SPECKLE INTERFEROMETRY DATA USING THE CCD

5.1 Introduction

This chapter describes the apparatus and programmes used in generating autocorrelation functions from stellar speckle interferometry data with single bit quantization. The data used were obtained with the Imperial College speckle interferometer (described in Chapter 4, section 4.2) and were recorded on cine film. Eventually it is intended that the speckle data will be reduced in real-time at a telescope site using a hard-wired autocorrelator (described in Chapter 8); the laboratory process is seen as an intermediate approach for studying the problems involved in computing the autocorrelation function.

It should be noted that throughout this chapter the word "event" refers to a pixel in the CCD whose stored charge is greater than the discriminator level and is thus recorded as a "1" in the computer memory.

5.2 The Hardware

Figure 5.1 is a photograph of the data reduction apparatus, showing the projector, light control, lens and CCD; the same arrangement is shown schematically in Figure 5.2. An incoherent (thermal) light source set in a simple condensing system illuminates each frame of the cine film as it is run through the projector. Both light source and film are mounted in a cine projector (Specto type FSQ) that was chosen because a single frame step facility was incorporated in this model. The speckle picture is imaged directly onto the CCD via a 102 mm f/2.9 lens that is moveable in order to optimally match the projected image scale to the CCD resolution. The CCD camera and computer interface are described in chapters 2

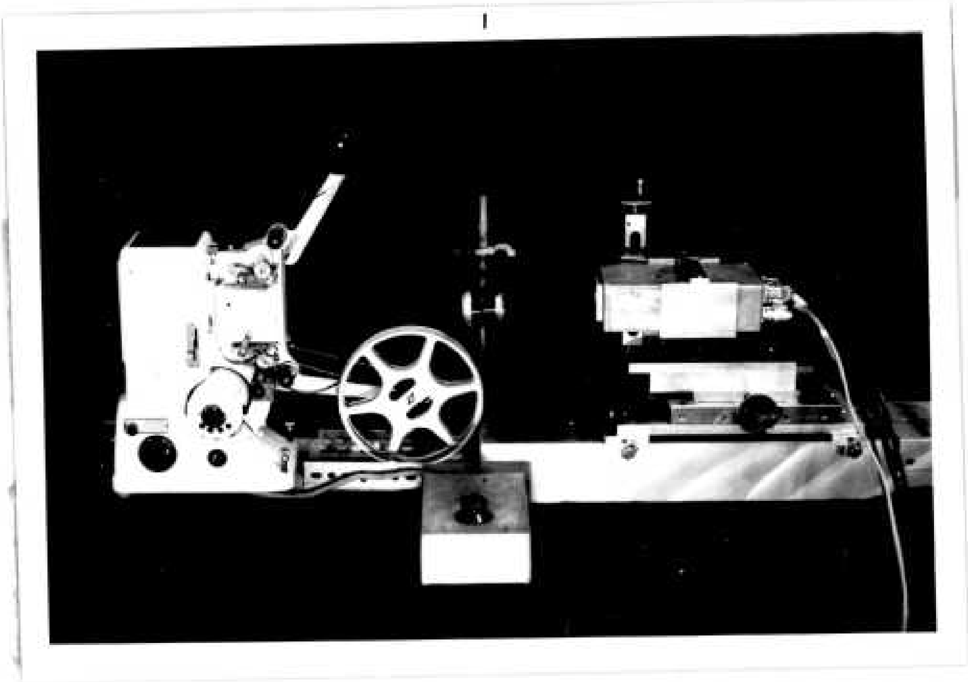

Film
Projector

CCD
Camera

FIG. 5.1: A PHOTOGRAPH OF THE DATA REDUCTION APPARATUS

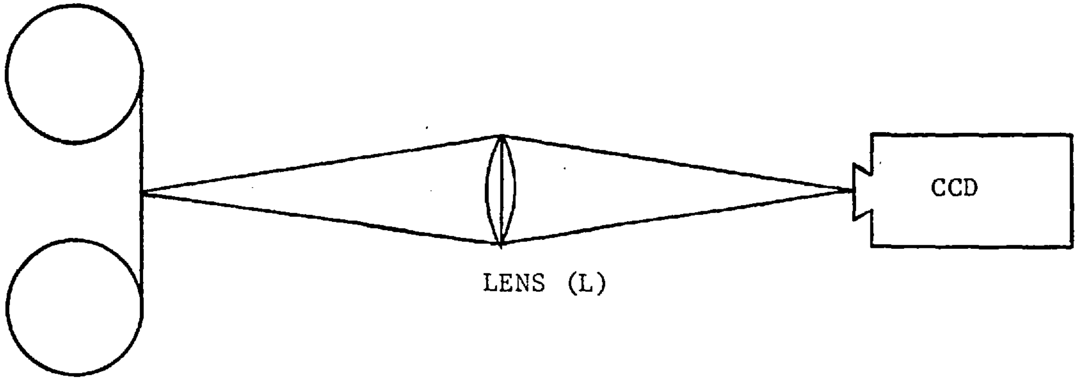

FIG. 5.2: SCHEMATIC DIAGRAM OF DATA REDUCTION APPARATUS

and 3.

The projector single step facility can be remotely controlled. When the computer has read a frame of video data into core, the restart pulse that reloads the buffer memory also increments the cine film.

5.2.1 Projector Control Circuit

The projector single step facility is controlled by the circuit shown in Fig. 5.3. A 32 μF electrolytic capacitor is charged up to about 220 volts via rectifying diode D and limiting resistors R_1 and R_2. When a change of frame is required, the capacitor is discharged through the solenoid S, activating the necessary mechanical section. The three contacts A, B and C can be connected to flying leads for remote operation via a relay located in the buffer store control logic.

There were two reasons for switching with a relay: the circuit operates between mains line and neutral with no reference to earth; the CMOS structure of the CCD must be kept electrically isolated from the large switching transients involved. A relay with very good contact ratings (250 v, 10 A : RS 348 - 807) was found to be necessary because of arcing between the contacts when they were switched back to recharge the capacitor. To minimise this problem, the capacitor C ($\sim$ 0.1 μF) was introduced across the relay contacts, and the value of R_1 was increased to 3.9 KΩ to reduce the initially current surge. The value of R_2 is about 470Ω. The slower charging rate limits the speed of operation of the projector, but this delay is far exceeded by the time taken to compute the autocorrelation of a single frame.

Activation of the switching relay was achieved in the following scheme :

i) After a frame of video has been read by the computer, the CLEAR pulse is returned to the control logic in the buffer store.

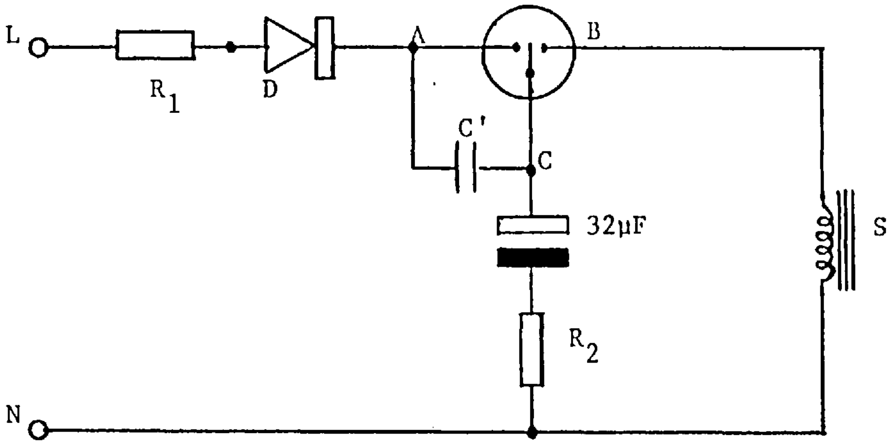

FIG. 5.3: SINGLE STEP CONTROL IN PROJECTOR

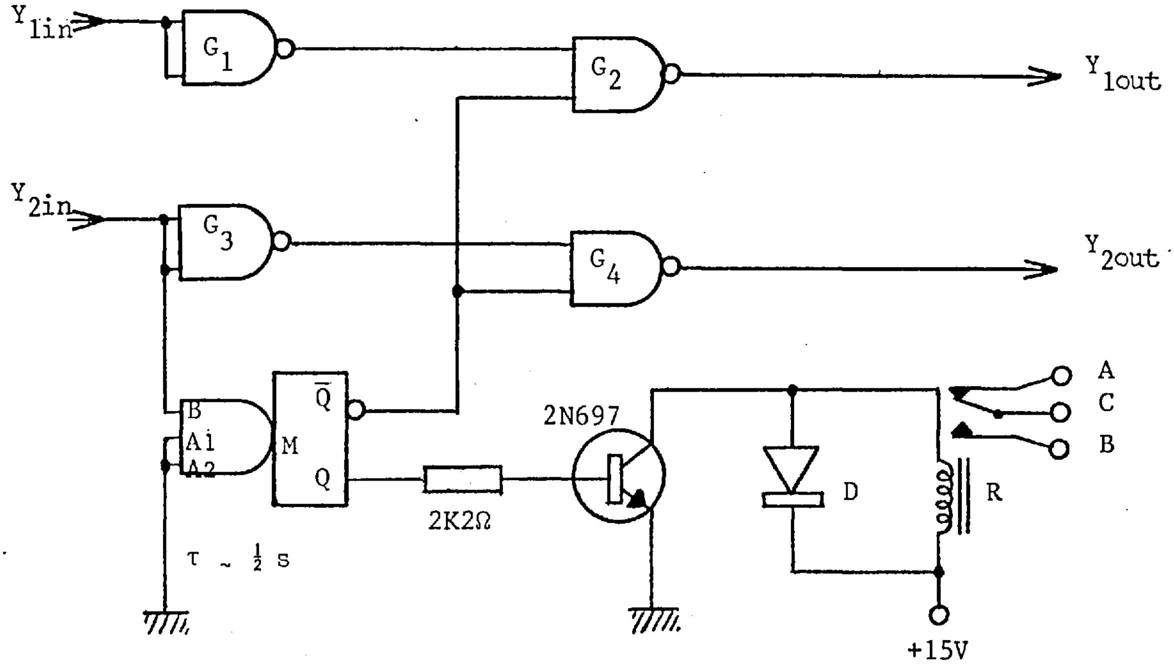

FIG. 5.4: RELAY CONTROL CIRCUIT

ii) This CLEAR pulse switches the relay but is prevented from reaching the rest of the logic to allow the projector a period of 0.5s to change frames and to mechanically settle.

iii) The stored CLEAR pulse is now communicated to the control logic and a new frame of video is read into the buffer store.

After data has been read into the computer the buffer store state changes from readout to write in by clocking two bistables. Firstly, the toggle bistable (D_1 in Chapter 3, fig. 3.2) which "remembers" whether the buffer store is being read-out or written-into is clocked by the CLEAR signal from CAMAC. This opens gates, allowing data into the RAMs and closes gates communicating with CAMAC. Once this state is established, data is prevented from reaching the RAMs by the "start" bistable (D_3 in Chapter 3, fig. 3.7) which changes state when the start-of-frame pulse is received from the camera, thus ensuring synchronisation of data with RAM addressing.

To delay the write-in cycle by ½ sec the CLEAR signal must be prevented from reaching D_1 and D_3 by interrupting these lines at points Y_1 and Y_2 in Figures 3.2 and 3.7 (Chapter 3). The relay control circuit inserted at these points is drawn in fig. 5.4. When gates G_2 and G_4 are closed, no further writing of data to the RAMs can take place : this is the settling down period. The detailed operation of this circuit is as follows.

When the transfer of data to the Interdata 70 is complete, the WRITE command line (i.e. $Y_{2\ in}$) goes HIGH. This triggers the monostable M that has a relaxation time of about 0.5s so that Q goes HIGH and $\bar{Q}$ LOW. With gates G_2 and G_4 now closed, no further information can be written into the buffer store while the projector is incremented. As Q goes HIGH, the 2N697 transistor is turned on, thus switching relay R which in turn fires the projector single step control. Diode D short circuits the back EMF from the relay solenoid. After 0.5 s the monostable relaxes to its former state and thus reconnects $Y_{1\,in}$ $Y_{1\,out}$ and $Y_{2\,in}$ $Y_{2\,out}$ (fig. 5.4).

5.2.2 Projector Light Control

The circuit, shown in Fig. 5.5, is adapted from a standard design. The projector lamp, which is rated as 10 amps at 12 v, was originally supplied from an A.C. source, but this caused the output of the CCD to "flicker". This circuit is intended to supply a chopped D.C. current, controlled by VR_1, to the lamp. The voltage across ZD and thus across the unijunction (2N2646) pulse generator circuit is unsmoothed D.C. clipped at 9 v, so that the power to the unijunction is interrupted in phase with the power line frequency. At the start of each new power line half cycle, the unijunction begins a timing sequence, determined by R_1, C_1 and VR_1, and after a delay it generates a positive pulse which turns on the thyristor (SCR : THY-500-26). Thus the unijunction gives delayed and variable firing of the thyristor.

The delayed pulse fires the thyristor at an arbitrary moment during the power line half cycle and the thyristor then remains conducting irrespective of the gate condition until its anode potential falls to near ground at the end of the half cycle. Hence varying the delay via VR_1 controls the light output of the lamp.

5.3 The Software

5.3.1 Data Reduction Programmes

Processing and storing a single frame of video data in the array PICTURE was described in Chapter 3. The programmes described in this section begin with

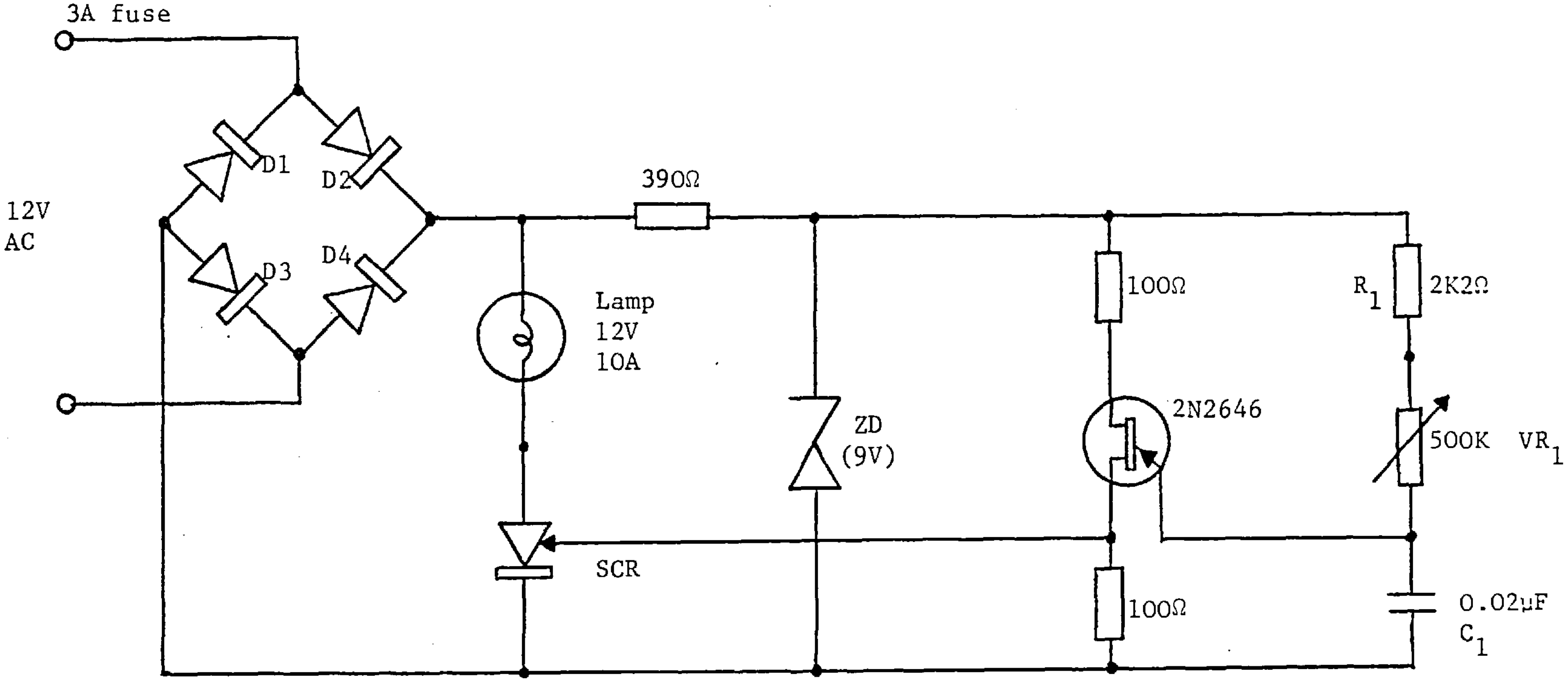

FIG. 5.5: LIGHT LEVEL CONTROL

the assumption that valid data will be found in this array.

The strategy adopted for the calculation of the vector separations is as follows.

i) The address of the first data point is taken as origin.

ii) The vector distance to all other data points is computed by subtraction of their x and y co-ordinates from those of the origin, and the resulting Δ x, Δ y components recombined to form a composite address. The contents of a store (initially set to zero) whose address is given by the vector separation, is incremented once every time that separation is found.

iii) The second data point is now selected as origin and the process repeated; the first data point, for which all possible distances have already been computed, is excluded.

iv) This process continues through all the data points.

A more detailed flow diagram is shown in figure 5.6. It is essential that the number of operations performed in the inner loop (from C to G in the diagram) is minimized to keep the overall execution time as low as possible. For this reason, the addresses of the events (given by $A = 100\ Y + X$) are already broken down into x and y components and held in corresponding but separate arrays. The inner loop has been written in assembler language to avoid unnecessary interpretation time. The loop limit parameter MM is the number of addresses that have been split into components and stored in the holding arrays (3STORE and 4STORE).

It was felt that a further increase in the speed of calculation could be achieved by inserting a "window" in the autocorrelation (c.f. Blazit et al 1975). The 100 pixel width of the CCD usually corresponds to about 1.5 arcsec of sky. Since it is not usual to use the speckle technique for binary systems with separations

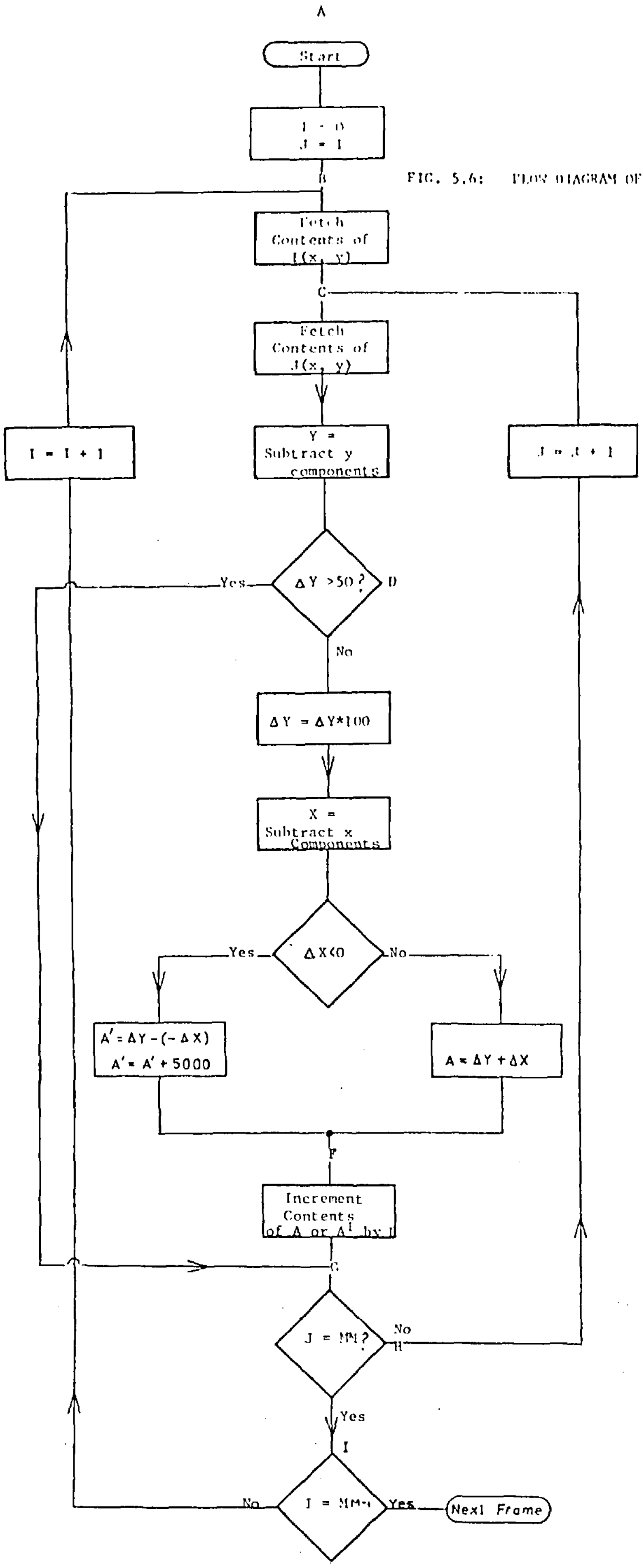

FIG. 5.6: FLOW DIAGRAM OF THE AUTOCORRELATION PROGRAMME

greater than about 0.75 arcsec, we will not gain any extra information by calculating separations greater than 50 pixels. Separations are tested against this 50 pixel limit during the inner loop; if the limit is exceeded then the inner loop is terminated and the next origin point chosen. The pixel limit can be altered to any required number.

As a result of the raster type scanning and addressing, the difference in y co-ordinates is always positive and ahead of the origin point, making it easy to test against the limit. If the difference is greater than 50 pixels the programme jumps to G (fig. 5.6). The difference in x co-ordinates, however, can be positive or negative, i.e. on either side of the origin point, so that constructing a "window" requires more complicated programming. Indeed, the extra steps required to do this nullify any advantage gained in employing a window in the x direction, and therefore this feature is not included.

The values of x and y obtained by subtraction are combined to form the composite address A, using the modulus value of x, i.e. $A = 100\Delta y + |\Delta x|$. Thus, A is the same value, whether x is positive or negative; to distinguish between the two cases, an offset of 5000 is added to A if x was initially negative, and this ensures it is stored in a different region of the memory. The entire sequence illustrated in fig. 5.6 will be referred to as AUTOCORRELATION.

For speed, the results of the vector subtraction, which occur in a random manner, must be stored in the fastest possible time. Random access to a disc store is a lengthy process; the trial programmes using disc storage took 45 minutes to compute the autocorrelation of a single frame. Hence a storage array in core is needed with an "area" of 5×10^3 pixels. With the essential read-in programmes and the array PICTURE loaded, there only remains some 2 K words of core storage.

To circumvent this problem, the information is passed around the arrays in the manner shown in fig. 5.7. Once stored in PICTURE, the addresses of events are split into x and y components that are held in 3STORE and 4STORE; PICTURE is zeroed during this step. The data in 3STORE, 4STORE is used by the AUTOCORRELATION routine which places the results back into PICTURE. From there the data is stored sequentially in a disc file and PICTURE, 3STORE and 4STORE are emptied ready for the next batch of data.

A more detailed flow diagram of the programmes used in this sequence is shown in fig. 5.8.

i) CCD and PROCESS

These are the programmes outlined in Chapter 3 that read in the data from the buffer store and carry out the necessary "tidying up".

ii) P-E

The events stored in PICTURE are resolved in their x and y components, storing the x component in 3STORE and the y component in 4STORE. It is assumed that in any single video frame of data, no more than 3000 pixels will contain events so that 3STORE and 4STORE are limited to 4 K words capacity each. This programme also counts the number of events (n) occurring in the frame and stores this as the parameter MM.

iii) 0 - PIC

With data transfer complete, the locations of array PICTURE are zeroed so that the results of AUTOCORRELATION can be stored.

iv) AUTOCORRELATION

This operates as described earlier and stores the results in PICTURE.

v) P-AD

The results of AUTOCORRELATION must be moved from PICTURE for two reasons; to make room for the next frame of data and so that data is not lost during

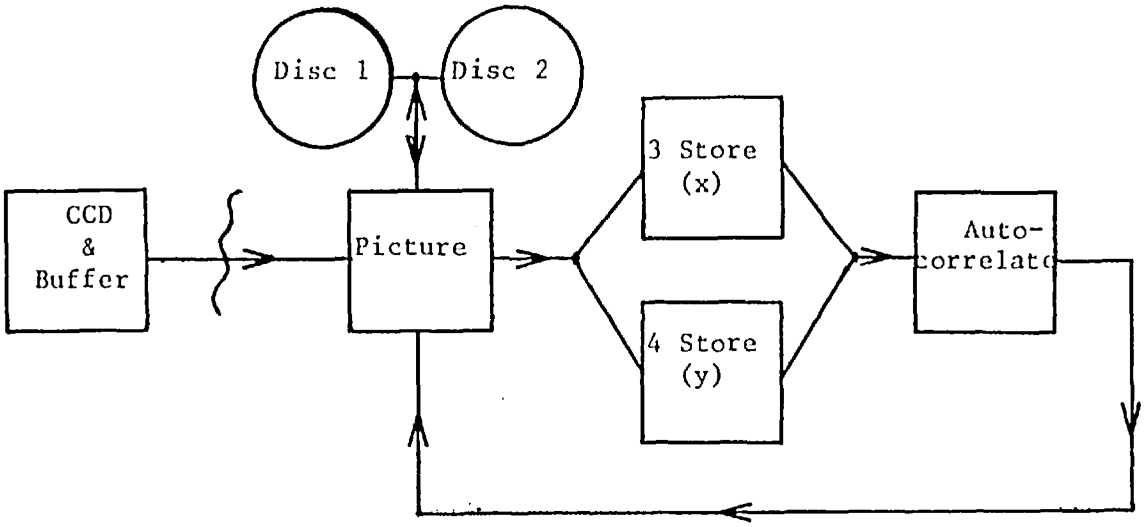

FIG. 5.7: THE FLOW OF INFORMATION AROUND THE STORAGE ELEMENTS IN THE COMPUTER

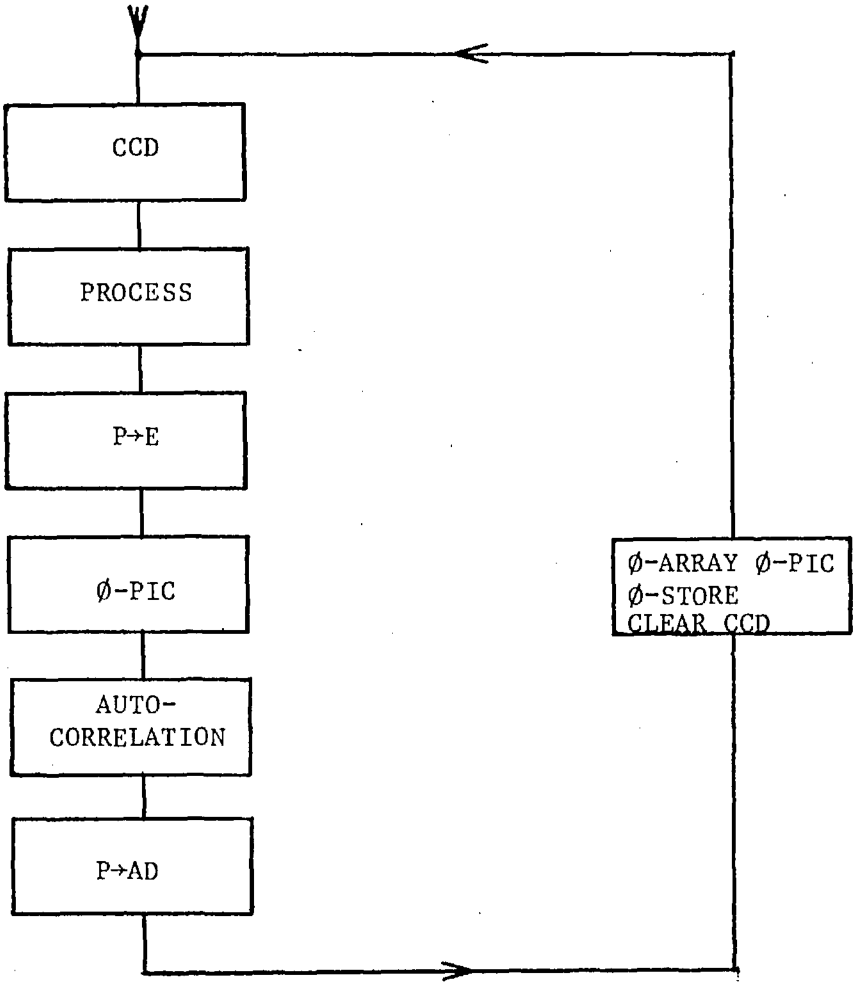

FIG. 5.8: FLOW DIAGRAM OF THE PROGRAMMES USED IN THE AUTOCORRELATION OF ONE FRAME OF VIDEO

one of the all too common computer "crashes". Transfer from PICTURE to a disc store (DISC 2) takes place sequentially to minimize transfer time (about 7 s) and is co-added to any previous results.

vi) 0-ARRAY

This consists of 0-PIC and 0-STORE. 0-STORE sets 3STORE and 4STORE to zero.

vii) CLEAR-CCD

The contents of the buffer store are read out by this programme, but the data is discarded thus allowing the buffer to be refilled with fresh data. This programme is not necessary if the cine-projector has already been incremented automatically.

Now that the autocorrelation of one frame of data is complete, the next frame of video is ready for processing.

5.3.2 Data Display Programmes

The acute shortage of core space outlined in the last section, means that the display programmes must be held on disc and only loaded into core for execution when the data processing is completed. Unfortunately, this does not allow the progress of the autocorrelation to be viewed in real-time.

The main display programme SHOW is a 2-D histogram map of the autocorrelation plane with 32 levels of grey scale, each grey level being 1/32nd of the autocorrelation value at $x = 1$, $y = 0$. An example of this display is shown in figure 6.2. The odd values of grey scale (1,3,5 ..... 31) are represented by the hexadecimal numbers (1,2,3,4 ..... D,E,F), while the even values of grey scale are blank in order to denote histogram level changes more clearly.

The actual values of each point in the autocorrelation plane are accessed by another programme (1NOS) which lists the values from (x,y) to (x + 13, y + 13) where x, y are co-ordinates specified by the user. The function of the other support programmes are described below.

TRANSFER-DATA

A second autocorrelation result store is held on disc (DISC 3). The contents of the first (DISC 2) can be loaded non-destructively (or co-added) into the second. This is useful if the contents of the locations in the first store are close to overflowing (i.e. location counts ~ 32,000).

2 A/C

This displays the contents of the second disc store in the same way as SHOW.

2 NOS

The autocorrelation values in the second disc store are displayed as in 1 NOS.

BLANK, 2BLANK

These programmes zero the two disc stores.

PEAK-FIND

This is designed to remove the autocorrelation function of a single point source. The algorithm is described in Chapter 6 (see 6.2.1).

5.4 System Tests

A series of experiments was designed to test various aspects of the digital autocorrelation system and are described below.

5.4.1 Computer simulation

A set of programmes was designed that would take place various test patterns of a fixed or statistical nature in the array PICTURE. Simple programmes for generating patterns such as straight lines and squares were used initially to ensure that the programme AUTOCORRELATION was working. In Block 339 (Appendix 2) the following programmes are listed.

i) EVENT. This is used to store a "1" in the array PICTURE at a specified location.

ii) PAIR uses EVENT to generate an artificial "speckle pair" separated by a specified distance and position angle, in the array PICTURE.

iii) S. Two random numbers read from a table and entered at the keyboard followed by the command S will generate the object PAIR whose centroid position is given by the random numbers.

These programmes are always available in the computer for checking the algorithms.

5.4.2 Autocorrelation of a known object

Slides of various objects and test patterns were prepared and imaged onto the CCD either by using a Baum projector (Baum 1962) or by placing them in the gate of the projector.

The first slide was a square of side 3 mm. This was reduced by the Baum projector so that the final image on the CCD measured 0.6 mm x 0.6 mm. If we assume that the intensity profile of the image is given by :

$$\begin{aligned} I(x,y) &= 1 \qquad 0{\cdot}3\,\mathrm{mm} \leqslant |x|,\ 0{\cdot}3\,\mathrm{mm} \leqslant |y| \\ &= 0 \qquad \text{otherwise} \end{aligned} \tag{5.1}$$

then the autocorrelation function is given by :

$$\begin{aligned} C(x',y') &= \left[1 - \frac{|x'|}{0{\cdot}6}\right] . \left[1 - \frac{|y'|}{0{\cdot}6}\right] \qquad \begin{matrix} 0{\cdot}6\ \mathrm{mm} \leqslant |x'| \\ 0{\cdot}6\ \mathrm{mm} \leqslant |y'| \end{matrix} \\ &= 0 \qquad \text{otherwise} \end{aligned} \tag{5.2}$$

The result, shown in figure 5.9, plotted in the x' direction is a clearly defined triangle and the half width (corresponding to the side of the square) gives a result of 0.58 ($\pm$0.04) mm.

A slide known as object R was produced on microfilm, cut to 16 mm size and inserted in the gate of the projector. This object is a pair of circles (diameter 0.182 mm) separated by 0.42 mm in the horizontal direction. The result of autocorrelating object R is shown in figure 5.10, and this can be shown to be the function :

$$C(r) = 2d^2 \left[\cos^{-1} r - r\sqrt{1-r^2} \right] \otimes \left\{ \delta(r) + \frac{1}{2} \left(\delta(r-s) + \delta(r+s) \right) \right\} \qquad (5.3)$$

where d is the diameter of each circle and s their separation. The calculated values are marked with a cross in figure 5.10. Figure 5.11 is a contour map of the autocorrelation of object R showing the central and secondary peaks.

A further slide that consisted of a series of object R's orientated in the vertical direction and placed randomly in a frame using a standard random number generator was constructed. As only one slide was available for processing, the result was somewhat noisy, but confirmed the separation of the circles deduced from object R.

It should be noted that the scale size in the x direction is 0.75 times that in the y direction due to the 4 : 3 aspect ratio of the CCD; i.e.

$$\Delta x = 0{\cdot}75\,\Delta y \qquad (5.4)$$

when Δ x and Δ y are measured in pixels.

Object R is used to calibrate the scale of the optical system before each

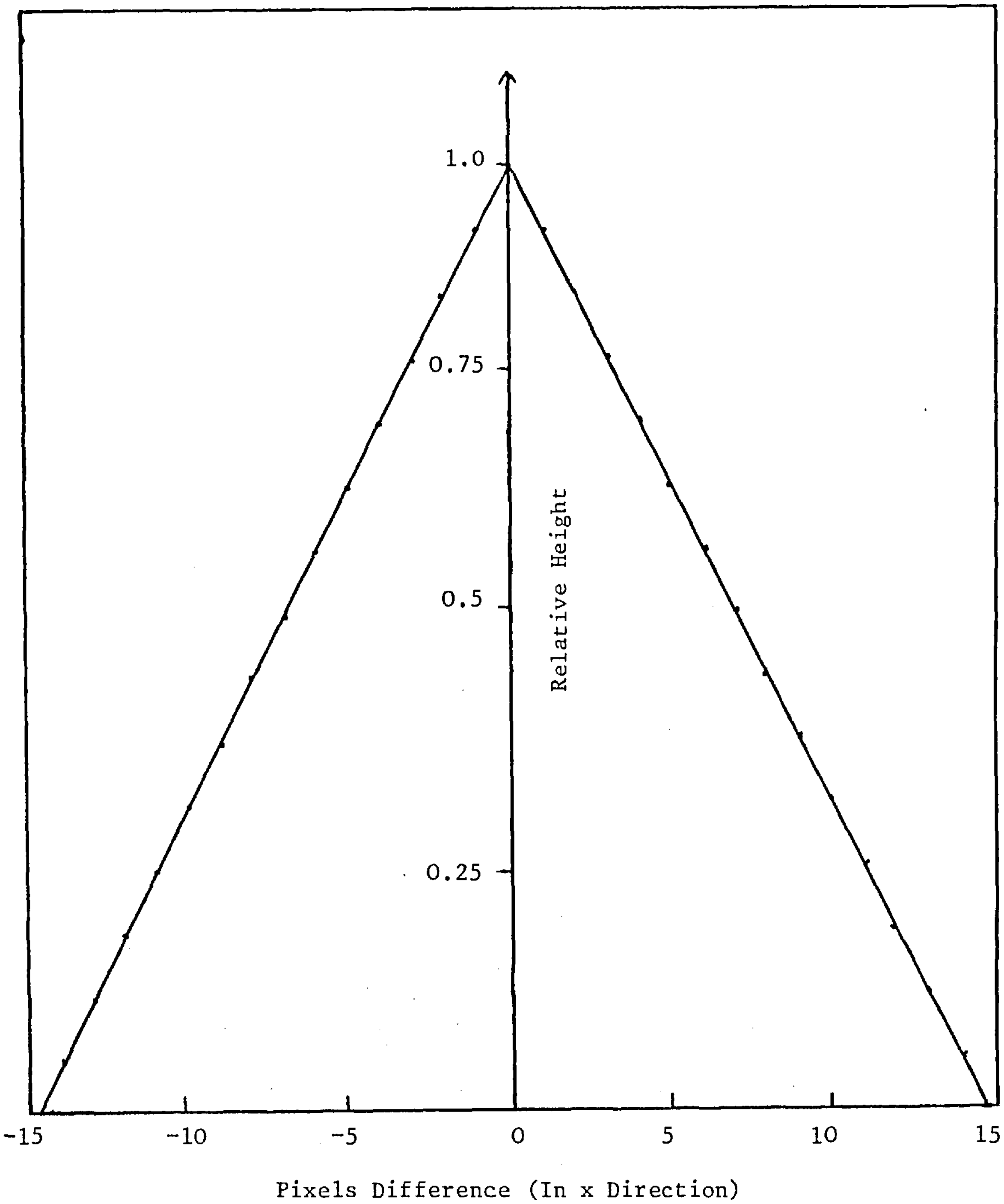

FIG. 5.9: THE AUTOCORRELATION OF RECT (x)

(1 Pixel difference = 0.04mm)

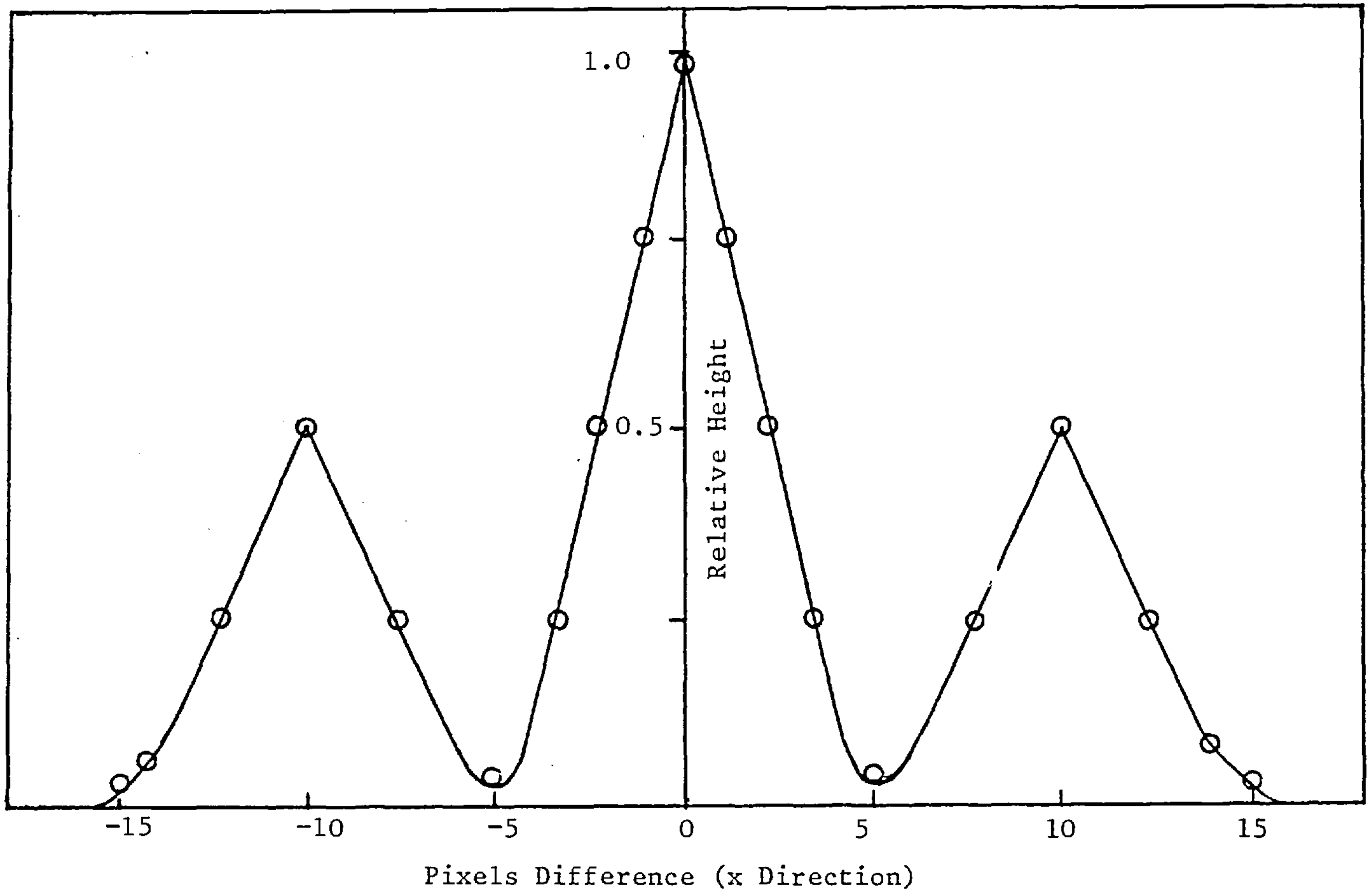

FIG. 5.10: AUTOCORRELATION OF OBJECT R

– = Calculated Curve

O = Experimental Results

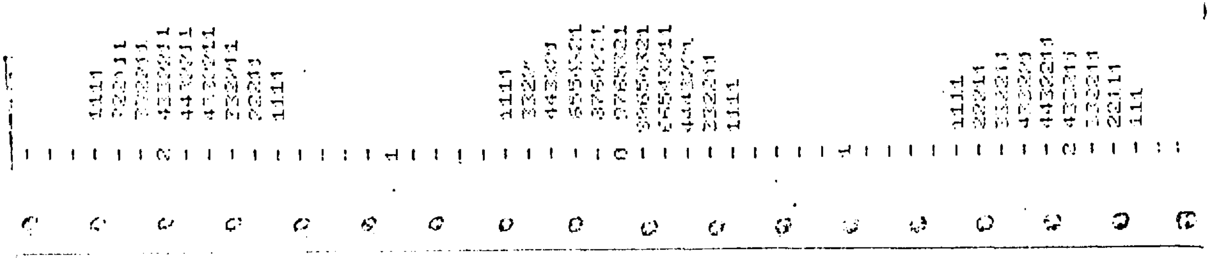

FIG. 5.11: THE CONTOUR MAP OF THE AUTOCORRELATION FUNCTION OF OBJECT R

(Double the Scale of Fig. 5.10)

autocorrelation of stellar speckle data.

5.4.3 Autocorrelation of a speckle pattern produced by Laser light

It was originally discovered by Goldfischer (1965) that the autocorrelation function of a laser speckle pattern is the Airy function of the optical system, and this was confirmed to a high degree of statistical accuracy by McKechnie (1974).

The optical system employed in this experiment is shown in figure 5.12. The beam from the laser is spread using a microscope objective, so that the illumination is slowly varying across the long slit. It is unfortunate that the laser used had several aberrations in the beam profile (nominally gaussian), but the expanded scale ensured that they would not greatly interfere with the diffraction pattern of the slit. It was not possible to "clean" the beam profile using a spatial filtering technique as too much light would be lost in this process. The scatterer was produced in the usual manner by grinding a flat glass plate with fine optical grinding powder.

From Goodman (1975), the resulting autocorrelation function is given by :

$$C(\Delta x,\Delta y) = \langle I\rangle^2 \left[1 + \mathrm{sinc}^2\left(\frac{L_x \Delta x}{\lambda z}\right).\mathrm{sinc}^2\left(\frac{L_y \Delta y}{\lambda z}\right)\right] \tag{5.5}$$

where $\langle I\rangle$ = mean intensity,

λ = wavelength of laser,

$L_{x,y}$ = slit width in x and y direction,

z = distance from aperture to image.

Treating the x and y components of the autocorrelation function separately,

$$C(\Delta x) \propto 1 + \mathrm{sinc}^2 \frac{L_x \Delta x}{\lambda z}$$

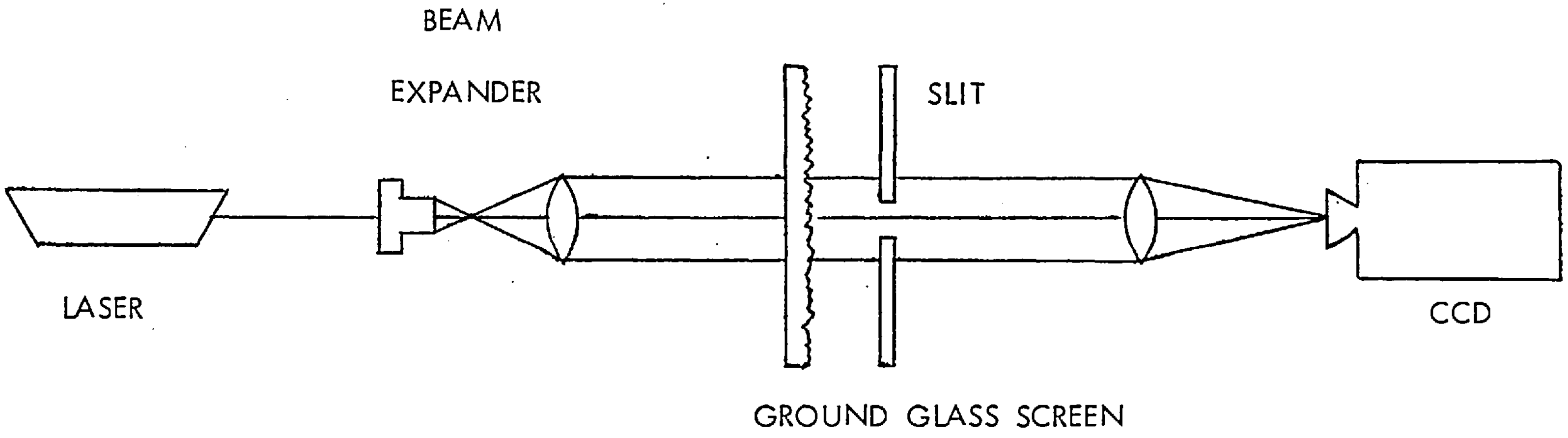

FIG. 5.12 : THE LASER SPECKLE EXPERIMENT

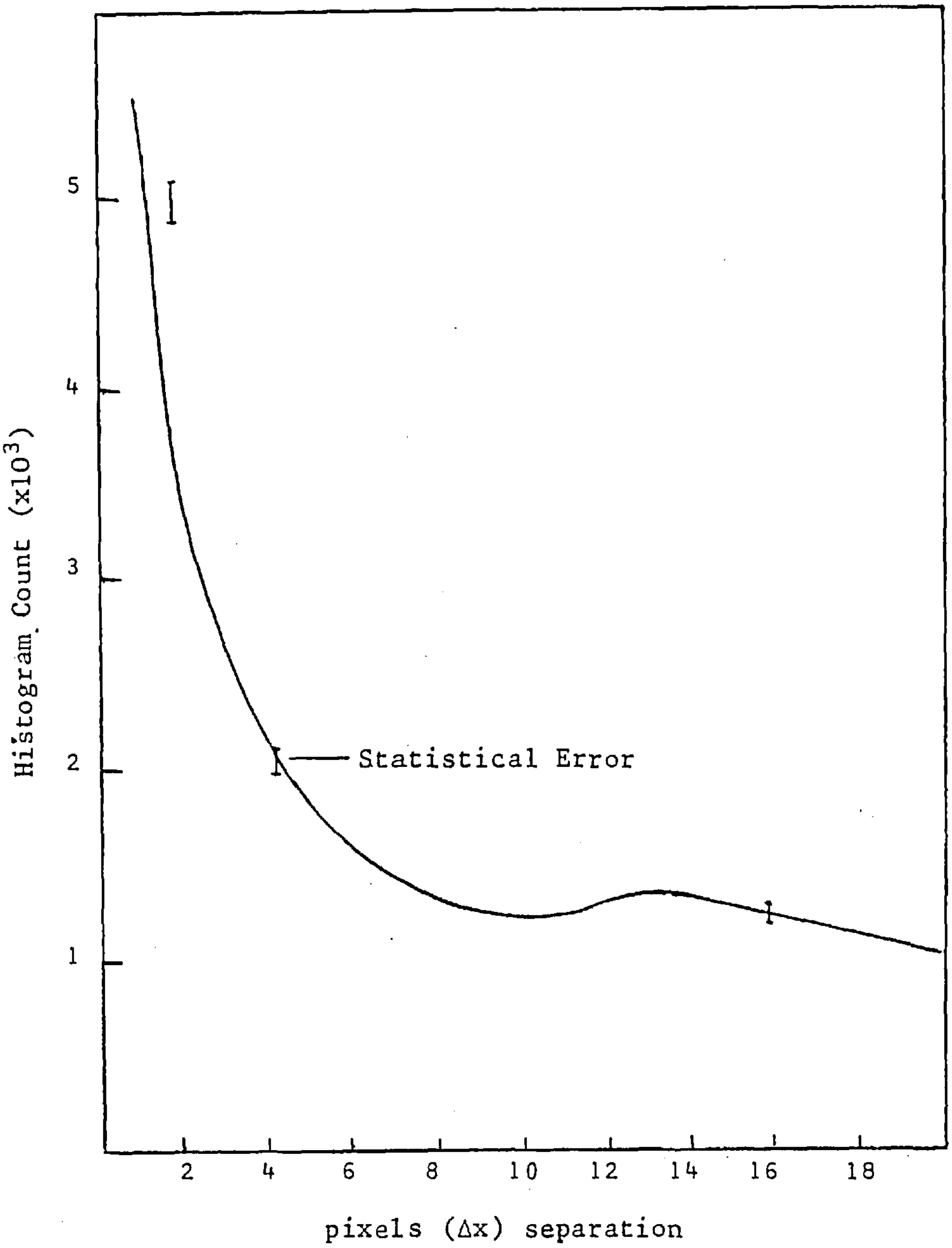

Fig. 5.13: The Autocorrelation of a Speckle Pattern created by a Laser Beam passing initially through a rectangular aperture. The $\left(\frac{\sin x}{x}\right)^2$ pattern is distorted by clipping but the position of the first minimum is visible.

where the sinc^2 expression first falls to zero at

$$\Delta x = \frac{\lambda z}{L_x} \qquad (5.6)$$

The result of the autocorrelation (in the x direction) is shown in figure 5.13. Although the curve is distorted by the clipping process, we know from Bates (1977) that the positions of the zero's of $\mathrm{sinc}^2\left(\frac{L_x \Delta x}{\lambda z}\right)$ are unchanged (see Chapter 4, section 4.5). The measured value of Δx from figure 5.13 (assuming a pixel separation in the x direction of 30 μm) is 0.300 ± .006 mm and from equation 5.6 using $\lambda = 6.33 \times 10^{-9}$m, z = 334.75 ± 0.3 mm, L = 0.705 ± .007 mm, we calculate Δ x as 0.301 ± .003 mm.

The length of the slit in the y direction is 1 cm, so that the distance to the first zero in the y direction would be 0.02 mm, which is below the resolution of the CCD.

CHAPTER SIX

The Results of Reducing Speckle Interferometry Data using a CCD

6.1 Experimental Precautions and Calibration

The results presented here were obtained by reducing the data recorded on cine film using the Imperial College speckle Interferometer (Chapter 4 and Beddoes et al 1976). Successive frames of data were imaged onto the CCD using the optical bench arrangement described in Chapter 5 ; the "hot spots" in the array were removed using the programmes also outlined in that chapter. Further precautions were taken as follows :

i) The light from the condensing optics of the projector was made as uniform as possible by careful alignment of the optics and the introduction of a diffusing screen. The uniformity was found to be ± 5% over the area of the CCD (4 mm x 3 mm) when the image was expanded to a size larger than the CCD imaging area (see section 6.4).

ii) The magnification, and thus the image scale, were measured by using object R (dot separation 0.419 mm ± .003 mm), as outlined in Chapter 5.

iii) Background illumination from the laboratory was reduced to about 5% of saturation level by screening with black cloth.

iv) The speckle images were carefully focussed onto the CCD since defocussing in this apparatus (or in the speckle interferometer) will smooth the statistics of the speckle pattern. The focal tolerance of the optical bench was calculated as about 20 wavelengths (e.g. Born and Wolf 1975). Defocussing by 28 and 55.5 wavelengths causes loss of resolution in the autocorrelation plane, as indicated in Fig. 6.1.

v) Using the light level control (Chapter 5), a level of illumination was set so that bright speckles did not cause blooming in the CCD.

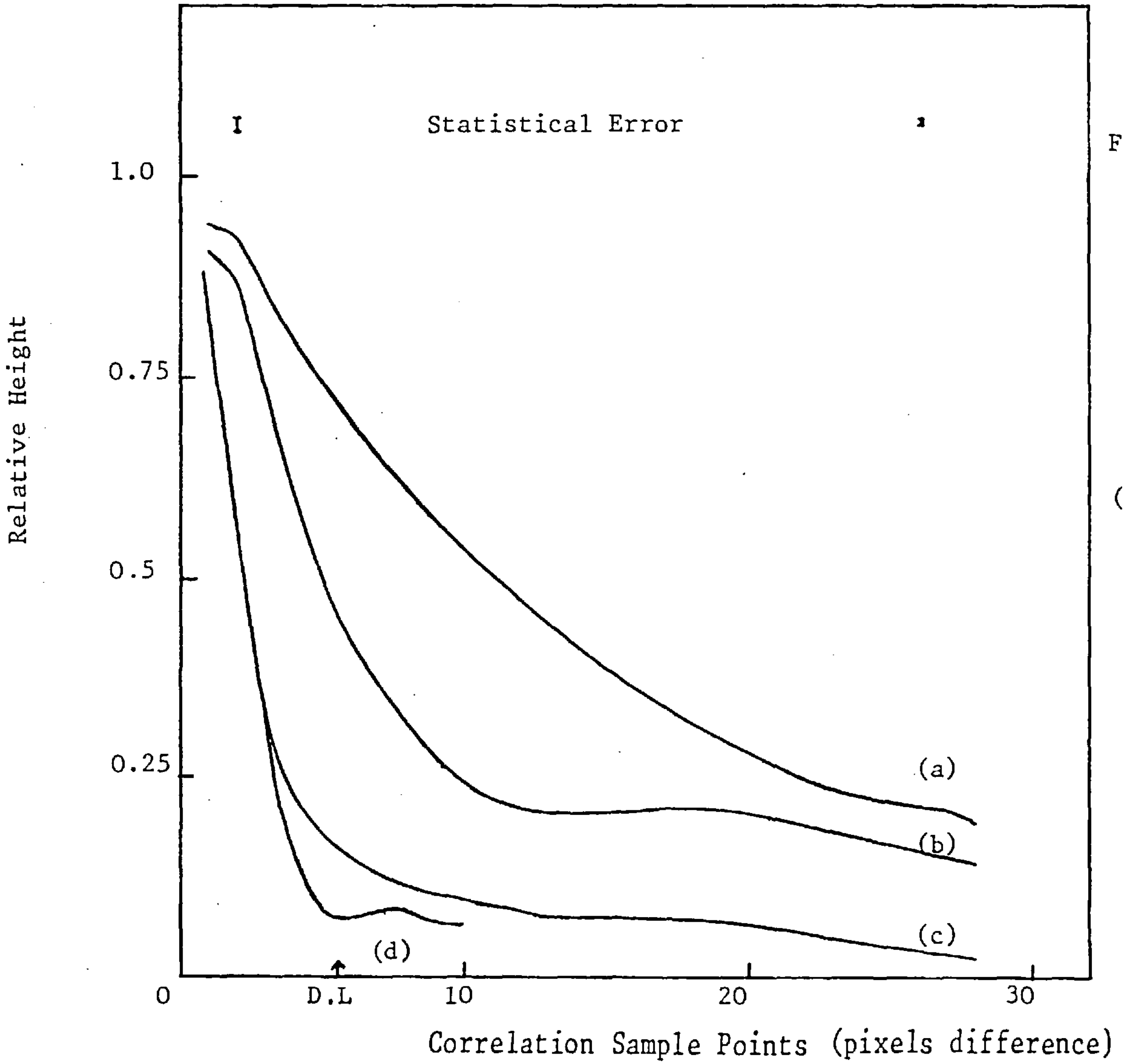

Fig. 6.1: The Effect of Defocussing on the Autocorrelation Function

(a) Defocus 55.5λ

(b) Defocus 28λ

(c) Experimental (Focussed) Curve (Focal Tolerance 20λ)

(d) Theoretical Curve

(D.L is the Telescope Diffraction Limit = 0.05 arseconds)

vi) The discriminator level was adjusted to obtain, on average, about 2.5×10^3 data points from the video picture without overloading the two storage arrays (3STORE and 4STORE ; each 4K data points).

vii) To ensure that the ratio of the average speckle intensity to the equivalent intensity threshold is constant during the experiment, ($\Gamma = \frac{I_D}{\langle I \rangle}$ in Chapter 4), the light level and discriminator level were set and not adjusted again.

viii) At the end of an experiment, the apparatus was again calibrated using object R (Chapter 5).

Calculation of Results and Errors

Once the x,y co-ordinates of the secondary peak in the autocorrelation plane have been determined, the separation and position angle are calculated in the following manner (refer to figures 6.2 and 6.3).

i) Separation

Due to the 4 : 3 aspect ratio of the CCD sampling, the separation r is given by :

$$r^2 = x^2 + \left(\frac{3}{4}y\right)^2 \qquad (6.1)$$

ii) Position Angle

The position angle is Θ where :

$$\Theta = \frac{2\pi}{3}(n-1) + \tan^{-1}\left(\frac{4x}{3y}\right) \qquad (6.2)$$

where n is the number of the quadrant in which the secondary is located (Fig. 6.3), i.e. n = 1 or 4.

There is, of course, an ambiguity of π radians in these angles due to the

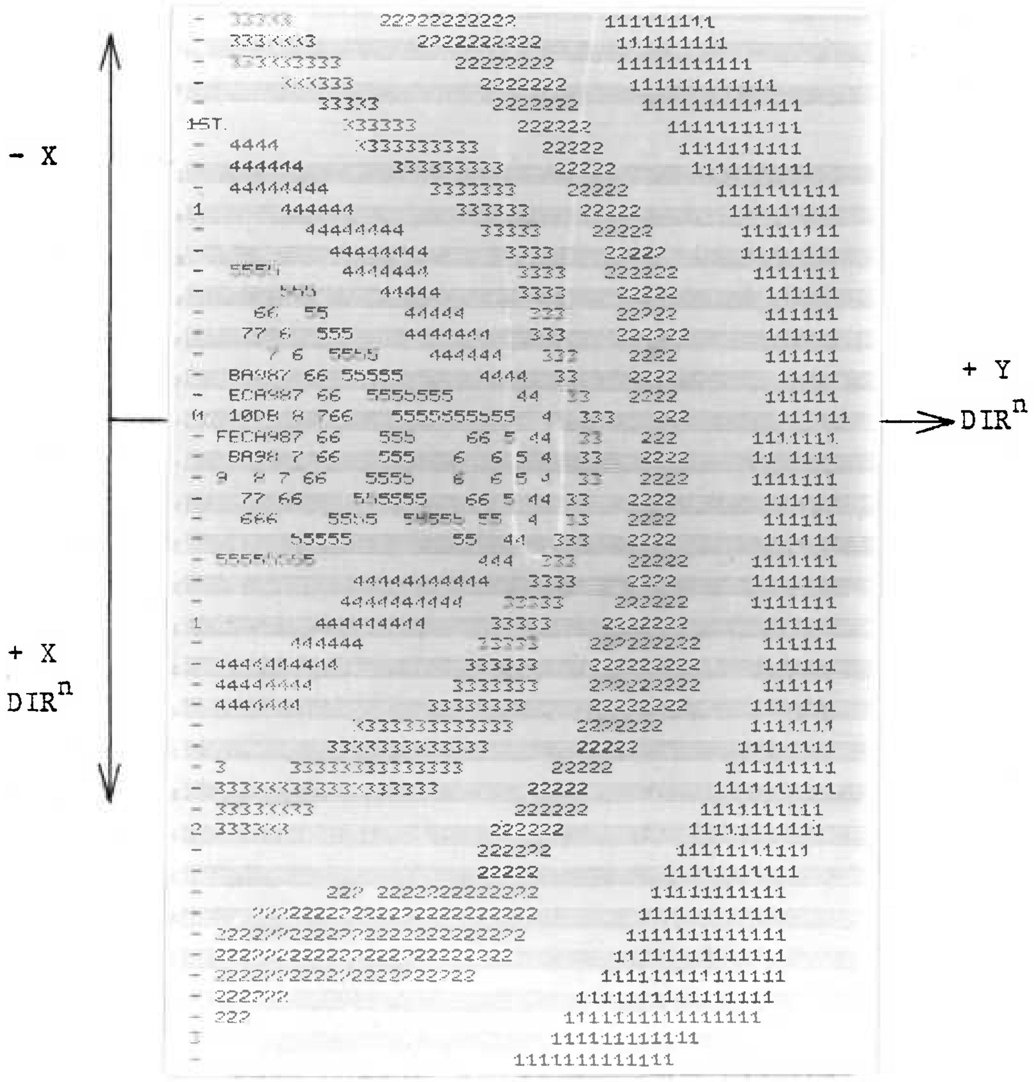

Fig. 6.2: The Two Dimensional Autocorrelation Function of an Artificial Binary Test Film. The Co-ordinate System is shown in more detail in Fig. 6.3. The Secondary Peak is visible to the right of 0, 0 and is surrounded by a Contour Ring of Level 6.

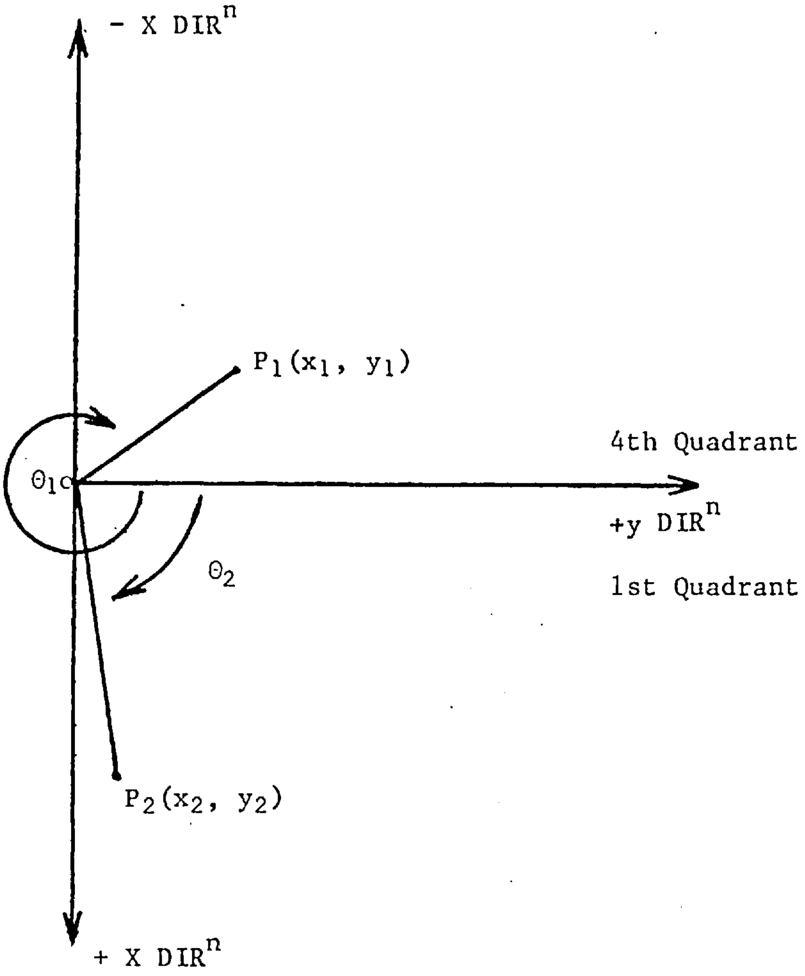

Fig. 6.3: Calculation of Position Angle and Separation from Distances measured in Autocorrelation Plane (c.f. Fig. 6.2)

symmetry of the autocorrelation of a binary star system. This ambiguity can be resolved by inspection of published visual elements, or by inspecting the original data.

Errors

i) Calibration

This is carried out using a slide of a pair of dots imaged onto the CCD. The separation of the dots is known to an accuracy of 0.75%. In general, the secondary peak will fall between two sampling points, and it is possible to judge its position to within half the spacing between sample points. Thus, if the separation of the binary is x divisions, the percentage error is given by :

$$\Delta x = \frac{25}{x} \% \qquad (6.3)$$

so that for a typical separation of 30 divisions, the error is about 1%. The combined error in calibrating is thus ± 1.25%.

ii) Error in reading results

a) Separation

The error in finding the peak of the secondary is the same as indicated above, i.e.

$$\Delta x = \frac{25}{x} \% \qquad (6.4)$$

so that for a separation in the range of 20-40 divisions, this is about 1%.

b) Position angle

The error in estimating the tangent of the position angle,

$$\tan\theta \sim \frac{4x}{3\bar{y}} \qquad (6.5)$$

is obtained by adding in quadrature the errors involved in estimating x and y (see ii a). This is typically about 1°- 2°.

6.2 Early Results

6.2.1 Calcite Test Films

Artificial binary-star systems have been generated from a single star (β Gem) by inserting doubly refracting calcite prisms into the light path of the interferometer. One or both of a pair of prisms is introduced to give apparent binary-star separations of approximately 0.08, 0.20, 0.28, 0.48 arcsec. for the Isaac Newton telescope. Assuming that the light from the star is unpolarized, these artificial binary stars are of equal magnitude. The films were originally created for magnitude difference calibration in the power spectrum (Fourier transform) method (Morgan et al 1978, and Chapter 4). An accurate figure for the separation and position angle of each pair has since been obtained using the power spectrum method. (See Table 6.1)

Three of the artificial binary star films were autocorrelated (e.g. Fig. 6.4) and a good agreement between the two methods of data reduction was found, once a systematic error in the results of the autocorrelation analysis was removed. This was traced to a displacement of the secondary peak caused by the overlap of the steep slope of the primary peak (Fig. 6.4). (The reasons for this are discussed in section 6.4). The profile of the primary peak in a direction perpendicular to the line joining the central and secondary peaks can be obtained, and it is assumed that the (much narrower) secondary peak has no significant effect in this direction. Subtraction of this profile from the area around the secondary peak shifts the secondary back to its original position. This is accomplished digitally using the programme PEAK-FIND (Appendix A). After this shift of about 0.01 arcseconds

Table 6.1 : Comparison of the results of calcite test films by both reduction methods

	POWER SPECTRUM METHOD	AUTOCORRELATION METHOD
i)	$0.278^{\Uparrow}$	$0.277^{\Uparrow}$
ii)	$0.506^{\Uparrow}$	$0.500^{\Uparrow}$
iii)	$0.205^{\Uparrow}$	$0.200^{\Uparrow}$
	Formal error less than 2%	$\pm 1.6\%$

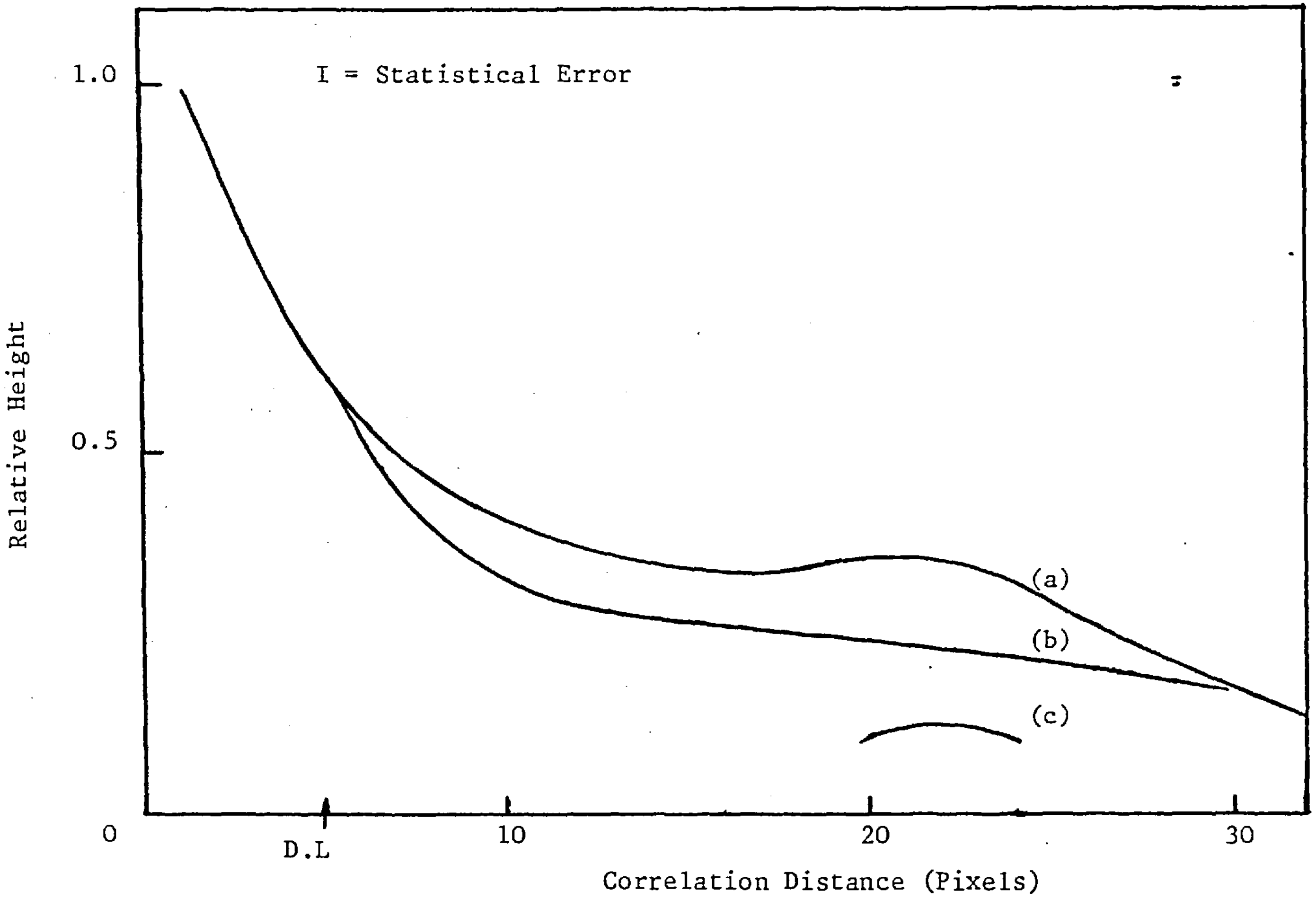

Fig. 6.4: The Autocorrelation of a Calcite Test Film
(D.L is the Diffraction Limit = 0.065 arcseconds)

(a) Secondary Peak (b) Background

(c) Corrected Peak

has been effected, the values of separation agree quite closely.

The profile of the primary and secondary peak of the autocorrelation function should correspond to the Airy function of the telescope used (Lowenthal and Arsenault (1970), Goodman(1975)). This was not found to be the case (see Fig. 6.4) and the investigation carried out is described in section 6.3 and 6.4.

6.2.2 The binary system ADS 10374 (η Oph)

The data for this system (Magnitude 2.46, magnitude difference 0.5) was obtained using the Sutherland 74 inch telescope and was originally reduced by the power spectrum method (Morgan et al 1978). This method arrived at a separation of 0.290 (± 2%) arcseconds and position angle 276.9° (± 2°).

Autocorrelation of 15 frames of data produced the curve shown in Fig. 6.5. Once again the secondary peak was displaced and the shape of the curve distorted. After correction, the result was 0.293 (± 0.01) arcseconds and 274° (± 2°).

6.2.3 The binary star system ADS 14073 (β Del)

The data for this system (magnitude 3.78, magnitude difference 1.0) was obtained using the Kottamia 74 inch telescope. Speckle interferometry data for two different epochs were reduced by the power spectrum method and the results published by Morgan et al (1978). The separation and position angle in these cases were :

i) 0.569 arcseconds, 336.5° (1975.450) ;

ii) 0.565 arcseconds, 348.5° (1975.956).

Data reduced by the autocorrelation method was recorded during the epoch 1978.580 and the separation and position angle obtained from autocorrelating 20 frames were 0.630 (± .01) arcseconds and 0° (± 2°) respectively. Using the previous results of Morgan et al (1978), the expected separation and position angle for this

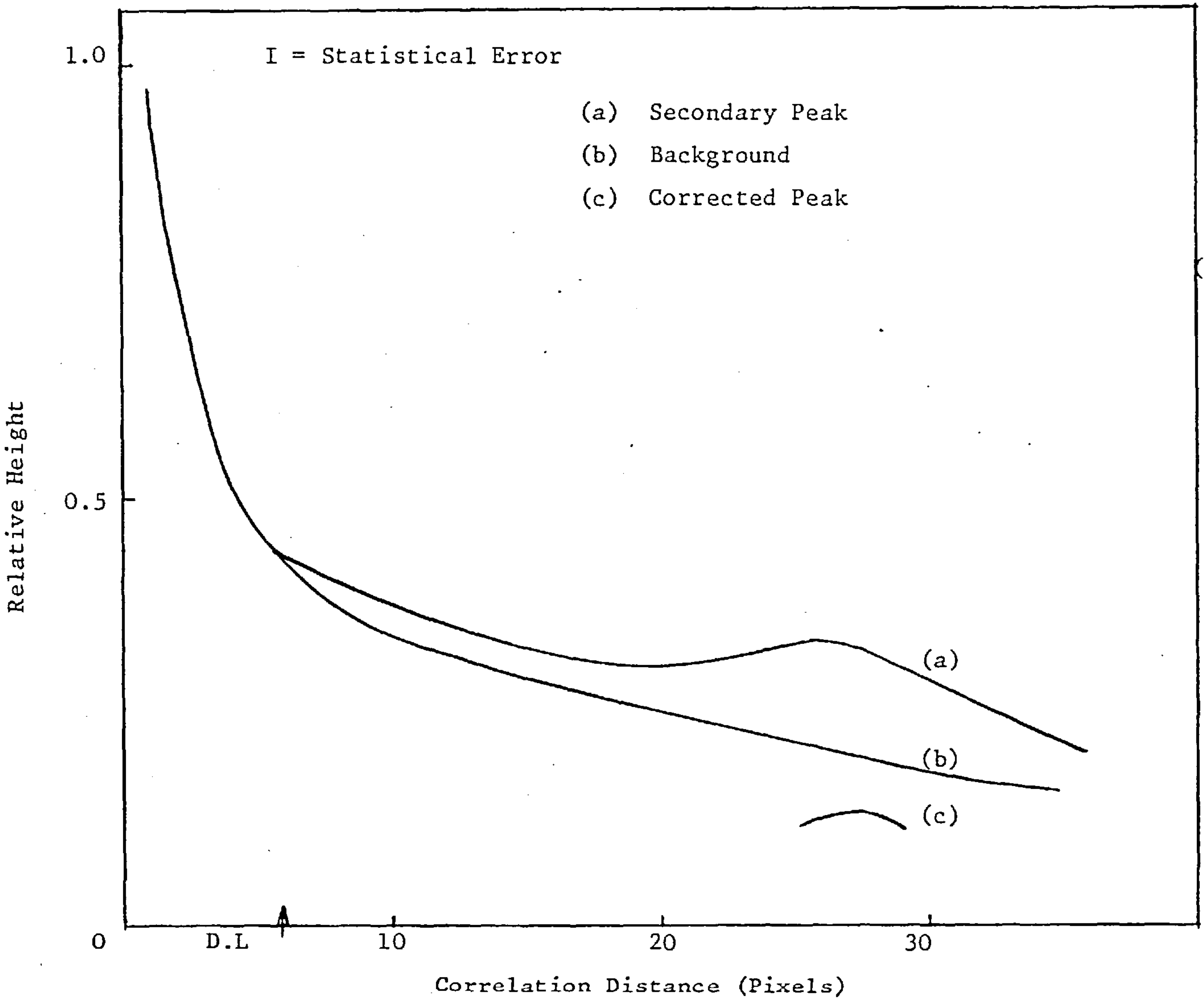

Fig. 6.5: Autocorrelation of η Oph.
(Diffraction Limit (D.L) = 0.065 arsec)

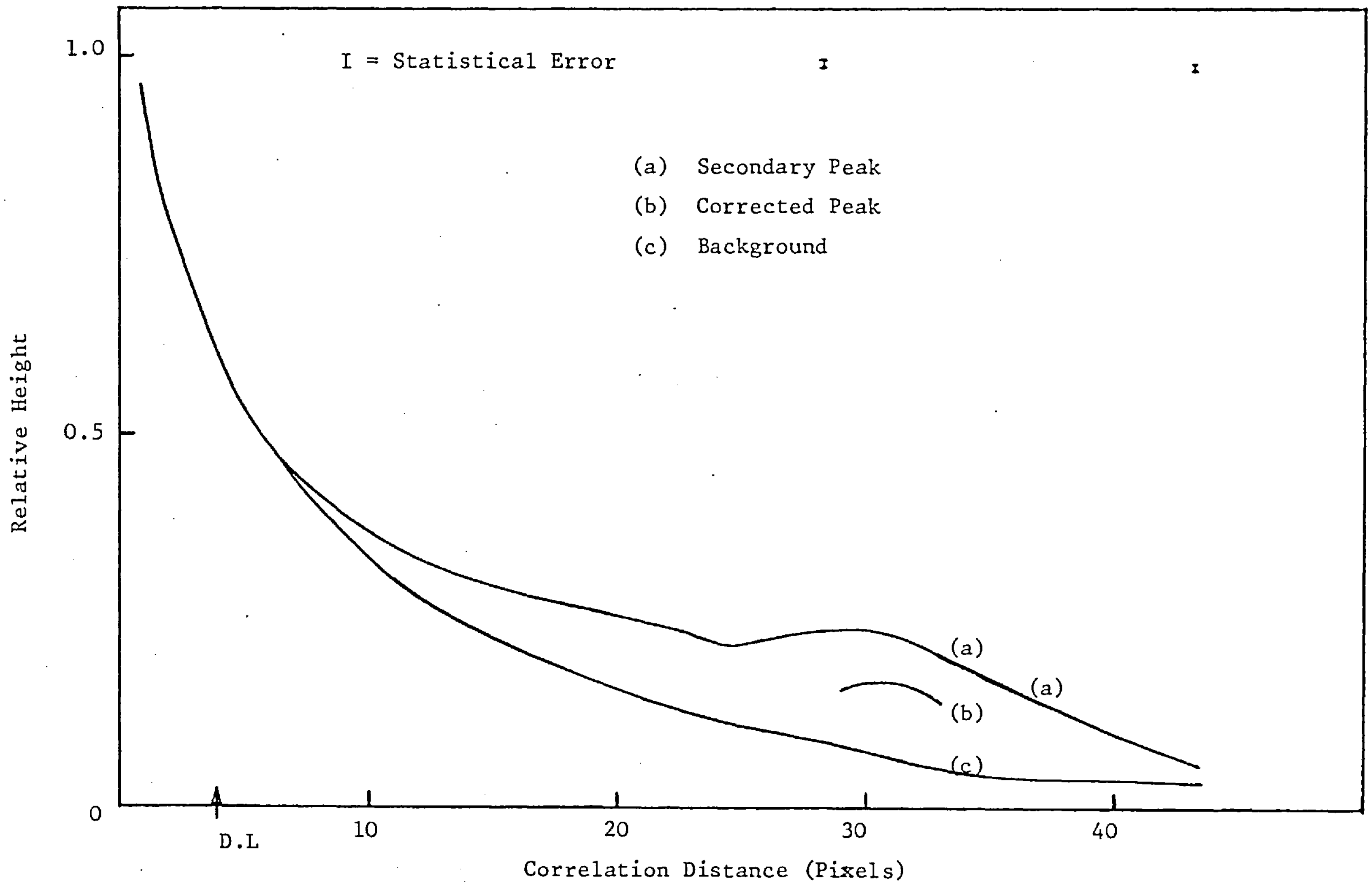

Fig. 6.6: Autocorrelation of β-Del (Diffraction Limit (D.L) = 0.065 arcsec)

epoch were calculated to be 0.626 arcseconds and 1.37°.

Again from figure 6.6, it is clear that the theoretical shape of the autocorrelation function was not obtained (see section 6.4).

6.2.4 The single stars α Ori and β Ori

As pointed out in Chapter 4, it is possible to measure stellar diameters using speckle interferometry because the resolved disc exhibits itself as a broadening of the central autocorrelation peak. Knowing the parallax and spectral type of α Ori (M2 IAB) and β Ori (B8 IA) (Norton 1964), and by using the relation between spectral type and typical diameter (Allen 1973), we can calculate the probable angular diameters to be 0.04 arcseconds for α Ori and 0.001 arcseconds for β Ori. Thus, using data obtained on the Anglo-Australian telescope (diffraction limit 0.03 arcseconds), we may hope to resolve α Ori. The diameter of α Ori has previously been determined using speckle techniques by Lynds et al (1976), who published a figure of 0.044 arcseconds in the TiO band.

The results obtained by autocorrelation are presented in figure 6.7, and it is immediately clear that the profile of β Ori does not correspond to the Airy function of the telescope (see fig. 4·5). In both cases the discriminator level (I_D) was the same and the mean intensity ($\langle I \rangle$) was set as described in section 6.1. Because of the approximate way in which the mean intensity level was set it is impossible to assert that the ratio of the discriminator level to mean intensity level, $\frac{I_D}{\langle I \rangle}$, is identical in both cases, although they are probably very similar.

Although the profile of α Ori is wider, there are two objections to calculating its diameter from this data.

i) In order to obtain the stellar diameter, it is necessary to fit the autocorrelation discs of various diameters to the function. Since the experimental curves do not

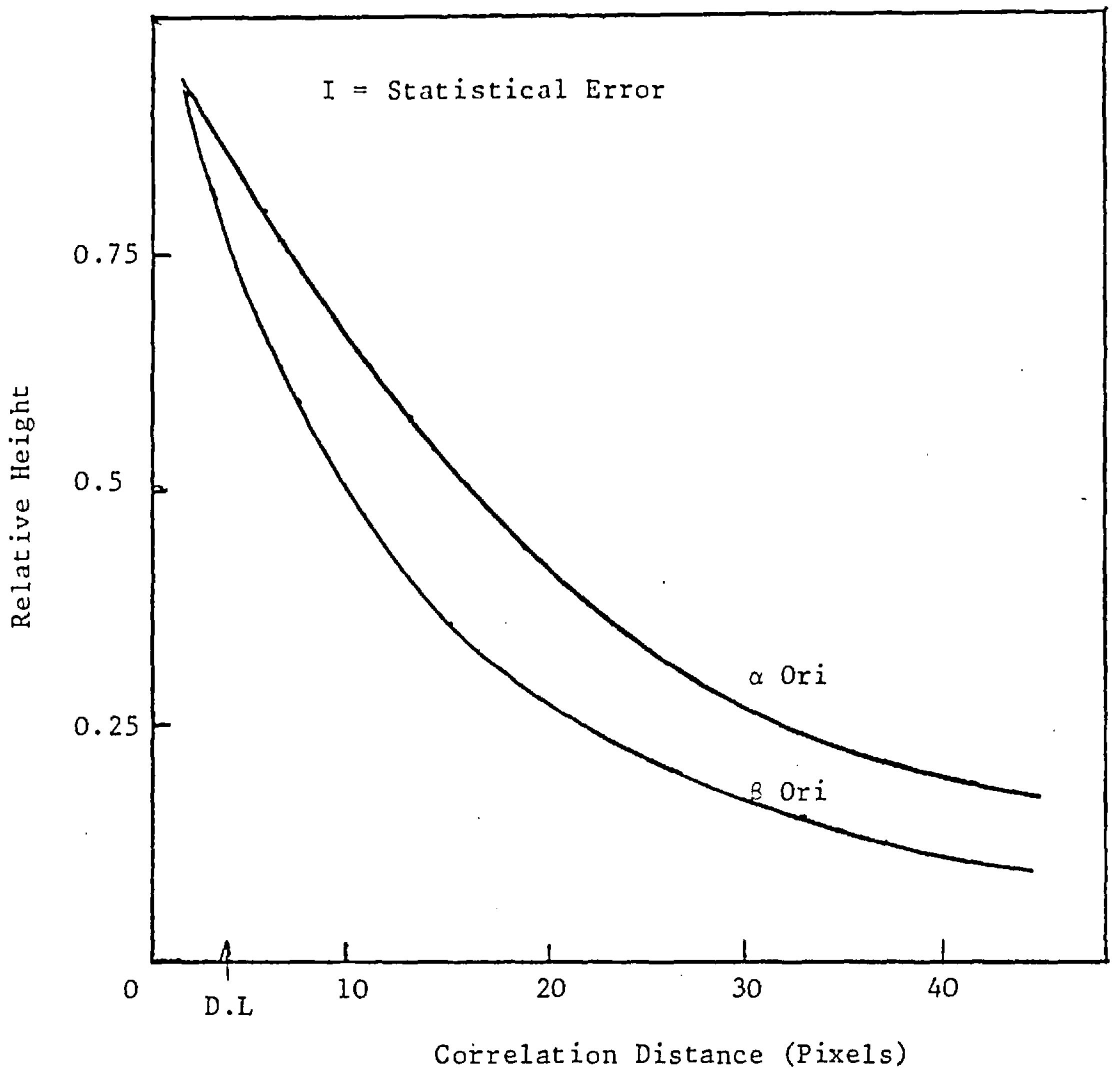

Fig. 6.7: Autocorrelation of α Ori and β Ori
(Diffraction Limit (D.L) = 0.033 arcsec)

conform to the theory and are unknown in analytic form, this procedure is invalid.

ii) From Bates (1977) it is to be expected that the width of the autocorrelation function (i.e. the position of the first minimum) is unaffected by the clipping level. Since the autocorrelation functions obtained departed considerably from the theoretically expected form, we can no longer be sure that this is the case.

The result of an experiment to test the effect of different threshold levels on the shape of the experimental curves is shown in figure 6.8. For the purposes of these experiments, the "width" of the autocorrelation curve is given by the position of the first minimum of the Airy function; any other determination of width will vary with discriminator level. No minimum of the Airy function can be observed in the curves of figure 6.8, making it difficult to arrive at any sensible measurement of "width". The shape of the curves is greatly affected by the ratio of the intensity threshold to the mean intensity level. Thus, if we cannot be certain that the ratio $\frac{I_D}{\langle I \rangle}$ is identical for both α Ori and β Ori (Fig. 6.7), it is uncertain as to whether the difference is caused by a resolved stellar disc.

If, however, we assume that the difference in the curves of figure 6.7 is due to a possibly resolved stellar disc, we can obtain an estimate of the angular diameter of α Ori. Knowing the value of the autocorrelation function of β Ori at the diffraction limit, it can be seen from figure 6.7 that the same value of autocorrelation function for α Ori occurs at an angular diameter of about 0.064 arcsec.

6.3 Discussion

The results presented so far indicate that although useful results can be obtained from the autocorrelation technique, there are several problems associated with it. These can be summarized as follows :

i) The distortion of the curve shape means that the background is not slowly varying

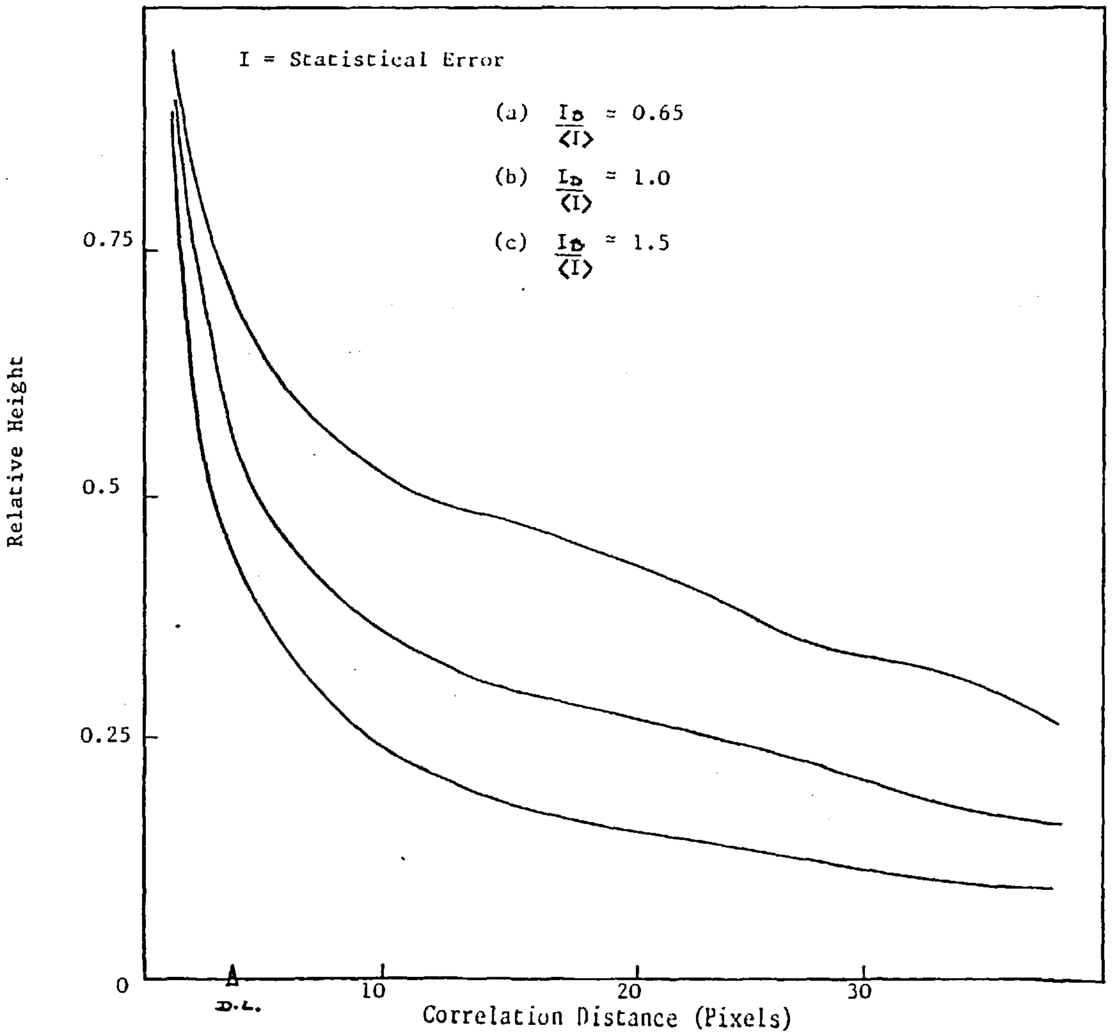

Fig. 6.8: Variation of Central Peak Width with Discriminator Level (Diffraction Limit (D.L) = 0.05 arcsec)

I_D = Discriminator Level

$\langle I \rangle$ = Mean Intensity

across the secondary peak, causing a displacement of the order of 0.01 arcseconds of the secondary peak position (see 6.3 and 6.4).

ii) The overlapping of the peaks may cause the secondary to appear as a "shoulder", making it difficult to locate in the autocorrelation plane.

iii) The secondary peak becomes smeared out and thus does not stand as far above the background as expected (Dainty 1978). This reduces the signal-to-background ratio.

iv) It becomes difficult to resolve stellar discs because the central peak is already wider than expected, and with an unknown form it is not possible to fit theoretical curves to the experimental data.

Difficulties in obtaining the expected autocorrelation function have been found by Lynds et al (1976) and Blazit et al (1977). Labeyrie (1978) has suggested that the peak shape remains intermediate between an Airy disc obtained in extremely poor seeing and an autocorrelated Airy disc obtained in diffraction limited seeing. This suggests that the atmosphere is not a strong scatterer, as assumed in theoretical models.

Recently, two studies of the statistics of stellar speckle patterns at a point in the image plane and the pupil plane have been carried out by Scaddan and Walker (1978) and Parry, Walker and Scaddan (1978). These studies confirm the predictions of classical speckle theory, which is based on the assumption that the atmosphere acts as a strong scattering medium, i.e. its phase fluctuations are greater than 2π.

Thus it is difficult to agree with Labeyrie's suggestion that in good seeing the autocorrelation function is proportional to the autocorrelation of the telescope Airy function. Welford (1975) has shown that speckle patterns formed by a weak scattering medium (phase fluctuation less than 2π) contain a central core that has the shape of the Airy function and Griffin (1973) has, somewhat controversially, claimed to have observed such phenomena by eye. Frame by frame examination of speckle data obtained using the Anglo-Australian telescope in good seeing (on one occasion less than 1 arcsec), reveals no such feature persisting from frame to frame.

It seems likely, therefore, that the statistics of stellar speckle patterns are those expected from a strongly scattering medium.

The finite extent of the seeing disc in the image plane implies that the atmospheric scattering cell size cannot be neglected in comparison to the telescope aperture. However, it has been shown by Goodman (1975) that this does not affect the second order statistics of the speckle pattern.

6.4 The effect of detector sampling

It is, of course, necessary to take account of the Shannon-Whittacker sampling theorem (e.g. Bracewell 1965) when deciding on the image scale. This theorem states that in order to sample every spatial frequency present in the speckle image, sampling must be carried out at at least twice that rate.

The cut off frequency of the power spectrum of a speckle pattern is given by (Goldfischer 1965, Goodman 1975, McKechnie 1974)

$$\omega_m = \frac{1}{\lambda f} \tag{6.6}$$

where λ is the wavelength of the light and f is the f-number of the optical system. Thus, for the Isaac Newton telescope Cassegrain focus, (f/14.2, plate scale 5.9 arcseconds per mm) and at a wavelength of 0.5 μm :

$$\frac{1}{\omega_m} = 0.042 \text{ arcseconds,}$$

i.e. the average "size" of a speckle, so that there must be at least two pixels per speckle to ensure correct sampling.

It has been pointed out by Dainty (1978) that the non-zero integration area of each pixel influences the signal to background ratio (Chapter 4) in two ways. First, the intensity measured by a spatially integrating detector will not be negative exponential. This has been studied by Goodman (1965) who showed that for the first-order statistics, the approximate probability distribution will be a gamma variate. (More exact solutions have been found, e.g. Dainty 1970). Secondly, the quantized sampling interval implies that the secondary peak will, in general, lie between sample points, and determination of the height of the peak above its local background may require the use of interpolation techniques.

Dainty (1978) concludes that it is desirable to make the sampling cell smaller than the speckle size, but that it is not clear whether there is any advantage in making it much smaller.

McKechnie (1974) studied the second order statistics of laser speckle with a finite aperture detector, and concluded that the resulting autocorrelation function is given by :

$$C'(x,y) = C(x,y) * A(x,y) \qquad (6.7)$$

where $C(x,y)$ is the true autocorrelation function, $A(x,y)$ is the autocorrelation of the aperture function and * denotes convolution.

A series of experiments was designed in which the scale of the image falling on the CCD could be varied in order to change the sampling rate. The approximate sampling rates used were :

i) 4 photosites per speckle,

ii) 25 photosites per speckle,

iii) 100 photosites per speckle,

iv) 256 photosites per speckle.

Cine films of two separate binary star systems were used in these tests. The first was a film of β - Cep (ADS 15032, HD 205021) taken with the 98 inch Isaac Newton Telescope (diffraction limit 0.05 arcsec) at Herstmonceux in about 3 - 4 arcsec seeing, and the second is a film of β - Del (ADS 14073, HD 196524) taken with the 74 inch Kottamia Telescope in Egypt (diffraction limit 0.065 arcsec) in 2 - 3 arcsec seeing. These films were chosen because they were well focussed and obtained at different sites in different seeing conditions. Details of previous results can be found in Morgan et al (1978).

With the size of scale used in these tests, the secondary peak lies outside the area of the CCD. Profiles of the central peak (as a measure of the success of the autocorrelation) were taken at right angles to the line joining the central and secondary peaks. The effect of progressively increasing the image scale of β - Cep is shown in fig. 6.9 for four different sampling rates. Although it is to be expected that the autocorrelation function is affected by the pixel area, the extent of the sensitivity of the speckle statistics to integration is surprising. As the sampling rate rises to about 49 pixels/speckle (Figure 6.9 (b)), the autocorrelation function begins to exhibit a slight minimum in the region of the diffraction limit (D.L.). When the sampling rate rises to about 100 pixels/speckle (Fig. 6.9 (c)), the form of the Airy function becomes fairly clear. For a more detailed comparison between the theoretical and experimental curves, they are plotted on a logarithmic scale. In fig. 6.10 the experimental curve is the central peak of the autocorrelation of β - Cep taken at the Isaac Newton telescope (diffraction limit 0.05 arcseconds). The calculated curve is the Airy pattern of this telescope (modified to include the central obscuration), placed on a Gaussian background (σ = 1 arcsecond) and

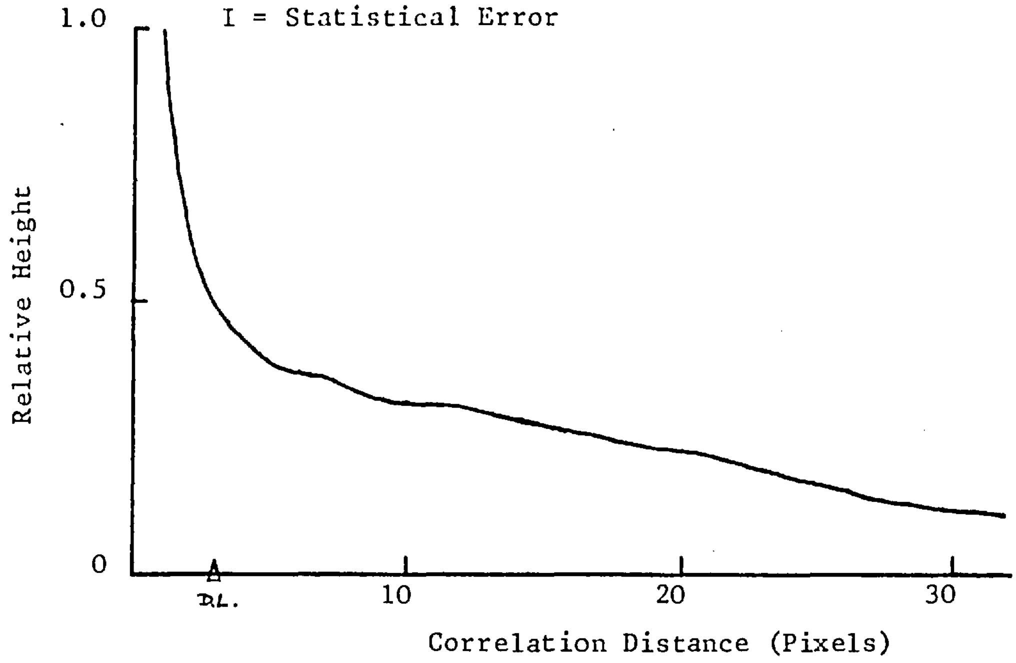

(a)

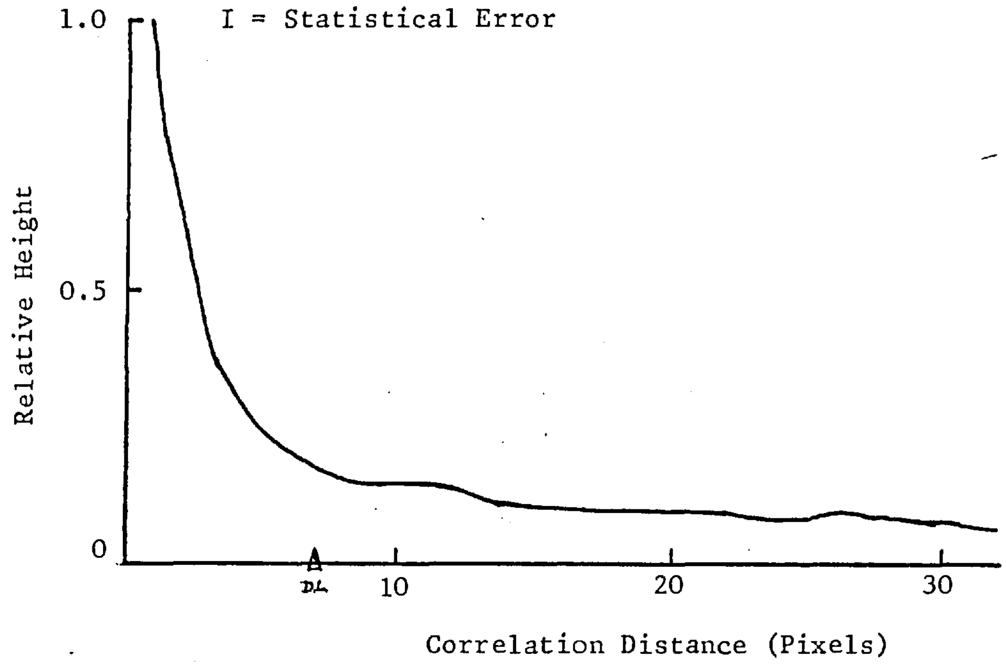

(b)

Fig. 6.9: Variation of Autocorrelation Function of β Cep with Sampling Rate (Diffraction Limit (DL) = 0.05 arcsec)

(a) 9 pixels/speckle

(b) 49 pixels/speckle

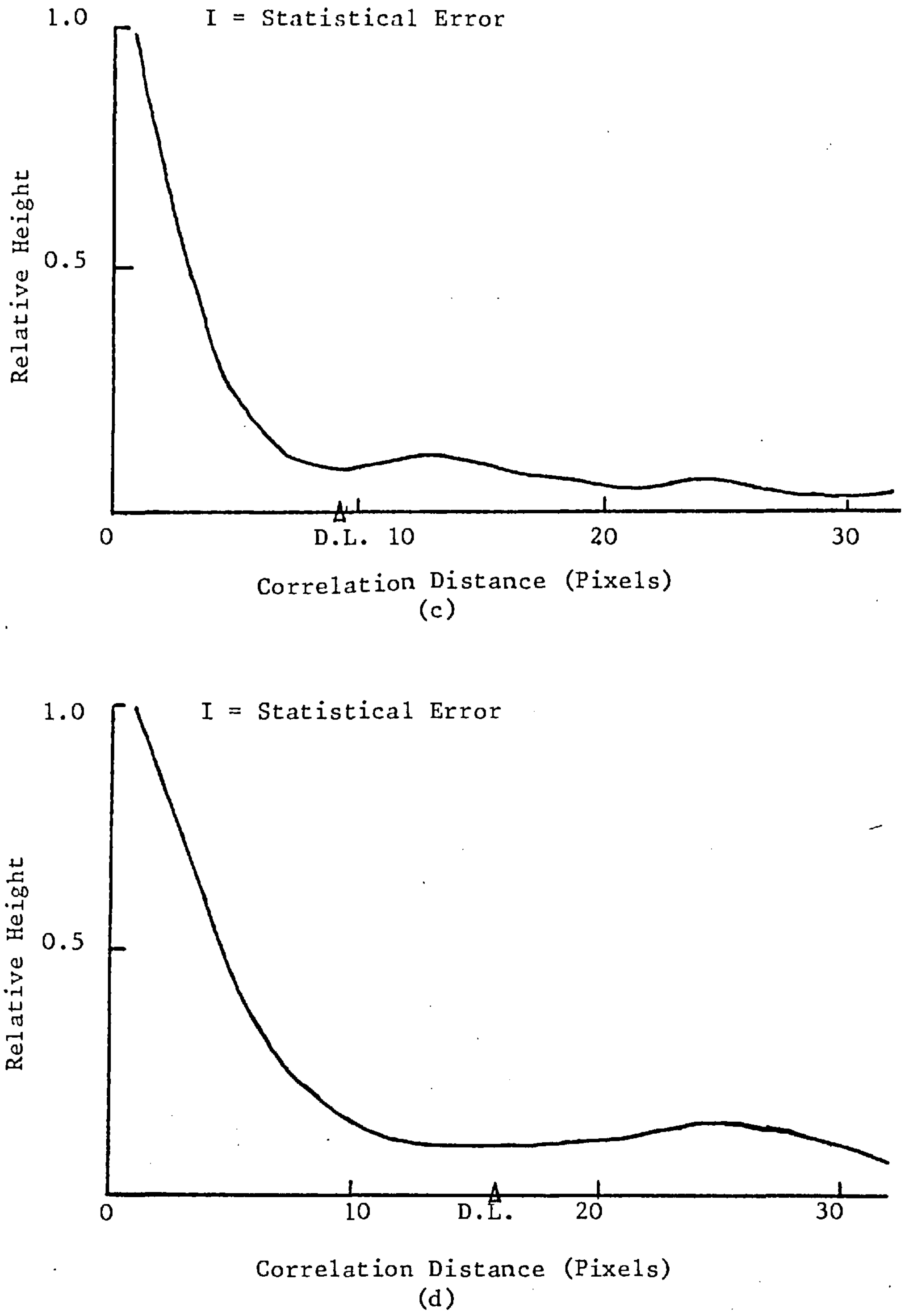

Fig. 6.9: Variation of Autocorrelation Function of β Cep with Sampling Rate (Diffraction Limit (DL) = 0.05 arcsec)

(c) 100 pixels/speckle

(d) 256 pixels/speckle

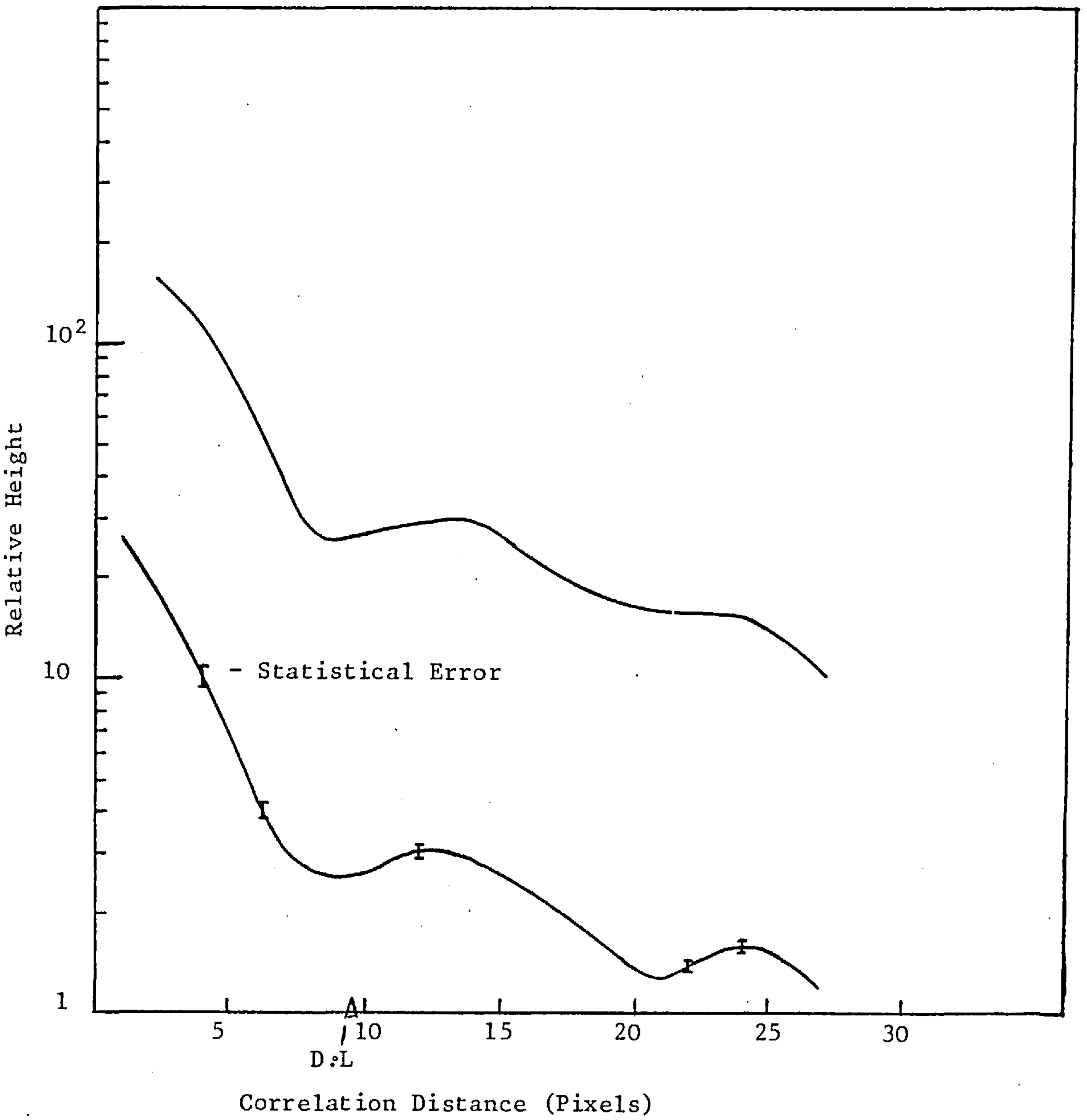

Fig. 6.10: Autocorrelation of β-Cep (Experimental Curve (b))
Diffraction Limit (D.L) = 0.05 arcsec.

Curve (a) is a Calculated Result Offset for Comparison distorted by clipping according to equation 5.31 ($I_D / \langle I \rangle = 1.8$). In figure 6.11 the autocorrelation central peak is that of β - Del with the profile taken at right angles to the line joining the central peak to the secondary, as for β-Cep. This data was obtained using the Kottamia telescope in Egypt (diffraction limit 0.065 arcseconds), and the comparison curve is calculated as for that in fig. 6.10 and scaled for the different diffraction limit.

There is good agreement in both cases, although the experimental curves tend to fall away slightly faster than the calculated curves with some anomalous features at around 30 pixels. This may be explained as due to the correlation being calculated over a finite range.

Two further illustrations of this are shown in figures 6.12 and 6.13. Figure 6.12 is the autocorrelation of the speckle pattern due to the single unresolved star Arcturus. A minimum in the function is clearly visible at the diffraction limit, but the second minimum occurs rather sooner than expected; the reasons for this are unknown. Fig. 6.13 is the autocorrelation of the single unresolved star Vega, with the first and second minima in the expected position. Both sets of data were obtained using the 74 inch telescope at Haute Provence (diffraction limit 0.065 arcseconds). Again we note that the background (dotted line) falls more steeply than expected for the first 30 pixels and then tends to flatten out.

To test the effect of a finite correlation range and clipping on the background of the autocorrelation function, the following calculation was made.

Assuming the statistics of a point in the speckle pattern are negative exponential (i.e. a high sampling rate), then the probability of a speckle being brighter than the discriminator threshold (I_D) is given by :

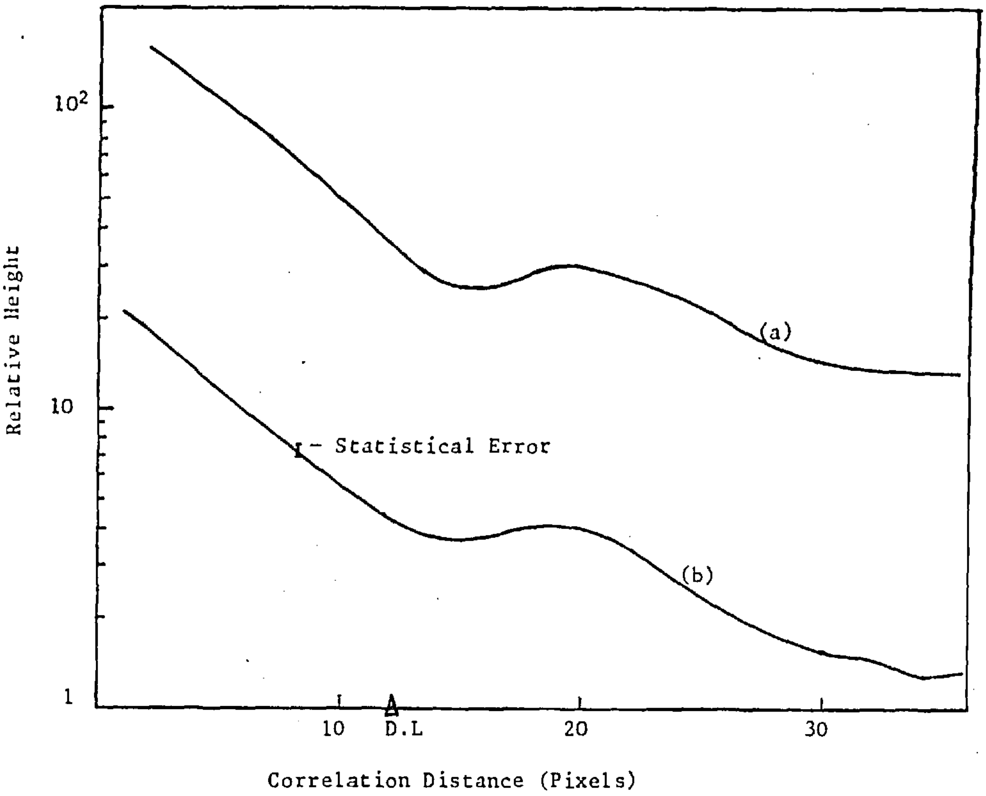

Fig. 6.11: Autocorrelation of β-Del (Curve (b))
Diffraction Limit (D.L) = 0.065 arcsec.

Curve (a) is a calculated Result Offset for Comparison

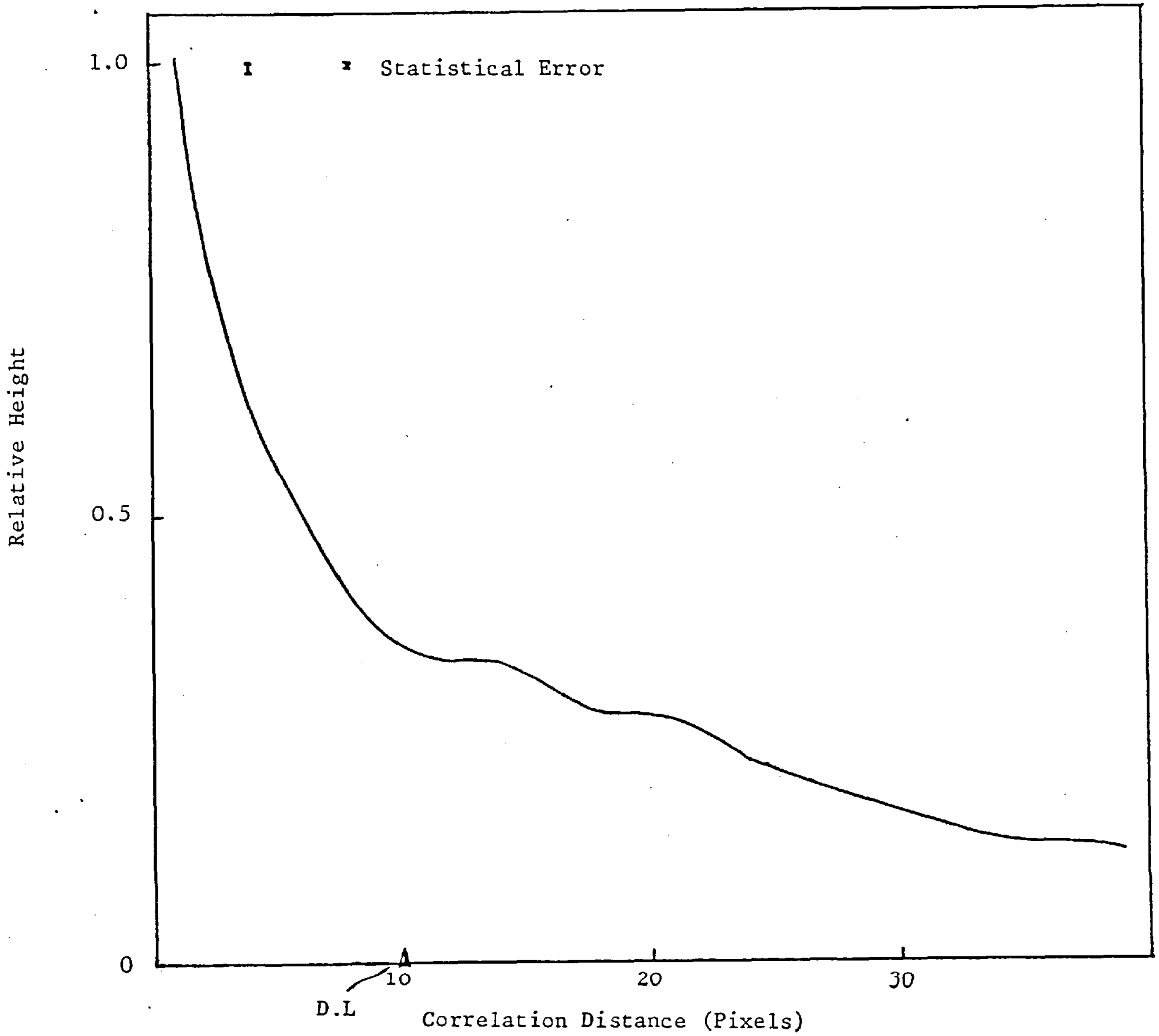

Fig. 6.12: Autocorrelation of Arcturus (Diffraction Limit = 0.065 arcsec)

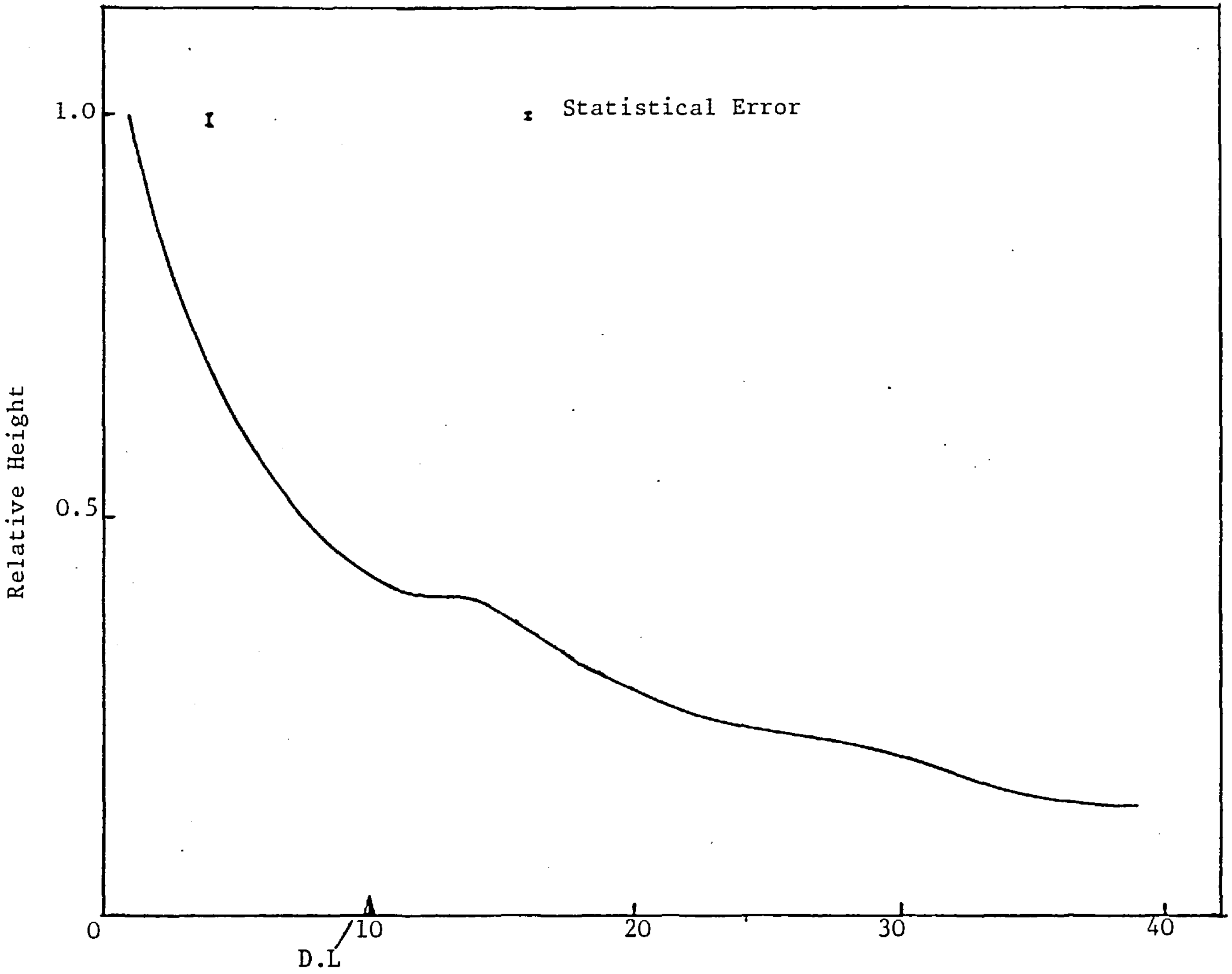

Fig. 6.13: Autocorrelation of Vega (Diffraction Limit (D.L) = 0.065 arcsec)

$$P(I > I_D) = \frac{1}{I_o} \int_{I_D}^{\infty} \exp\left(-\frac{I}{I_o}\right) dI \ ,$$

$$i.e. \quad P(I > I\ ) = \exp\left(-\frac{I_{D-}}{I_o}\right) \tag{6.8}$$

where I_o is the mean speckle intensity.

If separations greater than the correlation length of the speckle pattern are considered (i.e. intensities at different points are independent), the autocorrelation function is given by :

$$C(\tau) \propto \int_{-\infty}^{+\infty} P\left(I(x) > I_D\right) . P\left(I(x+\tau) > I_D\right) dx \tag{6.9}$$

In a real speckle pattern, there is an envelope which makes the statistics non-stationary and a finite limit to the separations in the correlation. Thus the autocorrelation function becomes (using 6.9 and 6.8) :

$$C(\tau) \propto \int_0^L \exp\left\{ -I_D\left[I_o^{-1}(x) + I_o^{-1}(x+\tau) \right]\right\} dx \tag{6.10}$$

It is normally assumed that the envelope can be approximated by :

$$I_o(x) = I_o e^{-x^2/\sigma^2} \tag{6.11}$$

where σ is a measure of the seeing disc. For convenience, we will assume that $I_o(x)$ is slowly varying and make the approximation :

$$\left[e^{-x^2/\sigma^2} \right]^{-1} \approx 1 + \frac{x^2}{\sigma^2} \tag{6.12}$$

Substituting into 6.10 and dropping constant terms, we obtain :

$$C(\tau) \propto e^{-\frac{I_D}{2}\frac{\tau^2}{\sigma^2 I_0}} \int_0^L \exp\left\{ -\frac{2 I_D}{I_0 \sigma^2}\left(x + \tau/2\right)^2 \right\} dx \tag{6.13}$$

Putting $k = \frac{2 I_D}{I_0 \sigma^2}$, substituting $t^2 = 2k\,(x + \tau/2)^2$ and rearranging gives :

$$C(\tau) \propto e^{\frac{-k\tau^2}{4}} \int_{\sqrt{2k}\,\tau/2}^{\sqrt{2k}\,(L + \tau/2)} e^{-t^2/2}\, dt \tag{6.14}$$

If $2w$ is the length of the image scanning area, then

$$L = 2w - \tau \tag{6.15}$$

so that :

$$C(\tau) \propto e^{\frac{-k\tau^2}{4}} \int_{\sqrt{2k}\,\tau/2}^{\sqrt{2k}\,(2w - \tau/2)} e^{-t^2/2}\, dt \tag{6.16}$$

and evaluating the integral :

$$C(\tau) \propto e^{\frac{-k\tau^2}{4}} \Big[\operatorname{erf}\left(\sqrt{2k}\,(2w - \tau/2)\right) - \operatorname{erf}\left(\sqrt{2k}\ \tau/2\right) \Big] \tag{6.17}$$

where erf (x) is the error function defined by :

$$\operatorname{erf}(x) = \frac{1}{\sqrt{2\pi}} \int_{-\infty}^{x} e^{-t^2/2}\, dt \tag{6.18}$$

This function is plotted in Fig. 6.14 for typical values of k and w. For comparison, the unclipped, undistorted background is also shown. Equation 6.17 when used with the formula derived by Bates (1977) (see Chapter 5) for the effect of clipping on the autocorrelation function, provides a complete description of the autocorrelation function.

6.5 Summary

We have shown that unless the detector sampling rate is very high (greater than 64 pixels/speckle : section 6.4), the autocorrelation function becomes distorted to the extent that the first minimum of the Airy function cannot be observed. This is important when studying stellar discs. In the case of binary star systems, such an image scale expansion will usually mean that the secondary peak falls outside the range of the autocorrelation function. Thus it is necessary to trade autocorrelation distortion for binary separation resolution in this case. The resulting distortion, as shown in section 6.2, will generally cause the secondary peak to become less visible above the background, thus altering the signal-to-background ratio.

The data for the results of autocorrelating β Cep, β Del, Arcturus and Vega were obtained at different telescope site in different seeing conditions, suggesting that the atmosphere acts as a rough transmitting medium (i.e. phase fluctuations greater than 2π) under a wide variety of conditions.

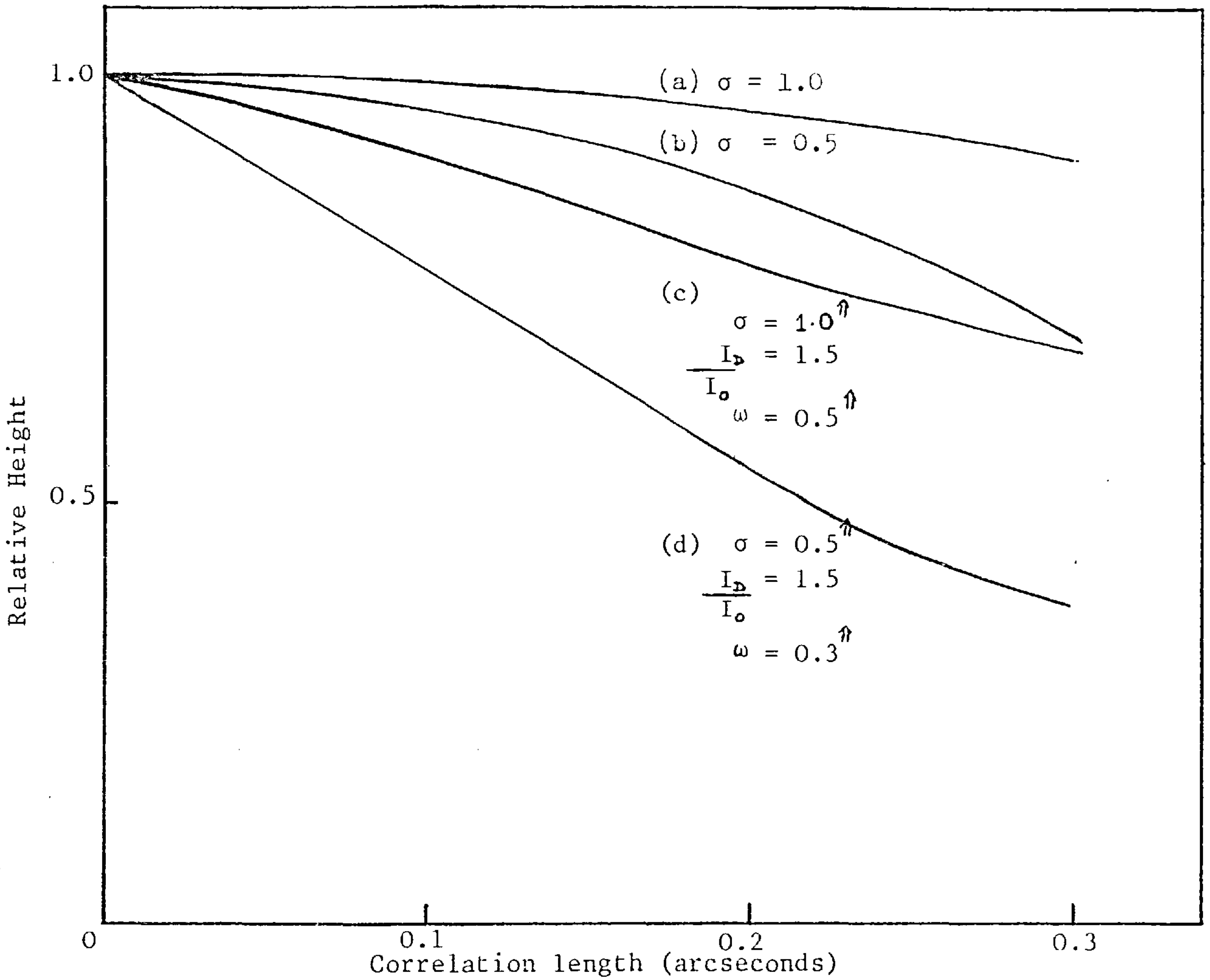

Fig. 6.14: Calculated Background. (a), (b): Unclipped, Unlimited, (c), (d): Clipped, Limited

CHAPTER 7

PHOTON COUNTING

7.1 Introduction

It is clear from the work reported in Chapter 2 that a prior stage of intensification is necessary if the CCD is to detect single photon events unambiguously. This chapter considers a possible design for a suitable image intensifier. For maximum detective quantum efficiency (DQE), it is important to record each photon event with the same weighting; this follows from the work of Mandel (1959), from which it can be deduced that:

$$E_D = \frac{E_r \ f}{1 + \frac{\overline{\Delta^2 g}}{\overline{g}^{\,2}}} \qquad (7.1)$$

where E_r is the responsive quantum efficiency, f the fraction of detected events recorded and $\overline{g}$ the weighting.

The output of an intensifier for a single photon event input will fluctuate around a mean value and clearly it will be a considerable advantage if the output of the intensifier is capable of saturating a CCD photosite so that each event is recorded with the same weighting.

Data transfer between the intensifier and the CCD is effected either by arranging that the CCD is directly bombarded by the photo-electrons or that the photo-electrons fall on a phosphor screen whose light output is imaged onto the CCD.

The first approach has been exploited in the Digicon device (Beaver and McIlwain 1971, Beaver et al 1976, Choisser 1976, Beaver 1978), and also in the instrument built by Currie (1976), but there are two objections to this design.

i) Difficulty is experienced in bringing the CCD leads out of the intensifier envelope.

ii) It has been suggested by Mende and Chaffee (1977) that direct electron bombardment can damage the CCD architecture, shortening its useful life.

Optical coupling is an easier approach using either a lens (e.g. Geary 1976) or a fibre-optic bundle (e.g. Reigler and More 1973). Transfer losses due to phosphor conversion inefficiency and lens or fibre-optic transfer inefficiency means that an intensifier of higher gain than in the direct bombardment case is needed, but this is offset by the ease with which intensifiers and CCD's could be interchanged when optically coupled. For a pair of lenses of aperture f/1.2 connected back to back (1 : 1 magnification), a transmission of 11.8% can be expected, whereas a fibre-optic plate (with resolution comparable to that of a good lens) has a transmission of about 70%. Fibre-optic plates must be polished flat to better than 1μm, before coupling and image defects such as Moire patterns, small scale image shear and "chicken-wire" effects can occur. It was felt, therefore, that lens coupling would simplify construction initially, although this could be replaced by fibre-optic coupling later should the extra light transmission be necessary.

7.2 Phosphor/CCD Spectral Matching

There are two factors governing the choice of phosphor screen at the output of the intensifier. The first is the efficiency with which the photo-electrons are converted into photons, and the second is the goodness of the match between the phosphor output spectrum and the CCD spectral response.

In general, for any radiation detector, the output response is given by (Eberhardt 1968):

$$I = S_p W_p \int_0^{\infty} \sigma_\lambda \, w_\lambda \, d\lambda \tag{7.2}$$

where σ_λ is the normalised detector spectral distribution, w_λ is the normalised light source spectral distribution, S_p is the peak monochromatic response of the detector and W_p is the peak monochromatic response of the light source. The integral luminous flux of a light source is given by:

$$F = W_p \int_0^{\infty} W_\lambda \, d\lambda \tag{7.3}$$

and hence the detector responsivity by:

$$R = \frac{I}{F} = \frac{S_p W_p \int_0^{\infty} \sigma_\lambda \, W_\lambda \, d\lambda}{W_p \int_0^{\infty} W_\lambda \, d\lambda} = S_p \alpha_{DS} \tag{7.4}$$

where $\alpha_{DS} = \dfrac{\int_0^{\infty} \sigma_\lambda \, W_\lambda \, d_\lambda}{\int_0^{\infty} W_\lambda \, d_\lambda}$ is the source detector spectral matching factor.

Values of α_{DS} for various phosphors and a typical CCD spectral response have been calculated by Airey (1974) and are listed below with the phosphor efficiencies.

	P.11(Zn.S.Ag)	P.20(Zn.CdS.Ag	P.22R(Gd.O_4.Eu)
Efficiency (E)	0.12	0.14	0.085
α_{DS}	0.258	0.563	0.832
$E.\alpha_{DS}$	0.031	0.079	0.071

Thus we see that the P.20 phosphor is slightly more efficient than the P.22R. However the P.22R phosphor has a decay time (to 10% of maximum signal) of 10μs compared to about 1ms for the P.20. In order to improve temporal resolution the P.22R phosphor was chosen for the intensifier. The peak wavelength of photons emitted by this phosphor is about 0.655μm and it is interesting to note from Chapter 2 that at 0.644μm, the CCD is saturated (at 28ms/frame) by 2.86×10^6 photons/pixel.

We are now in a position to calculate the gain required from the intensifier if saturation of the CCD is to occur. Denoting the phosphor efficiency by E, and the lens coupling transmission by L, then the amount of energy that must be incident on the phosphor for a single photon input is:

$$E' = \frac{2.86 \times 10^6}{E\ L} \cdot \frac{hc}{\lambda} \qquad (7.5)$$

and for $E = 0.085$, $L = 11.8\%$, $\lambda = \cdot 655\mu m$, this is:

$$E' \simeq 5.5 \times 10^8 \text{ eV}.$$

Clearly, such a gain can only be provided by a cascade image intensifier or by a micro-channel plate intensifier. Two experiments were conducted in which the output of a commercially available intensifier was imaged by a lens onto the CCD.

7.2.1 Varo Image Intensifier

This intensifier (of unknown type number) was a 3-stage, electro-statically focussed tube with a P.11 phosphor. The phosphor screen was imaged onto the CCD by two Canon f/1.2 lenses in a 1 : 1 magnification configuration. The dark current (approximately 6 counts/cm^2/sec) was used as a "signal" as this ensured that events on the phosphor screen were due to single photo-electrons. From Chapter 2, the CCD requires about 3.5 x 10^6 photons at this wavelength to saturate the CCD. With a gain of about 10^6, a phosphor efficiency of 15% and lens transmission of 10% the number of photons reaching the CCD for a single photon input is about 1.5 x 10^4, i.e. about 0.4% of the saturation level. As expected, there was no clearly visible signal from the CCD.

7.2.2 EMI Intensifier

This is a 4-stage, magnetically focussed cascade intensifier with a P.11 phorphor and a measured blue light gain of better than 10^6 (type number 9912). The phosphor screen was lens coupled to the CCD in the same manner as for the Varo intensifier. The photon flux due to a single photo-electron event incident on the CCD was about 10^5/pixel/frame giving a signal about 1/35 of the saturation level as expected from calculation. Unfortunately this was not quite high enough above the noise to reliably trigger the discriminator. It follows from the conclusions reached in Chapter 2 that the light pulse must be as close to saturating the CCD as possible for best detective quantum efficiency.

The conclusions to be drawn so far are:

a) that the wavelength of the phosphor output must peak towards the red end of the spectrum for best matching to the diode array spectral response,

b) that possibly more than three stages will be required in a lens coupled cascade intensifier to ensure unambiguous detection of light pulses.

Cascade image intensifiers of three or more stages will tend to have very long output phosphor decay times (e.g. Miller et al (1976), Robinson and Wampler (1976), Gaskell and Robinson (1978), Stapinski et al (1978)). As an example, the Lick Observatory device (Gaskell and Robinson (1978)) uses an image intensifier chain in which 1% of the initial signal may persist for several minutes; as a result the pulse height distribution is not peaked and the counting statistics are poor.

For these reasons, it was decided that a small micro-channel plate intensifier with a single short persistence, red (P.22R) phosphor would be a suitable intensifier for the CCD. Unfortunately, such a device was not commercially available and so it was necessary to design a tube for construction at Imperial College.

7.3 The Micro-channel Plate

The micro-channel multiplier was first introduced by Goodrich and Wiley (1962) as a very small, tubular, continuous dynode. Each multiplier consisted of a small glass tube that was relatively long compared to its diameter and coated on the inside with a metallic oxide. When a uniform electric field is established within the channel, an electron entering at one end creates secondary electrons by collision with the tube walls in a process that is ultimately limited by space charge effects. A large number of such multipliers can be placed together to form a close packed, hexagonal, two-dimensional array for image intensification. Typically, a micro-channel plate (MCP) will have a pore diameter between 10 and 50μm and a thickness of about 0.5mm. The gain is a function of the applied potential and the length-to-diameter ratio (Manley, Guest and Holmshaw 1969). For a straight micro-channel, gains of 10^6 are theoretically possible before space charge effects become important, but in practice the gain is limited to 10^4 because of feedback of ions released from the channel walls to the photo-cathode causing damage and showers of secondary electrons (Sackinger and Johnson 1969).

There are two principal solutions to the problem of ion feedback.

7.3.1 The Chevron Plate (Colson et al 1973)

In this arrangement, two MCP's with their channels cut at a small bias angle are placed close together so that there is no line of sight for an ion. This arrangement tends to reduce the overall resolution (Colson et al 1973) and has a very broad gaussian pulse height distribution (about 150% FWHM). This is caused by the output of a single pore in the first MCP exciting several pores in the second. Wiza et al (1977) have shown that with suitable inter-microchannel plate bias, the number of pores excited in the second MCP is reduced, because this acts as a form of proximity focussing. The FWHM is then improved to about 60%. The collection efficiency at the input face of the Chevron arrangement is about 90% (Gott et al 1970).

When used in a saturated mode gains of about 10^6 are possible with an ion count of 1 per cm^2 per sec using a micro-channel plate with 50μm pores and an accelerating potential of 3kV (Colson et al 1973).

The temporal resolution of a micro-channel plate is very good. A single electron input can cause an output pulse of width less than one nanosecond and rise time less than half a nanosecond (Colson et al 1973).

7.3.2 Curved Micro-channel Plates (Boutot et al 1976)

In this device, the micro-channels are curved so that ions released from the channel walls are re-absorbed and thus only one channel plate is required to operate in a saturated mode. The pulse height distribution is initially negative exponential but as the gain is increased to around 10^7, the pulse height distribution becomes sharply peaked with a FWHM of about 30 - 50% (Boutot et al 1976). This gain (with a collection efficiency of 85%) was measured for a plate of length-to-diameter ratio 80, pore size 40μm and accelerating potential of 1.5kV. (The ion count was measured as 50/sec/cm^2 at a gain of 2×10^6). The temporal resolution is 20ns (Oba and Maeda 1976).

Unfortunately, it appears that these devices are difficult to obtain (Airey et al 1978) and so it will be assumed that a Chevron arrangement will be used initially in the image intensifier.

7.4 Electro-Optic Focussing

There were three types of focussing considered for use in the proposed intensifier.

7.4.1 Electrostatic Focussing

Electrostatic focussing makes use of specially shaped electric fields for focussing the photo-electrons, and has the advantage that no bulky solenoids are required. The image produced suffers from pincushion distortion, image inversion and de-magnification. Although these defects can be corrected for, it was felt that this would introduce an unnecessary complication into the intensifier construction.

7.4.2 Electromagnetic Focussing

This is capable of very high resolution with small aberrations, but requires a uniform aerial magnetic field provided by a cooled solenoid. For emitted electrons (e.g. from a photo-cathode) with a Maxwellian velocity distribution and Lambertian angular distribution, the point spread (r.m.s) radius introduced by the focussing system is (Beurle and Wreathall 1962):

$$r_e = 0.93 \frac{V_o \pi}{B} \sqrt{\frac{2m}{eV_T}} \qquad (7.6)$$

where Vo is the most probable energy, B the magnetic field, V_T the accelerating potential and e/m the electronic specific charge.

7.4.3 Proximity Focussing

By making the gap between the emitting and receiving surfaces very small (<1mm) and the field gradient very high (O(5kV/mm)), the transit time of the electron can be kept very short, confining its lateral motion during the time of flight. Thus the electron image can be focussed onto the receiving surface. For an emitting surface that emits electrons with a Lambertian angular distribution and Maxwellian velocity distribution, it can be shown (e.g. Goodson et al 1972) that the MTF is given by:

$$\psi(f) = \exp\left[-f^2/{f_o}^2\right] \qquad (7.7)$$

where $f_o = \frac{1}{2\pi D}\left(\frac{V_T}{E_o}\right)^{\frac{1}{2}}$

and D is the distance between the emitting and receiving surfaces (in mm), V_T is the accelerating potential and Eo the mean initial energy (in electron volts).

7.4.4 Focussing Arrangements for the Proposed Intensifier

There are two regions in the proposed intensifier where electron-optic focussing is required. The first is from the photo-cathode to the micro-channel plate and the second is from the micro-channel plate to the phosphor screen.

For most common photo-cathodes, photo-electrons released have a most probable energy around 1eV. These photo-electrons have a Lambertian angular distribution and a Maxwellian velocity distribution and it is now well established that excellent resolution up to 100 lp/mm or more can be obtained using electromagnetic focussing. As an example, for $V_T = 5KV$, $B = 300G$, $Vo = 2V$ it can be calculated using equation 7.6 that the root mean square radius of the disc of confusion (r) is 9×10^{-3}mm. A crude estimate of the limiting resolution in this case can be given by:

$$fL = \frac{1}{2r} = 56 \text{ lp/mm}$$

In the case of priximity focussing (equation 7.7) it is suggested by Goodson et al (1972) that the limiting resolution occurs when $\psi(f)$ falls to 5% of its value at $f = 0$ and it can be calculated that in order to obtain a resolution of 56 lp/mm with a 0.5mm gap between the photocathode and microchannel plate requires a potential of 20KV. Thus better resolution can be obtained with electromagnetic focussing when the field gradient must be kept as low as possible.

In the second focussing region between the output of the microchannel plate and the phosphor screen, the choice of means of focussing is more difficult. Measurements made by Hill (1976) reveal that the energy distribution of secondary electrons from a microchannel plate is pseudo-negative exponential in character (i.e. the most probable energy occurs at about 3eV rather than at 0eV) and this is supported by the mathematical model of Guest (1971). Furthermore, measurements made by Woodhead and Ward (1977) suggest that the angular distribution of electrons emitted from a microchannel plate forms an ill-defined ring and is more forward peaked than a Lambertian distribution. Hence equations 7.6 and 7.7 do not apply because they are based on the assumption of a Maxwellian velocity distribution and a Lambertian angular distribution;

calculations based on these assumptions appear to underestimate the limiting resolution of existing microchannel intensifiers (Basyaeva et al 1972). In electromagnetic focussing, the size of the disc of confusion depends on the distribution of the axial velocity of the electrons only and the greatest velocity occurs when the electron is emitted parallel to the axis of the tube. For photocathodes the range of the distribution is about 0 - 2eV compared to about 0 - 50eV for microchannel plates, so it would be expected that for the same accelerating potential and magnetic field, the disc of confusion formed by a microchannel plate would be much larger. On the other hand, the accuracy of proximity focussing depends on the distribution of transverse velocities and since it appears that the distribution of electrons from microchannel plates is more forward peaked than that from photocathodes, then it seems that proximity focussing is more appropriate. This is borne out by experimental evidence (Guest 1971, Yeadon and Clark 1972, Woodhead and Ward 1977) that resolution of the order of 15 lp/mm, i.e. limited by the microchannel pore dimensions, is possible using proximity focussing.

7.5 A Preliminary Design of the Complete Intensifier

A schematic cross-section of the proposed intensifier is shown in Figure 7.1.

Photo-electrons released from the photo-cathode generally have a most probable energy of around 1eV so that electromagnetic focussing of the photo-electrons onto the MCP is desirable for best resolution in this section. It is proposed that the axial magnetic field will be of the order of 10^2 Gauss and the accelerating potential will be about 1kV, shared equally between the accelerating electrodes (in order to keep the field uniform).

The MCP's are about 0.5mm thick spaced by about two-thousandths of an inch with about 1kV across each. Initially there will be no inter-MCP potential.

The final stage of the intensifier will proximity focus the output of the MCP onto the phosphor screen using an accelerating potential of 2kV across a gap of about 0.7mm. The gap size will be reduced in later versions of the intensifier.

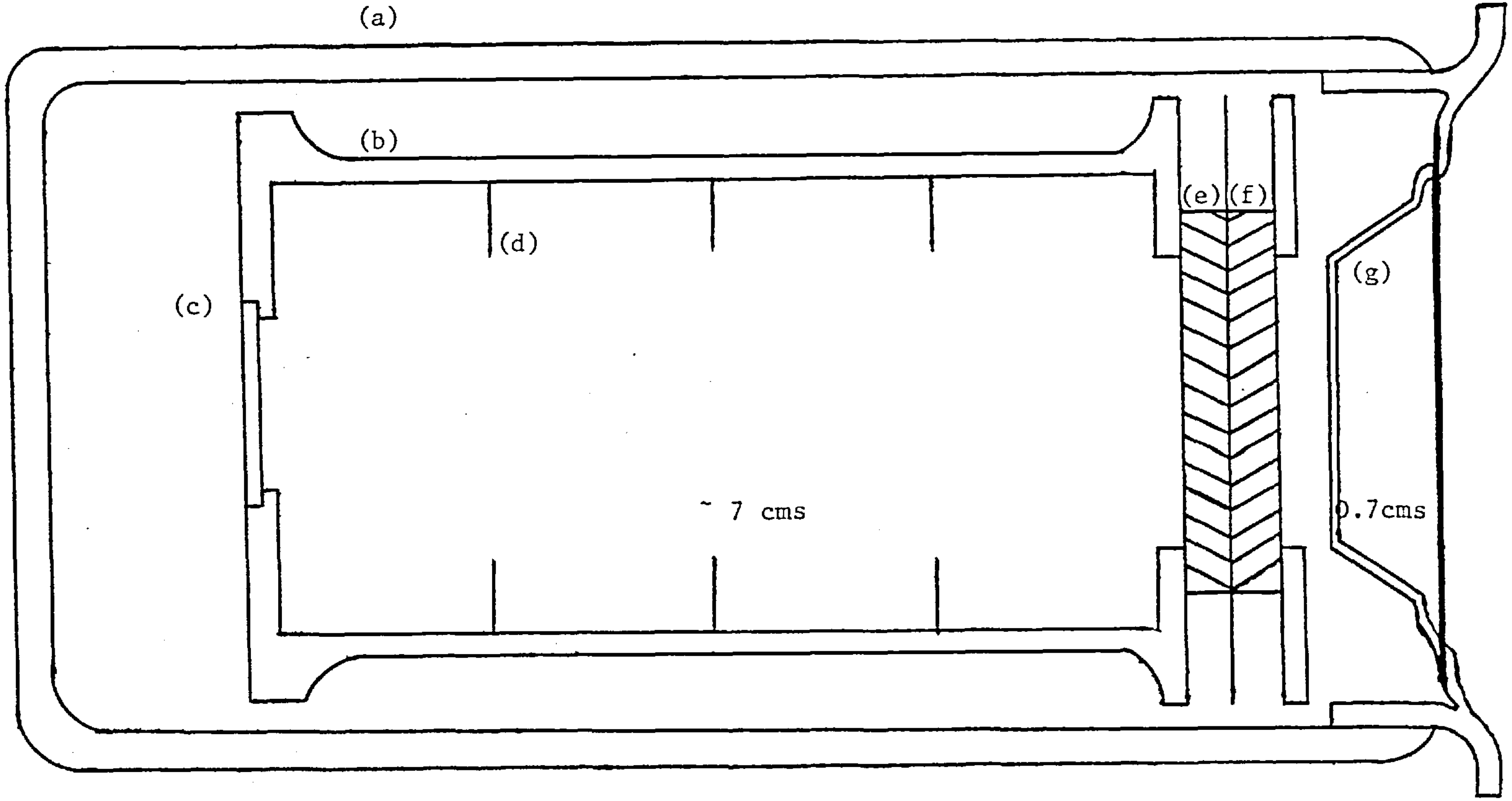

FIG. 7.1: THE PROPOSED INTENSIFIER

(a) Outer glass envelope (b) Inner glass envelope

(c) Photo-cathode (d) Accelerating anodes (e) (f) Micro-channel plates

(g) Phosphor screen

Further preliminary constructional details can be found in Airey et al 1978, and the design shown in Figure 7.1 will of course be subject to change as constructional difficulties become apparent.

7.6 Centroid Finding

Any real linear, stochastic imaging system will introduce a point spread function (PSF) that degrades the original image according to:

$$g(x^1) = \int_{-\infty}^{+\infty} f(x)\ h(x^1 - x)\ dx \qquad (7.8)$$

where $g(x^1)$ is the observed image, $f(x)$ the original image and $h(x^1 - x)$ the point spread function. In the spatial frequency domain, 7.8 becomes

$$G(u) = F(u).\ H(u). \qquad (7.9)$$

where $G(u)$, $F(u)$ and $H(u)$ are the Fourier transforms of $g(x)$, $f(x)$ and $h(x)$ respectively.

In principle, by applying a filter, $M(u) \approx H^{-1}(u)$ to the observed image, we could obtain:

$$M(u)\ G(u) \approx F(u) \qquad (7.10)$$

and thus recover the original image, but in the presence of an additive, uncorrelated noise, however, a filter that enhances the higher spatial frequencies of $G(u)$, will also boost the noise and this limits the range to which the power spectrum of $G(u)$ can be extended.

Nevertheless, using the a priori knowledge of the PSF to partially de-convolve the observed image has been successfully used in the nuclear community and Mende (1971) suggested that centroid finding could be applied to astronomical photon counting photometry. The first practical implementation of this technique in astronomy was introduced by Boksenberg and Burgess (1972).

The principle of centroid finding (as applied, for example, to the CCD) is illustrated in Figure 7.2.

The CCD array (marked by numbers in Figure 7.2) is associated with an array in the processing computer that is twice as large (marked by letters in Figure 7.2). Two possible event centres are indicated; (a) where the photo-electron event centre falls inside a pixel, and (b) where the event centre falls between two pixels. The result of single bit digitising is shown in Figure 7.2(iii). It is relatively simple to programme a logic network to assign events that excite two pixels to the cell between them in the computer array, or to assign events that excite three pixels to the middle one. Thus the limiting resolution of the CCD/computer combination is doubled. The scheme can, of course, be extended to two dimensions.

The gain of the University College Image Photon Counting System is high enough to enable recovery of the resolution of the first stage of the cascade intensifier (Boksenberg 1976).and in the same way, it may be possible to recover the resolution afforded by the first MCP of the intensifier described in this chapter, (cascading two MCP's will halve the limiting resolution (Colson et al 1973)).

A detailed mathematical study of the University College IPCS by Fort, Boksenberg and Coleman (1976) reveals that beside gains in the

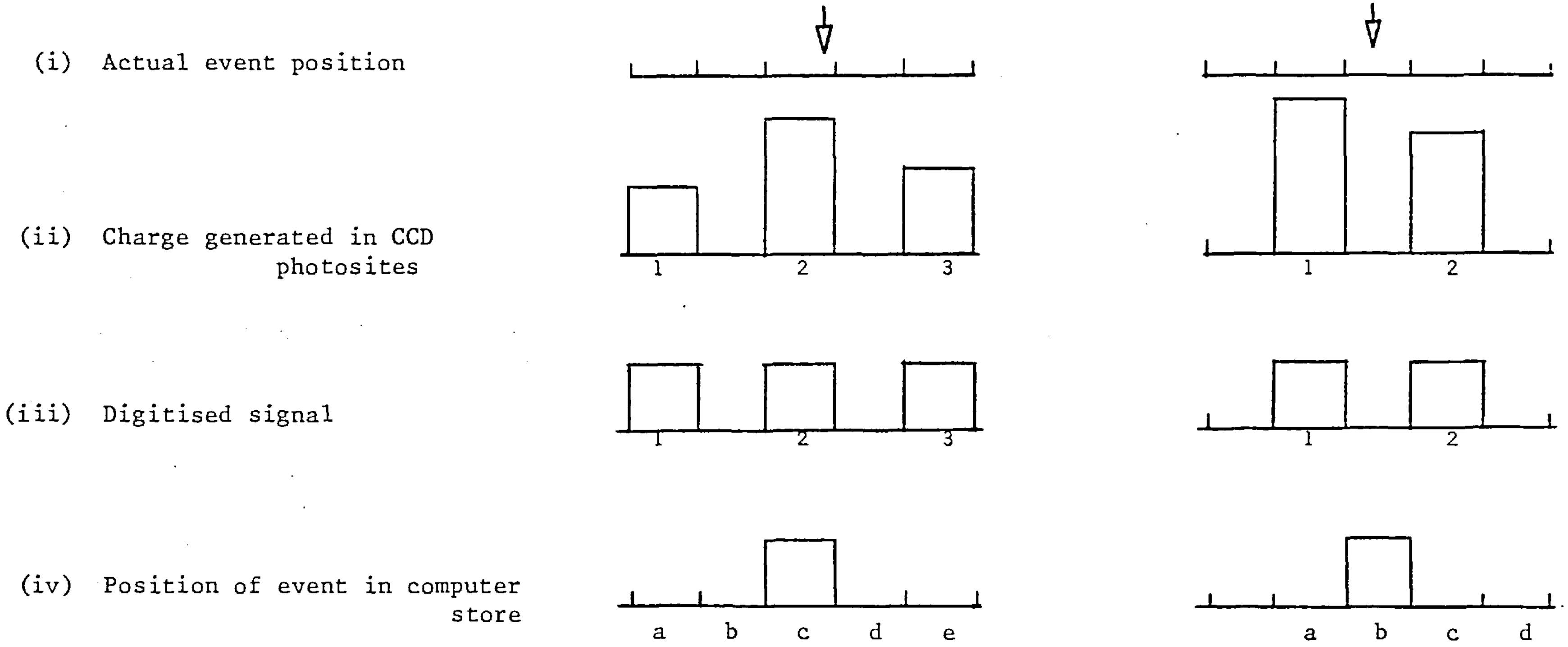

(a) (b)

FIG. 7.2: CENTROID FINDING

modulation transfer function, the centroiding scheme ensures equal weighting to photo-electron events, thus improving the DQE, and also prevents multiple counting of events to improve the linearity.

Centroid finding is essential for true photo-electron counting and is now being included in other photon counting systems (e.g. Blazit et al 1977).

A more detailed treatment of the particular photon counting system discussed in this chapter will have to wait for experimental knowledge of the PSF of the micro-channel plate tube.

7.7 Digital Data Handling

When fully operational, the intensified CCD could be used as a "front end" to the hard wired speckle interferometry correlator (Chapter 8). A further use of this device is for photon counting photometry, where it is necessary to integrate the image for a long period in order to minimize photon shot noise (Chapter 1). One of the advantages of digital image processing is that the storage can be extended indefinitely. A possible configuration is shown in Figure 7.3.

The video signals from the CCD, after undergoing centroid finding, are added into a 16 bit deep integrating memory, in which when full, the photon shot noise will be 0.15% of the signal. The integrated result could be stored on a digital magnetic tape or processed on-line by a computer via the CAMAC interface. The video monitor will keep the observer informed of the progress of integration. On-line manipulation will allow operations such as sky background

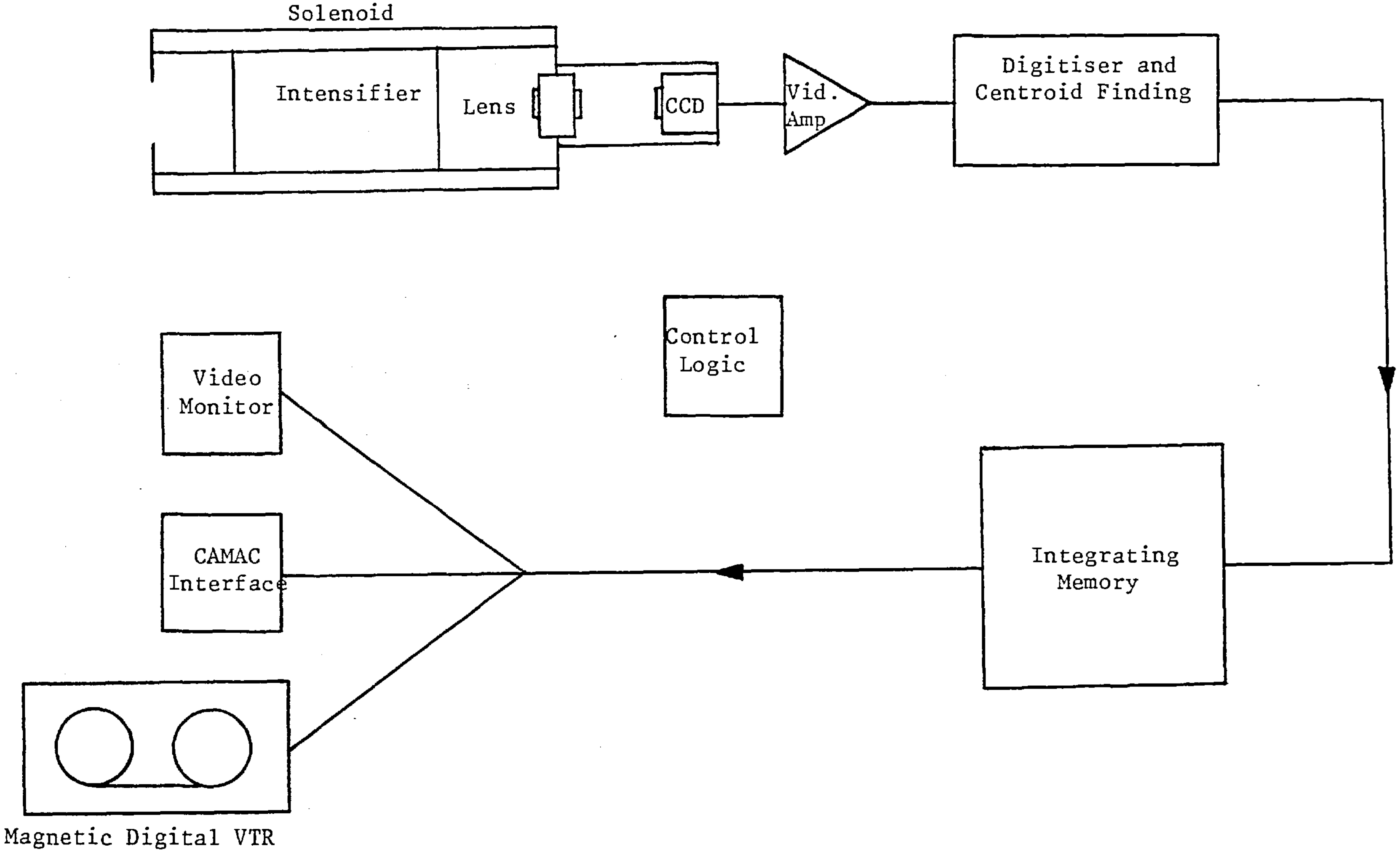

FIG. 7.3: A POSSIBLE SIGNAL PROCESSING SCHEME

subtraction and photo-cathode non-uniformity removal to take place (e.g. Hardwick 1978, Harrison et al 1978) and telescope time could be used more efficiently.

CHAPTER EIGHT

CONCLUSIONS AND FUTURE WORK

A brief survey of existing electro-optic detectors in Chapter One, revealed the charge coupled imaging device to be a new technology that shows great promise. The Fairchild 202 device with 100 x 100 pixels obtained for use in a computer based image processing system was tested with the image processing requirements in mind and was found to have the following properties (Chapter Two).

i) The photo-response is strictly linear from the noise level to saturation with a dynamic range of better than 10^3.

ii) There appeared to be no Fabry-Perot fringing effect in the $Si\ O_2$ layer in the optical region 500nm to 1100nm with a resolution of 10nm.

iii) Crosstalk conforms to the manufacturing limits and transfer efficiency is better than 99.99%.

iv) There is no measurable lag.

v) Blooming does not damage the CCD.

vi) With a thermally generated background charge (fat zero) the photosite non-uniformity is limited to 5%, but the number of "hot-spots" is quite large.

For the processing schemes discussed in this thesis (speckle interferometry and photon counting photometry), only single bit digitising is necessary, relaxing the signal generator requirements so that while the CCD has some drawbacks as far as analogue integrating photometry is concerned, e.g. the rather high inter-photosite non-uniformity, it is a very good detector for single bit digitised applications. The major drawbacks are the "hot-spots", that is the photosites with anomalously high dark current which can appear above a digitising threshold to be counted as spurious photon events or speckles, and the rather limited number of resolution elements (10^4). As discussed in Chapters Two and Three, the position of these events can be stored in the computer memory or possibly in a circulating store and subtracted from subsequent data fields because the hot-spots remain in a fixed position in the array. Larger CCD's are now becoming available to the astronomical community. A Fairchild CCD 211 device with 244 x 190 pixels has recently been acquired by Imperial College Astronomy Group, and preliminary tests indicate that the number of hot-spots has been reduced. A new digitiser, buffer and integrating memory which will be transportable to remote telescope sites is being constructed for this device. It is also reported that the Jet Propulsion Laboratory in America has placed a contract with Texas Instruments Ltd. to produce an 800 x 800 photosite CCD for spaceborne applications and an experimental 400 x 400 device has already been produced. Preliminary tests by Fahlman et al (1978) reveal that the problem of non-uniformities and "hot-spots" is still a serious one and it is to be hoped that the NASA contract will speed up the solution of this manufacturing difficulty.

The tests performed on the CCD were not exhaustive but were sufficient to determine the suitability of the array for the work described in this thesis. A more sophisticated series of tests for more general purposes is at present under way and will be more easily carried out when multi-bit quantization (with an on-line computer) is available (e.g. Chodil et al 1978).

The digitised CCD was successfully interfaced via CAMAC to an Interdata 70 mini-computer such that, on average, only 2 bits of data were dropped per frame. The different data rates were matched by using a single frame buffer store. Although this sacrificed real-time operation it meant that any number of events (up to 10^4) could be tolerated in a single frame.

Direct memory access (DMA) would permit a faster transfer of data than allowed by CAMAC when communication with a flexible mini-computer is desired although it is intended to use hard wired logic for the applications described here when all instrument problems have been solved.

Image intensification is, of course, necessary in order to extend the dynamic range of the CCD into the photon counting region. The preliminary experiments (Chapter Seven) involving commercially available intensifiers demonstrated that a gain of around 10^7 would be necessary for an unambiguous detection of photo-electron events, and there have been a number of approaches to this problem in recent years, although most of these systems have some drawbacks. Further design criteria such as the need for a physically small, robust, low power construction and lens coupling between the phosphor screen of the intensifier and the CCD for easy interchange, ruled out commercially available intensifiers so that a preliminary design of a new tube was drawn up (Chapter Seven).

The proposed tube is based on a pair of angled microchannel plates arranged in a Chevron formation for minimum ion feedback. Photo-electrons emitted from the photocathode will be accelerated onto the first microchannel plate and focussed by an axial magnetic field. The potential difference between the front face and back face of the microchannel plates should be sufficient to cause the cascade of electrons produced in each microchannel pore to be limited by space charge effects, i.e. the microchannel plate will be saturated. The resultant shower of electrons will be proximity focussed onto a P22R (red) phosphor that is optically coupled to the CCD. Preliminary calculations suggest that this arrangement should provide sufficient gain to saturate a CCD photosite.

In practice, of course, the image of a photoelectron event on the phosphor will be spread over several photosites, because of the point spread function of the tube. Following the work of Mende (1971), Boksenberg and Burgess (1972) and Fort et al (1976), the importance of photoelectron event centroid finding is well established and such a scheme can improve both the modulation transfer function and the linearity. Further work on this will have to wait for a detailed experimental study of the point spread function of the prototype tube.

Until the intensifier is available for direct work at a telescope site, the CCD and computer were used in the laboratory to reduce speckle interferometry data recorded by the Imperial College Speckle Interferometer. Speckle images, stored on cine film, were illuminated by an incoherent thermal light source and imaged onto the CCD. The diffraction limited data were recovered by calculating a two dimensional ensemble space auto-correlation using the mini-computer.

Previous experiments involving auto-correlation of speckle interferometry data (Lynds et al 1976, Blazit et al 1977, Hubbard et al 1978) (Chapters Five and Six) have produced results which do not correspond to the theory that the average speckle size is determined by the aperture of the optical system (Goldfischer 1965). In particular, the anomaly was attributed by Lynds et al (1976) to an "accumulation of small errors" or by Labeyrie (1978) to seeing effects. Similar results were initially obtained using the apparatus described in this thesis, although the separation and position angles of three binary systems (faintest at 4th magnitude) were deduced. It was later found during a detailed study of four stellar systems that the distortion of the auto-correlation was due to the surprising sensitivity of the speckle statistics to spatial integration. The data for the four systems (η Oph, β Del, Betelgeuse and Arcturus) were obtained at four different telescope sites in very different seeing conditions, suggesting that the condition for strong atmospheric scattering is usually met. It was also discovered that it is particularly important to ensure a large number of sampling pixels per "speckle" when the object in question is a possibly resolved stellar disc, because it is difficult to attribute a "width" to the auto-correlation function if it does not exhibit the expected minimum at the diffraction limit.

Unfortunately, the expansion of the image scale required to avoid distortion will often mean that "corresponding speckles" in a binary star speckle pattern will not fall within the detector area. From the results of Chapter Six for instance, a sampling rate of 10 x 10 pixels per speckle would mean (for a computation "window" of 50 pixels), that the maximum separation of the binary star would have to be less than 0.25 arcsec. (for a diffraction limit of 0.05 arcsec.).

Distortion of the auto-correlation function for binary star systems in these experiments took two forms.

i) The peaks were smoothed by convolution with the sampling aperture making the secondary peak difficult to locate.

ii) The finite extent of the auto-correlation increased the slope of the background so that it was no longer slowly varying across the secondary peak. Again there was greater difficulty in locating the secondary peak, and its centre position was displaced inwards by a few hundredths of an arc second.

Effects due to the background could possibly be removed using a processing technique due to Welter and Worden (1977), who have shown that subtraction of the cross-correlation of frames of speckle separated in time by an amount greater than the coherence time of the speckle pattern, from the auto-correlation of successive frames of data leaves the auto-correlation of the object intensity distribution. More formally,

$$< O(x) \otimes O(x) > = < I(x) \otimes I(x)> - < I(x) \otimes I^1(x) > \quad (8.1)$$

where $O(x)$ is the object intensity distribution, $I(x)$ the speckle intensity distribution, $I^1(x)$ is that of a speckle pattern that is separated from $I(x)$ by a time interval greater than the coherence time of the speckle pattern, $\otimes$ denotes spatial auto-correlation and <> denotes ensemble averaging.

This could be implemented on the computer system described in this thesis using the same cine films on which the speckle data is recorded. It would be necessary to store some ten successive frames of data in the mini-computer. The 10K array in core contains a 16 bit store at each of the 10K locations. At present, because the data is single bit digitised, only one of the bits is used at each location. Thus up to 16 frames (although 10 would be sufficient) could be "stacked" in this array. As the algorithm auto-correlated the first frame, cross correlation between the first and tenth frames (sufficiently separated in time to ensure no correlation) could also take place. Once the information contained in the first frame has been used, it can be discarded, and the stack of pictures pushed down to make room for the next video frame.

If, however, the statistics are smoothed because of sampling effects, then from equation 6.7,

$$I_D(x) = I(x) * D(x)$$

where I(x) is the true image intensity distribution and D(x) is the pixel aperture.

Using

$$I(x) = S(x) * O(x),$$

since convolution (*) obeys the distributive law, we can write that

$$I_D(x) = S(x) * O^1(x) \qquad (8.2)$$

where

$$O^1(x) = O(x) * D(x)$$

The result of applying equation 8.1 is:

$$(O^1(x) \otimes O^1(x)) = (O(x) \otimes O(x)) * (D(x) \otimes D(x)) \qquad (8.3)$$

that is, the auto-correlation of the apparent object obtained from the method of Welter and Worden (1977) is the true object auto-correlation convolved with the auto-correlation of the area shape of each photosite, so that the problems due to detector spatial integration remain.

At present, a hard wired auto-correlator that can compute auto-correlations and cross-correlations in real time is under construction at Imperial College. It is projected that this apparatus will process a frame of 256 x 256 pixels containing a maximum of 512 photon events in 20ms; the increased efficiency should allow study of stellar systems down to magnitude +12. The correlator could also be used in an analogue mode with clipping as a form of data compression. This results in a distortion of the auto-correlation function which, although inconvenient, can be corrected using a formula due to Bates (1977).

If the use of speckle interferometry or even speckle imaging is to be expanded to include arbitrary objects, then these results clearly indicate that it is essential to find a detector with as large a number of pixels as possible.

In the future, the intensified CCD (Chapter Seven) and hard-wired real time correlator (Chapter Four) could be combined to form a composite real-time speckle interferometer. Two further options are to use the CCD intensifier and an integrating memory store for photon counting photometry, or to use a cooled CCD with many-bit quantisation for direct analogue photometry, since using a mini-computer will permit considerable correction for CCD defects.

The laboratory apparatus described in this thesis has shown that the CCD is capable of providing useful astronomical data in speckle interferometry and can easily be expanded in future into a flexible real-time image processing system which can be used in a variety of modes.

APPENDIX A

The CCD Waveform timing logic is shown in Figure A.1 and is reproduced from Fairchild (1974b) with some slight modification caused by replacing the original components by 7400 series TTL logic. All NAND gates are SN7400, the OR gate is SN7432, the counters are SN74163 and the multiplexer is SN74153.

The ramp generators used to generate the digitised video display are shown in Figure A.2, and these are also a modified design from Fairchild (1974b).

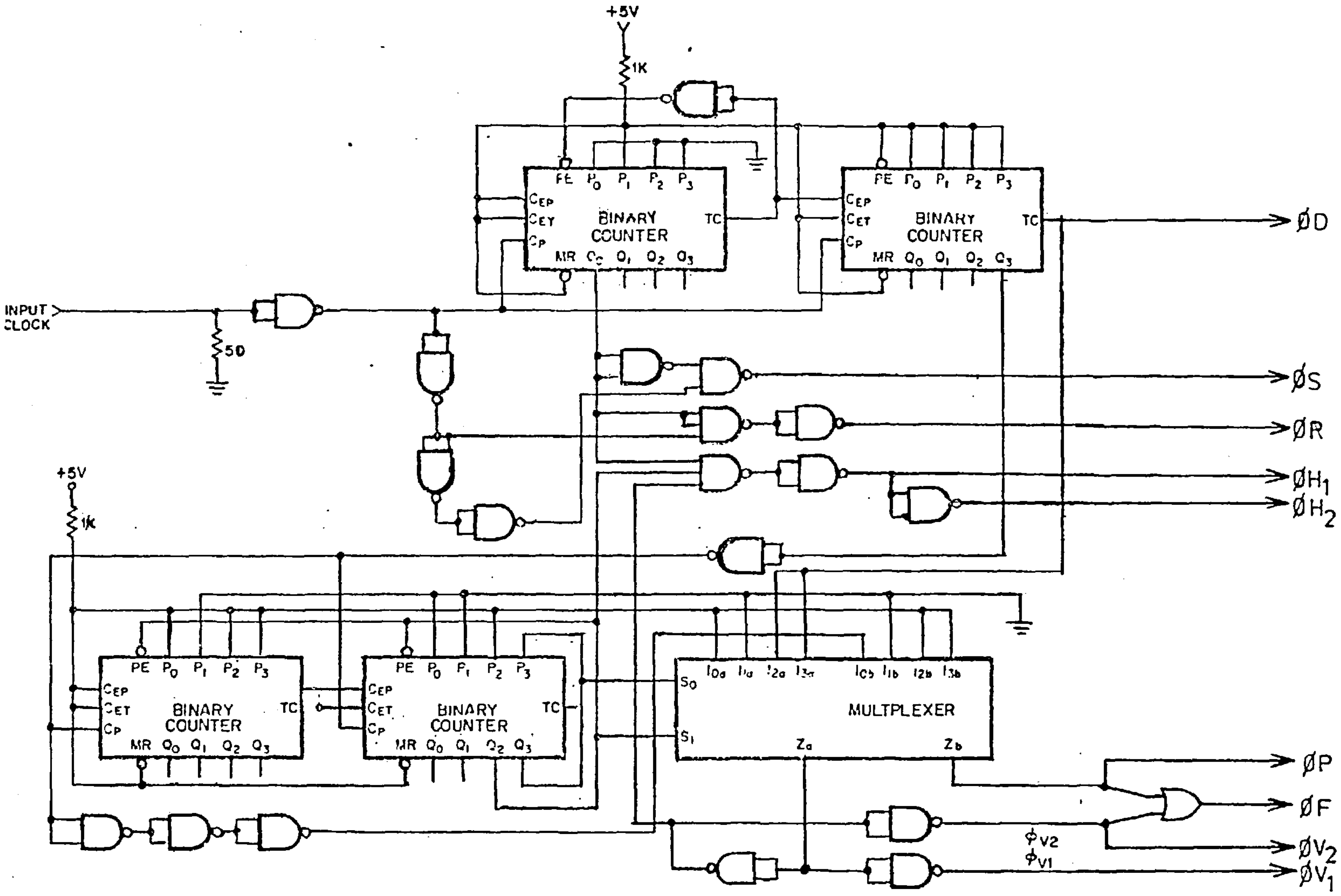
+5V
1K
PE P0 P1 P2 P3
CEP
CET
CP
BINARY COUNTER
TC
MR Q0 Q1 Q2 Q3
ØD
INPUT CLOCK
50
ØS
ØR
ØH1
ØH2
+5V
1K
S0
S1
I0a I1a I2a I3a I0b I1b I2b I3b
MULTPLEXER
Za
Zb
ØP
ØF
φV2
φV1
ØV2
ØV1

FIG. A·1

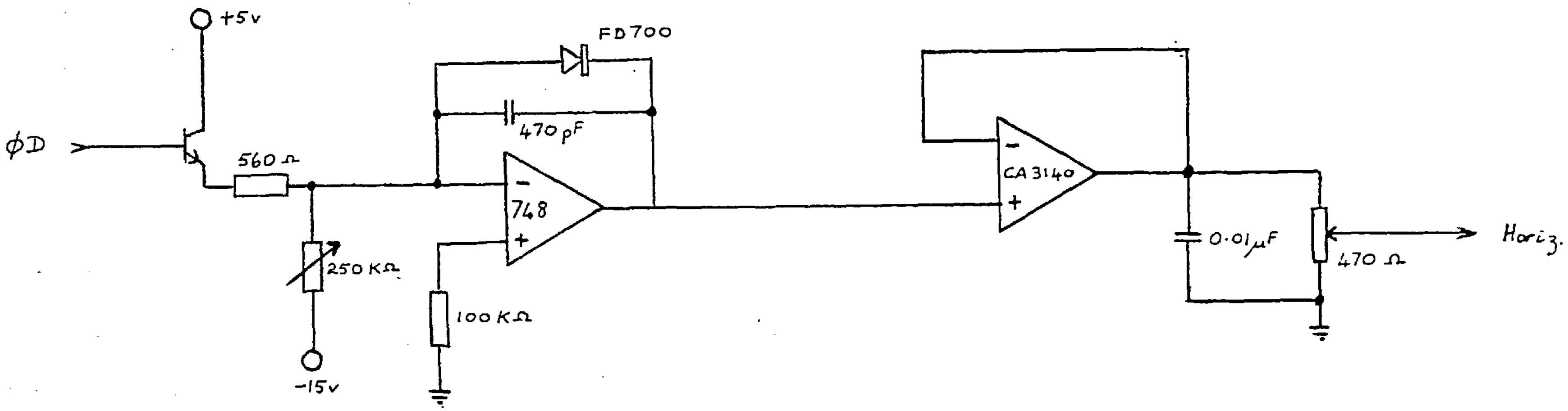
+5v
FD700
470 pF
φD
560 Ω
748
CA 3140
250 KΩ
100 KΩ
-15v
0·01 μF
470 Ω
Horiz.

FIG. A·2

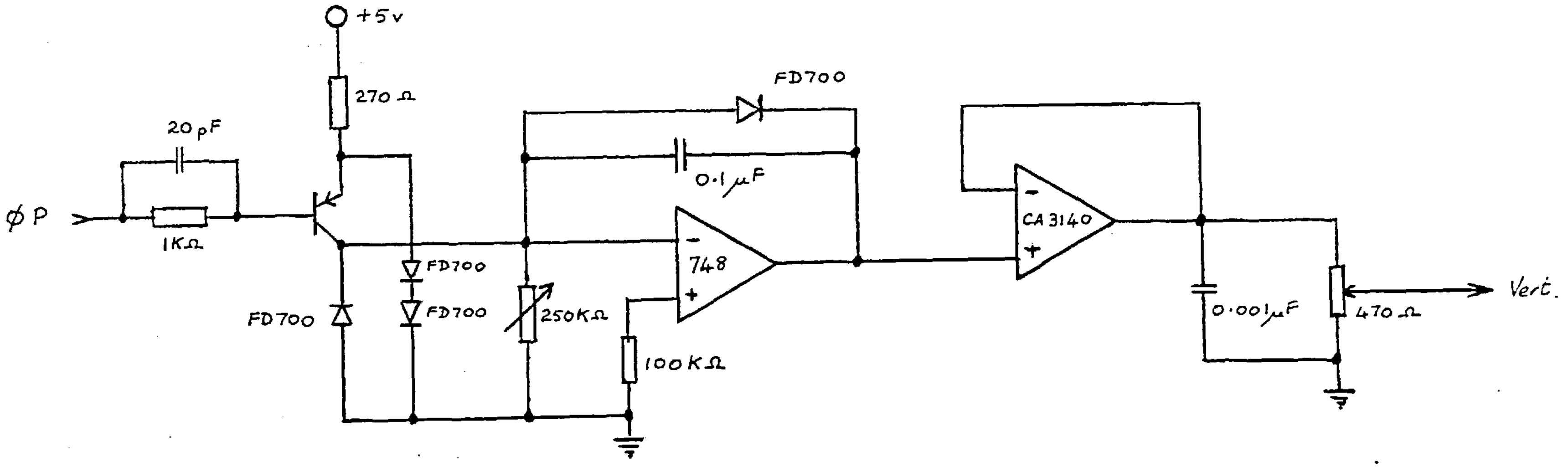
+5v
270 Ω
FD700
20 pF
0·1 μF
φP
1KΩ
FD700
FD700
FD700
748
250KΩ
100 KΩ
CA 3140
0·001 μF
470 Ω
Vert.

Appendix B

The Computer Programmes

The data processing and display programmes are written in FORTH language (Moore 1974). The layout is as follows:

Block 330: CAMAC interface words
Block 331: CLEAR-CCD, CCD
Block 332: O-PIC, ACNE
Block 333: P-E, O-STORE
Block 334: CRUX; Assembler language programme for AUTOCORRELATION
Block 335: CRUX
Block 336: TRANSFORM
Block 337: P-AD
Block 338: CLEAR-ARRAYS, ONESHOT
Block 339: Test Programmes
Block 340: NOFRAME, VID
Block 341: BLANK
Block 342: Component Programmes
Block 343: SHOW, INOS
Block 344: Component Programmes
Block 345: Component Programmes
Block 346: 2A/C, ZNOS
Block 347: TRANSFER-DATA
Block 348: PEAK-FIND

```
                              BLOCK NO.  330
( CAMAC          STANDARD MODULE NAMES                    CLD 27/ 6/78  )
    FORGET MARK : MARK ;   : TEST ;   CAMAC
RCRT CRATE !   ( THESE ARE IN REMOTE CRATE )
 4  0 NA IO
SYSCRT CRATE ! ( THESE ARE IN THESYSTEMS CRATE )
 6  0 NA CRY              6  1 NA CRX
 8  0 NA PRESET           8  1 NA PRESET-NO
11  0 NA INT-REG
 9  0 NA ADC
10  0 NA DELAY      10  1 NA DELAYS      10  2 NA DELAY-PL
11  0 NA INT-REG
13  0 NA SC1        13  1 NA SC2         13  2 NA SC3
13  3 NA SC4        13  0 NA SCALER      13 14 NA SC-CONT
: WAIT-L BEGIN DUP TLM SA Q @ END DROP ;
: WAIT-STAT BEGIN DUP TST SA Q @ END DROP ;
-->


                              BLOCK NO.  331
( CAMAC OPERATIONS                                        CLD 27/ 6/78  )
   10001 ARRAY PICTURE  9900 VARIABLE LIMIT 0 VARIABLE NN
: OPEN 0 NN ! ." A" IO ENB SA    IO CLM SA CR ;
: PART1 IO WAIT-L IO RD2 SA           NN @ 1000 /MOD DROP 0 =
  IF DUP . CR  THEN       DUP 0< ;
: CLOSE IO DIS SA NN @ . CR ;
: PROCESS DUP 105 /MOD 2 * ROT 5354 > IF 101 -
                                        THEN 100 * + 2 - ;

: CLEAR-CCD OPEN BEGIN PART1 IF DROP 1 ELSE 10000 <
           IF 1 NN +! THEN 0 THEN END CLOSE ;
: CCD OPEN BEGIN PART1 IF  .   1 ."    B " ELSE PROCESS
                                           DUP
   10000 > IF DROP ELSE
   1 SWOP PICTURE +!   1 NN +! THEN 0 THEN END CLOSE ;
-->


                              BLOCK NO.  332


      10000 0 DO I PICTURE @ DUP 0 > IF 1 DLC +! THEN  I 512
  /MOD 270 + BLOCK + +!  UPDATE                   LOOP DLC @ . ;

: 0-PIC 10000 0 DO 0 I PICTURE ! LOOP ;

: ACNE  10000 0 DO I 512 /MOD 270 + BLOCK + @ 0>
                 IF 0 I PICTURE !  THEN
              LOOP ;




=?????>
```

```
                              BLOCK NO. 333
( PICTURE PROCESSING - 2                                    CLD 27/ 6/78 )
    50 VARIABLE HI    0 VARIABLE OO
     0 VARIABLE MM    4000 ARRAY 1STORE  4000 ARRAY 2STORE
: P-E   0 MM !  97 3 DO I . CR  97 5 DO
                J 100 * I +      PICTURE @  0>
                     IF I J MM @ 1STORE ! MM @ 2STORE !
                        1 MM +!
           THEN             LOOP LOOP MM @ . ;

: 0-STORE 4000 0 DO 0 I 1STORE ! 0 I 2STORE ! LOOP ;

```

```
                              BLOCK NO. 334
( CRUX       MACHINE CODE ROUTINE                           CLD 12/ 7/78 )
HEX 2400 SHORT LSI, DECIMAL   ( ** TEMPORARY FIX  LIS, = LIST )
 CODE CRUX  2 2 S) LH,         ( R2 = LOOP LIMIT )
            3 4 S) LH,         ( R3 = J )
            4 1    LSI,        ( R4 = 1 )
            1 0 S) LH,         ( R1 = I )
HERE 2*     5  0 1STORE 2*  1 LH,
            6  0 1STORE 2*  3 LH,
            5 6    RSH,        ( X DIFFERENCE )
            7  HI 2*  0 LH,       ( PICK UP LIMIT )
            7 5 RSH,




-->
```

```
                              BLOCK NO. 335
( CRUX CONTD.                                               CLD 12/ 7/78 )
      IF>,  7 100 0 LHI,          ( * 100 )
            6 5      RMH,         ( RESULT IN R7 )
            5  0 2STORE 2*  1 LH,
            6  0 2STORE 2*  3 LH,
            5 6    RSH,           ( Y DIFFERENCE )
        IFL,  7 5    RSH,           ( X - - Y )
              7 5000 0 AHI,         ( ADD IN OFFSET )
        ELSE. 7 5   RAH,            ( X + Y )
        THEN, 7 7   RAH,            ( 2* FOR BYTE ADDRESS )
               4  0 PICTURE 2*    7 AHM.     ( MEMORY INC )
      THEN, 1 2 AIS,              ( I = I + 1 )
            1 2 RCH,              ( TEST I AGAINST LIMIT )
            3 SWAP 0 BTC,         ( BRANCH BACK TO 'HERE' )
            S) 6 AIS,             ( CLEAR STACK )
NEXT -->
```

```
                          BLOCK NO  336
( AUTOCORRELATION PROGRAMME                        CLD 13/ 7/78 )





: TRANSFORM  NN @ 1 - 2* 0 DO I 100 /MOD DROP 0 = IF I . CR THEN
               I     NN @ 2* I 2 +

                                          CRUX



-->
```

```
                          BLOCK NO. 337
( RESULT TO DISC                                   CLD 27/ 7/78 )


: P-AD  5000 0 DO
               I PICTURE @ I 512 /MOD 260 + BLOCK + +!
               UPDATE                LOOP'
        5000 0 DO
        5000 I + PICTURE @ I 512 /MOD 250 + BLOCK + +!
               UPDATE                LOOP ;







-->
```

```
                          BLOCK NO. 338
( COMPLETE A/C PROGS.                              CLD 27/ 6/78 )


: CLEAR-ARRAYS 0-PIC 0-STORE ;
: INTEGRATE  CCD P-D CLEAR-ARRAYS ;
: KRASH 100 0 DO I . CR CCD 0-PIC ."     " CR LOOP ;

: A/C CCD ACNE  P-E 0-PIC TRANSFORM P-AD 0-PIC 0-STORE ;

: TRIAL 100 0 DO ."     " CR  I . ." TRIAL" CR
                 A/C
         LOOP ;

: ONESHOT CLEAR-CCD A/C ;
: CTEST 5 0 DO CLEAR-ARRAYS  CCD P-E   LOOP ;
;S
```

```
                                   BLOCK NO. 339
( TEST PROGRAMMES                                                   CLD 27/ 6/78 )
     0 VARIABLE YY    0 VARIABLE XX
: EVENT J 100 * I + 1 SWOP PICTURE ! ;
: PAIR YY @ 2 + YY @ DO XX @ 2 + XX @ DO
        EVENT LOOP LOOP
       YY @ 10 + YY @ 8 + DO XX @ 10 + XX @ 8 + DO
        EVENT LOOP LOOP ;
: 5 YY ! XX ! PAIR ;
: MESS  1000 0 DO 1 56 I + PICTURE ! LOOP ;







;S
```

```
                                   BLOCK NO. 340
( MEMORY-1 INPUT/OUTPUT WORDS                                       CLD 12/ 7/78 )
   FORGET TEST : TEST ;
: STOVAL     512 /MOD 270 + BLOCK +  ! UPDATE ;
: DIUP 1 SWOP STOVAL ;
: GETVAL     512 /MOD 270 + BLOCK + @ ;
: NOFRAME 10710 0 DO 0 I      STOVAL  LOOP ;
: AXIS  10 /MOD SWOP 0 = IF .. ELSE DROP ." -" THEN ;
: 1VID 102 0 DO I AXIS ."   " 100 50 DO J 100 * I +
     GETVAL 0> IF ." *"  ELSE ."  " THEN LOOP CR LOOP ;
: 2VID 102 0 DO I AXIS ."   " 50 0 DO J 100 * I +
     GETVAL 0> IF ." *"  ELSE ."  " THEN LOOP CR LOOP ;

: VID ." 1ST. 1/2 FIELD" CR  ."    " 50 0 DO I AXIS LOOP CR 2VID
  CR ." 2ND 1/2 FIELD" CR ."    " 100 50 DO I AXIS LOOP CR 1VID ;

-->
```

```
                                   BLOCK NO. 341
( MEMORY-2  INPUT/OUTPUT WORDS                                      CLD 27/ 6/78 )
          0 VARIABLE QW
: NAME  512 /MOD 250 + BLOCK + ;
: BLANK 5001 0 DO 0 I      NAME ! UPDATE 0 I
        512 /MOD 260 + BLOCK + ! UPDATE  LOOP ;
  0 VARIABLE SCALED
: MAXVAL 0 SCALED ! 0 50 0 DO 50 0 DO J 100 * I +
          512 /MOD 250 + BLOCK + @ MAX LOOP LOOP
           50 0 DO 50 0 DO J 100 * I +
      512 /MOD 260 + BLOCK + @ MAX LOOP LOOP
          DUP 32 > IF 32 / 1 +  SCALED ! 1 QW !
                 ELSE SCALED ! 0 QW ! THEN ;




-->
```

BLOCK NO. 342

```
( DISPLAY PROGS. CONTD .                                          CLD 27/ 6/78 )
   0 VARIABLE REF.-LEVEL  0 VARIABLE AX   60 VARIABLE BX

: ZMOD QW @ 1 < IF 32 * SCALED @ / ELSE SCALED @ / THEN
   DUP REF.-LEVEL @ > IF   DUP 2 /MOD DROP 0 = IF ."  " DROP
   ELSE 1 + 2 /    HEX .. DECIMAL   THEN
                                ELSE DROP ."  " THEN ;

: 1SHOW 50 0 DO 50 I - AXIS ."  " 50 0 DO I 100 * 50
    J - +  512 /MOD 250 + BLOCK + @ ZMOD     LOOP CR LOOP ;


: 2SHOW 51 0 DO I AXIS ."  " 50 0 DO I 100 * J + 512
        /MOD 260 + BLOCK + @ ZMOD
         LOOP CR LOOP ;
-->
```

BLOCK NO. 343

```
( TEMP. GRAPH                                                    CLD 27/ 6/78 )


: SHOW MAXVAL SCALED @ QW @ 0 > IF 32 * THEN
      ." MAXVALUE = " . CR ."   " 51 0 DO I AXIS LOOP CR
      1SHOW 2SHOW ."   " 51 0 DO I AXIS LOOP CR ;

: HARDCOPY PRINTER SHOW TERMINAL ;

: 1NOS AX ! BX ! BX @ .  AX @ .  CR 14 0 DO 14 0 DO
      AX @ 100 /MOD I + 100 * SWOP J + + 512 /MOD
      BX @ + BLOCK + @ .  LOOP CR LOOP ;



-->
```

BLOCK NO. 344

```
(   DISPLAY PROGS. CONTD.                                       CLD 27/ 6/78 )
     0 VARIABLE QWE
: 2NAME 512  /MOD 500 + BLOCK + ;
: 2BLANK 5001 0 DO 0 I      2NAME ! UPDATE 0 I
        512  /MOD 510 + BLOCK + ! UPDATE  LOOP ;
  0 VARIABLE 2SCALE
: 2MAXVAL 0 2SCALE ! 0 40 0 DO 50 0 DO J 100 * I +
          512  /MOD 500 + BLOCK + @ MAX LOOP LOOP
            40 0 DO 50 0 DO J 100 * I +
          512  /MOD 510 + BLOCK + @ MAX LOOP LOOP
          DUP 31 > IF 31 / 1 + 2SCALE ! 1 QWE !
                  ELSE 2SCALE ! 0 QWE ! THEN ;



-->
```

```
                                BLOCK NO. 345
( TEMP. GRAPH                                            CLD 27/ 6/78 )


: 22MOD QWE @ 1 < IF 31 * 2SCALE @ / ELSE 2SCALE @ / THEN
   DUP REF.-LEVEL @ > IF   DUP 2 /MOD DROP 0 = IF ."   " DROP
   ELSE 1 + 2 /   HEX .. DECIMAL THEN  ELSE DROP ."   " THEN ;

: 21SHOW 50 0 DO 50 I - AXIS ."   " 50 0 DO I 100 * 50
   J - + 512  /MOD 500 + BLOCK + @ 22MOD  LOOP CR LOOP ;

: 22SHOW 51 0 DO I AXIS ."   " 50 0 DO I 100 * J +  512
        /MOD 510 + BLOCK + @ 22MOD
         LOOP CR LOOP ;



-->
```

```
                                BLOCK NO. 346
( TEMP. GRAPH                                            CLD 27/ 7/78 )
        0 VARIABLE 2AX   60 VARIABLE 2BX

: 2A/C  2MAXVAL 2SCALE @ QWE @ 0> IF 31 * THEN
           ." MAXVALUE = " . CR ."   " 51 0 DO I AXIS
            LOOP CR 21SHOW 22SHOW ."   " 51 0 DO I AXIS
            LOOP CR ;

: 2HARDCOPY PRINTER 2SHOW TERMINAL ;

: 2NOS 2AX ! 2BX ! 2BX @ . ."   " 2AX @ . CR 14 0 DO 14 0 DO .
        2AX @ 100 /MOD I + 100 * SWOP J + + 512 /MOD 2BX @ +
        BLOCK + @ .      .   LOOP CR LOOP ;



-->
```

```
                                BLOCK NO. 347
( DISPLAY PROGRAMS                                       CLD 27/ 6/78 )

: HRDCPY PRINTER  SHOW TERMINAL ;
: 2HRDCPY PRINTER  2A/C  TERMINAL ;
: TRANSFER-DATA
      50 0 DO ." 1   " I . CR 100 0 DO
           J 100 * I +      DUP
            512 /MOD 250 + BLOCK + @
      SWOP  512 /MOD 500 + BLOCK + +!
           UPDATE LOOP LOOP
      50 0 DO ." 2   " I . CR 100 0 DO
           J 100 * I +     DUP
            512 /MOD 260 + BLOCK + @
      SWOP  512 /MOD 510 + BLOCK + +!
           UPDATE LOOP LOOP ;
-->
```

```
                                      BLOCK NO. 340
( SUBTRACT BACKGROUND                                              CLD 27/ 6/78 )


: PEAK-FIND
   50 2 DO I . CR  50 2 DO J 100 * I +
        DUP 512  /MOD 500 + BLOCK + @
       SWAP 512  /MOD 510 + BLOCK + @ - ABS
       J 100 * I + 512 /MOD
      260 + BLOCK + ! UPDATE
           LOOP LOOP ;






;S
```

Appendix C

Published work:

1) "Interfacing a CCD Imaging Device through CAMAC". Proceedings of the ESO/CERN Conference on Applications of CAMAC to Astronomy, Geneva, 27th - 29th Sept. 1978.

2) "The use of a CCD in the reduction of Speckle Interferometry data". Preprints of the Seventh Symposium on Photo-Electronic Image Devices, Blackett Laboratory, Imperial College, 4th - 8th Sept. 1978.

3) "Astronomical Applications of a CCD". Advances in Electronics and Electron Physics, vol. 52, ed. Morgan and McMullan, 1979. Published by Academic Press.

INTERFACING A CCD IMAGING DEVICE THROUGH CAMAC

C.L. Davies

Astronomy Group, The Blackett Laboratory,
Imperial College of Science and Technology,
Prince Consort Road, London SW7 2BZ England

This paper describes the interfacing of a CCD to a minicomputer via CAMAC and its subsequent performance. The system is currently used in the reduction of speckle interferometry data and will eventually form part of a photon counting system.

INTRODUCTION

The better linearity and quantum efficiency of photo-electronic data gathering, combined with digital techniques that allow arbitrarily large data storage and interactive working, are overwhelming advantages over the photographic process in astronomy. In particular charge coupled devices show great promise as area image detectors, and although not yet matching television camera tubes in some aspects of performance, they have many significant advantages; they are small and robust, requiring only low voltages and small currents, and they have no need for solenoids. The CCD performs with strict linearity and avoids the problems associated with electron beam scanning;[1] in particular there is accurate positional information, limited only by the masks used during manufacture. These properties make the CCD ideal for transporting to telescope sites.

In the Astrononomy Group at Imperial College we have two particular areas of research that need a video picture digitised into a two level format for computer image processing.

The first is two dimensional photoelectron counting for photometry of faint extended sources such as galaxies. The linearity of photon counting allows operations such as sky background subtraction in the outer regions of galaxies to take place, where the signal is one-thousandth of the ambient light level.[2,3] Preliminary experiments are described later in this paper.

The second application is in the reduction of stellar speckle interferometry data. Speckle interferometry is a method of obtaining diffraction limited resolution from a large telescope despite the presence of atmospheric turbulence[4]. It has been shown that short exposure (5-25 ms) images of astronomical objects contains diffraction limited information. This information can be derived in one of two equivalent ways:

(a) By obtaining the fourier transform of each short exposure. This has been achieved in an analogue fashion using coherent optics.

(b) By obtaining the autocorrelation of each short exposure image. This approach is well suited to digital techniques.

In both cases the results of the computation of each frame are co-added in order to improve the S/N ratio [5,6].

The images are recorded on cine film using the apparatus shown in figure 1, [7] and until now have been reduced using analogue technique, which, although successful introduces extra sources of noise and non-linearity into the system. Observations have therefore been limited to fairly bright stars [8,9]. In future we intend to use a real time autocorrelator on site that will eliminate the need for cine film recording, but as an interim measure, we are reducing the cine film data by performing autocorrelations of each cine frame via the CCD and minicomputer. The CCD has been interfaced to a minicomputer via the CAMAC interfacing system that is now internationally used [10]. In order to match the data rate of the CCD output to the data rate of the CAMAC/computer system, it has been found necessary to use a single frame store. This store can be accessed by the CCD at T.V. framing rates in order to store the data and can be read out at a rate compatible with CAMAC operations.

THE CAMAC SYSTEM

The laboratory computing configuration is shown in Figure 2.

The minicomputer used is an Interdata 70 that has been programmed using FORTH language [11]. FORTH is an interactive, high level language that makes extremely efficient use of core, allowing the manipulation of large core arrays for image processing. The CCD, store and CAMAC crate are located remotely, with operations controlled from VDU-1. The remote crate and the systems CAMAC crate are connected via a differential branch driver.

The functional unit used is a Nuclear Enterprises type 9017 driver. The module contains a 24 bit parallel access register which functions as a one word store. There are two modes of operation:

(i) Data can be loaded, on command, into the register from an external unit, via a multi-way front panel connector, and gated onto the dataway.

(ii) Data can be loaded into the registrer from the CAMAC dataway and driven onto 24 output lines available in a second front panel connector. In our system, we only use the module in the first mode.

An interrupt signal level input can establish a LAM status within the module that is tested in the programme.

It has been found useful to modify this module so that the F(1) Read command also clears the LAM bistable and causes an output signal, called CLEAR, to be communicated to the external unit via a front panel connector.

THE CCD AND BUFFER STORE

The charge coupled device chosen is the Fairchild 202 CCD which is commercially available in chip form. 10^4 image sensing elements (pixels), each 18 μm x 30 μm, are arranged in an array of 100 horizontal lines by 100 vertical columns. The drive circuitry is a slightly modified version of that provided by Fairchild [12]. As explained earlier, the analogue output from the CCD is digitised into a two level binary signal. A complete frame of video is stored in the 10K by 1 bit memory. While the CCD scanning logic continues, the interfacing logic locates the presence of a '1', representing a photoelectron event, in the store and raises a LAM status in the CAMAC driver module. The address of this location is then read into a core memoery location. The CLEAR signal from the driver module increments the memory to the next event. At the end of readout, the buffer is rewritten by the CCD. At present, in non-optimized form, it takes about two seconds to read a single frame of about 1000 events into the computer, during which time further data from the CCD is lost. It is intended that in order to improve on the data collection efficiency, the ouput of the CCD will be recorded on video-tape at the telescope site, and then replayed at a slower rate compatible with the digitising process in the laboratory.

IMAGING PROPERTIES OF THE SYSTEM

At present, the CCD is uncooled and reaches a maximum temperature of about 37°C after an hour's use. Consequently, the noise performance is dominated by thermal effects, but it was felt that in the preliminary experiments, cooling was not an immediate requirement.

(a) Linearity and Dynamic Range

In Figure 3 the CCD output is averaged over one line. The dynamic range at this temperature is about 200 with strict linearity.

(b) Dark Current Defects

This is probably the most serious source of noise in the CCD and exhibits itself as "white spots" i.e. image sensing elements where the localized dark current is many times higher than the uniform dark current background. Figure 4 shows a digitised picture of the blemishes at 37°C with the discriminator set at 50% of the saturation level. The number of these can be substantially reduced by cooling; a reduction from 35°C to 25°C decreasing the number by at least 50%. We intend to cool the CCD to a moderately low temperature possibly using a Peltier cooler. This noise is, however, of the fixed pattern variety, and could be corrected for in the software.

(c) Spectral Response

The spectral response is typical of silicon devices, with no evidence of the interference effects reported by some authors[13]. This is probably due to the fact that the Fairchild CCD is a frontside illuminated device.

(d) Most other properties conformed to those reported previously in the literature [14 -18].

SOME RESULTS OF SPECKLE DATA REDUCTION

Autocorrelation of eachframe of speckle film yields diffraction limited information about the object. The autocorrelation is calculated using an algorithm due to Blazit et al[20] (1975).

$$C(h,l) = \sum_i \sum_j (x_i - x_{j-h}, y_i - y_{j-l})$$

That is, the vector separation of every possible pair of speckles is found, and a two-dimensional histogram of the results is built up.

The apparatus currently in use is shown in Figure 5. The cine film, mounted on a stop motion projector is imaged onto the CCD by lens L which is movable to allow the scale of the film to be optimally matched to the resolution of the CCD[19].

The entire process of reading in a single frame, computing the autocorrelation and integrating the result into a disc store takes approximately 1 → 1¼ minutes. At the end of each frame, the stop-motion projector is incremented by a single frame.

Figure 6 shows a typical contour map of the autocorrelation plane. The autocorrelation of a binary star system consists of a large central peak, flanked by two secondary peaks in a position that corresponds to the separation and position angle of the binary system. Figure 7 is a cross-section through a contour map. This was obtained by integrating 15 frames of film of the binary star ADS 10374. The separation obtained is 0.285 arc secs. ± .005 arc secs. at a position angle of 277± 3°. This agrees well with the previous result[8] 0.290 ± 0.006 arc secs. at a position angle of 276± 2° obtained by reducing 300 frames in the analogue method. This method of reduction is more efficient than the analogue system and, indeed, a computer simulation by Dainty (1978) suggests that objects as faint as 18th magnitude could be reached in a processing time of about 35 minutes.

THE USE OF THE CCD IN A PHOTON COUNTING SYSTEM

Considerable interest has been shown in recent years in the construction of photon counting systems using CCDs (e.g. [21,22]). It was felt that an important design factor would be that the image intensifier and CCD sections should be easily separable in order to take immediate advantage of improved tubes and/or CCDs.

Initially the output of a commercially available image intensifier was imaged onto the CCD by a fast lens. Two types were tried:

(i) a four stage, magnetically focussed, EMI Cascade intensifier with green output phosphor

(ii) a three stage, electrostatically focussed VARO cascade intensifier with green output phosphor.

In both cases images of granular nature were observed, but it is not certain that single photoelectron events could be distinguished.

In order to provide a small, simple, high gain intensifier without phosphor decay problems, it was decided to use a microchannel plate with an output phosphor screen chosen to have relatively short persistence and with a spectral output that is well matched to the spectral response of a silicon solid state imager. By using a "Chevron" arrangement, of angled channel plates, it is possible to run the microchannel plates in a saturated mode and thus obtain the best possible pulse height distribution.

Unfortunately, there is no intensifier available from manufacturers that adequately satisfies these requirements, so it was necessary to design and build the prototype here at Imperial College. If it is successful, a manufacturing company has expressed interest in producing a commercial version of the system. Details of the construction of the tube can be found in Airey, Morgan and Ring 1978.[13] Figure 8 shows a section through the tube. Photoelectrons are magnetically focussed onto the chevron arrangement whose output is proximity focussed onto the phosphor screen. The image is then optically coupled by means of a fast lens onto the CCD. Calculations by Airey indicate that there should be more than enough gain to saturate a pixel of the CCD with the signal generated by a single photoelectron.

Video signals from the CCD are then subject to digitising and centroid-finding before storage. (Figure 9).

CONCLUSION

The output of a CCD has been digitised and interfaced using CAMAC to a minicomputer which computes two-dimensional autocorrelations. This allows the reduction of speckle interferometry in a more efficient manner than achieved previously, but this system is not designed to detect single photoelectrons. However, a magnetically focussed, microchannel plate, image tube with a red phosphor is being built specifically to intensify astronomical images to a level that will allow detection of single photoelectrons by the CCD.

ACKNOWLEDGEMENTS

The author would like to thank Dr. B.L. Morgan for advice and encouragement, Messrs. R.W. Airey and P.A. Sharp for technical assistance, Mr. N.L. Vine for computing assistance, and the S.R.C. for provision of a CASE studentship.

REFERENCES

1. McCord, T.B., Frankston, M.J. June 1975 App. Optics 14, no. 6 p. 1437.

2. Hardwick, M.A.R., in "Seventh Symposium on Photo-electronic Devices (Preprints) p. 235, 4-8th Sept. 1978.

3. Harrison, A.B., Hardwick, M.A.R., Morgan, B.L. in "Seventh Symposium on Photoelectronic Devices (Preprints) p. 251 4-8th Sept. 1978.

4. Labeyrie, A. Astron. & Astrophys, 6, 85-87, 1970.

5. Dainty, J.C. Mon. Not. R. astr. Soc. 169, 631-641 1974.

6. Worden, S.P. "Vistas in Astron." 20, 301-317, 1977.

7. Beddoes, D.R., Dainty, J.C., Morgan, B.L., Scaddon, R.J., J. Opt. Soc. Am. 66, no. 11, 1976.

8. Morgan, B.L., Beddoes, D.R., Scaddan, R.J., Dainty, J.C. Mon. Not. R. Astr. Soc. 183, 701-710, 1978.

9. McAlister, H.A. Astrophys. J. 215, 159-165, 1977.

10. Stephens, C.L., van Breda, I.C., ESO/CERN Conf., Geneva May 1972.

11. Moore, C.H., Astron. & Astrophys Suppl., 15, 497-511.

12. Fairchild CCD 202 Data Sheet 1976.

13. Childs, I. in "Seventh Symposium on Photoelectronic Image Devices" (preprints) p. 349, 4-8th Sept. 1978.

14. Livingston, W.C., I.A.U. Colloquium no. 40., p.22-1 Paris-Meudon Obs., 6-8 Sept. 1976.

15. Livingston, W.C., in "Image Processing Techniques in Astr." p.21-30, ed. de Jager 1975.

16. Loh, E.D., Wilkinson, D.T., in "Imaging in Astronomy" Cambridge, Mass., June 18-21, 1975.

17. Geary, J.C. IAU Colloquium no. 40, p. 28-1. Paris-Meudon Obs., 6-8 Sept., 1976.

18. Dravins, D. "Image Processing in Astr." p. 97-102 ed. de Jager 1975.

19. Davies, C.L., Morgan, B.L., Scaddan, R.J., Dainty, J.C., *in* "Seventh Symposium on Photoelectronic Image Devices"(preprints) p. 377, 4-8 Sept., 1978.

20. Blazit, A., Koechlin, L., Oneto, J.L., *in* "Image Processing Techniques in Astron." 79-84 ed. de Jager 1975.

21. Hier, R.G., Beaver, E.A., Schmidt, G.W. *in* "Seventh Symposium on Photoelectronic Image Devices" (preprints) p. 401, 4-8 Sept. 1978.

22. Currie, D.G., IAU Colloquium no. 40, p. 30-1, Paris-Meudon Obs., 6-8 Sept. 1976.

23. Airey, R.W., Morgan, B.L., Ring, J., *in* "Seventh Symposium on Photoelectronic Image Devices" (preprints) p. 329, 4-8 Sept. 1978.

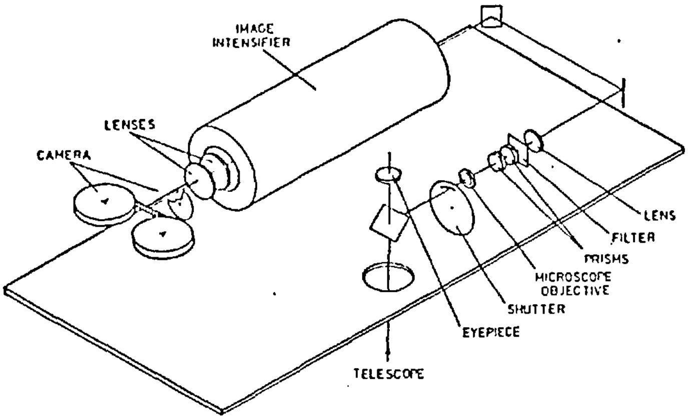

Figure 1. Schematic diagram of the speckle interferometer

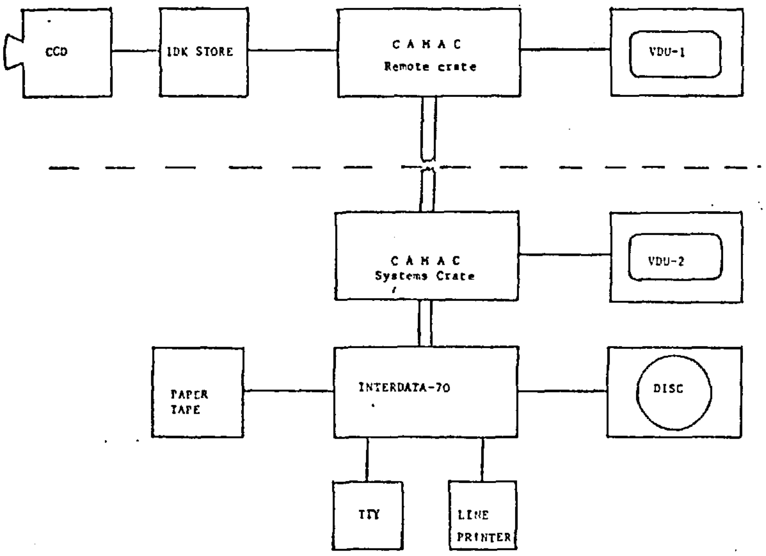

Figure 2. The laboratory computing configuration

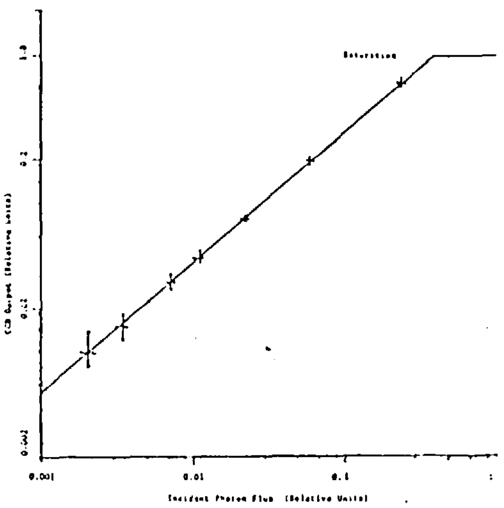

Figure 3. Graph of CCD output (averaged over 1 line of video) versus photon flux

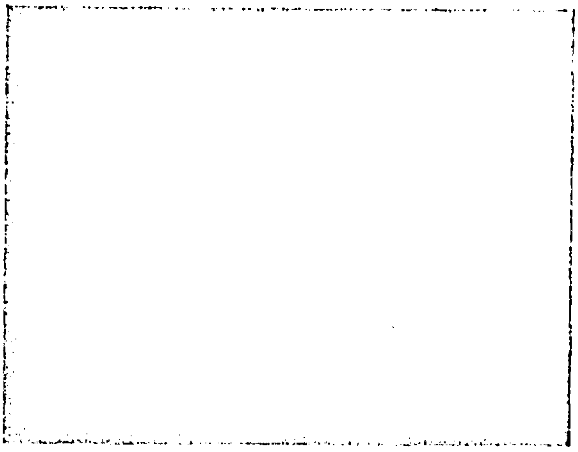

Figure 4. Dark current defects at 35°C with the discriminator set at 50% of diode saturation level

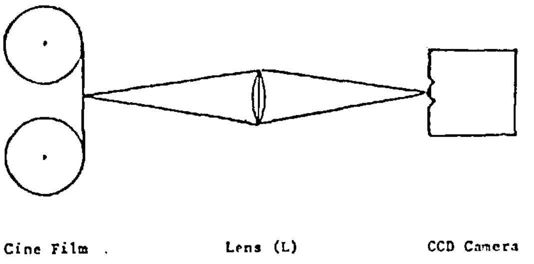

Schematic diagram of the digital technique of data analysis

Figure 5. Schematic diagram of the digital technique of data analysis

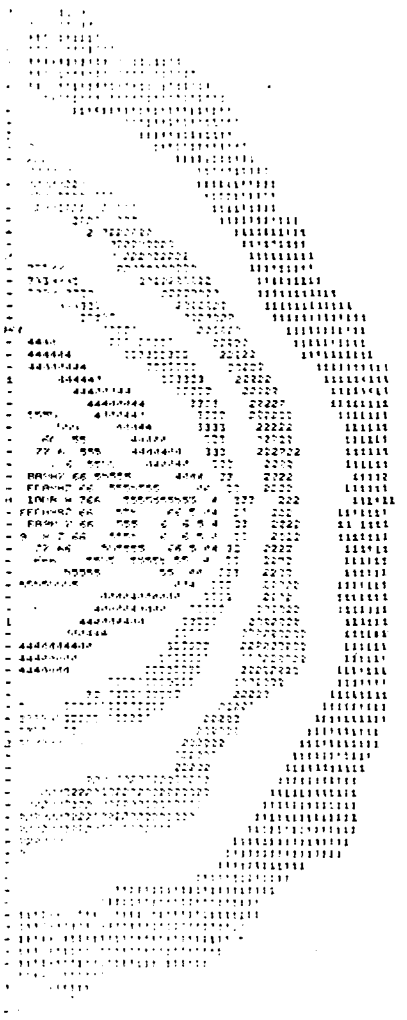

Figure 6. Contour map of autocorrelation plane showing secondary peak

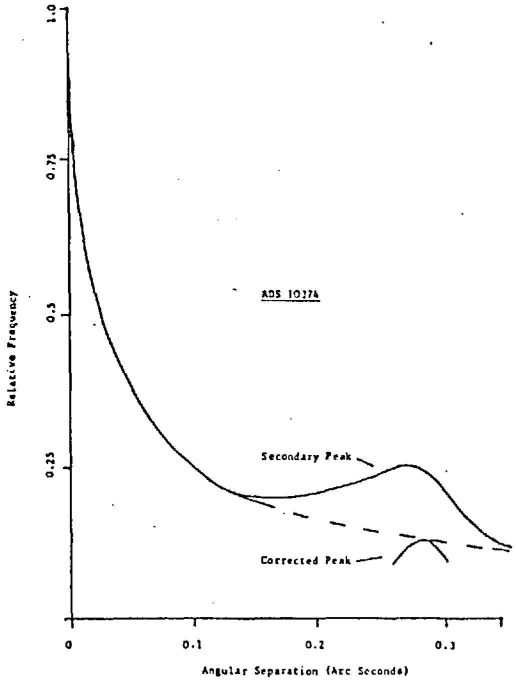

Figure 7. The autocorrelation of 15 frames of the binary system ADS 10374

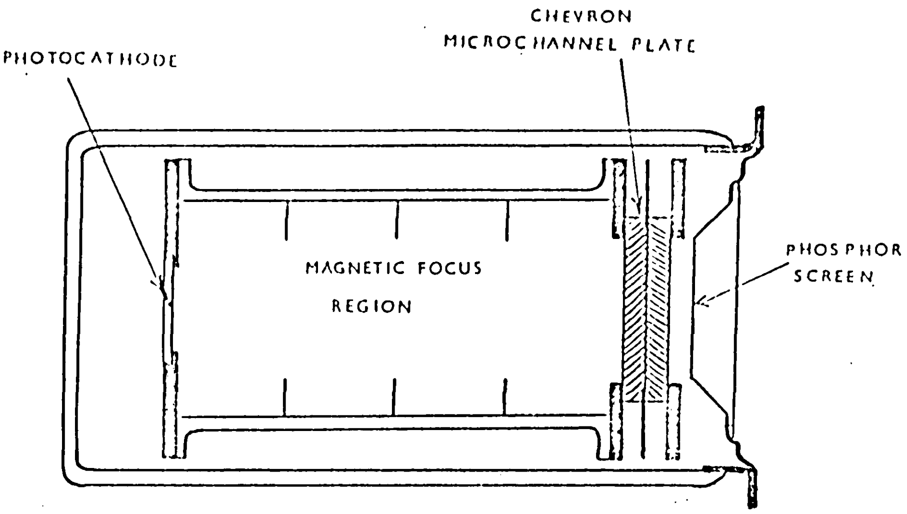

Figure 8. The microchannel plate image tube

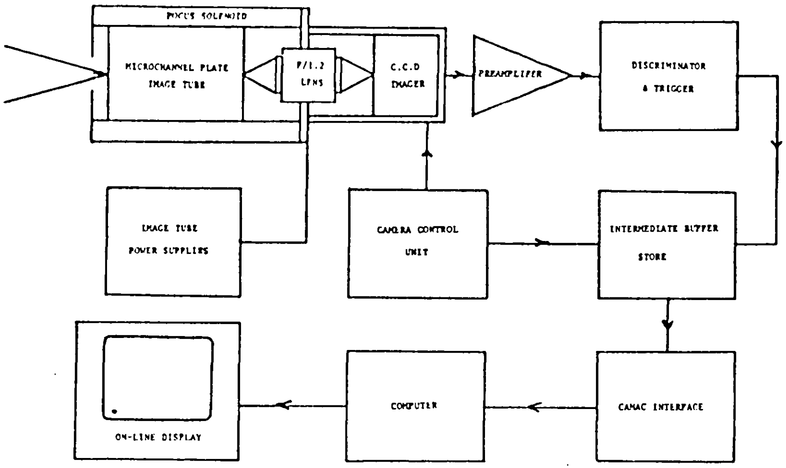

Figure 9. The Photon Counting System

THE USE OF A CCD IN THE REDUCTION OF SPECKLE INTERFEROMETRY DATA

C.L. Davies, B.L. Morgan, R.J. Scaddan

Astronomy Group, The Blackett Laboratory,
Imperial College of Science and Technology,
Prince Consort Road, London SW7 2BZ, England.

and

J.C. Dainty

Department of Physics, Queen Elizabeth College,
Campden Hill Road, London W8 7AH, England.

This paper describes the application of a charge coupled imaging device to the digital reduction of data obtained using the Imperial College stellar speckle interferometer. The method involves the calculation of two-dimensional auto-correlation functions using an Interdata 70 mini-computer. The method has several advantages over analogue analysis techniques. Eventually data will be reduced in real time using a hard wired autocorrelator which is now being constructed.

INTRODUCTION

Speckle interferometry is a method of obtaining diffraction limited resolution from a large telescope, despite the presence of atmospheric turbulence. It is a particularly useful technique for the accurate measurement of the separation and position angles of binary systems, the measurement of stellar diameters and the reconstruction of extended objects. Reviews of the technique, which was suggested by Labeyrie (Ref. 1), can be found in Dainty (Ref. 2) and Worden (Ref. 3).

The Imperial College speckle interferometer records a large number of short exposure (5-25 ms) images on ciné film via an E.M.I. 4-stage cascade image intensifier. The system has been described by Beddoes et al (Ref. 4) and is shown schematically in Fig. 1. There are two approaches by which diffraction-limited information can be derived from these images.

The object and image are related by the equation

$$I\ (x,y) = O\ (x,y) \otimes P\ (x,y) \tag{1}$$

where $\otimes$ denotes convolution.

(i) In the first approach, the average squared modulus of the Fourier transform of the image intensity, that is the power spectrum is found

$$\text{i.e. } W\ (u,v) = \left\langle \left| i\ (u,v) \right|^2 \right\rangle = \left\langle \left| T\ (u,v) \right|^2 \right\rangle . \left| O\ (u,v) \right|^2 \tag{2}$$

In this equation the transfer function, $\langle |T\ (u,v)|^2 \rangle$, can be shown (Ref. 5) to contain a component which extends to the diffraction limit of the telescope.

In the case of a binary star system, the power spectrum obtained is a set of cosine squared fringes whose spacing, orientation and contrast depend upon the angular separation, orientation and magnitude difference of the components of the system.

The method is applied by an analogue technique, the analysis being effected by a coherent optical system, in which the Fourier Transforms of successive frames of the ciné film are co-added onto a single photographic plate (Ref. 4). A typical result is shown in Fig. 2.

Good results using this method have been obtained (Ref. 6,7) with binaries as faint as $M_V = 9.5$ with errors of a few per cent. The analogue analysis, however, introduces additional sources of noise due to the granularity and surface scattering effects arising in the ciné film and non-linearity in the photographic plate. In practice, it has not been found possible to add more than about 10^3 images, limiting observations to fairly bright stars.

(ii) In the second approach, the ensemble average spatial autocorrelation of the image intensity is found i.e.

$$C\ (x,y) = \langle I\ (x,y) \star I\ (x,y) \rangle$$

where $\star$ denotes autocorrelation.

Thus

$$C\ (x,y) = \left\{ O(x,y) \star O\ (x,y) \right\} \otimes \left\{ \langle P(x,y) \star P\ (x,y) \rangle \right\} \qquad (3)$$

In the case of a binary star system, the two-dimensional autocorrelation function contains a central peak with secondary peaks at locations corresponding to the separation and position angle of the binary system. The amplitude ratio of the central and secondary peaks is determined by the magnitude difference of the stars.

The second method lends itself more easily to digital techniques. For photon noise limited images, the picture is digitised into two levels and the centre finding logic determines the position of each photoelectron event. The images of bright stars which contain many photons per speckle can be correlated by the same process using clipping as a form of data compression. This is possible since only the position of the speckles in the x,y plane is of interest although, of course, photometric information is sacrificed in this process.

It can be shown (Ref. 8) that the autocorrelation reduces to

$$C\ (h,\ell) = \sum_i \sum_j (x_i - x_{j-\ell}\ ,\ y_i - y_{j-h}) \qquad (4)$$

Thus, the process of vector autocorrelation involves computing the differences of photon co-ordinates, for all possible pairs of detected photons in all of the images, and incrementing memory locations whose addresses are given by the differences.

The speed of calculation is limited by the computer access time and is improved by the use of hard-wired circuitry. A hard-wired, real-time correlator has been constructed and used by Blazit et al (Refs. 8,9) which can autocorrelate up to 110 photon events per frame at a frame rate of 50 per second. We are at present constructing a correlator to perform auto-correlations and cross-correlations at up to 500 events per frame at a rate of 25 frames per second. A computer simulation (Ref. 10) has shown that the technique should permit measurement of binary stars as faint as 18th magnitude in an observation time of about 35 minutes.

OFF-LINE AUTOCORRELATION USING A CCD AND MINI-COMPUTER

Pending the completion of the real-timeautocorrelator, as an interim measure we are using a Fairchild CCD type 202 having a 100 x 100 pixel output field which we have digitised into two levels and interfaced to an Interdata 70 minicomputer to reduce data previously obtained on cine film. The apparatus is shown schematically in Fig. 3. The ciné film is imaged by a stop motion projector onto the CCD where each frame is scanned in a raster fashion. The lens L is moved to alter the size of the image falling onto the CCD, in order to optimally match the resolution to the binary star spacing.

Various properties of the CCD were examined to determine its suitability for this application; the linearity of the CCD was measured and the results shown in Fig. 4 indicate that it has an extremely linear response over a dynamic range of at least 200 at room temperature. A serious source of noise is that due to some elements of the array which exhibit a high dark current. The number of these can be substantially reduced by cooling, a reduction from 35°C to 25°C decreasing the number by at least 50 per cent. Figure 5 shows oscilloscope displays of the spatial distribution of the dark signal in the array at 35°C. In Figure 5 (a) the threshold has been set at 20 per cent of saturation. In Figure 5 (b) the digitisation threshold has been set at 50 per cent of the diode saturation level. This is the setting used in normal operation. Those elements with high dark current add little to the resulting autocorrelation function as the vector separations of the elements occur only once per frame whereas the vector separation between pairs of speckles occurs many times in each frame.

After digitisation the output of the CCD is read into a 10K by 1 bit buffer store. When a single frame has been stored, the interfacing logic is programmed to search through the 10K array until it finds a location containing a "1". On discovery a LAM interrupt signal is flagged in a CAMAC input/output register and the address in read into a core memory bin. During this process the frame is interlaced and the cycle continues. At present, using CAMAC, it takes about two seconds to read a single frame containing 1000 photoelectron events into the minicomputer. The autocorrelation is performed analogously to equation 4. When the autocorrelation is complete, a signal from the minicomputer advances the cine film by one frame. The autocorrelations of successive frames of the cine film are integrated into a disc store.

Figures 6 and 7 show examples of the resulting autocorrelation functions. In each case the initial autocorrelation function and that corrected for the effects of the envelope due to a single, unresolved star are given. Figure 6 was derived from 50 ciné film frames of a simulated binary system generated by means of a calcite crystal (Ref. 7).

Figure 7 is obtained from 15 frames of film of the binary system ADS 10374. The separation of the stars, as derived from these results is 0.285 ± 0.005 arc seconds at a position angle of 277 ± 3°. The values derived by adding the Fourier transforms of 300 frames by the analogue method are 0.290 ± 0.006 arc sec. and 276 ± 2°.

CONCLUSIONS

The output of a 100 x 100 pixel CCD has been digitised and interfaced to a minicomputer in which two-dimensional autocorrelation functions of the image have been computed and stored. The system has been used to reduce data obtained by speckle interferometry.

ACKNOWLEDGEMENTS

C.L.D. was in grateful receipt of an S.R.C. CASE studentship during the course of this work.

References

1. Labeyrie, A., Astr. Astrophys, 6, 85 (1970).
2. Dainty, J.C., In "Laser speckle and related phenomena (Topics in Applied Physics vol. 9)" ed. Dainty, J.C., Springer-Verlag (1975).
3. Worden, S.P., Vistas Astr., 20, 301 (1977).
4. Beddoes, D.R., Dainty, J.C., Morgan, B.L., Scaddan, R.J., J. Opt. Soc. Am., 66, No. 11, 1247 (1976).
5. Korff, D., J.Opt.Soc.Am., 63, 971 (1973).
6. McAlister, H.A., Astrophys. J., 215, 159 (1977).
7. Morgan, B.L., Beddoes, D.R., Scaddan, R.J., Dainty, J.C., Mon. Not. R. Astr. Soc., 183, 701 (1978).
8. Blazit, A., Koechlin, L., Oneto, J.L., In "Image Processing Techniques in Astronomy" ed. de Jager, Nieuwenhuijzen, 79, D. Reidel Publishing Company, Dordrecht-Holland (1975).
9. Blazit, A., Bonneau, D., Koechlin, L., Labeyrie, A., Astrophys. J., 214, L 79-L84 (1977)
10. Dainty, J.C., Mon. Not. R. Astr. Soc., 183, 223 (1978).

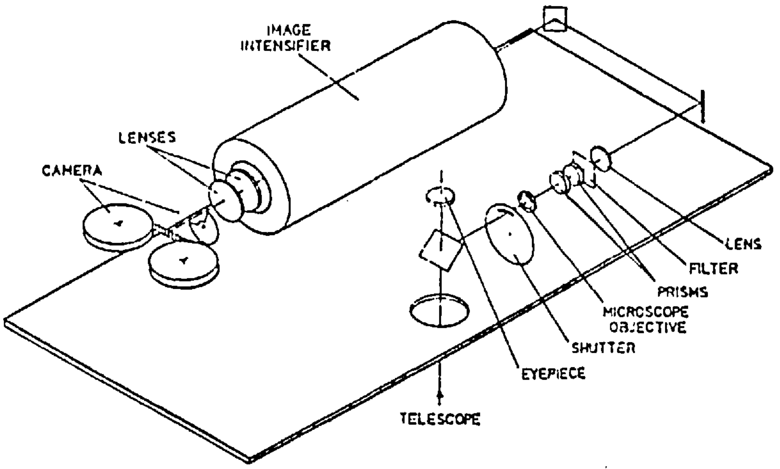

Fig. 1. Schematic diagram of the speckle interferometer.

Fig. 2. Fringes obtained from 700 frames of the binary star system λ Lupi. The fringe spacing corresponds to an angular separation of 0.563 arc secs.

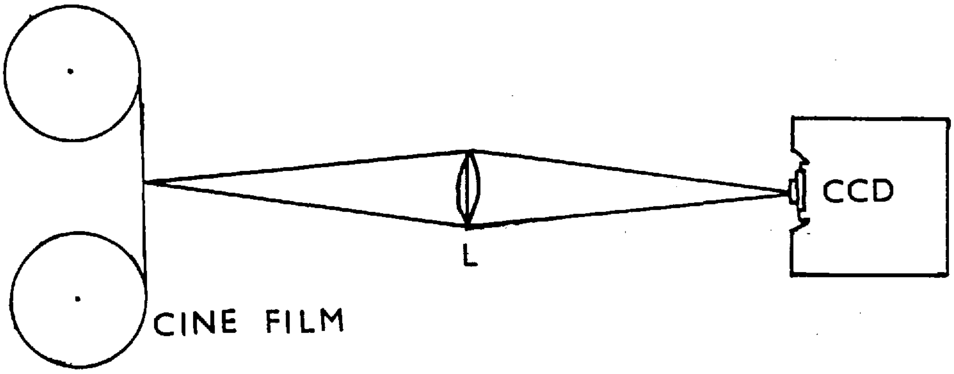

Fig. 3. Schematic diagram of the digital technique of data analysis.

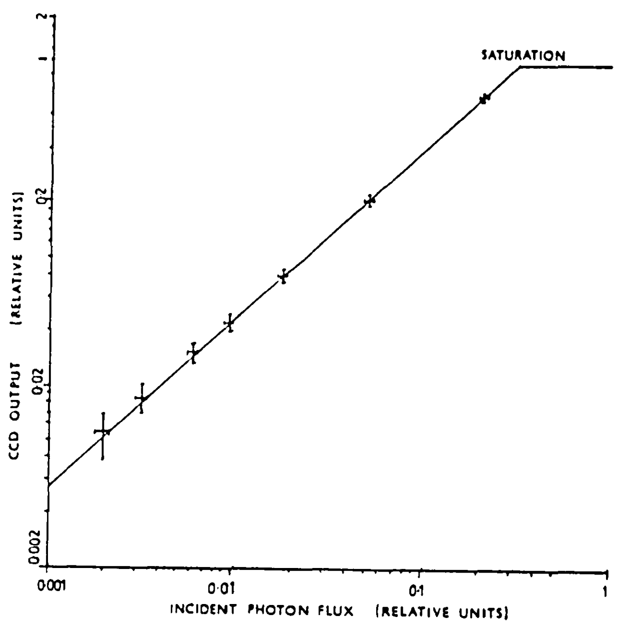

Fig. 4. Graph of CCD output (averaged over 1 line of video) versus photon flux.

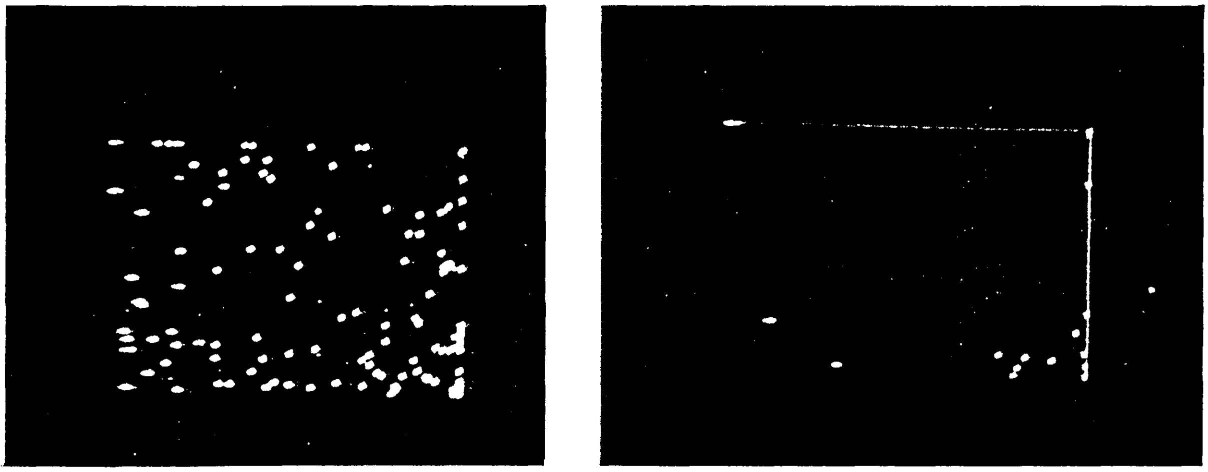

(a) Figure 5 (b)

Fig.5. Dark current defects at 35°C with the discriminator set at (a) 20% (b) 50% of diode saturation level.

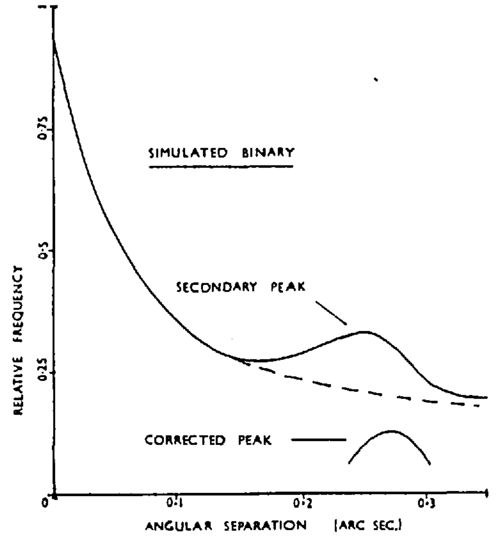

Fig. 6. The autocorrelation of 50 frames of the simulated binary system showing the corrected secondary peak.

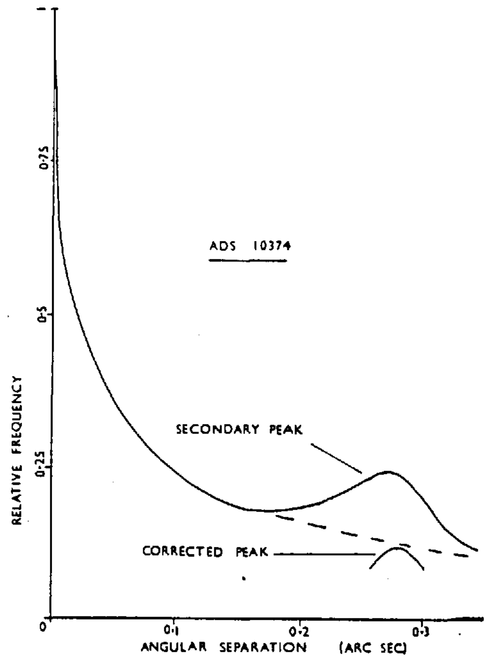

Fig. 7. The autocorrelation of 15 frames of the binary system ADS 10374. The corrected peak indicates a separation of 0.285 arc secs.

Astronomical Applications of a CCD

C. L. DAVIES, B. L. MORGAN, R. J. SCADDAN and R. W. AIREY

Astronomy Group, The Blackett Laboratory, Imperial College of Science and Technology, London, England

and

J. C. DAINTY†

Department of Physics, Queen Elizabeth College, London, England

INTRODUCTION

This paper describes the interfacing of a CCD to an Interdata 70 minicomputer and its subsequent performance. The system is currently used in the computation of two-dimensional autocorrelation functions for digital reduction of speckle interferometry data. This method has several advantages over the analogue analysis techniques. The interfaced CCD is also intended for use in a photon counting system using a specially designed microchannel plate image intensifier, which is described below.

Charge Coupled Devices (CCDs) show great promise as area image detectors. Although not yet matching television camera tubes in respect of uniformity of target response, they have many significant advantages: they are small and robust; they require only low voltages and small currents; they exhibit good linearity characteristics and high sensitivity over a wide range of wavelengths.

The CCD which is in use at Imperial College is the Fairchild type 202 device, which has 10^4 image sensing elements, each $18 \times 30\ \mu m^2$, arranged in a 100×100 matrix. It is driven by circuitry derived from that suggested by Fairchild. The analogue output is digitized into a two level signal.

Eventually the interfaced CCD will be used in a two-dimensional photon counting system. One of its many applications will be to the photometry of faint extended sources such as galaxies. In the outer

---

† Now at The Institute of Optics, The University of Rochester, Rochester. N.Y. 14627, USA.

regions of galaxies, the required signal can be as little as one-thousandth of the ambient sky background level and the extreme linearity of the photon counting approach enables the necessary precise subtraction of the sky background to be achieved. Preliminary photon counting experiments are described later in this paper.

APPLICATION OF THE CCD TO SPECKLE INTERFEROMETRY

The limit to angular resolution of a telescope is given by

$$\theta = 1{\cdot}22\ (\lambda/D),$$

where θ is the angular resolution (radians), λ is the wavelength of the light and D is the diameter of the telescope aperture. Thus for a telescope of aperture 2·5 m the angular resolution at a wavelength of 500 nm is about 0·05 arcsec. In practice however, atmospheric turbulence limits angular resolution to about one or two arcsec; consequently for the largest astronomical telescopes, the angular resolution limit may be a factor of fifty better than is actually observed.

Speckle interferometry is a method of deriving diffraction limited resolution from a large telescope despite the presence of atmospheric turbulence. Reviews of the technique have been given by Dainty[1] and Worden.[2]

Labeyrie[3] has shown that short exposure (5–25 msec) images of astronomical objects taken with large telescopes retain diffraction limited information. There are two approaches by which this information can be derived from such images.

Assuming that the quasi-monochromatic imaging equation applies, then

$$I(x, y) = O(x, y) * P(x, y), \tag{1}$$

where $I(x, y)$ is the image intensity distribution, $O(x, y)$ the object intensity distribution, $P(x, y)$ is the short exposure point spread function of the imaging system, and $*$ denotes convolution.

In the first approach, the average squared modulus of the Fourier transform of the image intensity, i.e., the power spectrum, is found:

$$\begin{aligned} W(u, v) &= \langle |i(u, v)|^2 \rangle \\ &= \langle |T(u, v)|^2 \rangle\, |O(u, v)|^2. \end{aligned} \tag{2}$$

In Eq. (2) $W(u, v)$ is the image power spectrum, $|O(u, v)|^2$ is the object power spectrum, $\langle |T(u, v)|^2 \rangle$ is the transfer function and $\langle\ \rangle$ denotes ensemble averaging. It can be shown[4] that the transfer function contains a component which extends to the diffraction limit of the telescope.

In the case of a binary star system, the object power spectrum is a set of cosine-squared fringes whose spacing, orientation and contrast depend on the angular separation, orientation and magnitude difference of the components of the system. These parameters may therefore be determined if the Fourier transforms of short exposure images of the binary system can be obtained. The Imperial College speckle interferometer is designed to record a large number of short exposure images on cine film via an E.M.I. 4-stage cascade image intensifier (Type no. 9912). The system has been described by Beddoes *et al.*[5] and is shown schematically in Fig. 1.

The two-dimensional Fourier Transform of each image is obtained by an analogue technique, the analysis being effected by a coherent optical system, in which the Fourier Transforms of successive frames of the cine film are co-added onto a single photographic plate. A typical result is shown in Fig. 2.

Good results using this method have been obtained with binaries as faint as $M_v = 9{\cdot}5$ and separations have been determined with errors of only a few per cent.[6,7] The analogue analysis, however, introduces additional sources of noise due to the granularity and surface scattering effects arising in the cine film and to non-linearity in the photographic plate. In practice it has not been found possible to add more than about 10^3 images, limiting observations to fairly bright stars.

In the second approach, the ensemble average spatial autocorrelation of the image intensity is derived from the speckle interferometer cine

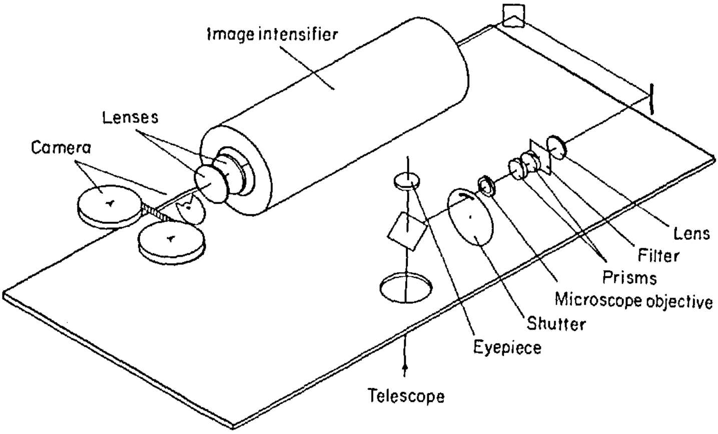

FIG. 1. The speckle interferometer.

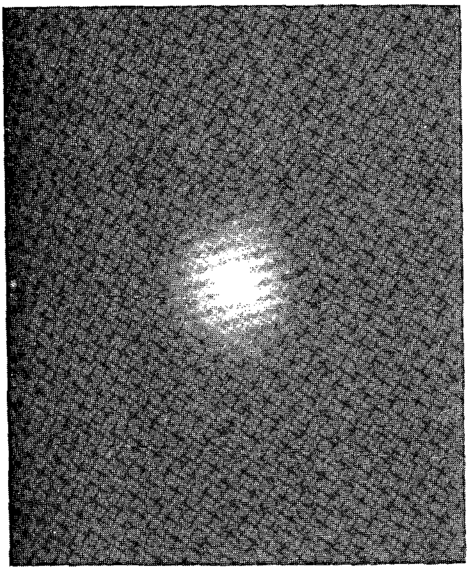

FIG. 2. Fringes obtained by adding the Fourier transforms of 700 frames of the binary star system γ Lupi. The fringe spacing corresponds to an angular separation of 0·563 arcsec.

film. In the case of a binary star system, the two-dimensional autocorrelation function contains a central peak, with secondary peaks at locations corresponding to the separation and position angle of the binary system. The amplitude ratio of the central and secondary peaks is determined by the magnitude difference of the stars, although this information may be difficult to recover.[8]

This method lends itself more easily to digital techniques, and off-line digital analysis has been carried out using a CCD in the system shown in Fig. 3. The cine film, mounted on a stop motion projector and illuminated by an incoherent light source, is imaged onto the CCD by a lens, which is movable to allow the scale of the film to be optimally matched to the resolution of the CCD. For photon noise limited cine frames the output of the CCD is digitized into two levels. The images of bright stars which contain many photons per speckle can be correlated by the same process using clipping as a form of data compression. This is possible because the position of speckles in the x, y plane yields valuable results although photometric information is lost and some distortion of the autocorrelation function may be introduced.

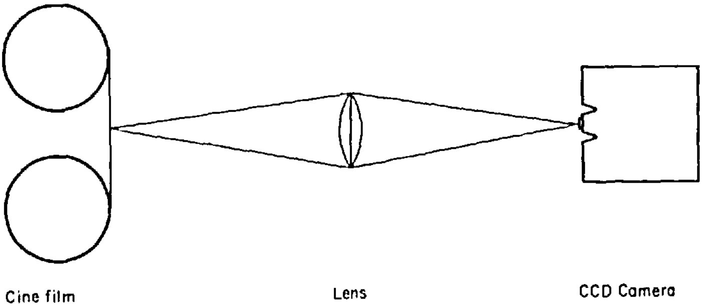

FIG. 3. The digital data analysis system.

It can be shown[9] that in these circumstances the autocorrelation function reduces to

$$C(h, l) = \sum_{i} \sum_{j} (x_i - x_{j-l}, y_i - y_{i-h}). \tag{3}$$

Thus, if the vector separation of every possible pair of speckles is found, a two-dimensional histogram of these separations yields the autocorrelation function directly. Aspects of the performance of the CCD were studied to determine its suitability for this purpose.

CCD PERFORMANCE

Properties of the CCD relevant to its use as a signal generating device have been widely reported.[10–13] The following characteristics are particularly important in the reduction of speckle data.

Noise Characteristics

The CCD is not cooled and reaches a maximum temperature of 37°C after one hour's use. Consequently the noise performance is dominated by thermal effects; it was felt that cooling was unnecessary in this application. The thermal noise comprises two components: the familiar random thermal background and a fixed pattern signal due to some photosites having a dark current many times greater than the average. This is a serious problem in the computing of autocorrelations. Figure 4 shows a digitized picture of the fixed pattern defects at 37°C, with the digitizing discriminator set at 20% of the diode saturation level. Figure 5 shows the same CCD output with the discriminator level set at 50% of

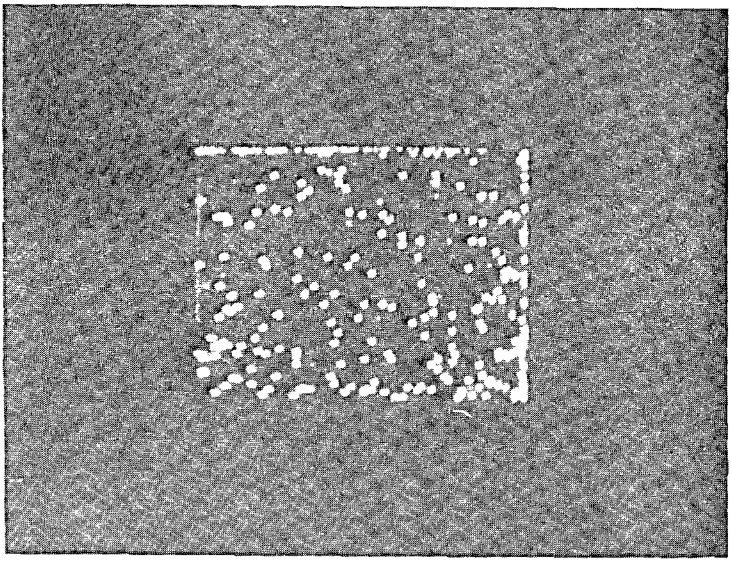

FIG. 4. Dark current defects at 37°C with the discriminator set at 20% of diode saturation level.

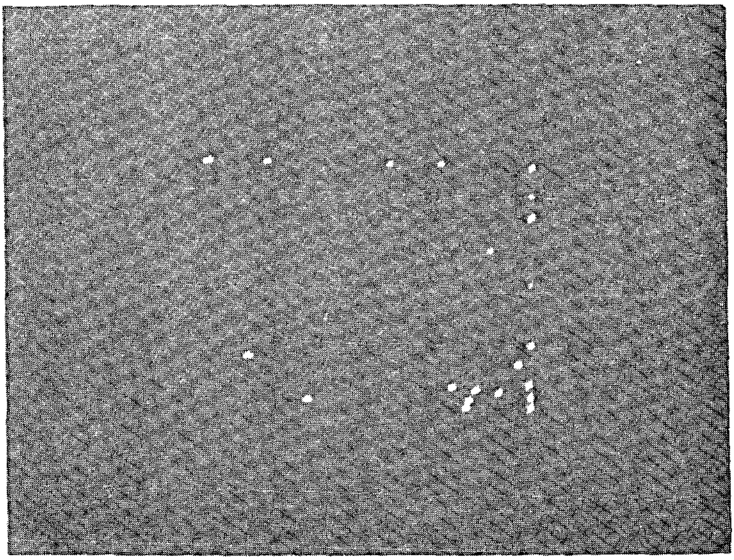

FIG. 5. Dark current defects at 37°C with the discriminator level set at 50% of diode saturation level.

the diode saturation level. Since this noise is "fixed pattern", a mapping of the defects can be stored in the computer and subtracted from each video frame.

Linearity and Dynamic Range

The random thermal background limits the dynamic range which can be achieved using the CCD. Figure 6 shows the relationship between input illumination and output signal level averaged over one line of the array. Photosites displaying the fixed pattern noise mentioned above were excluded from the measurement. It can be seen that the response is linear over a range of at least 100 to 1 at this temperature.

THE DATA PROCESSING SYSTEM

The processing of data from a single cine frame is carried out in four stages: the output of the CCD is firstly written into a buffer store, this store is then read into an Interdata 70 minicomputer where the two-dimensional autocorrelation function is computed and lastly the result is integrated into a disc store. The speed of this process is limited by the time taken for the calculation of the autocorrelation function to about ½ to

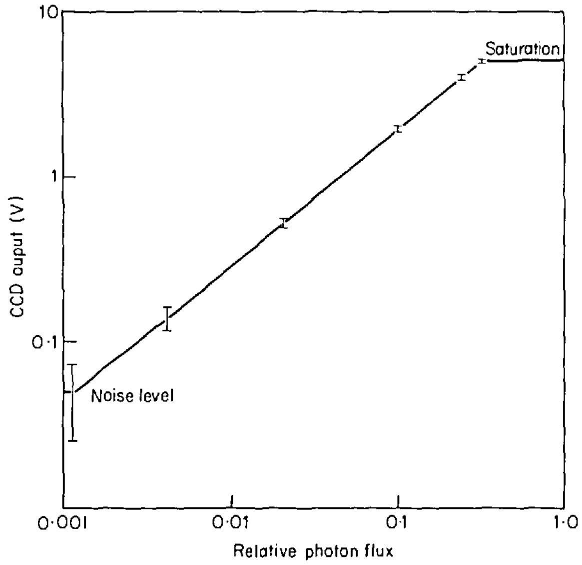

FIG. 6. Graph of CCD output (averaged over one line of video) versus photon flux.

1 min. At the end of this time, the stop motion projector is automatically incremented by one frame. In order to improve the processing time, a hard wired correlator is being constructed which will compute autocorrelations and cross correlations at a rate of 25 frames per second with up to 500 photoelectron events in each frame. This system will operate in real time on the telescope.

The Computing System

The laboratory computing configuration is shown in Fig. 7. The minicomputer is an Interdata 70 which has been programmed using FORTH language.[14] FORTH is an interactive, high level language that makes extremely efficient use of core, thus allowing the manipulation of the large arrays needed in image processing. The CCD, buffer store and CAMAC crate are remotely located and operations are controlled from VDU-1. A 24 bit I/O register CAMAC module is used as a one word store. The address of a photoelectron event is loaded on command from the control logic associated with the buffer store and this establishes a LAM status within the module which is continually sampled in the programme. The module has been modified so that the READ command also clears the LAM bistable and causes a restart signal to be communicated to the control logic of the buffer store.

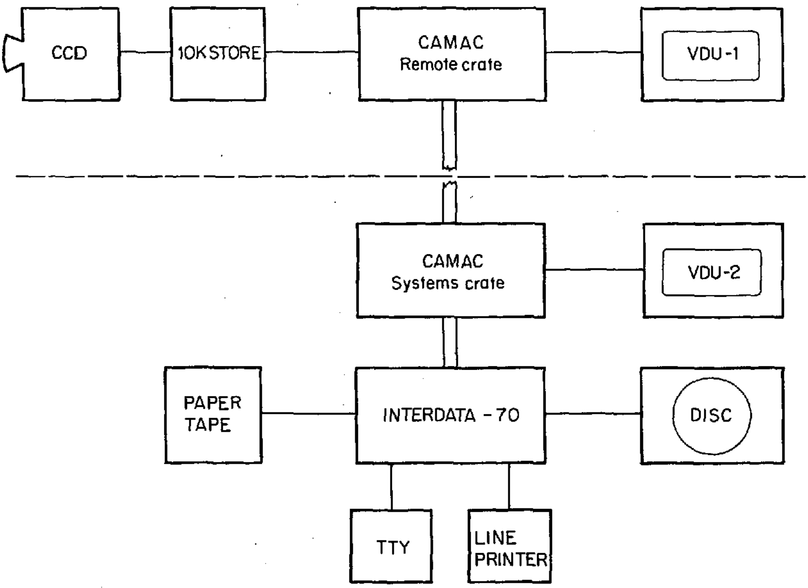

FIG. 7. Block diagram of the laboratory computing configuration.

The Buffer Store

After digitizing the output of the CCD, a complete frame of video is stored in a 10k × 1 bit store so that the output bit rate of the CCD ($\sim 3 \times 10^5$ bits $\sec^{-1}$) is matched to the input bit rate of the CAMAC/INTERDATA combination ($\sim 7 \times 10^3$ bits $\sec^{-1}$). The CCD scanning logic continues to operate while the control logic associated with the buffer store searches sequentially through the array for a location with a "1" stored (corresponding to a photoelectron event). It then raises a LAM status in the I/O module and the address is read into the appropriate memory location. A restart command from the module triggers the control logic and the search continues. At the end of readout, the buffer store is rewritten by the CCD. A single frame containing about 1000 events takes approximately two seconds to read into the computer.

AUTOCORRELATION RESULTS

The system is calibrated using a simulated binary star created by filming a single unresolvable star through a calcite crystal to create a double image.[7] Figure 8 shows a typical contour map of the autocorrelation plane for the simulated binary, and Fig. 9 shows a cross section through it. Tables I and II show a comparison of preliminary results using the autocorrelation technique and those obtained using the analogue apparatus.[7]

TABLE I

Comparison of the separations obtained by analogue and digital methods

Object	Analogue	Digital
Simulated binary	0·278″ ± 0·006″	0·277″ ± 0·005″
(η Oph) ADS 10374	0·278″ ± 0·006″	0·277″ ± 0·005″
(β Del) ADS 14073	0·290″ ± 0·006″	0·285″ ± 0·005″

TABLE II

Comparison of the position angles obtained by analogue and digital methods

Object	Analogue	Digital
Simulated binary	7° ± 2°	8·9° ± 3°
(η Oph) ADS 10374	276 ± 2°	277° ± 3°
(β Del) ADS 14073	0° ± 2°	0° ± 3°

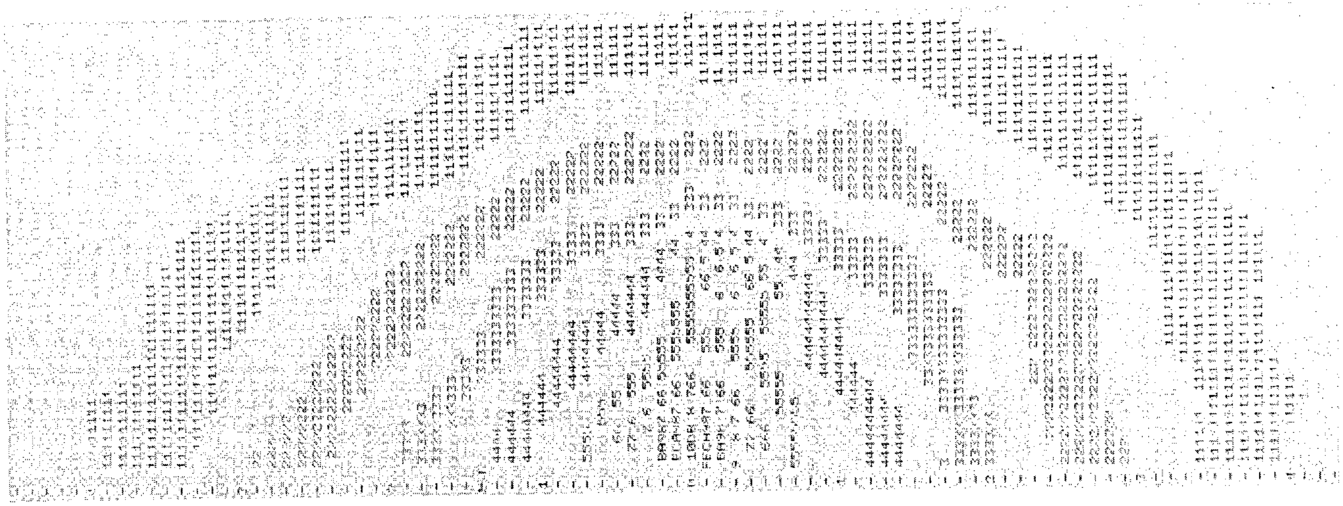

FIG. 8. Typical contour map of autocorrelation plane showing secondary peak.

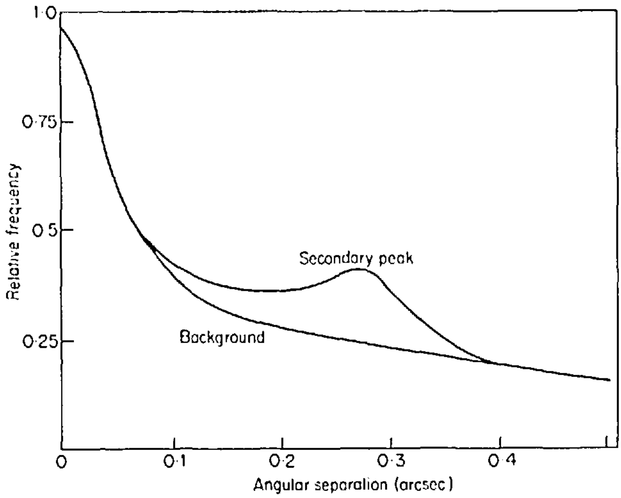

FIG. 9. Cross section through the contour map of Fig. 8 along the line of the secondary peak.

In each case, the digital result is obtained by co-adding less than thirty frames while the analogue method uses at least 250 frames. The digital reduction of speckle data is more efficient than the analogue technique, and a computer simulation by Dainty[8] suggests that objects as faint as 18th magnitude could be resolved in a processing time of about 35 min.

THE USE OF A CCD IN A PHOTON COUNTING SYSTEM

It is eventually intended to use a CCD as part of a photon counting detector on telescopes. For the detection of single photoelectron events it is of course necessary to add a prior stage of image intensification.[15]

In a preliminary experiment, the output of a commercially available image intensifier tube was imaged onto the CCD using a fast lens coupling. Two types of image intensifier were tried.

(i) A four stage, magnetically focused, E.M.I. cascade intensifier with green P·20 output phosphor.

(ii) A three stage, electrostatically focused VARO cascade intensifier with green P·20 output phosphor.

In both cases, images of a granular nature were observed, but it is not certain that single photoelectron events could be distinguished. This and other measurements suggest that a suitable intensifier must have:

(i) Very high gain to allow optical coupling with a lens to the CCD. Lens coupling is desirable rather than fibre optic coupling or direct electron bombardment, since it permits simple interchanging of CCDs and enables intensifiers with different photocathodes to be used.

(ii) A red phosphor for optimal matching to the CCD spectral response.

(iii) A relatively short phosphor decay time so that each event is only counted once.

(iv) Small physical size.

No image intensifier meeting these criteria was commercially available and one was therefore designed at Imperial College,[16] and its construction is now nearing completion. If it is successful, a manufacturing company has expressed interest in producing a commercial version.

The final design (Fig. 10) consists of a short magnetically focused section which images electrons from the photocathode onto the channel plate input face. Two 12·5 μm pore microchannel plates are arranged in chevron configuration and are run in the saturated gain mode. Their output pulses (approximately 10^7 electrons) are proximity focused with a field gradient of 3 kV mm^{-1} onto a rare earth phosphor screen which has spectral emission peaked in the red. This phosphor was chosen for its excellent match to the spectral response of a silicon CCD.

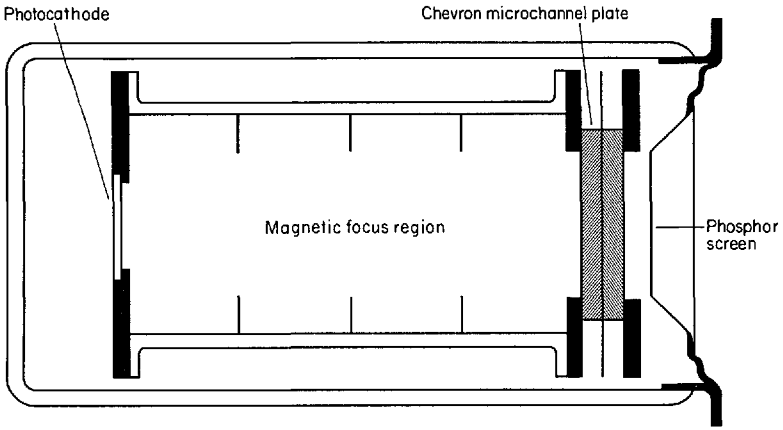

FIG. 10. A schematic cross section of the image intensifier tube.

The photocathode holder, the accelerating electrodes for the magnetically focused region, together with the assembly which holds the microchannel plates and the phosphor screen, are all mounted to form a single rigid structure that can be inserted into the glass vacuum envelope of the tube which is then sealed by means of an argon arc weld at the output end.

The photocathode is prepared separately in a photocathode processing cell, fitted with a special thin glass breakbulb which can be ruptured in vacuum to permit transfer of the photocathode into the tube through a flattened pumping stem, after the tube has been baked out. This photocathode transfer procedure is similar to that which has been well established for the manufacture of the Spectracon electronographic image tube.[17] The advantage of this technique is that alkali vapours used in the photocathode formation process are not liberated within the image tube envelope where they could contribute to spurious electron emissions by lowering the work function of surfaces. Moreover, damage to the microchannel plates by alkali contamination is avoided. The prototype microchannel intensifier has a posted-in S·11 photocathode; later tubes will have S·20 photocathodes. Barium getters are used in the tube to absorb any residual gases liberated by the microchannel plates when the tube is operated. The intensifier is designed to focus its magnetic section in a field of approximately 0·01 T produced by a small solenoid, wound to give a uniform magnetic field over the working region of the tube.

CONCLUSIONS

A charge coupled device has been successfully interfaced, via CAMAC, to an Interdata 70 mini-computer for the computation of two-dimensional autocorrelation functions. Although the video picture is digitized with only one bit accuracy, useful information is obtained. The current system allows the off-line reduction of speckle interferometry data to be achieved in a more efficient manner than with analogue techniques. This system is not designed to detect single photoelectrons. However, a magnetically focused, microchannel plate image tube with a red phosphor is being built specifically to intensify astronomical images to a level that will allow detection of single photoelectron events by the CCD.

ACKNOWLEDGMENTS

C.L.D. was in grateful receipt of an S.R.C. CASE studentship during the course of this work.

REFERENCES

1. Dainty, J. C. *In* "Laser speckle and related phenomena (Topics in Applied Physics, Vol. 9)" ed. by J. C., Dainty, p. 255. Springer-Verlag, Berlin (1975).
2. Worden, S. P., *Vistas Astron.* **20,** 301 (1977).
3. Labeyrie, A., *Astron. & Astrophys.* **6,** 85 (1970).
4. Korff, D., *J. Opt. Soc. Am.* **63,** 971 (1973).
5. Beddoes, D. R., Dainty, J. C., Morgan, B. L. and Scaddan, R. J., *J. Opt. Soc. Am.* **66,** 1247 (1976).
6. McAlister, H. A., *Astrophys. J.* **215,** 159 (1977).
7. Morgan, B. L., Beddoes, D. R., Scaddan, R. J. and Dainty, J. C., *Mon. Not. R. Astron. Soc.* **183,** 701 (1978).
8. Dainty, J. C., *Mon. Not. R. Astron. Soc.* **183,** 223 (1978).
9. Blazit, A., Koechlin, L. and Oneto, J. L., *In* "Image Processing Techniques in Astronomy" ed. by C. de Jager and H. Nieuwenhuijzen, p. 79, Reidel, Dordrecht, (1975).
10. Fairchild CCD 202 Data sheet (1976).
11. Loh, E. D. and Wilkinson, D. T., *In* Proc. Conference on "Imaging in Astronomy" Cambridge, Mass., June 18–21 (1975).
12. Livingston, W. C., *In* "Astronomical Applications of Image Detectors with Linear Response" (IAU Colloquium No. 40) ed. by M. Duchesne and G. Lelièvre, p. 22–1. Paris-Meudon Observatory (1976).
13. Dyck, R. H. and Jack, M. D., "Low Light Level Performance of the CCD 201", Fairchild Semiconductor Components Group Information Sheet (1974).
14. Moore, C. H., *Astron. & Astrophys. Suppl. Ser* **15,** 497 (1974).
15. Currie, D. G., *In* "Astronomical Applications of Image Detectors with Linear Response" (IAU Colloquium No. 40) ed. by M. Duchesne and G. Lelièvre, p. 30–1. Paris-Meudon Observatory (1976).
16. Airey, R. W., Morgan, B. L. and Ring, J. *In* "Seventh Symp. P.E.I.D. Preprints," p. 329 (1978).
17. McGee, J. D., Khogali, A., Ganson, A. and Baum, W. A., *In* "Adv. E.E.P." Vol. 22A, p. 11 (1966).

References

Note: AEEP refers to "Advances in Electronics and Electron Physics" published by Academic Press.

Aikens R.S., Lynds C.R., Nelson R.E., 1976.
Proc. Soc. Photo-optical Instrumentation Engineers, vol. 78, pp 65 - 72.

Aime C., Roddier F., 1977.
Opt. Comm., vol. 21, p. 435

Airey, R.W., 1974.
Internal Report: "Preliminary Appraisal of a Photon Counting Image Tube System". Blackett Laboratory, Imperial College, London SW7.

Airey R.W., Morgan B.L., Ring J., 1978.
Preprints of the 7th Symposium on Photo-Electronic Devices, Blackett Laboratory, Imperial College, London SW7. 4th - 8th Sept. 1978. p.329

Allen C.W., 1973.
"Astrophysical Quantities". 3rd Edition. Pub. Athlone Press, London Univ.

Barbe D.F., 1975 (Jan.) Proc. IEEE,
vol. 63, no. 1, p. 38.

Barnett M.E., Parry G., 1977. Opt. Comm.
vol. 21, no. 1, p. 60.

Basayaeva L.I., Pletneva N.I., Semenov E.P., 1972
Sov. J. Opt. Techn. vol. 39, no. 6.

Bates R.H.T., 1977. Mon. Not. R. Astr. Soc.,
vol. 181, p. 365.

Baum W.A., 1962. AEEP vol. 16, p. 391.

Beaver E.A., 1978. Preprints of the 7th Symposium on
Photo-Electronic Devices, Blackett Laboratory,
Imperial College, London SW7.
4th - 8th Sept. 1978 o. 393.

Beaver E.A., McIlwain C.E., 1971.
Rev. Sci. Inst. vol. 42, no. 9, p. 1321.

Beaver E.A., Harms R.J., Schmidt G.W., 1976.
AEEP vol. 40B, p. 745

Beddoes D.R., 1979.

Ph. D. Thesis, Imperial College, London Univ.

Beddoes D.R., Dainty J.C., Morgan B.L., Scaddan R.J., 1976.

J. Opt. Soc. Am. vol. 66, no. 11, p. 1247.

Berglund C.N., 1971 (Dec.) IEEE

Journal of Solid State Circuits, vol. SC-6, no. 6, p. 391.

Beurle R.L., Wreathall W.M., 1962. AEEP

vol. 16, p. 333.

Blazit A., Koechlin L., Oneto J.L. 1975.

In "Image Processing Techniques in Astronomy".

pp 79 - 84. ed. De Jager/Nieuwenhuijzen

pub. D. Reidel Pub. Comp. Holland

Blazit A., Bonneau D., Koechlin L., Labeyrie A., 1977.

Astrphys. J. vol. 214, L79 - L84.

Boksenberg A., 1972. Proc. ESO/CERN Conf. on Auxiliary

Instrumentation for Large Telescopes. ed. Lausten and Reiz

Geneva, May 2 - 5, 1972.

Boksenberg A., 1976. Proc. IAU Colloquium no. 40
ed. M. Duchesne, G. Lelievre.
Paris - Meudon, 6 - 8 Sept. 1976.

Boksenberg A., Burgess D.E., 1972.
AEEP vol. 33B, p. 835.

Boksenberg A., Burgess D., Fordham L.A., Shortridge K.,
Wright S.L., 1976. AEEP vol. 40B, p. 877.

Born M., Wolf E., 1975. "Principles of Optics"
5th ed. pub. Pergamon Press.

Boutot J.P., Eschard G., Polaert R., Duchenois V., 1976.
AEEP vol. 40A, p.103.

Boyle W.S., Smith G.E., 1970.
Bell Sys. Tech. Journ. vol. 49, pp 587 - 593.

Bracewell R., 1965. "The Fourier Transform and its applications".
pub. McGraw-Hill.

Brignell J.E., Young R., 1979. J. Phys. E:
Sci. Inst. vol. 12, p. 455.

Brown, R.H., 1968.
"The Intensity Interferometer", pub. Taylor and Francis.

Childs I., 1978. Preprints of the 7th Symposium on Photo-Electronic Devices, Blackett Laboratory, Imperial College, London SW7. 4th - 8th Sept. 1978. p. 349.

Chodil G.J., Hoshiko H.H., Johnson J.J., McConaughey R.M., 1978. Preprints of the 7th Symposium on Photo-Electronic Devices, Blackett Laboratory, Imperial College, London SW7. 4th - 8th Sept. 1978, p. 369.

Choisser 1976. AEEP vol. 40B, p. 735.

Colgate S.A., Moore E.P., Colburn J., 1975. Appl. Opt. vol. 14, no. 6, p. 1429.

Colson W.B., McPherson J., King F.T., 1973. Rev. Sci. Inst. vol. 44, no. 12, p. 1694.

Currie D.G., 1976. Proc. IAU Colloquium no. 40. ed. M. Duchesne and G. Lelievre. Paris - Meudon, 6th - 8th Sept. 1976.

De Vorkin D. H., 1975. J. Hist. Ast. vol. 6, no. 1.

Dainty J.C., 1970. Opt. Acta vol. 17, p. 761.

Dainty J.C., 1973. Opt. Comm. vol. 7, p. 129.

Dainty J.C., 1974. Mon. Not. R. astr. Soc.
vol. 169 pp 631 - 641.

Dainty J.C., 1975. In "Laser Speckle and Related Phenomena".
ed. J.C. Dainty. Topics in Applied Physics vol. 9.
pub. Springer-Verlag.

Dainty J.C., 1976. "Progress in Optics". vol. 14.
ed. E. Wolf, pub. North-Holland.

Dainty J.C., 1978. Mon. Not. R. astr. Soc. .
vol. 183, pp 223 - 236.

Davies J.D., Ponsonby J.E.B., Pointon L., de Jager G., 1969.
Nature vol, 222, p. 933.

Debrus S., Francon M., May M., 1969.
ICO 8 Conference, Reading.

Dravins D., 1975. In "Image Processing Techniques in Astronomy"
pp 97 - 102. ed. de Jager/Nieuwenhiujzen.
pub. D. Reidel Pub. Comp. Holland.

Dyck R.H., Jack M.D., 1974. "Low Light Performance of the
CCD 201". Paper available from Fairchild Semiconductor
Components Group, California. Oct. 1974.

Eberhardt E.H., 1968. App. Opt. vol. 7, no. 10
Oct. 1968 p.2037.

Eur 5100e & Eur 4100e. Specifications for the CAMAC system
pub. Commission of the European Communities.

Fahlman G.G., Mochnacki S.W., Pritchet C., Condal A.R.,
Walker G.A.H., 1978.
Preprints of the 7th Symposium on Photo-Electronic Image
Devices. Blackett Laboratory, Imperial College, London SW7.
4th - 8th Sept. 1978 p. 375.

Fairchild 1974(a) CCD201 Preliminary Data Sheet
(b) CCD201 Design Brochure
pub. Fairchild Semiconductor Components Group, California.

Fairchild 1976 (April) CCD202 Preliminary Data Sheet.
pub. Fairchild Semiconductor Components Group, California.

Fairchild 1978. CCD321A Data Sheet (Aug. 1978).
pub. Fairchild Camera and Instrument Group, California.

Farrow A.S.J., 1974. Oxford Conf. on Computer Scanning, vol. 2
pp 407 - 422.

Fort B., Boksenberg A., Coleman C., 1976.
Proc. IAU Colloquium no. 40, ed. M. Duchesne and
G. Le Lievre. Paris - Meudon 6th - 8th Sept. 1976.

Fry P.W., 1975. J. Phys. E: Sci. Inst. vol. 8, p. 337.

Gaskell C.M., Robinson L.B., 1978.
Preprints of the 7th Symposium on Photo-Electronic Image Devices, Blackett Laboratory, Imperial College, London SW7. 4th - 8th Sept. 1978 p. 301.

Geary J.C., 1976. Proc. IAU Colloquium no. 40.
ed. M. Duchesne and G. LeLievre. Paris - Meudon, 6th - 8th Sept. 1976.

Geary J.C., Beetz M.A., Fath D., 1976.
Proc. IAU Colloq-ium no. 40,
ed. M. Duchesne and G. LeLievre. Paris - Meudon, 6th - 8th Sept. 1976.

Gezari D.J., Labeyrie A., Stachnik R.V., 1972.
Astrophys. Journ. vol. 173, L1 - L5.

Gibbs J.E., 1977. Electr. Lett. vol. 13 p. 122

Gilbert G.R., Angel J.R.P., Grandi S. 1976.
AEEP vol. 40B p.699.

Goldfischer L.I., 1965. J. Opt. Soc. Am. vol. 55, no. 3, p. 247.

Goldman S., 1953. "Information Theory",
pub. Prentice-Hall Inc. N.Y.

Goodman J.W., 1965. Proc. IEEE vol. 53, no. 11
p. 1688.

Goodman J.W., 1975. In "Laser Speckle and Related Phenomena"
ed. J.C. Dainty, Topics in Applied Physics vol. 9.
pub. Springer-Verlag.

Goodrich G.W., Wiley W.C., 1962. Rev. Sci. Inst., vol. 33,
p. 761.

Goodson J., Woolgan A.J., Higgins J., Thumbwood R.F., 1972.
AEEP vol. 33A, p. 83.

Gott R., Parkes W., Pounds K.A., 1970.
Nuc. Inst. and Methods, vol. 81, p. 152.

Gough P.T., Bates R.H.T., 1974.
Optica Acta vol. 21, p. 243.

Griffin R.F., 1973. Observatory vol. 93, p. 3.

Guest A.J., 1971. Acta Electronica vol. 14, no. 1.
p. 79.

Hale J.A.G., Saraga P., 1974.
Opto-electronics, vol. 6, pp 333 - 348.

Hardwick M.A.R., 1978. Preprints of the 7th Symposium on Photo-Electronic Image Devices, Blackett Laboratory, Imperial College, London SW7. 4th - 8th Sept. 1978, p. 235.

Harrison A.B., Morgan B.L., Hardwick M.A.R., 1978. Preprints of the 7th Symposium on Photo-Electronic Image Devices, Blackett Laboratory, Imperial College, London SW7. 4th - 8th Sept. 1978, p. 251.

Hill G.E., 1976. AEEP vol. 40A, p. 153.

Horton J.W., Mazza R.V., Dym H., 1964. Proc. IEEE vol. 52, p. 1513.

Hubbard G., Reed M., Strittmatter P., Hege K., 1978. Proc. IAU Colloquium no. 50, "High Angular Resolution Stellar Interferometry". ed. J. Rouis: Maryland Aug. 1978.

Jakeman E., 1973. In "Photon Correlation and Light Beating Spectroscopy". ed. H.Z. Cummins and E.R. Pike, p. 94. pub. Plenum Press.

Joyce W.B., Bertram W.J., 1971. Bell Sys. Tech. Journ. vol. 50 no. 6. p. 1741.

Kaiser J.F., Angell R.K., 1956. Technical Memo. no. 7668-TM-2, Servomechanisms Lab. MIT, 17th Dec. 1956.

Karo D.P., Schneiderman A.M., 1979. App. Optics vol. 18, no. 6, p. 828.

Kazan 1974. In "Advances in Image Pickup and Display" vol. 1. ed. Kazan, pub. Academic Press.

Knox K.T., Thompson B.J., 1974. Astrophys. Journ. vol. 193, L 45 - L 48.

Kodak 1967. "Kodak Wratten Filters". 3rd ed. pub. Kodak Ltd. (London).

Koechlin L., 1978. Proc. IAU Colloquium no. 50. "High Angular Resolution Stellar Interferometry". ed. J. Rouis: Maryland, Aug. 1978.

Korff D., 1973. J. Opt. Soc. Am. vol. 63, no. 8. p.971.

Labeyrie A., 1970. Astron. & Astrophys. vol. 6., p. 85.

Labeyrie A., 1976. In "Progress in Optics" vol. 14. p. 47. ed. E. Wolf. pub. North-Holland

Labeyrie A., 1978. In "Annual Review of Astronomy and Astrophysics". p. 78.

Leskovar B., 1977 (Nov.). Physics Today vol. 30
no. 11, p. 42.

Lipson S.G., Nisenson P., 1974. App. Optics vol. 13.
p. 2052.

Livingston W.C., 1975. In "Image Processing Techniques in
Astronomy" p. 21.
ed. de Jager/Nieuwenhuijzen.
pub. D. Reidel Pub. Comp. Holland.

Livingston W.C., 1976. Proc. IAU Colloquium no. 40
ed. M. Duchesne & G. LeLievre. Paris - Meudon,
6th - 8th Sept. 1976.

Livingston W.C., Harvey J., Slaughter C., Trumbo D., 1976.
App. Optics vol. 15, no. 1.

Loh E.D., Wilkinson D.T., 1975. "Imaging in Astronomy"
Technical Digest Conf: Cambridge, Mass.,
June 18 - 21, 1975.

Lowenthal S., Arsenault H., 1970.
J. Opt. Soc. Am. vol. 60, no. 11, p. 1478.

Lowrance J.L., Renda G., Zucchino P., 1976.
AEEP vol. 40B, p. 711.

Lynds C.R., Worden S.P., Harvey J.W., 1976.
Astrophys. Journ. vol. 207, pp 174 - 180.

McAlister H.A., 1977. Astrophys. Journ. vol. 215,
pp 159 - 165.

McCord T.B., Frankston M.J., 1975. App. Optics vol. 14,
no. 6, p 1437.

McKechnie T.S., 1974. Optics vol. 39, p. 258.

Mandel L., 1959 (May). British Journ. App. Phys.
vol. 10, p. 233.

Manley B.W., Guest A., Holmshaw R.T., 1969.
AEEP vol. 28A, p. 471.

Marcus S., Nelson R., Lynds R., 1979.
SPIE Conf. "Instrumentation in Astronomy - III".
Tuscon, Arizona, Jan. 29th - Feb. 1st, 1979.

Mende S.B., 1971. App. Optics, vol. 10, no. 4, p. 829.

Mende S.B., Chaffee F.H., 1977. App. Optics vol. 16,
no. 10, p. 2698.

Miller J.S., Robinson L.B., Wampler E.J., 1976.
AEEP vol. 40B, p. 693.

Millet E.J., 1976. J. Phys. E: Sci. Inst. vol. 9, p. 794.

Moore C.H., 1974. Astron. & Astrophys. Suppl. vol. 15, pp 497 - 511.

Morgan B.L., Beddoes D.R., Scaddan R.J., Dainty J.C., 1978. Mon. Not. R. astr. Soc. vol. 183, pp 701 - 710.

Morton D.C., 1972. ESO/CERN Conf. "Auxiliary Inst. for Large Telescopes". Geneva. 2nd - 5th May.

Nisenson P., Stachnik R.V., 1975. "Imaging in Astronomy" Technical Digest Conf.: Cambridge, Mass. 18th - 21st June, 1975.

Norton P.A., Inglis J.G., 1964. "Norton's Star Atlas" pub. Gall and Inglis, London.

Oba K., Maeda H., 1976. AEEP vol. 40A, p. 123.

Parry G., Walker J.G., Scaddan R.J., 1979. Optica Acta, vol. 26, p. 563.

Reigler G.R., More K.A., 1973. IEEE Trans. Nuc. Sci., vol. 20, no. 1, p. 102.

Robinson L.B., Wampler E.J., 1976. Proc. IAU
Colloquium no. 40, ed. M. Duchesne and G. LeLievre.
Paris - Meudon, 6th - 8th Sept. 1976.

Roddier F., 1975.
"Imaging in Astronomy". Conf. Preprints. Boston.

Roddier C., Roddier F., 1975. J. Opt. Soc. Am.,
vol. 65, no. 6, p. 834.

Rösch J., Wlerick G., Boussuge C., 1962.
AEEP vol. 14., p. 357.

Rose A., 1946. Journ. Soc. MPTE., vol. 47, p. 273.

Rosenfeld A., 1969.
"Computer Science & Applied Maths Series: Picture
Processing by Computer".
pub. Academic Press, NY & London.

Sackinger W.M., Johnson J.M., 1969.
AEEP vol. 28A, p. 487.

Sargent W.L., Young P.J., Boksenberg A., Shortridge K.,
Lynds C.R., Hartwick F.D.A., 1978.
Astrophys. Journ. vol. 221, p. 731.

Scaddan R.J., Walker J.G., 1978.
App. Optics, vol. 17, no. 23, p. 3779.

Shaw R., 1963. J. Phot. Sci., vol. 11, p. 199.

Shaw R., 1975. "Imaging in Astronomy" Tech. Digest Conf: Cambridge, Mass. 18th - 21st June 1975.

Solomon A.L., 1974.
"Parallel Transfer Register Charge Coupled Imaging Devices". pub. Fairchild Camera & Instrument Corp., California.

Stapinski T.E., Rodgers A.W., Ellis M.J., 1978.
Preprints of the 7th Symposium on Photo-Electronic Devices, Blackett Laboratory, Imperial College, London SW7. 4th - 8th Sept. 1978, p. 335.

Stephens C.L., van Breda I.G., 1972.
ESO/CERN Conf. on Auxiliary Instrumentation for Large Telescopes. ed. Lausten & Reiz. p. 499. Geneva, 2nd - 5t- May, 1972.

Stupp E.H., Levitt R.S., 1971. In "Photo-Electronic Imaging Devices", vol. 2. p. 275, ed. Biberman & Nudelman, pub. Plenum Press.

Swihart T.L., 1968.

"Astrophysics & Stellar Astronomy",

pub. Wiley & Sons Inc.

Texas 1970. "Transistors" Data Book 3.

TI Semiconductor Comp.

Texas 1971a. "Digital Integrated Circuits" Data Book 2.

TI Semiconductor Comp.

Texas 1971b. "Linear - ECL - Mach IV Spec." Data Book 1.

TI Semiconductor Comp.

Texas 1974. "MOS - LSI Static RAM".

TI BUlletin no. DL - S7412189 Oct. 1974.

TI Semiconductor Comp.

Toner M.C., Dix M.J., Sawistowski H., 1978.

J. Phys. E: Sci. Inst., vol. 11, p. 960.

Van Vleck J.H., Middleton D., 1966. Proc. IEEE vol. 54,

no. 1, p. 2.

Vicars - Harris M., 1975. Proc. Symposium on Charge Coupled

Device Technology for Scientific Imaging Applications.

J.P.L., Pasadena, California, March 1975.

Vogt S.S., Tull R.G., Kelton P., 1978. App. Optics. vol. 17, no. 4, p. 574.

Wattson R.B., Rappaport S.A., Fredrick E.E., 1976. Icarus vol. 27, p. 417.

Weinreb S., 1963. Mass. Inst. of Tech. Research Laboratory of Electronics, Technical Report No. 412, 20th August, 1963.

Welford W.T., 1975. Optical and Quantum Electronics, vol. 7, pp 413 - 416.

Welter G.L., Worden S.P., 1977. J. Opt. Soc. Am., vol. 68, no. 9, p. 1271.

Westphal J.A., Kristian J., 1976. IAU Colloquium no. 40, Paris-Meudon, 6 - 8th Sept. 1976. ed. M. Duchesne, G. Lelievre.

Wilcock W.L., 1966. AEEP vol. 22A, p. 535.

Wiza J.L., Henkel P.R., Roy R.L., 1977. Rev. Sci. Inst., vol. 48, no. 9, p. 1217.

Woodhead A.W., Ward R., 1977. The Radio & Electronic Engineer, vol. 47, no. 12, p. 545.

Yeadon E.C., Clarke J.A., 1972. AEEP, vol. 33B, p.593.